



8-2022

Numerical and Experimental Investigation of Machinery Isolation Featuring Gap-Type Nonlinear Rotational Inertial Mechanisms for Marine Applications

Alexandra C. Shafer

University of Tennessee, Knoxville, ashafer4@vols.utk.edu

Follow this and additional works at: https://trace.tennessee.edu/utk_gradthes



Part of the [Structural Engineering Commons](#)

Recommended Citation

Shafer, Alexandra C., "Numerical and Experimental Investigation of Machinery Isolation Featuring Gap-Type Nonlinear Rotational Inertial Mechanisms for Marine Applications. " Master's Thesis, University of Tennessee, 2022.

https://trace.tennessee.edu/utk_gradthes/6465

This Thesis is brought to you for free and open access by the Graduate School at TRACE: Tennessee Research and Creative Exchange. It has been accepted for inclusion in Masters Theses by an authorized administrator of TRACE: Tennessee Research and Creative Exchange. For more information, please contact trace@utk.edu.

To the Graduate Council:

I am submitting herewith a thesis written by Alexandra C. Shafer entitled "Numerical and Experimental Investigation of Machinery Isolation Featuring Gap-Type Nonlinear Rotational Inertial Mechanisms for Marine Applications." I have examined the final electronic copy of this thesis for form and content and recommend that it be accepted in partial fulfillment of the requirements for the degree of Master of Science, with a major in Civil Engineering.

Nicholas Wierschem, Major Professor

We have read this thesis and recommend its acceptance:

Mark D. Denavit, Nicholas E. Wierschem, Timothy J. Truster

Accepted for the Council:

Dixie L. Thompson

Vice Provost and Dean of the Graduate School

(Original signatures are on file with official student records.)

Numerical and Experimental Investigation of Machinery Isolation Featuring Gap-Type Nonlinear
Rotational Inertial Mechanisms for Marine Applications

A Thesis Presented for the
Master of Science
Degree
The University of Tennessee, Knoxville

Alexandra Shafer

August 2022

Acknowledgements

There are several people I would like to thank that made the work completed in this thesis possible. First, I would like to thank Dr. Wierschem, the PI for this project, my advisor, and member of my defense committee. He has been a great mentor over the last year and a half and has shown immense support and patience, not only with me, but all the students in our research group. Many of the topics I studied and issues I ran into throughout this thesis were new to me, so there were many hours, meetings, emails, and questions that were necessary to lead to the completion of this thesis. I would also like to thank Dr. Mark Denavit and Dr. Timothy Truster for serving as committee members. Additionally, I want to say a huge thank you to Andy Baker for fabricating the parts needed for our experimental tests. I thoroughly enjoyed working with Andy because he was always so timely, helpful, patient and kind. I would also like to thank our undergraduate research assistant, Jonathan Snell, for assisting with experimental testing. He has been so eager to help in the lab and would do any task necessary to complete the testing.

Last but certainly not least, I would like to thank my parents, Steve and Katherine Shafer for their constant support, love and always believing in me.

This research was supported in part by the Office of Naval Research under Agreement #N00014-21-1-2122. The findings, opinions, recommendations, and conclusions in this work are those of the authors alone and do not necessarily reflect the views of others, including the sponsor.

Abstract

Transmitted noise and vibration from equipment and machinery is an ongoing and serious priority onboard marine vessels as noise and vibrations interfere with system operations and can compromise the functionality of the vessel. Vibration isolation systems have been widely studied for civil and mechanical applications because of the damage that can occur from extreme vibrations and excessive motion. Conventional vibration isolation systems often include components such as springs and dampers in the isolation layer, but researchers have begun to incorporate other devices including, linear rotational inertial mechanisms (RIMs), often known as inerter, to enhance traditional vibration isolation systems. The inerter is a mechanical device with two terminals in which the equal and opposite force produced is equal to a constant known as inertance multiplied by the relative acceleration between the two terminals. The inertance is a calculated value based on characteristics of the inerter including the geometry of its flywheel. When an inerter is incorporated in an isolation system, the inerter reduces the natural frequency of the system and reduces displacements, but also results in high-frequency transmitted forces, or loads induced back into the system. The high-frequency transmitted forces caused by inerters have encouraged the investigation of nonlinear rotational inertial mechanisms (NRIMs). The objective of this thesis was to investigate the behavior of NRIMs, with an emphasis on gap-type mechanisms, for use in machinery isolation in marine environments. A numerical study was performed to compare a conventional inerter with three different NRIMs. To experimentally investigate linear rotational inertial mechanisms and nonlinear rotational inertial mechanisms, a test apparatus was designed to analyze the effects of incorporating these devices in an isolation layer. A gap-type NRIM, referred to as the bushing-crown gap inerter that would engage and disengage a flywheel based on the primary mass displacement, was designed, fabricated, and tested to determine the effectiveness of the device. The test apparatus was tested without a RIM, with a linear RIM, and with a NRIM to compare responses. The bushing-crown gap inerter significantly reduced high-frequency transmitted forces compared to the RIM. The natural frequency of the isolation mode of the system increased slightly with the gap-type NRIM compared to the no RIM case. Additionally, the amplitude of the peak at the natural frequency was decreased compared to the no RIM case but was still slightly higher than the conventional inerter. The gap-type NRIM flywheel configuration has potential to reduce the natural frequency peak amplitude while avoiding high-frequency transmitted forces that is observed with the inerter when subjected to broadband loading. The results of this research indicate the potential of gap-type NRIMs and encourage further study of them.

Table of Contents

| | |
|---|----|
| Chapter 1 Introduction | 1 |
| Chapter 2 Literature Review | 2 |
| 2.1 Passive Structural Vibration Control..... | 2 |
| 2.1.1 Linear Vibration Isolation Systems | 3 |
| 2.1.2 Nonlinear Isolation Systems..... | 5 |
| 2.2 Inerter..... | 6 |
| 2.2.1 Inerter-based Energy Dissipators | 11 |
| 2.2.2 Inerter-Based Dynamic Vibration Absorbers | 12 |
| 2.2.3 Inerter-Based Vibration Isolation Systems | 14 |
| 2.3 Inerter Nonlinearity | 16 |
| 2.3.1 Inherent Inerter Nonlinearities | 16 |
| 2.3.2 Intentional Inerter Nonlinearities | 18 |
| 2.4 Existing Studies & Real Applications of Inerter | 19 |
| Chapter 3 Marine Application..... | 22 |
| Chapter 4 Numerical Simulations | 27 |
| 4.1 Linear Simulations | 27 |
| 4.2 Nonlinear Simulations..... | 30 |
| 4.2.1 Acceleration Gap..... | 32 |
| 4.2.2 Displacement Gap | 38 |
| 4.2.3 Geometrically Nonlinear Inerter..... | 45 |
| Chapter 5 Experimental Design | 48 |
| 5.1 Phase 1 Experimental Testing | 48 |
| 5.1.1 Die Set Apparatus & Modifications | 48 |
| 5.1.2 Instrumentation & Sensor Layout | 50 |
| 5.1.3 Data Analysis & Discussion..... | 50 |
| 5.1.4 Conclusions..... | 53 |
| 5.2 Phase 2 Experimental Testing | 53 |
| 5.2.1 Conventional RIM Device | 53 |
| 5.2.3 Instrumentation & Sensor Layout | 57 |
| 5.2.4 Data Analysis & Discussion..... | 57 |
| 5.2.5 Conclusions..... | 61 |
| 5.3 Phase 3 Experimental Testing | 70 |
| 5.3.1 Bushing – Crown Gap Inerter Device | 70 |
| 5.3.2 Instrumentation & Sensor Layout | 71 |

| | |
|--|-----|
| 5.3.3 Data Analysis & Discussion..... | 71 |
| 5.3.4 Conclusions..... | 82 |
| Chapter 6 Conclusion & Recommendation for Future Work..... | 83 |
| References | 85 |
| Appendices | 87 |
| Vita..... | 192 |

List of Tables

| | |
|---|----|
| Table 1 Base loaded linear isolation system results | 28 |
| Table 2 Mass loaded linear isolation system results..... | 31 |
| Table 3 Base loaded acceleration gap results compared to linear simulations | 36 |
| Table 4 Mass loaded acceleration gap results compared to linear simulations | 37 |
| Table 5 Base loaded displacement gap results compared to linear simulations..... | 41 |
| Table 6 Mass loaded displacement gap results compared to linear simulations | 44 |
| Table 7 Geometrically nonlinear inerter compared to linear simulations | 47 |
| Table 8 Sensor identification number, model number, serial number, location, and direction for experimental testing | 51 |
| Table 9 Damping ratio of die set at amplitude = 0.8, 1.6, 2.0 | 52 |
| Table 10 Sensor 3 to Sensor 8 CPSD, Frequency Peaks and Angle | 56 |
| Table 11 Phase 2 flywheel inertance values, percent of mass, and natural frequency of the system considering inertance | 59 |
| Table 12 Phase 2 Identified natural frequency from experimental results and calculated inertance values from identified natural frequency..... | 65 |
| Table 13 Phase 3 flywheel inertance values, percent of mass, and set screw, bolt, and nut configurations | 73 |
| Table 14 Numerical values from all experimental values tested at Amplitude = 0.8..... | 78 |
| Table 15 Numerical values from all experimental values tested at Amplitude = 1.6..... | 79 |
| Table 16 Numerical values from all experimental values tested at Amplitude = 2.0..... | 80 |

List of Figures

| | |
|--|----|
| Figure 1 Schematic of an isolated rigid mass | 4 |
| Figure 2 Schematic of a QZS Mechanism..... | 7 |
| Figure 3 Schematic drawing of an ideal two-terminal mechanical inerter | 9 |
| Figure 4 Schematic drawing of a ball-screw inerter..... | 9 |
| Figure 5 Schematic drawing of a rack-and-pinion inerter | 9 |
| Figure 6 Model of a SDOF isolated system with an inerter | 10 |
| Figure 7 SDOF system with two ODRIVD..... | 13 |
| Figure 8 SDOF system incorporating TMDI configuration | 15 |
| Figure 9 MDOF system incorporating TMDI configuration | 15 |
| Figure 10 (a) SDOF structural system; (b) a traditional TMD system; (c)TID system..... | 15 |
| Figure 11 Proposed inerter-based isolation system configurations | 17 |
| Figure 12 Comparison of displacement transmissibility of conventional and parallel-connected isolator systems | 17 |
| Figure 13 Schematic of Geometrically Nonlinear Inerter | 21 |
| Figure 14 (a) Mare Island Navy Mount; (b) rubber cylinder isolator; (c) enclosed spring isolators..... | 23 |
| Figure 15 Vibratory Acceleration Acceptance Criteria for Structureborne Equipment..... | 23 |
| Figure 16 (top) Unfiltered white noise signal (b) Filtered and scaled white noise signal for Type I equipment | 25 |
| Figure 17 Time-scaled filtered white noise signal for Type 1 equipment and systems with natural frequency less than 250 Hz | 25 |
| Figure 18(a) Isolated building subjected to ground motion force (b) Isolated machinery subjected to machine generated force | 26 |
| Figure 19 Base loaded relative displacement time histories for isolation with an inerter, without an inerter, and system with low stiffness | 28 |
| Figure 20 Relative displacement and absolute acceleration estimated transfer function results for linear base loaded systems | 28 |
| Figure 21 Mass loaded displacement time histories for isolation with an inerter and without an inerter .. | 31 |
| Figure 22 Absolute displacement and isolator force estimated transfer function results for linear mass loaded system | 31 |
| Figure 23 Inerter force vs. acceleration relationship with a dead zone gap implemented..... | 33 |
| Figure 24 Base loaded acceleration gap inerter results for various gap sizes. a-d: Relative Displacement, e-h: Absolute Acceleration | 36 |
| Figure 25 Mass loaded acceleration gap inerter results for various gap sizes. a-d: Absolute Displacement TF, e-h: Isolator Force TF..... | 37 |
| Figure 26 Harmonic oscillator network with a series in parallel with an inerter and ideal play | 39 |
| Figure 27 Base loaded displacement gap inerter results for various gap sizes. a-d: Relative Displacement, e-h: Absolute Acceleration | 39 |
| Figure 28 Time step convergence study for without RIM, with RIM, and Displacement gap NRIM at time steps 1/200, 1/250 and 1/300..... | 40 |
| Figure 29 Noise study for base-loaded displacement gap NRIM absolute acceleration at various time spans | 43 |
| Figure 30 Mass loaded displacement gap inerter results for various gap sizes. a-d: Absolute Displacement transfer function, e-h: Isolator Force transfer function..... | 43 |
| Figure 31 Geometrically Nonlinear Inerter, a-b: Absolute displacement transfer function, e-g: Isolator Force transfer function..... | 47 |
| Figure 32 Die set that the test apparatus is built up around | 49 |

| | |
|--|----|
| Figure 33 Die set test apparatus with springs | 49 |
| Figure 34 Accelerometer layout. (a) top of die set (b) front of die set | 51 |
| Figure 35 Figure 33 Ground Motion CPSD, Z direction | 54 |
| Figure 36 Sensor 2 CPSD, Z direction | 54 |
| Figure 37 Sensor 5, 6 and 7 transfer function estimate, Z direction | 55 |
| Figure 38 Sensor 4 auto power spectral density plot, Y Direction | 55 |
| Figure 39 Sensor 3/8 CPSD and angle plot for amplitude = 2.0..... | 56 |
| Figure 40 Conventional RIM installed in die set for phase 2 testing..... | 58 |
| Figure 41 Thrust bearing and shaft collar used to secure the conventional RIM in the die set..... | 58 |
| Figure 42 Fabricated flywheel hub | 59 |
| Figure 43 Examples of flywheel configurations (a) $b=24.6\%$ (b) $b=39.7\%$ (c) $b=194.5\%$ | 59 |
| Figure 44 Ground motion APSD for all flywheel configurations and phase 1 testing..... | 62 |
| Figure 45 Sensor 5, 0-100 Hz Estimated Transfer Function for all Flywheel Configurations at Amp = 0.2, 0.4, 0.8, 1.6, 2.0 | 63 |
| Figure 46 Sensor 5, 0-500 Hz Estimated Transfer Function for all Flywheel Configurations at Amp = 0.2, 0.4, 0.8, 1.6, 2.0 | 64 |
| Figure 47 Phase 2 Estimated transfer function with increased nfft value used for calculated inertance values from identified natural frequency..... | 65 |
| Figure 48 Sensor 4, 0-100 Hz APSD for all Flywheel Configurations at Amp = 0.2, 0.4, 0.8, 1.6, 2.0 | 66 |
| Figure 49 Sensor 8, 0-100 Hz APSD for all Flywheel Configurations at Amp = 0.2, 0.4, 0.8, 1.6, 2.0 | 68 |
| Figure 50 Gap inerter notched bushing and crown engaged (left) and disengaged (right) | 72 |
| Figure 51 Displacement gap inerter with labeled components | 72 |
| Figure 52 Sensor 5 estimated transfer function for all flywheel configurations, 2 – 30 Hz, compared to no flywheel case at Amp = 0.8, 1.6, and 2.0 | 74 |
| Figure 53 Sensor 5 estimated transfer function for all flywheel configurations, 2 – 10 Hz, compared to no flywheel case at Amp = 0.8, 1.6, and 2.0 | 75 |
| Figure 54 Sensor 5 estimated transfer function for 300% gap-type NRIM configuration compared to no flywheel case and linear flywheel cases from phase 2 at Amp = 0.8, 1.6, and 2.0 | 76 |

Chapter 1 Introduction

The objective of this thesis was to investigate the behavior of nonlinear rotational inertial mechanisms, with an emphasis on gap-type mechanisms, for use in machinery isolation in marine environments. Vibration isolation systems have been widely studied for civil and mechanical applications. Vibration isolation systems have been developed and implemented in mechanical applications because extreme vibrations, or excessive motion can cause costly damage to equipment, decrease effectiveness, cause noise, and impact system operations. Conventional vibration isolation systems often include components such as springs and dampers in the isolation layer, but researchers have begun to incorporate other devices, like linear rotational inertial mechanisms (RIMs), to enhance traditional vibration isolation systems. A linear RIM, otherwise known as an inerter, is a mechanical device with two terminals in which the equal and opposite force produced is equal to the inertance multiplied by the relative acceleration between the two terminals (Smith 2020). The inertance is a function of certain properties of the system and can be easily increased, resulting in significant mass effects. The inerter is commercially available and has numerically and experimentally proven to be efficient in reducing displacements and the natural frequency of the isolation mode of an isolated system. Although the inerter is effective by some measures, as inertance is increased, the high-frequency loads transferred through the isolation system are increased. The transmitted high-frequency forces caused by inerters have encouraged the investigation of nonlinear rotational inertial mechanisms (NRIMs) numerically and experimentally for specific marine applications.

The contents of this thesis include an extensive literature review on passive structural control, specific considerations for marine applications, numerical simulations of linear and nonlinear rotational inertial mechanisms, and the experimental design and testing of one of the numerically modeled NRIMs. The literature review in chapter 2 details linear and nonlinear passive structural vibration isolation. There is an in-depth review of the inerter and inerter-based systems that have been researched. Although the primary focus of this thesis is vibration isolation systems, the literature review details several inerter-based systems including inerter-based energy dissipators, inerter-based dynamic vibration absorbers, and inerter-based vibration isolation systems. Furthermore, the literature review summarizes inherent inerter nonlinearities that have been discovered, as well NRIMs with intentional nonlinearities. Currently, there is a lack of full-scale experimental testing utilizing linear and nonlinear RIMs, but the literature review summarizes existing studies and real applications of the inerter. Chapter 3 details specific considerations that are necessary for marine applications. Chapter 4 details the numerical simulation of a conventional inerter and three different NRIMs. Additionally, in chapter 5, a test apparatus was designed to effectively analyze the effects of incorporating rotational inertial mechanisms in an isolation layer. A version of one of the NRIMs numerically simulated was then designed, fabricated, and tested to determine the effectiveness of the device. The test apparatus was tested without a RIM, with a RIM, and with a NRIM to compare responses. Chapter 6 draws conclusions from the experimental tests and provides recommendations for future work.

Chapter 2 Literature Review

Extensive research has been conducted on passive vibration control and vibration mitigation techniques in civil and mechanical applications. The following literature review will detail passive structural vibration control, which includes linear and nonlinear isolation systems, and will provide a foundation for the research in this thesis. An overview of the conventional tuned mass damper (TMD), a fundamental passive vibration control device, will be given. Following this is the introduction to the novel inerter device which is the focus of this thesis. Inerter-based energy dissipators, dynamic vibration absorbers and vibration isolators will be discussed in detail regarding the current research being done to enhance conventional systems. Next, nonlinearities in inerters, both inherent and intentional, will be discussed. Finally existing studies and real applications of the inerter in mechanical and civil applications will be discussed to show how the device has been physically realized and where improvements and/or additional research is needed.

2.1 Passive Structural Vibration Control

The vibration, or oscillation of a rigid or elastic body from its equilibrium position, is a common issue in civil applications. Often there is a focus on civil engineering structures, but excessive vibrations frequently occur in mechanical applications. Mechanical equipment isolation is essential because extreme motion can cause damage to equipment or the surrounding structure, decrease effectiveness of the equipment, cause excessive noise, and impact system operations. Due to the impact vibrations have on system performance, serviceability, and safety in mechanical applications, vibration isolation systems have been developed and implemented in civil and mechanical engineering applications (Ma, Bi, and Hao 2021).

Structural vibration control systems can be classified as passive, semi-active, active, or hybrid. When structural motion, oscillations, or vibrations occur, a passive vibration control system can generate a force in response to the motion without a dependence on an external source of power (Ma, Bi, and Hao 2021). This contrasts with active, semi-active, and hybrid systems which rely on sensors and controllers to record real time data regarding structural motion. Using this real time information, an external power source can produce control forces to respond to the motion. Passive vibration control is favorable in civil engineering applications due to their independence from external energy and generally more simplistic design (Ma, Bi, and Hao 2021).

Passive vibration control systems can be classified into three categories: energy dissipators, dynamic vibration absorbers, and vibration isolation systems (Ma, Bi, and Hao 2021). Conventional energy dissipators, like metallic yield dampers, friction dampers, viscoelastic dampers, and viscous fluid dampers, convert kinetic energy into heat to reduce structural vibrations (Ma, Bi, and Hao 2021). Dynamic vibration absorbers transfer vibration energy to auxiliary systems. An example of a dynamic vibration absorber that is commonly used is the tuned mass damper (TMD). Although the TMD is not the focus of the work presented in this thesis, the TMD is an important and foundational passive vibration control device and should be reviewed when discussing passive structural control. The TMD has a secondary mass, spring, and damper connected to the primary structure. The frequency of the damper is tuned or designed to interfere when the system is oscillating in resonance. The resulting TMD modifies the dynamics of the combined system, where the TMD splits the mode it is tuned to into two modes. One where the TMD is in phase with the structure and one where it is out of phase with the structure. The TMD then resonates out of phase from the structural motion to reduce large vibration amplitudes (Connor 2003). Taipei 101, a 509 m high skyscraper located in Japan, employs the use of a TMD to reduce structural vibrations caused from frequent typhoon storms and earthquakes (Wagg 2021). A 660-ton mass

suspended by cables swings when the building is shaken by natural events. The swinging of the mass is tuned to interfere and thus cancel the large amplitudes that the building is subjected to. The TMD mass is increased in size and weight as the primary structure and damping effects required increase (Wagg 2021). Increasing the size of the TMD mass results in an increase in cost and space for the TMD which is a major limitation of the TMD. Additionally, the TMD is tuned to dissipate vibrations at one resonance peak, therefore, if system parameters or the resonance peak changes, or if the structure has multiple problematic modes of vibration, the device will be less effective (Wagg 2021). Lastly, a vibration isolation layer will add a degree of freedom to the system which will create a new, lower fundamental frequency that becomes the new natural frequency of the system. The new fundamental frequency is effectively shifted meaning it will occur at a sooner period and will be lower than the original natural frequency of the system and thus forces and vibrations can then be attenuated (Ma, Bi, and Hao 2021). Energy Dissipators, Dynamic vibration absorbers and vibration isolation systems are all used in engineering applications, but for the purpose of this thesis, there will be a focus on isolation systems. The following chapters detail linear and nonlinear vibration isolation systems.

2.1.1 Linear Vibration Isolation Systems

A single degree of freedom (SDOF) system with an isolated rigid mass (m) supported on an isolator that has stiffness (k) and damping (c) as shown in Figure 1 can be used to explain the concept of linear vibration isolation. It should be noted that not all isolated systems are SDOF, and this model does not include the dynamics of the mass being isolated. In this SDOF case, the presence of an isolation system effectively adds a low frequency mode to the system, but in a dynamic system that is already isolated, the natural frequency will be effectively shifted. The system is excited by a harmonic base excitation, P with loading frequency, ω . The equation of motion for this isolated rigid mass in terms of u , the displacement, is $m\ddot{u} + c\dot{u} + ku = P$. The natural frequency of the system can be calculated using the equation: $\omega_n = \sqrt{k/m}$ (Balaji and Karthik SelvaKumar 2021).

The system is in resonance when the natural frequency is equal to, or in practice near, the loading frequency. When the system is in resonance, the amplitude of the response will be very high. Due to this high response amplitude, the goal of the isolation system is to shift the natural frequency of the system away from the loading frequency, which results in the system staying out of a resonance condition. Therefore, to attenuate vibrations using an isolation system, either of the following must occur: 1. The loading frequency, or excitation needs to be adjusted, or 2. The natural frequency of the system needs to be tuned to a specific natural frequency that ensures the system stays out of resonance (Balaji and Karthik SelvaKumar 2021). Option 1 is not easily controllable in real applications, so researchers have focused on enhancing linear and nonlinear vibration isolation systems to shift the natural frequency of a system which effectively reduces vibrations by keeping the system out of its resonance condition.

A linear vibration isolation system consists of a flexible supporting mechanism, usually provided by a linear spring and an energy dissipation mechanism, typically modeled as a linear damper (Balaji and Karthik SelvaKumar 2021). The linear isolation system mass, stiffness and damping elements do not vary with time and behave linearly (Deshpande, Mehta, and Jazar 2006). This can be seen in the equation of motion for the linear SDOF system in Figure 1. The force in the spring, or stiffness element in the EOM, is calculated by multiplying the stiffness coefficient, a property of the spring, by the displacement of the system relative to the base, u . The stiffness coefficient, k , is represented by a constant value; therefore, the force due to the stiffness element increases linearly with increasing relative displacement. In a perfectly linear system, the stiffness coefficient will stay constant for the entirety of the isolation system lifetime.

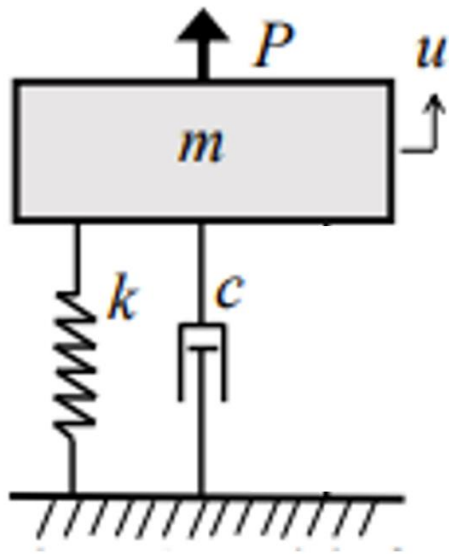


Figure 1 Schematic of an isolated rigid mass

This linearity can also be seen with the force due to damping, which is represented by a damping coefficient, c , multiplied by the velocity of the system, \dot{u} . Like the stiffness force, the damping force also increases linearly with time due to a constant damping coefficient. The behavior of springs and dampers in SDOF systems, like in Figure 1, are modeled as perfectly linear, but it is important to acknowledge that springs and dampers can have inherent nonlinearities (Deshpande, Mehta, and Jazar 2006). Despite inherent nonlinearities that can occur in a system, modeling stiffness and damping forces linearly creates a relatively simple system for analytical and numerical analysis that is manageable and typically still sufficiently accurate (Deshpande, Mehta, and Jazar 2006).

Researchers have found linear isolation systems can be effective for vibration control, but that linear systems do not work well at low loading frequencies. A linear isolator dissipates vibrations best when the frequency ratio, the ratio of the loading frequency divided by the isolation mode natural frequency, is equal to or greater than $\sqrt{2}$ (Balaji and Karthik SelvaKumar 2021). To achieve this desired frequency ratio when the loading frequency is low, the isolation layer natural frequency will need to be decreased. Using the mathematical definition of natural frequency, the stiffness of the system will often need to be reduced to decrease the natural frequency of a system. However, stiffness reductions can lead to excessive static and dynamic displacements (Balaji and Karthik SelvaKumar 2021). In other words, as the stiffness of the isolation layer is decreased, the displacement of the isolated mass tends to increase. This is a major limitation of linear isolation systems because there is a practical limit where the stiffness cannot be further decreased; therefore, there is a limited range of frequencies in which the linear isolation system can be effective. Damping is effective at dissipating vibrations at resonance, but can have negative effects on the transmissibility of the system, or the ratio of the force experienced by the isolated mass to the external load applied to the system, at higher frequencies (Balaji and Karthik SelvaKumar 2021). In engineering applications, there is a need for vibration mitigation for a wideband low-frequency spectrum, like for random excitations, white noise and shocks which are often necessary when isolating machinery and equipment (Balaji and Karthik SelvaKumar 2021). This need for low-frequency isolation has encouraged researchers to turn toward nonlinear isolation systems.

2.1.2 Nonlinear Isolation Systems

A nonlinear isolation system is a system with a stiffness or energy dissipation mechanism that has the ability to change characteristics based on loading or response of the system (Balaji and Karthik SelvaKumar 2021). Variable stiffness and variable damping can be used in the system either through a mechanism, such as a geometric nonlinearity, or by using materials with nonlinear properties (Balaji and Karthik SelvaKumar 2021). Nonlinear isolation systems are attractive due to the ability for the system to have low dynamic stiffness, resulting in a low natural frequency, while also having low static deflection. A key difference between linear and nonlinear isolation systems is that the effectiveness of nonlinear isolation may not be robust to changes in the amplitude of the loading. Because superposition does not apply to nonlinear isolation system, the behavior will change based on the loading and is not predictable compared to linear isolation systems. This nonlinearity could be an advantage or disadvantage and can change based on the nonlinear device, loading, and configuration of the system. Additionally, nonlinear isolation systems are more complex than linear isolation systems (Lu, Brennan, and Chen 2016).

Nonlinear passive systems can drastically reduce the dynamic stiffness of the system or attain zero stiffness by utilizing a negative stiffness mechanism (Balaji and Karthik SelvaKumar 2021). An isolator with zero dynamic stiffness is called a quasi-zero-stiffness (QZS) mechanism and is obtained by combining a positive stiffness element with a negative stiffness element (Carrella, Brennan, and Waters 2007). A negative stiffness effect can be physically realized by utilizing different spring orientations or taking advantage of buckling. Many configurations of QZS mechanisms have been proposed, like the

simple QZS mechanism shown in Figure 2. Carrella et al. (2007) investigated this QZS mechanism utilizing a vertical spring, k_v and two oblique springs, k_0 to determine the relationship between the geometry of the springs and the relative stiffness.

When an appropriately tuned load is applied to the QZS system in Figure 2, the vertical spring compresses and the oblique springs become horizontal. When the oblique springs are horizontal, i.e., when θ_0 is equal to zero, the QZS system is in its static equilibrium position. When motion from loading occurs about the static equilibrium position, the vertical spring acts as a positive stiffness element and the oblique springs act as negative stiffness elements in the vertical direction (Carrella, Brennan, and Waters 2007). There have been many quasi-zero stiffness systems proposed and they have become attractive due to the ability for the isolators to dissipate vibrations for a broadband range of frequencies and reduce force transfer but there are limitations to QZS mechanisms (Z. Zhang, Zhang, and Ding 2020). One drawback of the QZS design is that the total linear stiffness of the system is reduced which results in the system having decreased resistance to deformation (Z. Zhang, Zhang, and Ding 2020). Additionally, due to the nonlinearities, it is common at low frequencies for the response to be very complex and induce several super-harmonic responses (Z. Zhang, Zhang, and Ding 2020). The drawbacks mentioned contribute to the hesitation for quasi zero stiffness to be used in practical engineering applications.

A Nonlinear energy sink is a passive isolation system that is configured with a small mass supported by a linear dashpot, or damping mechanism, and a nonlinear spring connected to the main structure (Balaji and Karthik SelvaKumar 2021). The NES absorbs excitation energy from the structure and locally dissipates it (Balaji and Karthik SelvaKumar 2021). The nonlinear spring makes the energy that is transferred from the structure to the NES irreversible, meaning energy cannot be returned into the system (Ma, Bi, and Hao 2021). The nonlinear spring also enables the NES to be effective at a wide range of frequencies (Balaji and Karthik SelvaKumar 2021). The nonlinear nature of the NES allows it to self-tune to the primary system, meaning that the NES does not have its own natural frequency. It is important to note that the amplitude of the loading is very important to the performance of the NES and must be considered in the design, but the ability for the NES to be effective at different frequencies and dissipate energy without returning it to the primary system leads to efficient vibration suppression.

2.2 Inerter

Limitations of conventional vibration mitigation devices and techniques have encouraged researchers to turn to inerter and inerter-based devices to mitigate vibrations in civil structural applications. The inerter was formally defined by Smith in 2001 as a mechanical device with two terminals in which the equal and opposite force produced is equal to the inertance multiplied by the relative acceleration between the two terminals (Smith 2020). An ideal two-terminal mechanical inerter can be seen schematically in Figure 3. The two terminals have absolute displacements x_1 and x_2 and are the connection points to other elements in the system (Smith 2020). The forces generated at both terminals are equal in value and opposite in direction. The governing equation for the force generated by an ideal inerter is $F(t) = b(\ddot{x}_2(t) - \ddot{x}_1(t))$ (Smith 2020). The inertance, b , is a calculated value measured in units of mass, and is based on certain characteristics of the system that are dependent on the geometry and components of the inerter (Smith 2020).

The inerter has been physically realized in many ways but the ball-screw inerter and rack-and-pinion inerter are the most significant types of realizations to the application in this thesis. A schematic of the ball-screw inerter is shown in Figure 4 and consists of a threaded rod, a ball screw nut, a radial bearing, a housing, and a flywheel fixed to a threaded rod (Smith 2020).

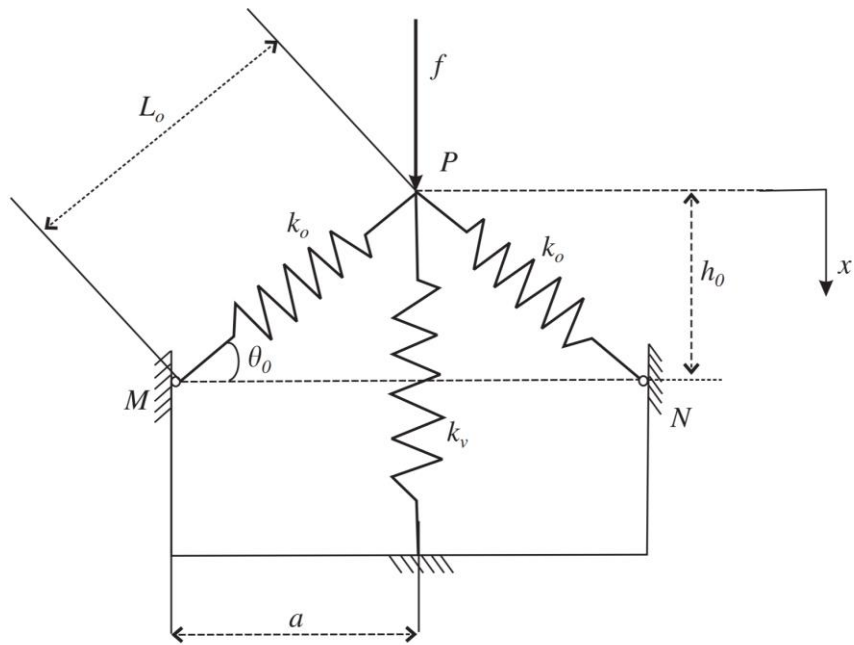


Figure 2 Schematic of a QZS Mechanism

Reproduced from (Carrella, Brennan, and Waters 2007).

When a force is applied to the inerter that makes the ball screw nut want to translate relative to the threaded rod, the threaded rod and the attached flywheel will rotate as this translation occurs (assuming the ball screw nut is prevented from rotating); thus this mechanism converts linear motion into rotational motion (Ma, Bi, and Hao 2021). The equation: $b = \left(\frac{2\pi}{l}\right)^2 \cdot I$, where l is the distance traveled for each complete turn of the ball-screw, known as the lead, and I is the moment of inertia of the flywheel, can be used to calculate the inertance of the ball screw inerter (Ma, Bi, and Hao 2021). The inertance can be increased by increasing the moment of inertia of the flywheel or decreasing the lead of the ball-screw.

A schematic drawing of a rack-and-pinion inerter which consists of a rack, housing, gears, pinions, and flywheel, is shown in Figure 5. When load is applied at the terminals, the rack will slide laterally which will drive the rotation of the flywheel through the pinions and gears; thus, this mechanism also converts lateral motion into rotational motion of the flywheel. The inertance of the rack-and-pinion inerter can be calculated using the following equation: $b = n^2 \cdot I$, where I is the moment of inertia of the flywheel and n is the gear ratio which is dependent on the radii of the gears (Ma, Bi, and Hao 2021). Like the ball-screw inerter, the moment of inertia of the flywheel (I) directly impacts the inertance of the rack-and-pinion inerter (Ma, Bi, and Hao 2021).

Researchers have found many benefits to incorporating the inerter into structural vibration control. Typical mechanical networks have previously consisted of a combination of springs, dashpots, and masses. The inerter is a two-terminal mass element, like the spring and dashpot. This means that an inerter can be used in a mechanical network with a spring and dashpot. The inclusion of the inerter opens up a wider design space that has the potential to yield more effective vibration control systems (Ma, Bi, and Hao 2021).

As previously mentioned, the force generated due to the relative motion of the two terminals of an inerter is directly impacted by the inertance of the inerter. There is a significant mass amplification effect that occurs when an inerter is incorporated into a mechanical network. The inertance can be modified by changing the geometry, or dimensions of the flywheel, or the mechanism that results in rotation. For example, making the lead of the lead screw smaller or the gear ratio of the rack and pinion bigger can result in feasible mass effects far greater than the actual mass in the system, and these mass effects can be modified relatively easily by making small changes to the components of the inerter (Ma, Bi, and Hao 2021). The mass effects on the system can be seen when looking at the resulting equation of motion for a system with an inerter incorporated in the isolation layer. Figure 6 shows a model of a SDOF isolated system with an inerter with inertance (b), spring (k), damper (c), mass (m), and a load (P) acting on the mass.

The force generated by the inerter is equal to the relative acceleration between the two terminals multiplied by the inertance, or $F_b = b(\ddot{u}_2 - \ddot{u}_1)$, but the ground is fixed in this case, so the force generated by the inerter is: $F_b = b\ddot{u}$. The resulting equation of motion for the system: $(m + b)\ddot{u} + c\dot{u} + ku = P$. The amplified mass effects can be seen in the equation of motion in two ways: 1. The mass and inertance are grouped together, thus the system thinks there is a larger mass in the system than there actually is, and 2. The inertance, b can be easily manipulated by changing the flywheel, or mechanism of rotation. For example, the inertance can be drastically increased while utilizing a relatively small flywheel. This is a major benefit to incorporating the inerter into isolation layers. Additionally, the inerter is like a negative stiffness element meaning the inerter lowers the natural frequency and at times generates a force that assists motion, rather than opposes motion, but unlike typical negative stiffness elements, the inerter is not affected by static loads and cannot compromise stability of the system (Ma, Bi, and Hao 2021).

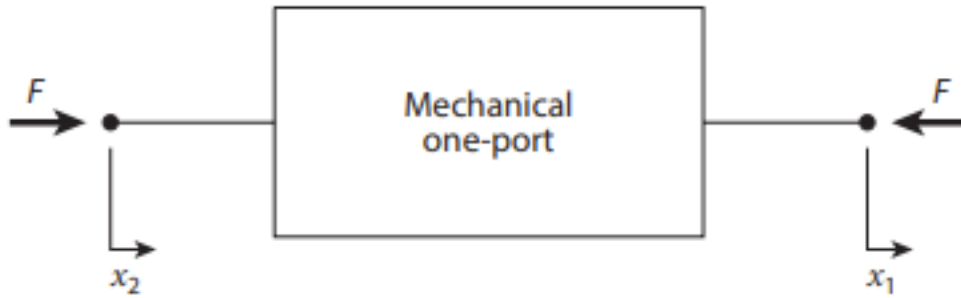


Figure 3 Schematic drawing of an ideal two-terminal mechanical inerter

Reproduced from (Smith 2020)

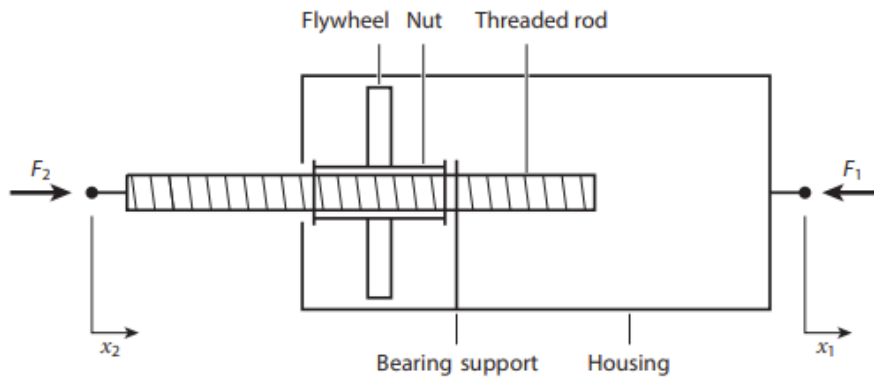


Figure 4 Schematic drawing of a ball-screw inerter

Reproduced from (Smith 2020)

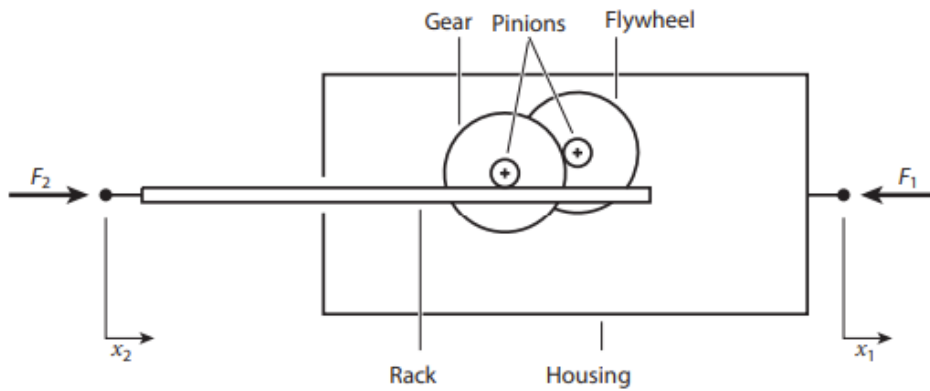


Figure 5 Schematic drawing of a rack-and-pinion inerter

Reproduced from (Smith 2020)

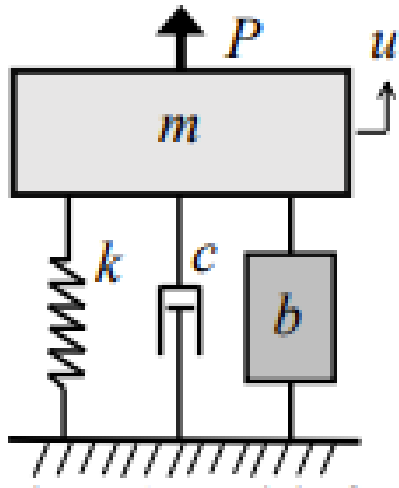


Figure 6 Model of a SDOF isolated system with an inerter

The characteristics and added benefits of inerters have encouraged researchers to incorporate the inerter in conventional passive control systems to mitigate structural vibrations. As previously mentioned, passive vibration control systems can be broadly classified into energy dissipators, dynamic vibration absorbers, and vibration isolation systems. The inerter has been incorporated into each of these types of passive control systems to create inerter-based energy dissipators, inerter-based dynamic vibration absorbers, and inerter-based vibration isolation systems. A broad overview of inerter-based vibration control systems is given in the following chapters.

2.2.1 Inerter-based Energy Dissipators

The addition of the inerter to a conventional energy dissipator has shown to result in large motion and consequently dissipates more vibrations because the ideal mechanical behavior of the system is the superposition of the mechanical behavior of the damper and the inerter (Ma, Bi, and Hao 2021). A variety of inertial mass dampers (IMDs) have been proposed and developed to enhance the conventional energy dissipator and increase vibration dissipating capabilities in mechanical networks and applications (Ma, Bi, and Hao 2021). The angular mass damper, rotational inertia viscous damper (RIVD), clutch inerter damper (CID), and one directional rotational inertia viscous damper (ODRIVD) are examples of effective inerter-based energy dissipators and are described in the following paragraphs.

Pradono et al. (2008) developed and tested an angular mass damper to dampen the relative acceleration between two joints in seismic applications. The device is a wheel that has an inner and outer perimeter with mass concentrated on the outer perimeter. The equivalent mass generated by the wheel is determined by the ratio of the outer radius to the inner radius of the wheel (Pradono et al. 2008). Pradano et al. found that using the angular mass damper in a friction-damped and base-isolated benchmark building further reduced seismic response. The reason for this outcome can be seen in the equation of motion for a SDOF system using an angular mass damper subjected to seismic forces. With mass m , equivalent mass m_{eq} , damping c , stiffness k , relative displacement u , and ground displacement z , the equation of motion is: $(m + m_{eq})\ddot{u} + c\dot{u} + ku = -m\ddot{z}$. The mass of the system is increased due to the equivalent mass, but the equivalent mass is not adding actual mass to the structure. Adding actual mass to the structure would result in an increase in seismic-induced forces. Essentially, the natural period is lengthened without increasing earthquake force, making the angular mass damper an effective way to reduce seismic energy and related vibrations (Pradono et al. 2008). Similar to the angular mass damper, a RIVD, or an inerter with viscous damping, increases a system's effective mass and dissipates energy by surrounding a rotational inertia mass, or flywheel, with a viscous material, or fluid (Javidialesaadi and Wierschem 2019b). When the structure starts moving, kinetic energy is stored in the flywheel. The structure then reaches its maximum velocity, relative to the base and sequentially, the motion of the structure will slow down. Any remaining kinetic energy in the flywheel is then transferred back to the primary structure (Javidialesaadi and Wierschem 2019b). Therefore, the flywheel, although dissipating energy, cannot permanently absorb energy in this configuration.

Makris et al. (2016) proposed a CID to exploit the benefits of the inerter by suppressing displacements of long periods, but also address the main disadvantage of rotational inertial mechanisms which is that energy is transferred back into the structure due to the energy stored in the rotating flywheel. The proposed system consisted of two parallel rotational inertia systems in a rack-pinion-flywheel configuration with a simple clutch mechanism that would allow the pinion-gearwell to be driven solely by the motion of the translating rack, and conversely not allow the pinion of the gearwheels to drive the rack (Makris, Asce, and Kampas 2016). The inertial element of the developed system ensures the resisting force is proportional to the relative acceleration between the mass and supports of the flywheel, but the addition of the clutch mechanism would allow the system to resist motion of the structure without causing

deformation (Makris, Asce, and Kampas 2016). Similar to the CID, Javidialesaadi and Wierschem (2019b) proposed a one directional rotational inertia viscous damper (ODRIVD), where energy is transferred one-directionally to the flywheel and locally dissipated, thus, energy is not transferred back to the primary structure. Javidialesaadi and Wierschem (2019b) proposed a mechanism that utilizes two ODRIVD, where one ODRIVD is engaged with the positive velocity of the structure and the second is engaged with the negative velocity of the structure. The proposed ODRIVD consists of a one-directional ball screw, flywheel and viscous fluid and the investigated system is a SDOF system subjected to base excitation controlled with two ODRIVD, as shown in Figure 7.

This configuration will behave or vibrate in three different ways. If the structure is moving left, the first ODRIVD will engage and will result in the flywheel of the farthest right ODRIVD to spin freely. If the structure is moving right, the farthest right ODRIVD will engage and the flywheel of the farthest left ODRIVD will spin freely. If neither condition is met in the previously described states, neither ODRIVD will engage which will result in both flywheels spinning freely (Javidialesaadi and Wierschem 2019b). Javidialesaadi and Wierschem (2019b) found that the two ODRIVD configuration has superior performance at low device damping levels. At zero damping, the ODRIVD has a significantly lower amplitude at resonance when compared with the RIVD. Additionally, at low damping levels, the two ODRIVD system has potential for superior performance compared to the RIVD due to the one direction energy mechanism and the ability for the flywheel to locally dissipate energy and not transfer energy back to the primary structure (Javidialesaadi and Wierschem 2019b).

2.2.2 Inerter-Based Dynamic Vibration Absorbers

Conventional dynamic vibration absorbers (DVAs), like a TMD, rely on a large secondary mass to improve vibration control, but including a large secondary mass is not practical in all applications. For typical civil engineering structures, even considering a small mass percentage, a very large mass would be necessary for a DVA to be effective. A larger mass increases construction and material costs, as well as requires a significant amount of space to design into the structure. DVAs require tuning which can create many limitations to the abilities of the device. For a DVA to properly dissipate vibrations, the device must be tuned to specific system parameters. If the system parameters change at any point within the device, or structure's lifetime, the device cannot adapt to the new parameters thus reducing effectiveness of the device.

Despite tuning limitations, researchers have investigated adding an inerter to conventional dynamic vibration absorbers to reduce the need for a large secondary mass and improve vibration control. Inerter-based DVAs, like the tuned mass damper inerter (TMDI) and the tuned inerter damper (TID) have proven to be effective inerter-based dynamic vibration absorbers and are described in the following paragraphs.

Marian and Giaralis (2014) proposed a tuned mass damper inerter (TMDI) to reduce oscillatory motion of SDOF and multi-degree of freedom (MDOF) structures excited by white noise. The SDOF system, as seen in Figure 8, has an inerter connected between the TMD oscillating mass and the ground. The MDOF system, as seen in Figure 9, has an inerter connected between the TMD oscillating mass and the primary structure.

Both configurations allowed the system to take advantage of the mass amplification effects which is a main benefit of using the inerter in mechanical networks. Compared to the conventional TMD configuration, both the SDOF and MDOF TMDI systems, had improved vibration mitigation performance and had increased effectiveness even with relatively low values for the TMD mass (Marian and Giaralis 2014). Essentially, a smaller secondary TMD mass could be used in conjunction with the inerter and still be effective at suppressing vibrations (Marian and Giaralis 2014).

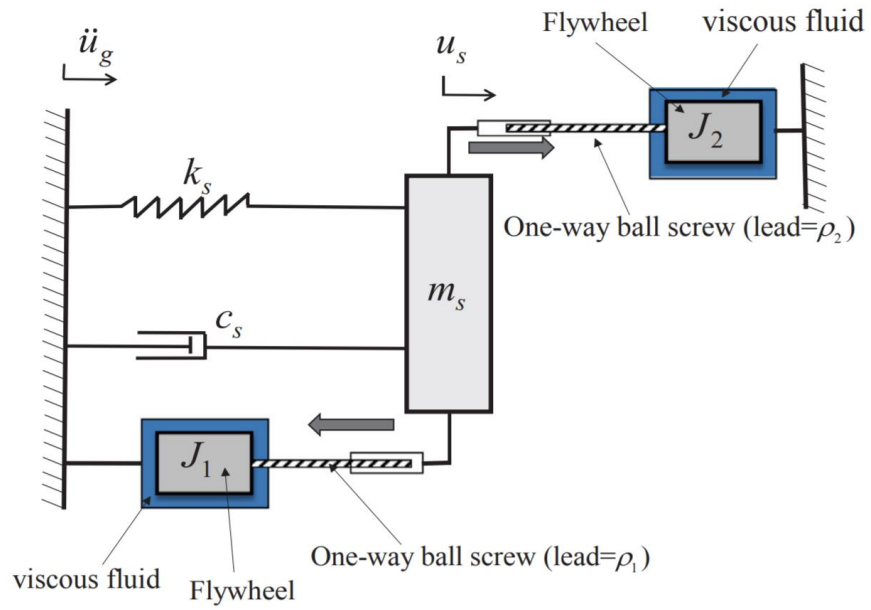


Figure 7 SDOF system with two ODRIVD

Reproduced from (Javidialesaadi and Wierschem 2019b).

Lazar et al. (2014) proposed a tuned inerter damper (TID) which has a similar configuration to the TMDI, but the inerter is installed in series with spring and damper elements and there is no secondary mass present. Figure 10 shows (a) a SDOF structural system, (b) a traditional tuned mass damper system, and (c) the proposed tuned inerter damper system. As seen in Figure 10, The TID is connected between stories of a structure, rather than on a single story, like a traditional TMD.

This configuration takes advantage of the large inertance-to-mass ratio that can be obtained without relying on a secondary mass element(Lazar, Neild, and Wagg 2014). Lazar et al. (2014) compared the TMD and TID transfer functions, developed a tuning procedure for SDOF and MDOF systems, studied different TID configurations, and studied the seismic performance of the TID. As the inertance-to-mass ratio increased, there was an increase in displacement response performance(Lazar, Neild, and Wagg 2014). For SDOF structures, the TMD and TID had identical performance when they had the same mass ratio, but the ability for the TID mass-to-inertance ratio to be easily increased is a major benefit of the TID system and makes it a good alternative to conventional dynamic vibration absorbers(Lazar, Neild, and Wagg 2014). Considering MDOF structures, the best structural response was observed with the inerter installed between the ground and the first story of the structure. When tested as a 3DOF system subjected to seismic excitation, the TID device placed at the bottom story level had a similar response to a traditional TMD placed at the top story level, however, the small size and mass of the device still point to the TID as an attractive alternative to a traditional TMD.

As seen with the TMDI and TID, an inerter can be added to linear DVA systems to reduce or eliminate a secondary mass due to its mass amplification affects.

2.2.3 Inerter-Based Vibration Isolation Systems

Recently, inerter-based configurations for vibration isolation systems have been proposed. The large inertance that can be achieved without increasing the physical mass of the system and the potential for that inertance to be used to positively alter the dynamics of the systems are motivations for applying inerters to isolation systems. Inerter-based vibration isolation systems have proven to be effective and are described in the following chapter. Hu et al. (2015) proposed five different inerter-based isolation systems and analytically studied the performance of each configuration. Figure 11 shows the five configurations investigated with two of the configurations consisting of only an inerter and damper and the other three consisting of inerter, damper, and spring.

The configurations varied in series-connected and parallel-connected SDOF configurations to evaluate how the configuration of the system affects the frequency response(Hu et al. 2015). It was found that both the series and parallel-connected inerter lowered the invariant points in the frequency domain response and outperformed traditional DVAs (Hu et al. 2015). Figure 8 compares the displacement transmissibility of a conventional isolator and a parallel-connected inerter isolation system(Ma, Bi, and Hao 2021). The parallel-connected inerter has a reduced natural frequency of the receiving mass, reduced peak, and unchanged static displacement. The negative stiffness and anti-resonance effects can be seen visually in the figure (Ma, Bi, and Hao 2021). For these reasons, the parallel-connected inerter has been primarily used and studied in research over series-connected inerters, but there are still limitations to this configuration. In Figure 12, the frequency plateau between points C and D is much higher for the parallel-inerter isolator than the conventional isolator. This is of concern because at higher frequencies, the parallel-connected isolator is not as effective at isolation performance(Ma, Bi, and Hao 2021). The inerter force increases as frequency increases and as the inerter force grows very large, the subsequent isolation performance decreases because high frequency forces are transmitted back into the system. It has been found that high frequency performance is increased if the inerter is further isolated from the ground; however, this can decrease isolation performance at lower frequencies(Ma, Bi, and Hao 2021).

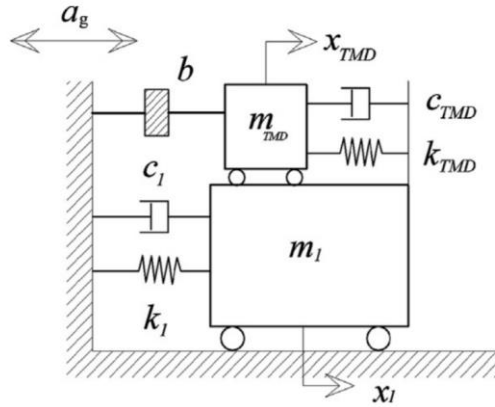


Figure 8 SDOF system incorporating TMDI configuration

Reproduced from (Marian and Giaralis 2014)

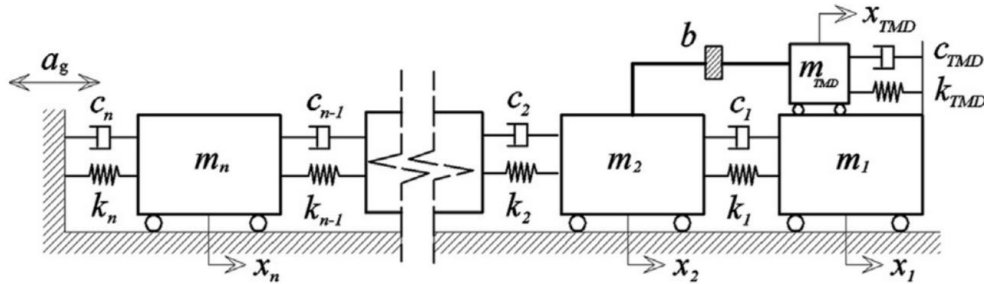


Figure 9 MDOF system incorporating TMDI configuration

Reproduced from (Marian and Giaralis 2014)

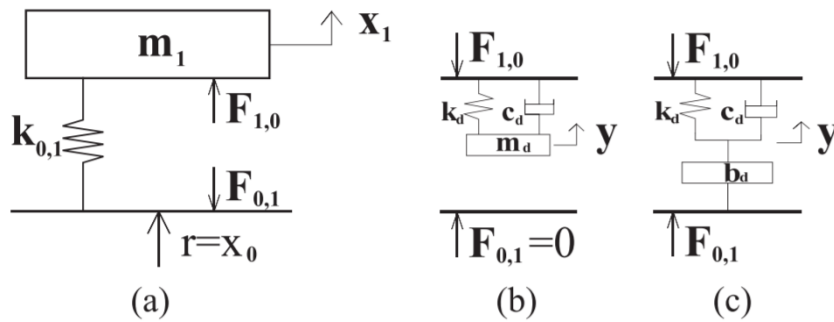


Figure 10 (a) SDOF structural system; (b) a traditional TMD system; (c) TID system

Reproduced from (Lazar, Neild, and Wagg 2014)

Inerter-based base isolation systems (BIS) have also been proposed to mitigate the response of structures exposed to ground motion. Inerter-based BIS systems include the BIS-TID and BIS-TMDI, which have both shown promising performance for structures subjected to ground motion (Ma, Bi, and Hao 2021). For this thesis, ground motion is not the primary applicable loading mechanism, so inerter-based isolation systems focused on mitigating the response from ground motion will not be thoroughly discussed.

2.3 Inerter Nonlinearity

The ideal force of an inerter in a mechanical system is the inertance multiplied by the relative acceleration between the two terminals. This concept for an ideal inerter is relatively straightforward and easy to incorporate into the equation of motion for a system, however, a perfectly ideal inerter is unavailable in practice (Ma, Bi, and Hao 2021). There are nonlinearities that influence the actual performance of the inerter which include backlash or play, dry friction, viscous damping and elastic effects (Ma, Bi, and Hao 2021). The following chapters will discuss the inherent nonlinearities present in the inerter and the influence they have on performance, as well NRIMs with intentional nonlinearities that can be exploited to improve aspects of the vibration mitigation performance.

2.3.1 Inherent Inerter Nonlinearities

Nonlinearities such as backlash or play, dry friction, complex damping forces, and elastic effect, all of which will be described below, impact inerter performance and cause deviation from ideal behavior. These nonlinearities can be modeled using complex nonlinear functions but are typically not considered in the equation of motion for a mechanical system.

Backlash, which is also referred to as play, is caused by gaps or spaces between mating components of the system that result in a loss of motion (Ma, Bi, and Hao 2021). This often occurs when gears are involved but can occur in any mechanical system with mated components. Dry Friction is a force that occurs when components of a mechanical system are in contact and slide against one another (Shaw 1986). In practice, ball-screw inerter devices can be lubricated to limit the production of major dry-friction forces (Wagg 2021). The elastic effect is a nonlinearity that occurs due to elastic deformation of the ball-screw under axial loads, which is often assumed to be rigid in simplified models (Ma, Bi, and Hao 2021). Complex damping forces can affect inerters in multiple ways. An inerter will dissipate energy during operation and the energy dissipation is often modeled as a viscous damper which can have nonlinear effects experimentally, but is often modeled as a linear element of the system (Brzeski and Perlikowski 2017). Complex damping forces that are nonlinear include Coulomb and viscous frictions and relate to various mechanical losses that occur in the system (Ma, Bi, and Hao 2021). Additionally, an inerter with viscous damping has a viscous material, or fluid surrounding the flywheel (Javidialesaadi and Wierschem 2019b), but the research conducted for this thesis will not be utilizing fluid inerters or other mechanisms that themselves provide true viscous damping to the flywheel.

Numerous studies have been performed to determine the effect of inerter nonlinearities in inerter-based vibration isolation systems, specifically in automobile and vehicle suspensions. Sun et al. (2016) investigated the influence of nonlinearities on the performance of ball-screw inerter used in vehicle suspension systems. They found that the vibration isolation performance was slightly influenced by the inerter nonlinearities when comparing the performances of the NRIM with the ideal linear inerter (Sun et al. 2016). Similarly, Wang and Su (2008) studied the effects of nonlinearities, including backlash, elastic effect, and friction in automotive suspensions. They found that there is a small reduction in suspension performance due to inerter nonlinearities, but suspension systems incorporating the inerter are still preferred over traditional suspension systems (Fu-Cheng Wang and Wei-Jiun Su 2008).

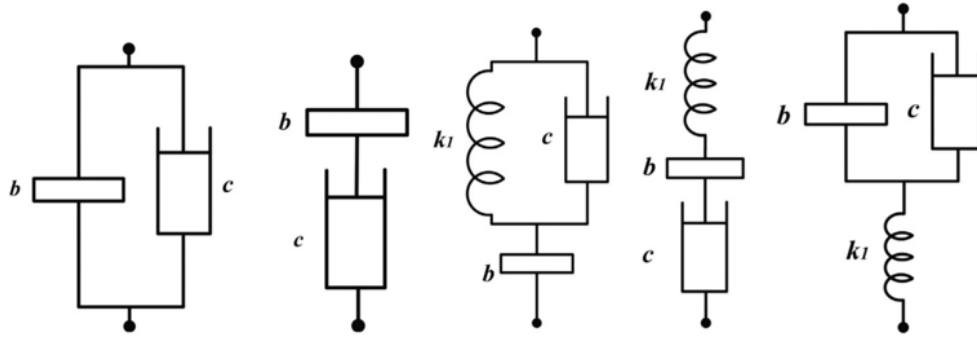


Figure 11 Proposed inerter-based isolation system configurations

Reproduced from (Hu et al. 2015)

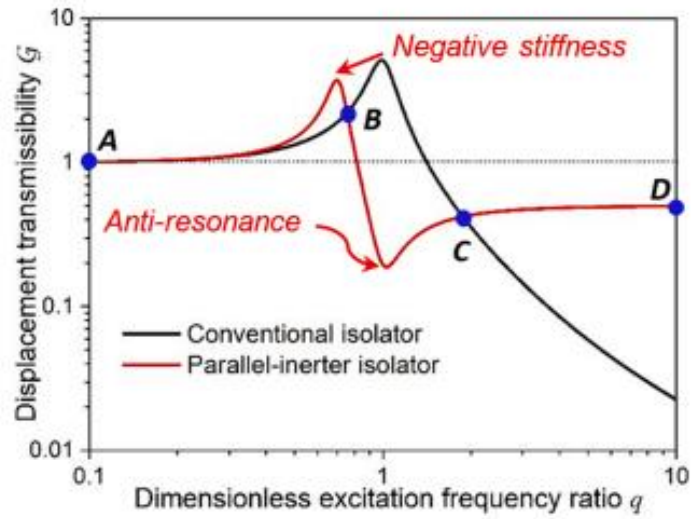


Figure 12 Comparison of displacement transmissibility of conventional and parallel-connected isolator systems

Reproduced from (Ma, Bi, and Hao 2021)

Researchers have also considered the effects of inerter nonlinearities in TID and TMDI systems. Gonzalez-Beluga et al. (2017) performed numerical and experimental studies with a TID to determine the effect of dry friction on performance. Backlash was not considered because a commercially available inerter was used and the ball-screw device was pretensioned to largely eliminate backlash. Gonzalez-Beluga et al. found that the nonlinearities in a commercially available inerter do affect the behavior, however, the effect is not dramatic. For a simple nonlinear model considering dry friction as a nonlinear parameter of the inerter, the inerter at high-amplitude loading can capture the behavior of an ideal inerter, but at low-amplitudes deviated from the ideal case(Gonzalez-Buelga et al. 2017). The deviations led the researchers to retune components of the TID which then allowed the model to capture the behavior of that of an ideal inerter despite including dry friction(Gonzalez-Buelga et al. 2017). This could present an issue if the structure were tuned for low amplitudes and then experienced high amplitudes later in its service life (Ma, Bi, and Hao 2021). Brzeski and Perlikowski (2017) investigated the effects of viscous damping, dry friction, and play in a TMDI. Like the previous study, they found that the effects of viscous damping and dry friction on system dynamics are qualitatively comparable and found that using a simplified model with just a viscous damper considered can yield satisfactory precision(Brzeski and Perlikowski 2017). Additionally, they found that the influence of play and backlash is not significant in this case, but it is acknowledged that the gap may have more influence in smaller scale systems (Brzeski and Perlikowski 2017).

Inherent inerter nonlinearities can impact vibration mitigation performance and can cause deviation from ideal behavior, but the effect of these nonlinearities is dependent on the system configuration and loading. It has been found that nonlinearities become less significant in large scale systems, especially when used with other linear elements, like springs and dampers (Wagg 2021). Similarly, the effect of inherent inerter nonlinearities can change based on the loads applied to the system. It has been found that at higher amplitudes, nonlinearities impact performance less than at lower amplitudes.

2.3.2 Intentional Inerter Nonlinearities

Researchers have begun to design NRIMs with intentional nonlinearities to exploit the benefits of nonlinearity. The CID discussed in chapter 2.2.1, the nonlinear energy sink inerter (NESI) and the geometrically nonlinear inerter are examples of inerters that were intentionally designed to be nonlinear. The intentionally nonlinear configurations allowed researchers to investigate if nonlinear performance is more effective than the ideal linear inerter.

A NESI can have many different layouts and types of nonlinear springs while reducing the need for a secondary mass (Wagg 2021). For example, Javidialesaadi and Wierschem (2019a) proposed a nonlinear energy sink-tuned mass damper inerter (NESI-TMDI) where the inerter was located between the primary mass and a fixed point. They found that the NESI-TMDI could decrease the RMS response by 20- 25% compared to the NES(Javidialesaadi and Wierschem 2019a). Increasing the inertance of the inerter can significantly increase the performance of the NESI compared to the NES without adding physical mass to the system. The NESI has potential to provide better structure control performance than the NES, despite having less physical mass (Javidialesaadi and Wierschem 2019a). Zhang et al. (2019) used a cubic nonlinear spring in a TID (NESI-TID) to reduce the large mass required for traditional NES. The NESI-TID has superior vibration suppression performance when compared to the traditional NES, while eliminating the need for a large secondary mass (Z. Zhang et al. 2019). Similar results were found when Zhang et al. (2019) used a nonlinear spring in a TMDI (NESI-TMDI). By comparing the amplitude frequency response and energy dissipation of the NESI-TMDI with a conventional NES, it was determined that the NESI-TMDI is more effective at suppressing vibrations(Y.-W. Zhang et al. 2019).

Adding an inerter to nonlinear energy sink configurations eliminates the need for a large secondary mass and shows great potential in vibration suppression performance.

Different inerter configurations can result in geometric nonlinearities and has also been studied by researchers. Yang et. al (2020) investigated a geometrically nonlinear inertance mechanism as shown in Figure 13. The schematic shows a pair of slanted ideal inerters, with inertance b , fixed at points A and B and hinged together at point O (Yang, Jiang, and Neild 2020).

The effective vertical force of the inerters is derived using the geometry of the system and an equation is given for this total effective vertical force of the inerters to point O (Yang, Jiang, and Neild 2020). The vertical force of the geometrically nonlinear inerter is dependent on the displacement, velocity and acceleration of the terminal O, which moves with loading (Yang, Jiang, and Neild 2020). This is a major difference from the force of an ideal linear inerter which is only dependent on the relative acceleration between the terminals. Based on the equation, the effective inertance of the device is dependent on the geometry of the system. For example, when x far exceeds l , or visually the inerters are oriented mostly vertically, the geometrically nonlinear inerters will provide an inertance equal to 2 times the individual inertance to the system (Yang, Jiang, and Neild 2020). Conversely, if the displacement x is very small, the effective inertance will be very small. Yang et al. found that compared to the linear inerter isolators, the isolators using geometrically nonlinear inerters had a reduction of the peak dynamic response and bending of the frequency response curve toward lower frequencies, reduction in peak transmissibility and bending of the transmissibility curve, and lower transmissibility at higher frequencies, thus showing that the geometrically nonlinear inerters have attractive vibration isolation performance benefits (Yang, Jiang, and Neild 2020).

2.4 Existing Studies & Real Applications of Inerter

The application of the inerter in the field of vibration isolation has grown immensely and has been proposed and studied in a variety of different industries and applications including car suspension systems, inerter-based vibration isolation systems as discussed in previous chapters, train suspension systems, and motorcycle steering compensators (Lazar, Neild, and Wagg 2014). The inerter, originally known as the J-damper, was initially developed for high performance suspensions in Formula One cars. The inerter made its debut in Formula One when it was raced at the Spanish Grand Prix in 2005 by McLaren Racing (Smith 2020). Incorporating the inerter in high performance motorsport vehicles resulted in improved mechanical grip, which is the ability for the suspension to keep the tire in contact with the road over a range of frequencies (Smith 2020). Since 2008, Penske Racing Shocks has commercially developed and supplied the Penske Formula One ball-screw inerter to Formula One teams for improved mechanical grip (Smith 2020).

The success of the inerter in Formula One has encouraged researchers to expand the application of inerter-based control systems for civil structures. As described in chapter 2.3, numerous studies have been performed utilizing inerters in vibration isolation systems, but there is a very limited number of applications of the inerter used in actual vibration control systems. Ma, Bi and Hao (2021) compiled a list of the experimental tests utilizing inerter-based vibration control systems in civil engineering and found that experimental studies using inerter-based vibration control are limited compared to analytical studies, and many of the experimental tests done are small-scale, with very few being large or full-scale tests. Additionally, there are only three known actual civil engineering applications of inerter-based vibration control systems, all of which are inerter-based energy dissipators, and include the NTT East Sendai Aobadori Building in Sendai Japan, the Zhangjiajie Grand Canyon Glass Bridge in Zhangjiajie China, and the Hongrui Dongting Bridge in Yueyang China (Ma, Bi, and Hao 2021). While inerter-based

vibration control systems have proven to be attractive analytically and experimentally in small scale tests, the field is still evolving and needs experimental studies and real applications of inerter-based vibration control in full scale civil engineering applications. Additionally, the complexity of this subject is increased when nonlinear aspects and configurations of the inerter are considered.

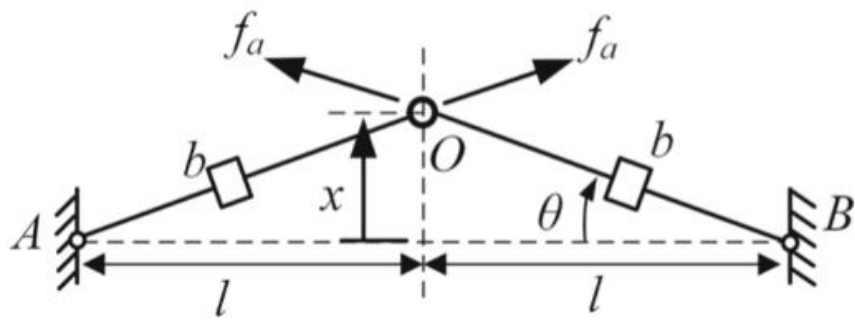


Figure 13 Schematic of Geometrically Nonlinear Inerter

Reproduced from (Yang, Jiang, and Neild 2020).

Chapter 3 Marine Application

Transmitted noise and vibration from equipment and machinery is an ongoing and serious priority onboard marine vessels as noise and vibrations interfere with system operations and can compromise the functionality of the vessel. The use of isolation mounts for vibration mitigation is a common technique, but with vibration mitigation requirements continuing to increase, this project aims to develop a compact and lightweight isolation system utilizing rotational inertial mechanisms, like the inerter, to mitigate vibrations.

Isolation mounts that are commonly used onboard vessels are shown in Figure 14 and include Mare Island Navy Mounts, rubber cylinder isolators, and enclosed spring isolators. Isolation systems introduce a low stiffness layer between a vibration source and a system which aims to reduce the transmission of vibrations. Due to the low stiffness of the isolator, high static and dynamic displacements are common in isolation systems. If the loading frequency aligns with the frequency of the isolation system (resonance), or if large amplitude loading is applied to the system, large isolator displacements will occur. If the displacement demands become too large for the isolator to accommodate, or the stroke limitations are exceeded, the isolator can bottom out. An isolator that bottoms out resembles an impact load on the system and the isolated machinery. This can impose additional loads on the system and cause damage to machinery which is counterintuitive to the original purpose of the isolator.

A rotational inertial mechanism, or inerter, can provide a large inertial mass even though the physical mass is quite small, shift system natural frequencies, and modify the dynamics of the system without compromising the systems stiffness, a known problem with conventional isolators. The use of inerters in isolation systems for machinery and marine applications has not been extensively studied. Current studies lack analysis of linear rotational inertial mechanisms subjected to marine specific broadband loading, limited stroke available for isolation systems, the amount of effective mass possible given size limitations, and all nonlinear rotational inertial mechanism considerations. Both linear and nonlinear rotational inertial mechanisms can enhance marine isolation systems by replacing or by their use in combination with the conventional isolator mounts.

Broadband shaped white noise is the primary loading that is analytically and experimentally considered. The Military Standard for Structureborne Vibratory Acceleration Measurements and Acceptance Criteria of Shipboard Equipment, or MIL-STD-740-2(SH) was used to determine appropriate loading levels. Figure 15 shows the vibratory acceleration acceptance criteria for structureborne equipment.

Before mechanical equipment is installed onboard, the equipment is tested in a laboratory setting where this figure is used to ensure that the maximum acceleration of the equipment falls under acceptable levels. Figure 15 gives the maximum acceptable acceleration in decibels that certain types of equipment are permitted to have while onboard naval vessels. Type 1 equipment includes compressors and internal combustion engines. Type 2 includes pumps, valves, and life support equipment. Type 3 includes any equipment not covered by Type 1, 2, and 4, and Type 4 equipment includes vaneaxial fans. Figure 15 presents the acceptable acceleration criteria using a 1/3-octave band frequency range. MATLAB was used to filter a random white noise signal through a 1/3-octave band filter. Using the maximum acceptable acceleration value at each listed frequency, the filtered signal was scaled and thus, an appropriate white noise signal was generated in MATLAB for each type of equipment. The generated signal ensures that the isolated mass is subjected to the maximum allowable acceleration that is permissible onboard for a particular type of equipment and then will be further isolated using rotational inertial mechanisms.

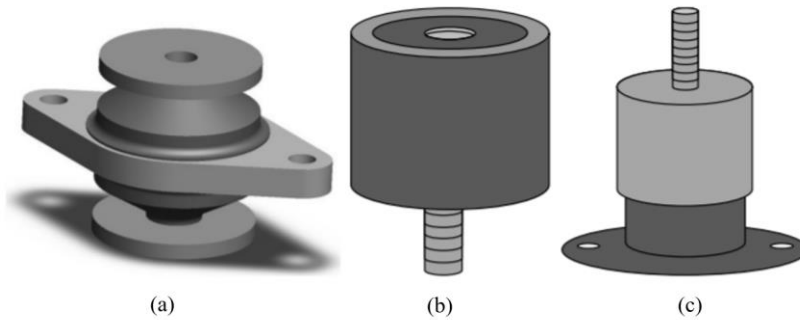


Figure 14 (a) Mare Island Navy Mount; (b) rubber cylinder isolator; (c) enclosed spring isolators

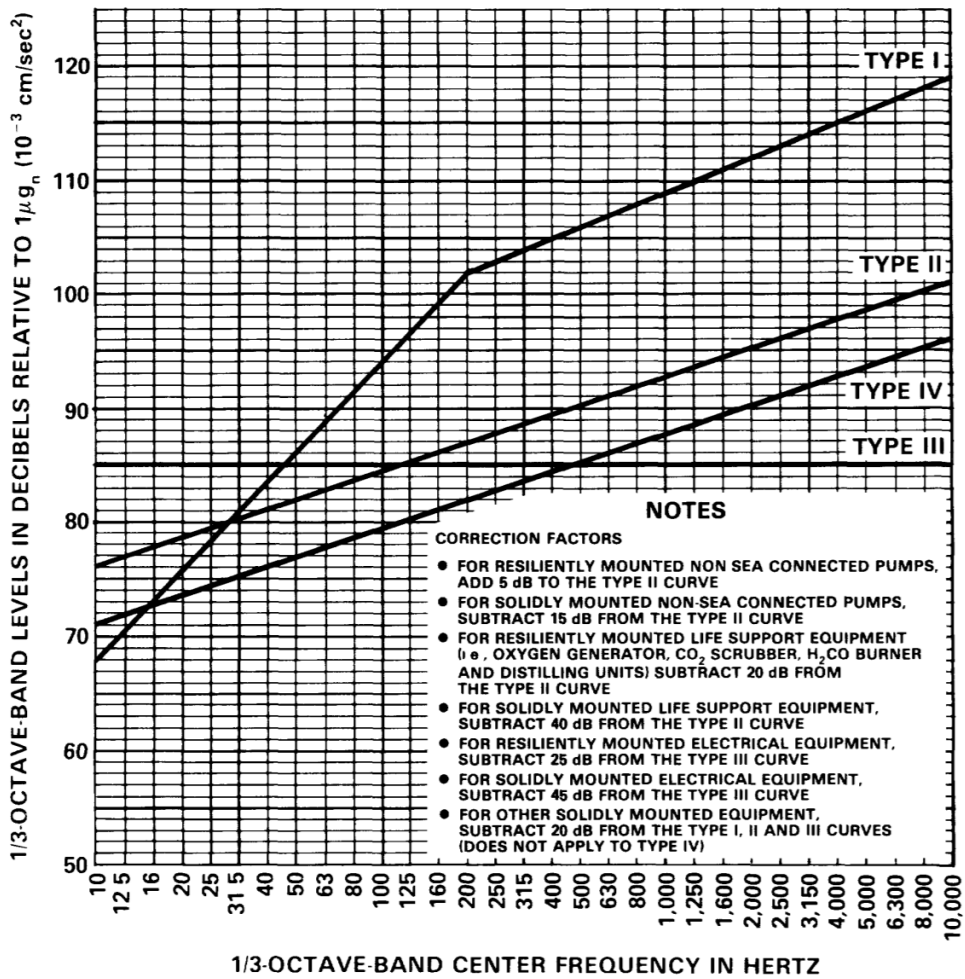


Figure 15 Vibratory Acceleration Acceptance Criteria for Structureborne Equipment

Reproduced from MIL-STD- 740-2(SH)

This will allow for consistent and accurate measuring of isolation progress. Figure 16 shows the white noise signal that will provide Type 1 equipment the maximum acceleration permitted for marine applications.

As shown in Figure 16, the filtered noise does not truly begin, or level out until around 250 Hz. The natural frequency of the systems being investigated in this thesis are between 3-5 Hz due to system parameters. Due to the MATLAB filtering process, the filtered noise demonstrated in Figure 16 will not accurately represent marine acceptable acceleration levels for systems with natural frequency less than 250 Hz. The initial stages of the experimental design, which will be explained in more depth in the next chapter, focused on systems with natural frequencies between 3-5 Hz. Therefore, the time vector used was scaled to be 100 times slower, which shifted the frequency values. This scaling allowed the filtered noise to begin, or level out, around 2 Hz. The scaled marine filtered white noise can be seen in Figure 17. This ensures an appropriate marine white noise is applied to any system with a natural frequency less than 250 Hz. As the experimental phase progresses and the natural frequency of the system being investigated increases, the original filtered white noise signal, seen in Figure 16, may be used.

Isolation of marine equipment subjected to white noise loading is very different when compared to isolation of a building from vibration forces, such as an earthquake. The load application and main goals of isolation differs between machine and building isolation. Isolation of machines aims to protect the surface, or ground from the load, where the load is typically generated from the equipment being isolated. In contrast, building isolation aims to protect the building from earthquake forces that are generated from the ground. The difference in the loads and the way they are applied in the two scenarios can be visually seen in Figure 18, where the ground acceleration generated from an earthquake is represented by $m\ddot{x}_g$ and the force generated from the machine is represented by F .

The main goals of machine isolation are to reduce displacements and transmitted forces. Reducing transmitted forces is important because when forces are transferred back into the system additional loads are induced which impacts system operations. The main goals of building isolation are to reduce the relative displacement of the building which would prevent structural failure and reduce the absolute acceleration of the building which relates to serviceability issues, such as controlling motion that occupants would feel. The stark contrast between the goals and load applications of machine and building isolation demonstrates the complexity of isolation systems and the need for research on specific isolation scenarios.

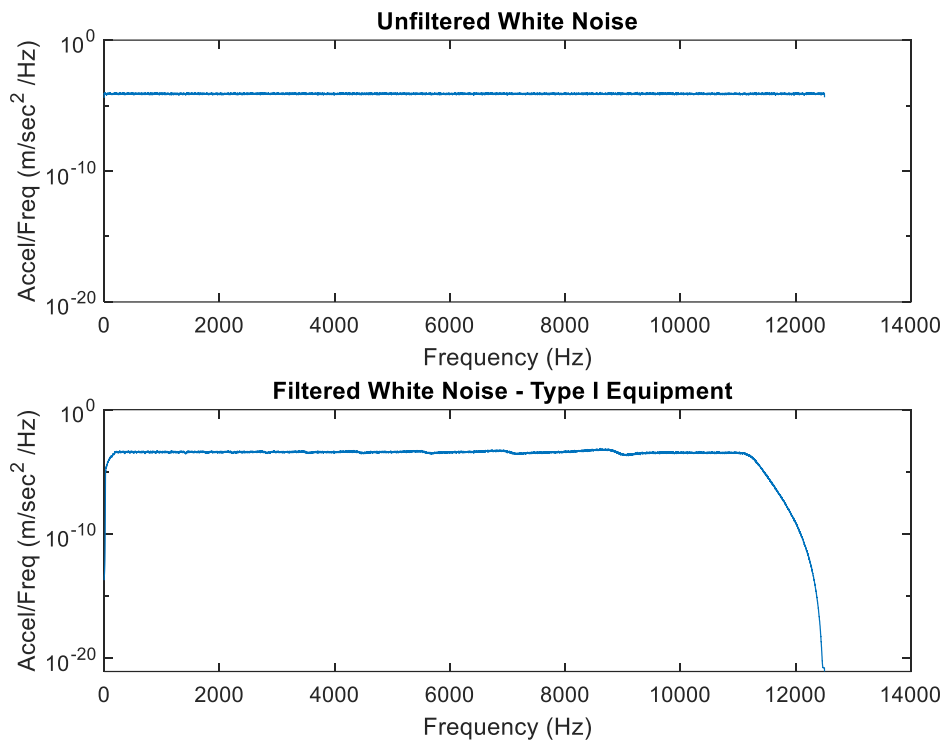


Figure 16 (top) Unfiltered white noise signal (b) Filtered and scaled white noise signal for Type I equipment

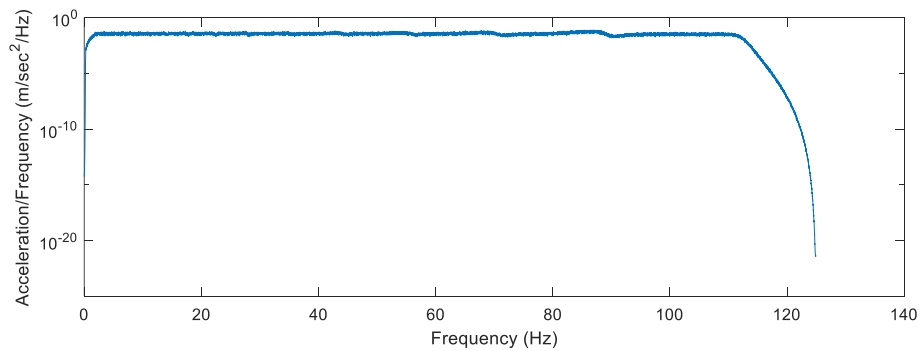


Figure 17 Time-scaled filtered white noise signal for Type I equipment and systems with natural frequency less than 250 Hz

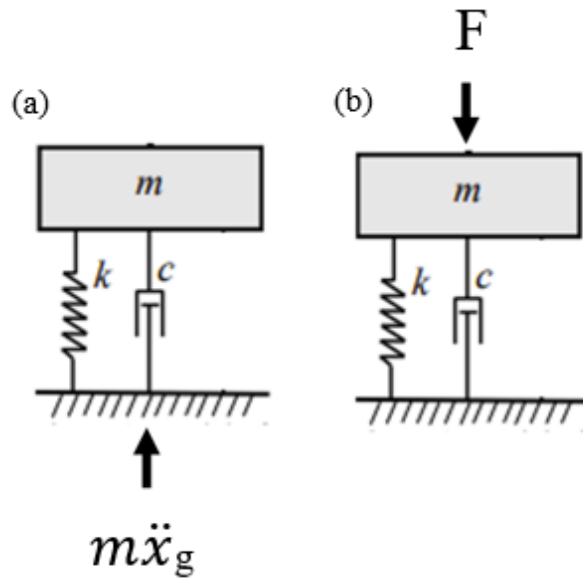


Figure 18(a) Isolated building subjected to ground motion force (b) Isolated machinery subjected to machine generated force

Chapter 4 Numerical Simulations

This chapter will investigate the advantages and disadvantages of incorporating inerters, and NRIMs in isolation systems. MATLAB was used to numerically simulate linear and nonlinear RIMs in isolation systems to better understand performance differences between the systems and to see if advantages to nonlinear systems are numerically realizable. To represent isolation systems in a marine application, a SDOF system with a force on its mass (referred to as mass loaded) was used to analyze displacements and transmitted forces for the modeled linear and nonlinear systems. To expand the potential applications of this work as well as match loading conditions that appear in shake table tests, a SDOF system loaded with a base acceleration (referred to as base loaded) will also be considered. This base loaded system was used to analyze relative displacement and absolute acceleration for the modeled linear and nonlinear systems. The linear simulations analyzed include a SDOF system without an inverter, a SDOF system with a linear inverter, and a SDOF system with reduced stiffness in the isolation layer. The nonlinear simulations are referred to as the acceleration gap inverter, the displacement gap inverter, and the geometrically nonlinear inverter. The MATLAB codes written for all the numerical simulations discussed in this chapter can be found in Appendix A.

4.1 Linear Simulations

MATLAB was used to numerically simulate linear isolation systems. A base loaded SDOF system, shown in Figure 6, was used to compare isolation system performance with an inverter, or RIM, without an inverter, and a system with low stiffness. As previously mentioned, to reduce the natural frequency of a system, the stiffness would need to be reduced, or a rotational inertial mechanism will need to be incorporated to add mass effects to the system. Stiffness reductions can lead to excessive static and dynamic displacements, so it was numerically simulated to compare to the conventional RIM and system without a RIM. The shifted marine filtered white noise discussed in Chapter 3 is identified as an acceleration and was used to analyze isolation system behavior with appropriate loading. The marine filtered white noise, or acceleration, was applied to the base of the isolation system to investigate isolation systems with and without a conventional RIM.

The mass of the system was 17.92 kg which was selected based on a 18"x18" aluminum plate. A damping ratio of 20% was used because of the focus on equipment vibration mitigation, so a higher damping ratio is expected and appropriate. The stiffness for the linear system with the RIM and without the RIM was chosen so that the natural frequency of the system without the RIM is 5.3 Hz. The low stiffness value was determined by calculating the required stiffness to have the natural frequency equal to the natural frequency of the system with the conventional RIM. The low stiffness value is about half of the stiffness for the other two systems. The inertance of the system was equal to 100% of the mass at 17.92 kg. Using the equation of motion for the system, state space matrices were derived and input into MATLAB. The `lsim` command, load, simulated time, and initial conditions were used to obtain the displacement, velocity and acceleration time responses of the dynamic system model defined from the state space matrices. The relative displacement time histories for isolation with an inverter, without an inverter, and a system with low stiffness can be seen in Figure 19 below. The MATLAB command `tfestimate` was used to estimate the relative displacement and absolute acceleration transfer functions from the response. The absolute acceleration was analyzed because it represents transmitted forces for base loaded cases. The relative displacement and absolute acceleration estimated transfer function results are displayed in Figure 20.

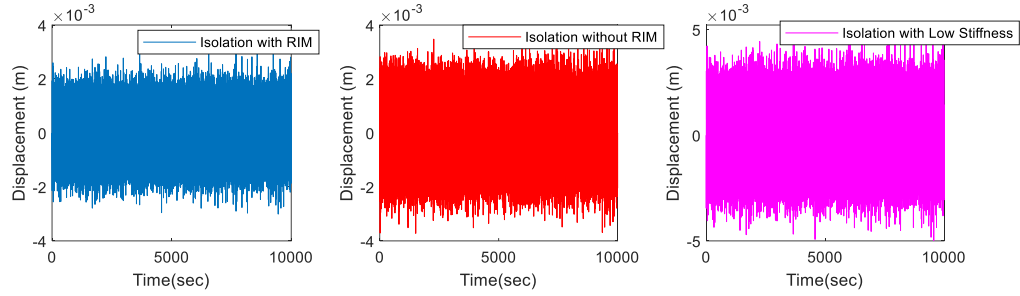


Figure 19 Base loaded relative displacement time histories for isolation with an inerter, without an inerter, and system with low stiffness

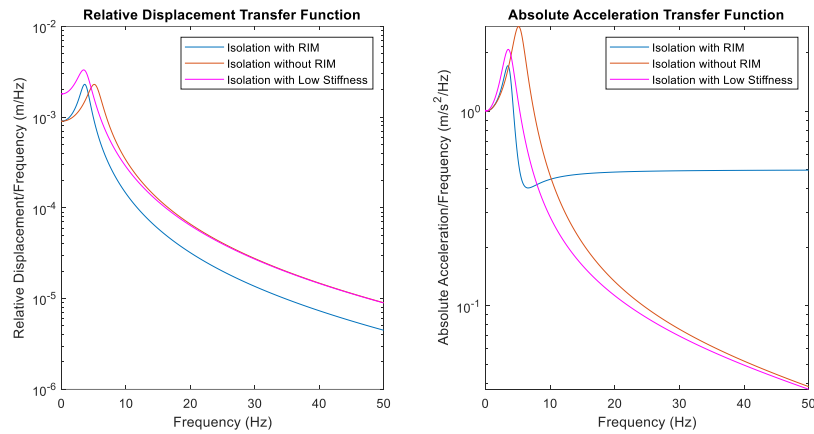


Figure 20 Relative displacement and absolute acceleration estimated transfer function results for linear base loaded systems

Table 1 Base loaded linear isolation system results

| | Isolation with RIM | Isolation without RIM | Isolation with Low Stiffness |
|---|--------------------|-----------------------|------------------------------|
| Natural Frequency | 3.75 Hz | 5.30 Hz | 3.75 Hz |
| Peak Relative Displacement Transfer Function | 0.0023 | 0.0023 | 0.0033 |
| Peak Absolute Acceleration Transfer Function | 1.72 | 2.73 | 2.08 |
| H₂ Norm Relative Displacement | 0.0013 | 0.0016 | 0.0022 |
| H₂ Norm Absolute Acceleration | 2.17 | 1.91 | 1.42 |

Referring to the relative displacement transfer function results in Figure 20, it can be visually seen that the peak relative displacement transfer function with the RIM occurs at a lower frequency than without the RIM. This is the natural frequency of the system. Effectively, the system with the inerter has shifted the natural frequency which can also be seen numerically in

Table 1. At lower frequencies, the system without the RIM is more effective at reducing displacements, but the isolation system with the RIM is more effective at reducing displacements at higher frequencies. This is visually shown in Figure 20, but also numerically demonstrated by calculating the H_2 norm, shown in

Table 1. The H_2 norm is the area under the squared curve from 0 to infinity. For all numerical simulations, the H_2 norm was calculated for a bounded frequency range of 1 – 100 Hz. For the conventional RIM case, the H_2 norm for the isolator force transfer function would be infinite if frequency bounds were not used. This also ensured accurate comparison to the nonlinear numerical simulations in later chapters. There is a 23.1% increase in the relative displacement transfer function H_2 norm for the system without the inerter, therefore the inerter significantly reduces displacements of the mass. When looking at the absolute acceleration transfer function results, the isolation system with the RIM has much higher transmitted forces at higher frequencies, shown visually in Figure 20 and numerically using the isolator force transfer function H_2 norm in

Table 1. This is because the inerter is engaged 100% of the time, so the inertance is always contributing to the total transmitted force. Additionally, the inerter transfers force proportional to the acceleration which increasingly grows relative to the displacement. The absolute acceleration transfer function for the system without the inerter has an H_2 norm that is 11.9% lower than the system with the inerter. As previously discussed, the transmitted forces that occur due to the incorporation of an inerter in an isolation system can be problematic in marine applications.

A low stiffness system was also modeled in Figure 20 to show the effects of reducing stiffness to shift natural frequency, rather than adding an inerter to an isolation system. Referring to the relative displacement transfer function plot in Figure 20, the natural frequency for the system with the RIM and the low stiffness system are the same, but the low stiffness system has a large static displacement at a frequency of 0 Hz compared to the other linear systems. Additionally, at higher frequencies, the displacement transfer function converges to the without RIM system. These observations are supported by the results in

Table 1 which shows a significantly higher peak relative displacement transfer function value and relative displacement H_2 norm for the low stiffness system compared to the other linear systems. Referring to the absolute acceleration transfer function plot in Figure 20, there is a higher peak for the low stiffness system compared to the conventional RIM system, but transmitted forces are equal to the linear system without a RIM. The transmitted forces are significantly lower than the system with a conventional RIM. The figure observations are supported by the results in

Table 1 where the peak absolute acceleration transfer function value for low stiffness is between the conventional RIM and system without a RIM, but significantly lower transmitted forces when referring to the absolute acceleration transfer function H_2 norm.

The mass loaded SDOF system shown in Figure 6 was used to compare isolation system performance with an inerter and without an inerter. The excitation was produced from the marine filtered white noise

by multiplying the filtered white noise signal by the mass of the system, i.e. ($F = ma$). This force was then applied to the mass of the system. The same system parameters were used as the previous system. Using the equation of motion for the mass loaded systems, the same MATLAB procedure for the base loaded case was used to simulate the dynamic response of the mass loaded system. The displacement time histories for isolation with an inerter and without an inerter can be seen in Figure 21 below. The isolator force, F_T , was calculated using the response and system parameters. The isolator force for the system with the RIM was calculated using the following equation: $F_T = ku + c\dot{u} + b\ddot{u}$ while the isolator force for the system without the RIM was calculated using: $F_T = ku + c\dot{u}$. The isolator force was analyzed for mass loaded cases because it represents transmitted forces. The MATLAB command `tfestimate` was used to estimate the absolute displacement and isolator force transfer functions from the response. The absolute displacement and transmitted force for the mass loaded linear systems can be visually seen in Figure 22 with relevant numerical values in Table 2.

Similar conclusions can be drawn for the mass loaded linear isolation systems as the base loaded linear isolation systems. The system without the RIM had a 18.8% higher relative displacement H_2 norm and a 19.4% lower absolute acceleration H_2 norm. The behavior and trends are the same for the mass loaded and base loaded linear cases. In fact, the difference between the mass loaded absolute displacement and the base loaded relative displacement is scaled by a factor of 17.92, or the mass of the system. Additionally, the mass loaded isolator force and the base loaded absolute acceleration are equal. Therefore, the absolute displacement transfer function for the mass loaded case and the relative displacement transfer function for the base loaded case are analogous to each other, while the isolator force transfer function for the mass loaded case and the absolute acceleration transfer function for the base loaded case are analogous to each other. Typically, machine isolation would be experimentally and numerically simulated using the mass loaded case, but due to the availability of experimental equipment, base loaded cases will also be analyzed for this thesis. This loading scenario is also of interest when considering isolation of equipment from loads originating from the structure it is connected to.

Isolation with a RIM significantly and effectively reduces mass displacements at higher frequencies, but the transmitted forces that occur at higher frequencies with the RIM are substantially higher than isolation systems without a RIM. The increased transmitted forces are apparent from the high frequency tail that is seen in the isolator force (mass loaded) and absolute acceleration (base loaded) transfer function estimates. Additionally, it was shown in the base loaded linear simulation how reducing the stiffness of a system led to larger static and dynamic displacements, therefore, the linear inerter is a superior option for reducing the natural frequency of the system and reducing displacements, despite high transmitted forces. Nonlinear isolation systems will be explored to determine if the displacements at low frequencies can be improved and the transmitted forces at high frequencies reduced, while keeping effective displacement performance at high frequencies. Additionally, the base loaded absolute acceleration transfer function and mass loaded isolator force transfer function behavior is comparable, as well as the base loaded relative displacement transfer function to the mass loaded absolute displacement transfer function.

4.2 Nonlinear Simulations

As previously discussed in the literature review, intentionally designed inerter nonlinearities have potential to outperform ideal linear inerters. Numerical simulations were performed to evaluate the effectiveness various nonlinear rotational inertial mechanisms have of reducing absolute displacement and transmitted force in the case of the mass loaded system and reducing relative displacement and absolute acceleration in the case of the base loaded system. An acceleration gap inerter and displacement gap inerter were numerically simulated in a SDOF system and are described thoroughly below.

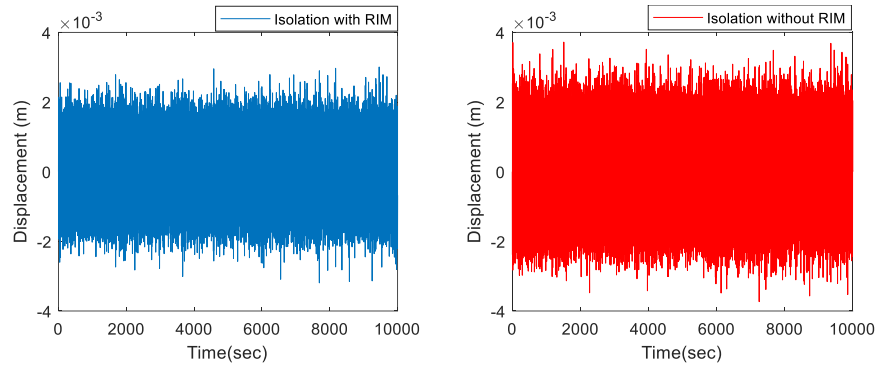


Figure 21 Mass loaded displacement time histories for isolation with an inerter and without an inerter

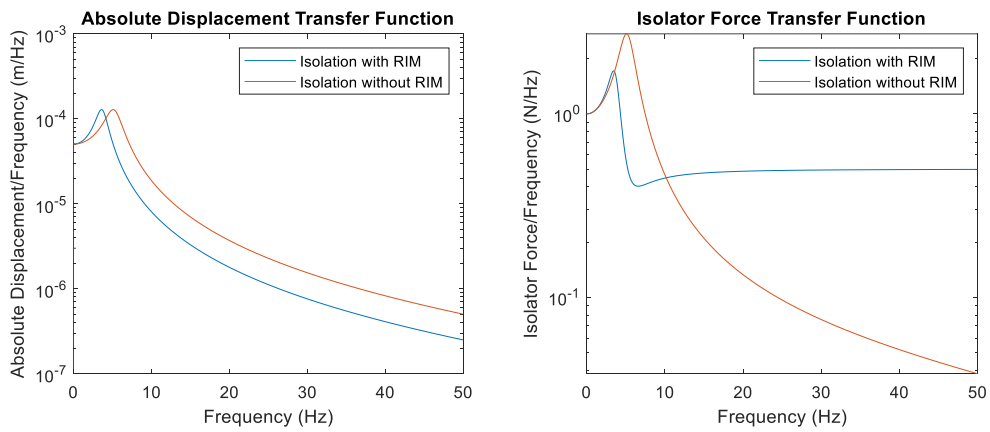


Figure 22 Absolute displacement and isolator force estimated transfer function results for linear mass loaded system

Table 2 Mass loaded linear isolation system results

| | Isolation with RIM | Isolation without RIM |
|--|---------------------------|------------------------------|
| Natural Frequency | 3.74 Hz | 5.30 Hz |
| Peak Absolute Displacement TF | 0.00013 | 0.00013 |
| Peak Isolator Force TF | 1.72 | 2.73 |
| H₂ Norm Absolute Displacement TF | 0.000074 | 0.000089 |
| H₂ Norm Isolator Force TF | 2.17 | 1.91 |

4.2.1 Acceleration Gap

The acceleration gap model was developed with intentions of exploiting the benefits of the inerter, but avoiding the negatives, like the high force transmission effects that occur at high frequencies. It is intended that incorporating an acceleration gap in the inerter will allow the inerter to engage and disengage based on system response. At low levels of system response, where displacement reduction performance lacks, the inerter is intended to disengage. At high levels of system response where it has superior performance in reducing displacements, the inerter is intended to be engaged. If the inerter disengages for periods throughout the response, the transmitted forces should subsequently be reduced. The acceleration gap is considered for instructional purposes because this gap is difficult to realize for passive isolation systems due to inerter engagement and disengagement being dependent on the acceleration of the system. A dead zone model, seen in Figure 23, was used in the inerter's force, F_B versus absolute acceleration, \ddot{u} relationship to create an acceleration gap model.

For the acceleration gap model, the inerter becomes engaged, or disengaged based on the value of the absolute acceleration compared to the gap size, g . Figure 23 visually shows that the force of the inerter is equal to 0, or the inerter is disengaged if the absolute acceleration of the system is less than the gap, or greater than the negative of the gap (i.e. $-g < \ddot{u} < g$). The inerter is reengaged if the absolute acceleration is greater than the gap or less than the negative of the gap (i.e. when $\ddot{u} > g$, or $\ddot{u} < -g$). When the inerter is reengaged, the inertance b , increases in value and thus increases the force of the inerter. The force of the inerter, F_B is equal to the inertance multiplied by the acceleration gap value subtracted from the absolute acceleration (i.e. $F_B = b(\ddot{u} - g)$).

The acceleration gap inerter was simulated in MATLAB using the same SDOF system and parameters used in the previous linear simulations (Figure 6). The MATLAB `lsim` command, time, load, and initial conditions were used to numerically simulate the acceleration gap, but for this system the response had to be evaluated at each time step individually. State space matrices were created for a system with the inerter engaged and for a separate system with the inerter disengaged. A for loop was created to evaluate the absolute acceleration and compare the value to the acceleration gap at each time step. Based on the changing absolute acceleration value, MATLAB would evaluate the next time step using the system with the inerter engaged or disengaged. A complete displacement, velocity, and acceleration time response of the dynamic system was evaluated. Using the time histories, the isolator force was calculated. When the inerter was engaged and the absolute acceleration was greater than the gap value, the transmitted force was calculated using the following equation: $F_T = ku + c\dot{u} + b(\ddot{u} - g)$, but when the inerter was engaged and the absolute acceleration was less than the negative of the gap value, the transmitted force was calculated using: $F_T = ku + c\dot{u} + b(\ddot{u} + g)$. Essentially, the subtraction or addition of the gap value, g was determined by the value and sign of the absolute acceleration. This can be seen visually in Figure 23.

When the inerter was disengaged, the transmitted force was calculated using the following equation: $F_T = ku + c\dot{u}$. Figure 24 shows the base loaded acceleration gap inerter results for various gap sizes. Plots a through d show the relative displacement of the mass for various gap sizes and plots e through h show the absolute acceleration. Relevant numerical information from Figure 24 is displayed in Table 3.

Plots a-d in Figure 24 show the relative displacement transfer function for various gap sizes converging to the linear without RIM case. Plots e-h in Figure 24 show the transmitted forces for various gap sizes and it can be seen visually that transmitted forces are decreased for every gap size when compared to the conventional RIM case.

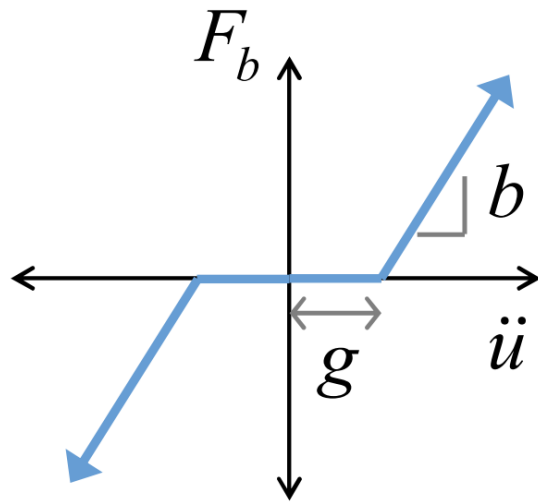


Figure 23 Inerter force vs. acceleration relationship with a dead zone gap implemented

This is expected because as inerter engagement is decreased, the inerter will not be contributing to the transmitted forces. The gap size directly relates to the engagement and disengagement of the inerter. As the gap increases, engagement decreases because more acceleration is needed to engage the inerter. Visually, it is apparent in Figure 24 that engaging and disengaging the inerter can result in lowered transmitted forces at higher frequencies. The H_2 norm using a 1-100 Hz bounded frequency range was calculated for the relative displacement and absolute acceleration for all gap scenarios. In addition to wanting an accurate comparison to the bounded H_2 norm calculations done in the previous chapter, bounding the H_2 norm calculations for the nonlinear gap cases ensured nonphysical numerical results at 0 Hz and after 100 Hz were not skewing results. There were nonphysical numerical issues at 0 Hz and after 100 Hz due to the ratio nature of the transfer function and the noise used which caused the results to not accurately depict the true behavior of the system. For example, at a frequency of 0 Hz, there were large peaks due to the transfer function ratio, but large displacements and forces are not possible at 0 Hz, so bounding the frequency for which the H_2 norm was calculated ensured that the results were not being skewed. The large peaks at 0 frequency can be seen in Figure 24. The bounded H_2 norm for the absolute acceleration transfer function was used to determine the amount transmitted forces were decreased compared to the conventional RIM case. With 93.1% engagement, gap = 0.1 m/s² had a 6% decrease in transmitted forces compared to the conventional RIM case. As engagement decreases, there were larger decreases in transmitted forces. For example, gap = 0.7 m/s² with 61.9% engagement, had a 21.7% decrease in transmitted forces. Additionally, gap = 1.3 m/s² had a 26.3% decrease in transmitted forces. Gap = 2.6 m/s² had a 24.4% decrease in transmitted forces from the conventional RIM. Gap = 2.6 m/s² had significant transmitted force reduction compared to the conventional RIM, which was expected due to the amount the RIM was engaged, but there was an increase in transmitted forces compared to gap = 1.3 m/s², despite there being 20% less engagement. This is interesting because there is significantly less inerter engagement for gap = 2.6 m/s² compared to gap = 1.3 m/s². This increase in transmitted forces, despite less gap size could be due to the significant increases in the peak absolute acceleration transfer function seen in Figure 24 and Table 3. The peak absolute acceleration transfer function for gap = 2.6 m/s² is larger than the linear without RIM case. Although the peak is increased as engagement decreases for all gap sizes, the peaks for gap = 0.1 m/s², gap = 0.7 m/s², and gap = 1.3 m/s² are all less than the linear without RIM case.

The engagement and disengagement of the inerter will impact the ability to reduce relative displacements. In Figure 24, the relative displacement transfer functions for gap = 0.1 m/s² and 0.7 m/s² resemble the conventional RIM case. As inerter engagement decreases, the relative displacement transfer function converges to the linear without RIM case, therefore, displacements will not be reduced effectively if the gap is too high. In addition to the displacement transfer function peak converging to the linear without RIM case, the H_2 norm for the relative displacement transfer function also converges to the without RIM case as inerter engagement is decreased. Table 3 shows the peak of the relative displacement transfer function increased, exceeding both the conventional RIM and linear case without the RIM as inerter engagement is decreased. For all gap sizes, the frequency at which the relative displacement transfer function peak occurs, or the natural frequency of the gap system, was increased compared to the linear case with the RIM. The gap system natural frequencies were all less than the linear case without the RIM.

For the ground loaded acceleration gap, there are significant reductions in the transmitted forces which is concluded from looking at the H_2 norm results for absolute acceleration, but the H_2 norm for the relative displacement transfer function is not reduced compared to the linear with RIM system. The acceleration gap may not be effective at reducing displacements while simultaneously reducing transmitted forces in ground loaded scenarios. A mass loaded case was also numerically simulated for the acceleration gap inerter. The system parameters and gap sizes were the same as the previous simulation. The load was

applied to the mass in the same way the load was applied for the mass loaded linear simulation in chapter 4.1. Figure 25 and Table 4 shows the mass loaded acceleration gap inerter results for various gap sizes. Plots a-d show the absolute displacement transfer function of the mass and plots e-h show the isolator force transfer function for various gap sizes.

Similar trends are observed for the mass loaded acceleration gap results in Figure 25 as was seen in the base loaded acceleration gap results in Figure 24. Like the base loaded case, plots a-d of Figure 25 show the absolute displacement transfer function for the acceleration gap inerter converging to the linear without RIM system, thus showing that the acceleration gap inerter is less effective at reducing displacements than the system with the conventional RIM as the gap increases. The divergence between the system results for the RIM case and for the gap inerter case becomes more drastic as the gap is increased, or with less inerter engagement. In plots e-h of Figure 25, transmitted forces were still decreased, but the isolator force transfer function peaks were also increased.

Numerical results from Figure 25 are presented in Table 4. Despite the same gap sizes being used for the base and mass loaded acceleration gap cases, the acceleration gap inerter had higher engagement levels than the base loaded case. Transmitted forces were assessed using the bounded H_2 norm for the isolator force transfer function. Although decreases in transmitted forces were seen for the mass loaded case, the transmitted force decreases are less drastic than the base loaded case. Even though the same gap sizes were used for the base loaded and mass loaded case, the mass loaded case had smaller decreases in transmitted forces for every gap size. Gap = 0.1 m/s^2 had a 1.38% decrease in transmitted forces, gap = 0.7 m/s^2 had a 4.61% decrease in transmitted forces, gap = 1.3 m/s^2 had a 11.1% decrease in transmitted forces, and gap = 2.6 m/s^2 had a 17.51% decrease in transmitted forces. These are all smaller decreases in transmitted forces compared to the base loaded case. Like the base loaded case, the peak for the isolator force transfer function increased as engagement decreased. As seen in Table 4, for all gap sizes, the isolator force transfer function peak was greater than the linear with RIM case, but less than the linear without RIM case.

As previously mentioned, Figure 25 shows the acceleration gap inerter converging to the without inerter case as inerter engagement decreases more drastically than was seen in the base loaded case. The mass loaded acceleration gap did not have as drastic of peak absolute displacement transfer function increases as was observed with the base loaded cases. The peak absolute displacement transfer function for gap = 0.7 m/s^2 was equal to the linear with RIM case with a value of 0.00013. Gap = 0.7 m/s^2 , 1.3 m/s^2 , and 2.6 m/s^2 , had a slight increase in the peak compared to the conventional RIM case of 0.00014. The frequency where the peak displacement transfer function occurred, or the natural frequency of the system, increased compared to the conventional RIM case but was less than the linear without RIM case. The mass loaded case had better displacement performance, but far greater natural frequency increases than the base loaded case. Additionally, the H_2 norm for the absolute displacement transfer function was greater than the conventional RIM case for all gap sizes, like the base loaded case.

Transmitted forces and displacements are of large concern in marine isolation. Mass loaded and base loaded systems with an acceleration gap of various sizes were analyzed to determine the effectiveness the concept could have with reducing displacements and transmitted forces. Similar trends were seen for both cases for the various gap sizes, but the base loaded acceleration gap seemed to be more effective with reducing transmitted forces and less effective with displacement reduction. The mass loaded case seemed to be more effective with reducing displacements but didn't reduce transmitted forces as much as was observed with the base loaded case. The acceleration gap has proven to be difficult to physically realize. Other nonlinear models have been numerically simulated to investigate if displacements and transmitted forces can be reduced with a realizable NRIM.

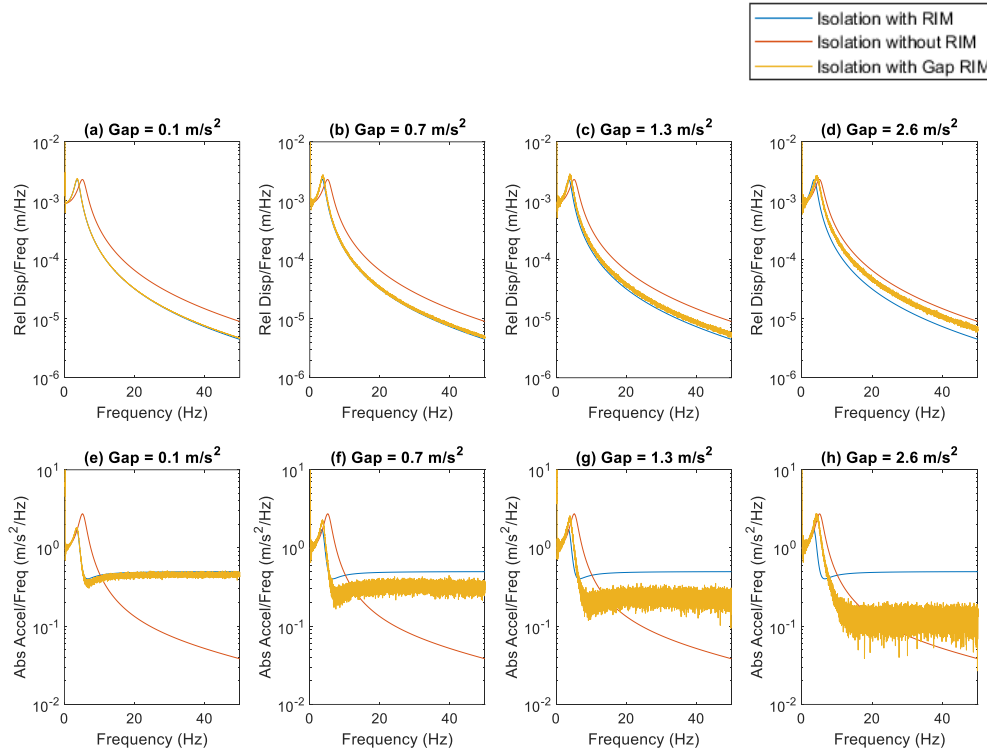


Figure 24 Base loaded acceleration gap inerter results for various gap sizes. a-d: Relative Displacement, e-h: Absolute Acceleration

Table 3 Base loaded acceleration gap results compared to linear simulations

| | Gap = 0.1 m/s ² | Gap = 0.7 m/s ² | Gap = 1.3 m/s ² | Gap = 2.6 m/s ² | With RIM | Without RIM |
|--|-------------------------------|-------------------------------|-------------------------------|-------------------------------|----------|----------------|
| Percent of time RIM is Engaged | 93.1% | 61.9% | 43.1% | 20.1% | 100% | 0% |
| Peak Relative Displacement TF | 0.0024 | 0.0028 | 0.0029 | 0.0027 | 0.0023 | 0.0023 |
| Frequency of Peak Relative Displacement TF | 3.62 Hz | 3.75 Hz | 3.87 Hz | 4.44 Hz | 3.60 Hz | 5.08 Hz |
| Peak Absolute Acceleration TF | 1.83 | 2.29 | 2.60 | 2.76 | 1.72 | 2.73 |
| H₂ Norm Relative Displacement TF (with bounds) | 0.0014 | 0.0015 | 0.0015 | 0.0015 | 0.0013 | 0.0016 |
| H₂ Norm Absolute Acceleration TF (with bounds) | 2.04 | 1.70 | 1.60 | 1.64 | 2.17 | 1.91 |

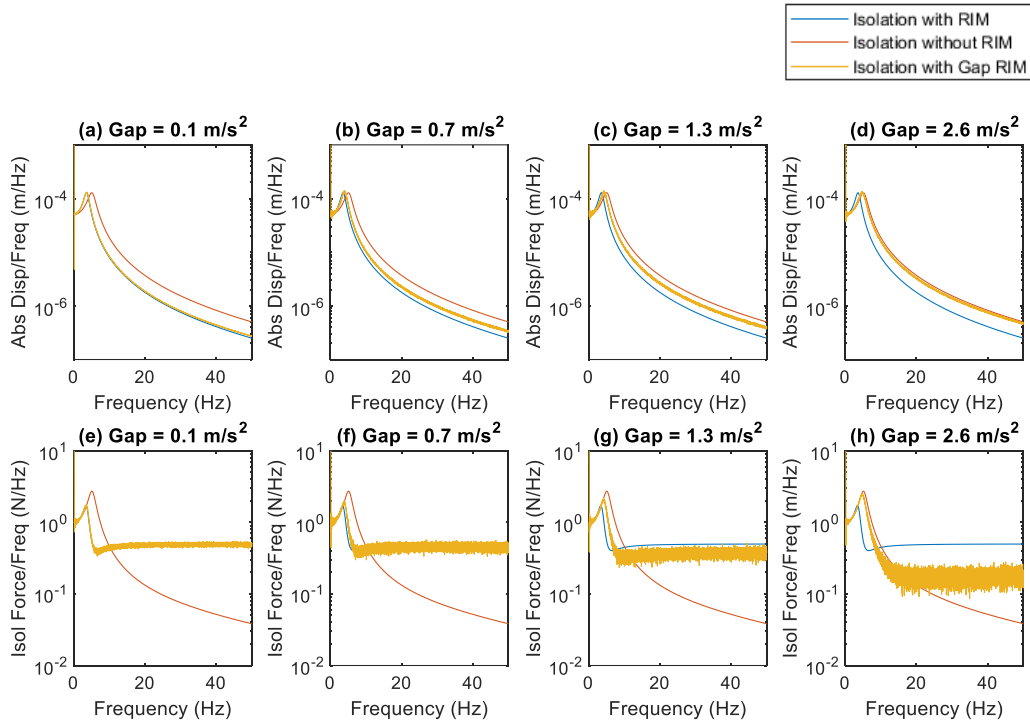


Figure 25 Mass loaded acceleration gap inerter results for various gap sizes. a-d: Absolute Displacement TF, e-h: Isolator Force TF

Table 4 Mass loaded acceleration gap results compared to linear simulations

| | Gap = 0.1 m/s ² | Gap = 0.7 m/s ² | Gap = 1.3 m/s ² | Gap = 2.6 m/s ² | With RIM | Without RIM |
|---|-------------------------------|-------------------------------|-------------------------------|-------------------------------|----------|----------------|
| Percent of time RIM is Engaged | 93.2% | 64.4% | 47.9% | 23.6.% | 100% | 0% |
| Peak Absolute Displacement TF | 0.00013 | 0.00014 | 0.00014 | 0.00014 | 0.00013 | 0.00013 |
| Frequency of Peak Absolute Displacement TF | 3.60 Hz | 3.92 Hz | 4.35 Hz | 4.75 Hz | 3.60 Hz | 5.08 Hz |
| Peak Isolator Force TF | 1.75 | 2.00 | 2.14 | 2.53 | 1.72 | 2.73 |
| H₂ Norm Absolute Displacement | 0.000076 | 0.000081 | 0.000083 | 0.000087 | 0.000074 | 0.000089 |
| H₂ Norm Isolator Force TF | 2.14 | 2.07 | 1.93 | 1.79 | 2.17 | 1.91 |

4.2.2 Displacement Gap

The displacement gap model has a very similar concept to the acceleration gap, but the inerter is engaged or disengaged based on the displacement of the mass, instead of the acceleration of the mass. A displacement gap was investigated because it was more likely to physically realize a passive device that was dependent on displacement of the mass. To be consistent with previous chapters, the same SDOF system and parameters used in chapter 4.1, shown in Figure 6 were used. The only change to the system was a different gap model, dependent on displacements, was applied to engage and disengage the inerter.

Scheibe and Smith (2009) developed displacement gap models for various system configurations, but there wasn't an exact model for the system shown simulated in this chapter (Figure 6). The model developed by Scheibe and Smith is shown in Figure 26, where the system has two oscillating masses, a spring and inerter with ideal play, or a gap. The system has three different states where the inerter is engaged and extended, engaged and compressed, or completely disengaged. Smith and Scheibe (2009) detail the solutions and dynamical equations for each state relating to this specific system.

The same displacement idea proposed by Scheibe and Smith (2009) was used for the system simulated in previous chapters (Figure 6) where there is a fixed based, spring, damper and gap inerter incorporated. The model and equation of motions were modified for the SDOF system in Figure 6, but the displacement gap model is very similar to the acceleration gap. The inerter will engage or disengage based on the gap size. This is a two-sided gap model where if the mass displaces more than the gap, vertically, the inerter will engage and extend. If the mass displaces less than the negative value of the gap, the inerter will engage and compress. Contrarily, if the mass displaces less than the gap, but more than the negative of the gap, the inerter will not engage (i.e. $-g < u < g$).

The same approach used for the acceleration gap in MATLAB was used to simulate the time histories response for the base and mass loaded displacement gap cases. Gap sizes of 0.0001 m, 0.0003 m, and 0.0005 m were used such that similar inerter engagement levels, observed for the acceleration gap, would be investigated for the displacement gap. The gap size required for significant engagement was much less than what was expected for marine loading applications. Due to the displacement model being dependent on the displacement of the mass, a more powerful loading would be required to have a gap size that is more physically realistic. However, the purpose of this chapter is to show and discuss the displacement gap concept. Figure 27 shows the base loaded displacement gap results with plots a-d showing the relative displacement of the mass and plots e-h showing the absolute acceleration. A time step convergence study was performed to ensure a time step of 1/250 was appropriate. Time steps of 1/200, 1/250 and 1/300 were investigated. Figure 28 shows the time step of 1/250 is appropriate due to the responses converging.

Error! Reference source not found. shows the numerical results for the base loaded displacement gap inerter compared to the systems with and without a RIM.

Figure 27 shows similar trends to the acceleration gap cases where figures a-d show the gap inerter converging to the linear without RIM case as inerter engagement is decreased, or gap size is increased. In figures e-h, the transmitted forces visually appear to be decreased at higher frequencies compared to the linear cases, but the peak of the absolute acceleration transfer function increases as the gap size is increased. Like the base loaded acceleration gap, transmitted forces were analyzed using the absolute acceleration H_2 norm. Additionally, transmitted forces were reduced for every displacement gap case compared to the conventional RIM. For example, gap = 0.0001 m with 89.4% engagement had a 9.22% decrease in transmitted forces compared to the conventional RIM case. Gap = 0.0003 m with 72.3% engagement had a 20.3% decrease in transmitted forces. Gap = 0.0005 m with 56.9% engagement had a 27.7% reduction in transmitted forces compared to the conventional RIM and gap = 0.001 m had a 33.2% reduction. The transmitted force reductions for gap = 0.0005 m and 0.001 m are significantly greater than

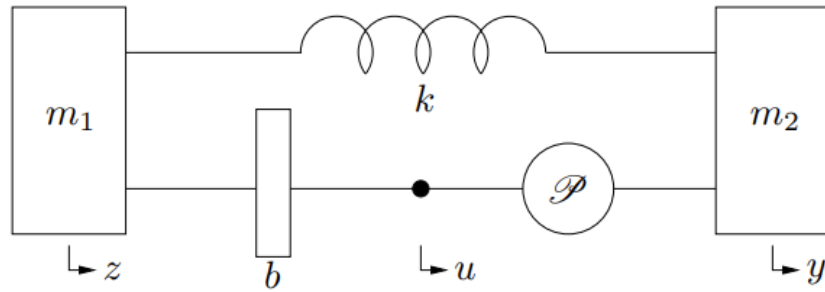


Figure 26 Harmonic oscillator network with a series in parallel with an inerter and ideal play

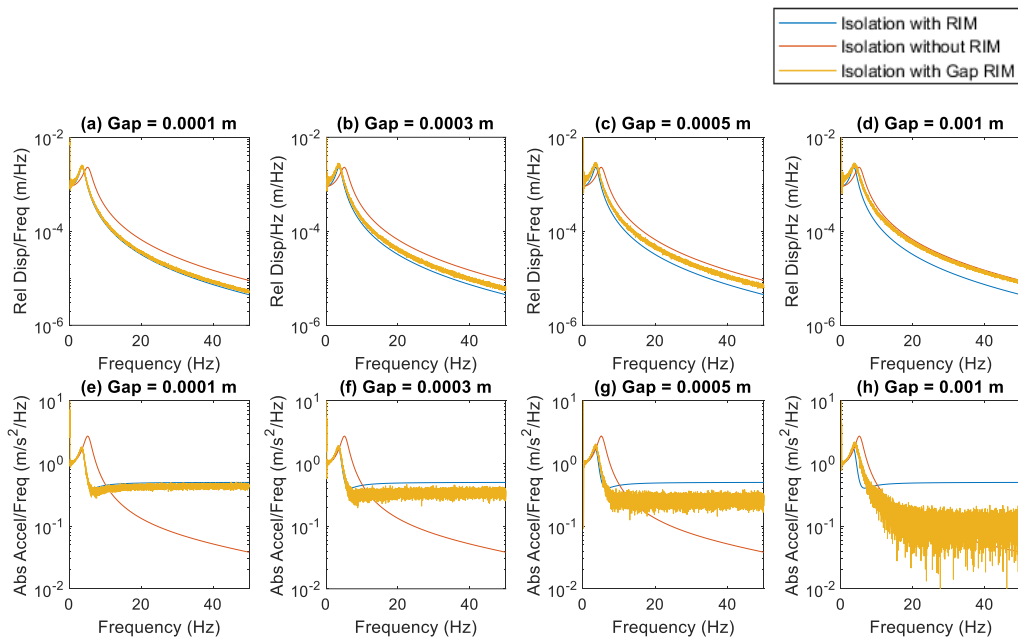


Figure 27 Base loaded displacement gap inerter results for various gap sizes. a-d: Relative Displacement, e-h: Absolute Acceleration

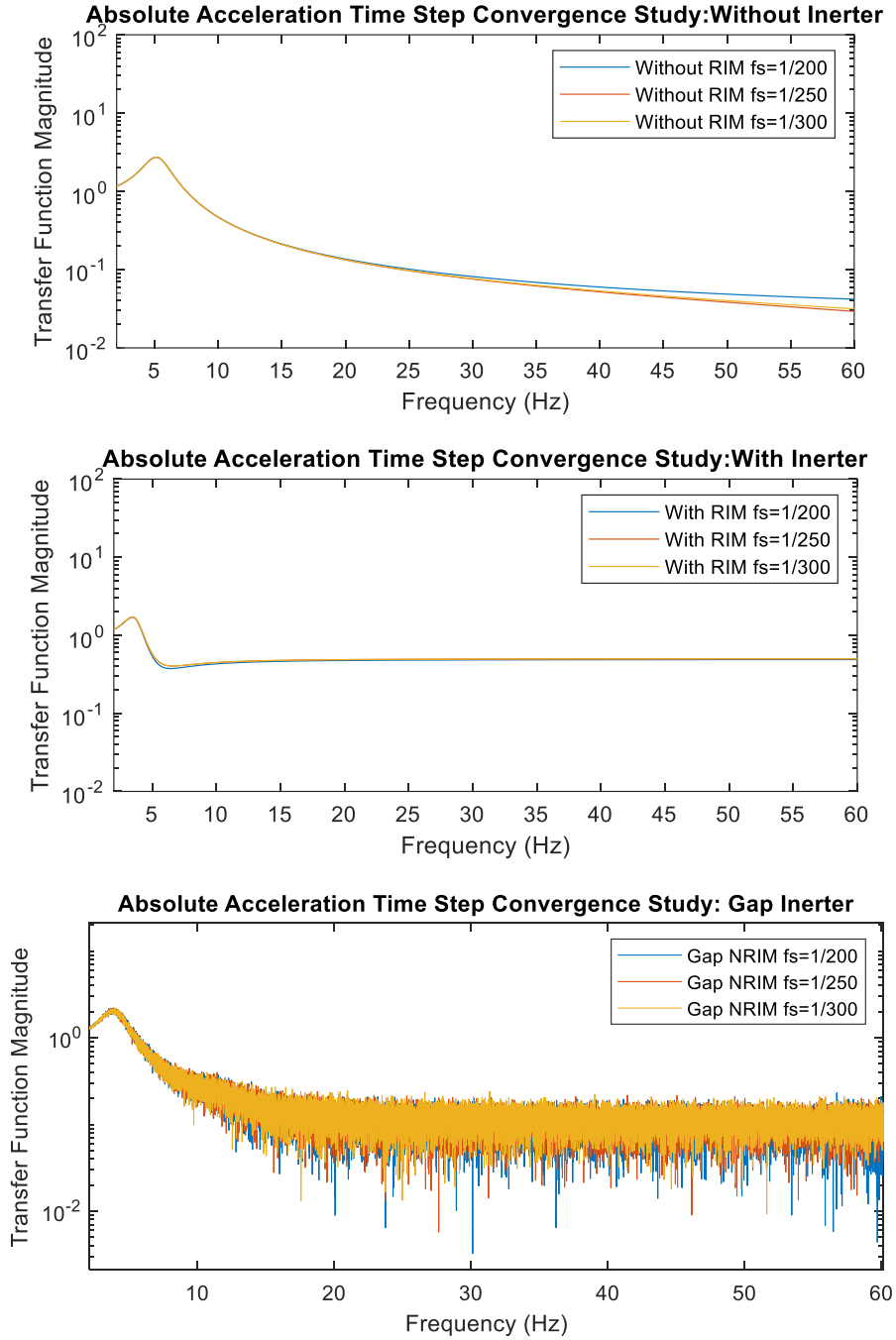


Figure 28 Time step convergence study for without RIM, with RIM, and Displacement gap NRIM at time steps 1/200, 1/250 and 1/300

Table 5 Base loaded displacement gap results compared to linear simulations

| | Gap = 0.0001 m | Gap = 0.0003 m | Gap = 0.0005 m | Gap = 0.001 m | With RIM | Without RIM |
|---|---------------------------|---------------------------|---------------------------|--------------------------|-----------------|------------------------|
| Percent of time RIM is Engaged | 89.4% | 72.3% | 56.9% | 25.7% | 100% | 0% |
| Peak Relative Displacement TF | 0.0026 | 0.0028 | 0.0029 | 0.0029 | 0.0023 | 0.0023 |
| Frequency of Peak Relative Displacement TF | 3.51 Hz | 3.36 Hz | 3.54 Hz | 3.65 Hz | 3.60 Hz | 5.08 Hz |
| Peak Absolute Acceleration TF | 1.83 | 1.93 | 2.05 | 2.20 | 1.72 | 2.73 |
| H₂ Norm Relative Displacement | 0.0014 | 0.0016 | 0.0017 | 0.0017 | 0.0013 | 0.0016 |
| H₂ Norm Absolute Acceleration | 1.97 | 1.73 | 1.57 | 1.45 | 2.16 | 1.91 |

what was observed for the acceleration gap with similar inerter engagement percentages. Also like the base loaded acceleration gaps, the peak absolute acceleration transfer function increases as gap size is increased, but the peaks for all gap sizes remain less than the linear without RIM case.

As previously mentioned, Figure 27 shows the relative displacement transfer function for the various displacement gap sizes. The figure visually shows relative displacement performance decreasing as inerter engagement decreases which is consistent with past simulations. The bounded relative displacement H_2 norm is consistent with Figure 27 in that the H_2 norm converges to the linear without inerter case. The H_2 norms for all gap sizes are less than the linear without inerter case, but greater than the conventional RIM case. For all gap sizes, the peak of the relative displacement transfer function was greater than the conventional RIM and without RIM cases. Gap = 0.001 m had a peak that was slightly larger than the conventional RIM case. Similarly, gap = 0.001 m was the only gap size that had no shift in the natural frequency. The natural frequency was increased compared to the conventional RIM case. For gap = 0.0001 m, gap = 0.0003 m, and gap = 0.0005 m, the natural frequency shifted to be less than the conventional RIM case. Gap = 0.0003 m had the most significant shift in natural frequency out of all the gap sizes. The natural frequency shifted .24 Hz from the conventional RIM case which is a 6.67% decrease.

The base loaded displacement gap significantly reduced transmitted forces and shifted the natural frequency of the system but was not as effective at reducing displacements as the conventional RIM case. The natural frequency shifts observed, and the increased displacement amplitudes could be attributed to the noise in the loading due to the transfer function estimates being evaluated. The noise in the simulation was also investigated by performing the simulation at a range of time values. The simulation in Figure 27 was performed for 100 seconds, but Figure 29 compares the base-loaded displacement gap NRIM absolute acceleration for gap= 0.001 m performed for 100 seconds, 200 seconds, 400 seconds, and 800 seconds. The noise in the figure is significantly reduced by increasing the time of the simulation. Like the acceleration gap, the displacement gap was also numerically simulated for the mass loaded case. Figure 30 shows the mass loaded displacement gap inerter results for the same gap sizes that were used in the previous simulation. The absolute displacement transfer function and isolator force transfer functions were analyzed to determine the efficiency of mass loaded displacement gaps. Relevant numerical information from the figures can be found in Table 6.

Many of the same trends seen in the base loaded displacement gap were observed for the mass loaded displacement gap. Like the base loaded case, Figure 30 visually shows the absolute displacement converging to the linear without RIM case as engagement decreases. Additionally, the isolator force transfer functions in Figure 30 show transmitted force reduction at higher frequencies as gap size is increased, but the peak also increases with gap size increases. The transmitted force percentage decreases from the conventional RIM are also very similar to the base acceleration case. For example, gap = 0.0001 m with 89.4% engagement had a 9.22% decrease in transmitted forces compared to the conventional RIM case. Gap = 0.0003 m with 72.3% engagement had a 19.4% decrease in transmitted forces. Gap = 0.0005 m with 56.9% engagement had a 25.8% reduction in transmitted forces compared to the IRIM and gap = 0.001 m had a 28.6% reduction. The peaks of the isolator force transfer function for the mass loaded displacement gaps differed numerically but had similar trends compared to the base loaded case. For example, both cases had transmitted force transfer function peaks less than the linear without RIM case, but greater than the conventional RIM case. Additionally, smaller gap sizes yielded smaller transmitted force peaks.

Like past numerical simulations, the absolute displacement transfer functions in Figure 30 converge to the linear without RIM case as gap size increases, or inerter engagement decreases. Similar displacement

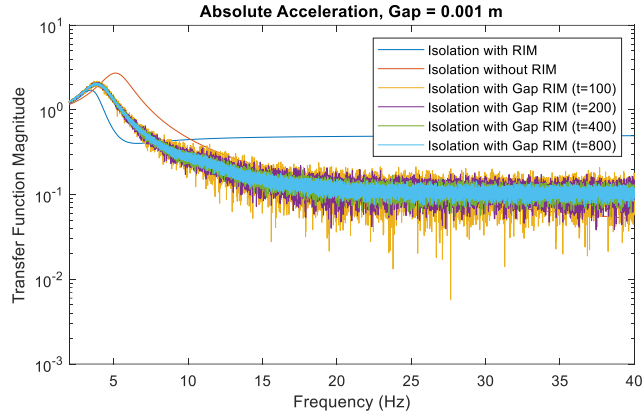


Figure 29 Noise study for base-loaded displacement gap NRIM absolute acceleration at various time spans

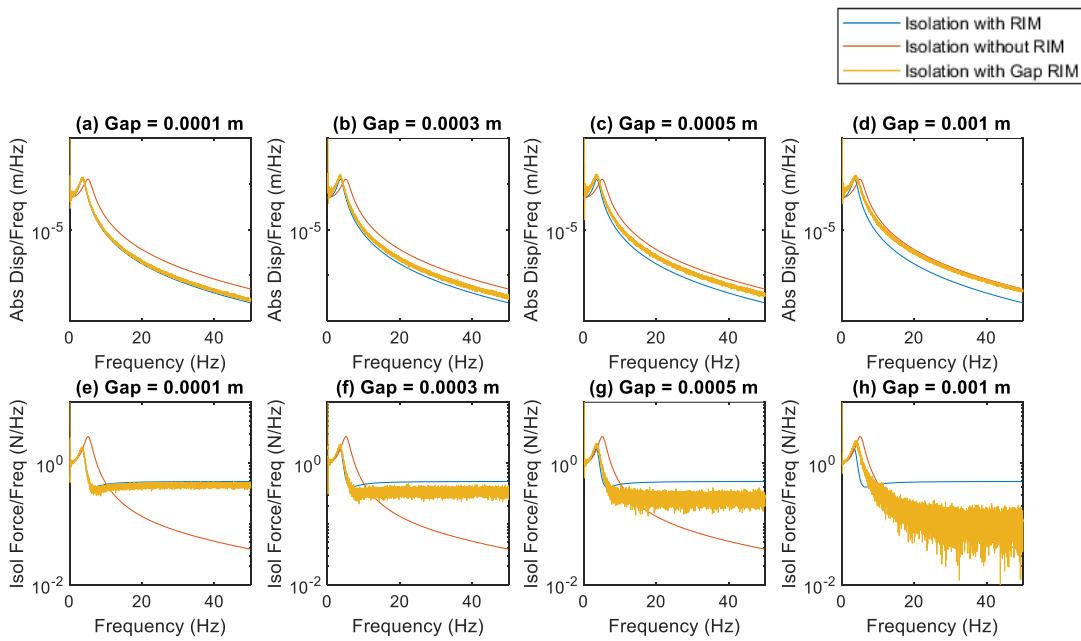


Figure 30 Mass loaded displacement gap inerter results for various gap sizes. a-d: Absolute Displacement transfer function, e-h: Isolator Force transfer function

Table 6 Mass loaded displacement gap results compared to linear simulations

| | Gap = 0.0001 m | Gap = 0.0003 m | Gap = 0.0005 m | Gap = 0.001 m | With RIM | Without RIM |
|--|---------------------------|---------------------------|---------------------------|--------------------------|-----------------|------------------------|
| Percent of time RIM is Engaged | 89.4% | 72.3% | 56.9% | 25.7% | 100% | 0% |
| Peak Absolute Displacement TF | 0.00014 | 0.00017 | 0.00017 | 0.00016 | 0.00013 | 0.00013 |
| Frequency of Peak Absolute Displacement TF | 3.53 Hz | 3.53 Hz | 3.43 Hz | 4.00 Hz | 3.60 Hz | 5.08 Hz |
| Peak Isolator Force TF | 1.83 | 2.05 | 2.11 | 2.33 | 1.72 | 2.73 |
| H₂ Norm Absolute Displacement TF | 0.000080 | 0.000088 | 0.000094 | 0.000096 | 0.000074 | 0.000089 |
| H₂ Norm Isolator Force TF | 1.97 | 1.75 | 1.61 | 1.55 | 2.17 | 1.91 |

trends discussed for the base loaded displacement gap cases were also observed for the mass loaded displacement gaps.

The absolute displacement transfer function H_2 norm was greater than the conventional RIM case for all gap sizes. For gap = 0.0001 m and gap = 0.0003 m, the H_2 norm is less than the linear without RIM case. As the gap increases, the H_2 norm increasingly exceeds the linear. Finally, the same trend for natural frequency shifting discussed for the base loaded case applies for the mass loaded case. The natural frequency was shifted for all gap sizes except gap = 0.001 m. For the mass loaded case, gap = 0.005 m had the largest natural frequency shift of .17 Hz from the conventional RIM case.

Both the base and mass loaded displacement gap inerter has not shown to significantly reduce displacements compared to the conventional RIM case, but there is potential for the gap inerter to reduce or shift the natural frequency of the system and reduce transmitted forces by disengaging the inerter when it is not necessary to be engaged. The displacement gap inerter model can be physically realized which makes it a viable passive RIM. As previously mentioned, the gap sizes used in the numerical simulation were based off the displacements induced by the shifted marine white noise signal. The displacement gap size used in the numerical simulations may not be physically realizable for a marine environment as it is much smaller than what was anticipated for an appropriate gap size. The physical realization and experimental design of the displacement gap will be explained in the following chapter.

4.2.3 Geometrically Nonlinear Inerter

The geometrically nonlinear inerter researched by Yang et. al (2020) was previously introduced in chapter 2.3.2. The equations outlined in Yang et. al (2020) were used to numerically simulate the geometrically nonlinear inerter compared to the conventional RIM and system without RIM subjected to random white noise loading. The loading used for the simulations was a randomly generated white noise loading applied to the mass. The power of the loading was specified such that the max displacement of the system with the conventional RIM was equal to 1.5 cm. This was deemed a reasonable and realistic displacement for the system and thus was used to investigate the geometrically nonlinear inerter. The parameters and methods used to numerically simulate the linear systems are identical to those used in chapter 4.1. The geometrically nonlinear inerter system was also modeled as a SDOF system with a stiffness element, damping element and the geometrically nonlinear inerter. The parameters of the system are identical to former nonlinear simulations, except the length, L , shown in Figure 13 will change. Changing the length, L , will show the effect length has on the GNI and will help determine if the device is physically realizable. The lengths numerically simulated were chosen such that the GNI exhibited nonlinear behavior. Due to the nature of the equations and the nonlinearity of the system, state space matrices and the `lsim` command were not used to numerically simulate the geometrically nonlinear inerter. Instead, the MATLAB command `ode45` was used to evaluate the system. `Ode45` integrates the system of differential equations using a specified set of initial conditions, a time span, and a function with equations that defines the system. Using `ode45`, the displacement and velocity of the system are determined. The acceleration of the system was calculated using the equation of motion and the equation for the total effective vertical force of the inerters to point O, f_b , that was presented by Yang et al. (2020). The equation of motion for the system shown in Figure 6 was given in chapter 2.2. This equation was modified to include the geometrically nonlinear inerter force, rather than the conventional RIM component. The resulting equation of motion for the system with a mass applied load, P was: $m\ddot{x} + c\dot{x} + kx + f_b = P$. The GNI force, f_b is dependent on the inertance (b), length (l), displacement, velocity, and acceleration of the system and was inserted into the EOM. The acceleration, \ddot{x} , was then derived. The resulting acceleration equation for the GNI can be found in Appendix A. The isolator force was then calculated using the stiffness, damping, and geometrically nonlinear inerter force contributions. Using MATLAB, the absolute

displacement transfer function and isolator force transfer functions were estimated to compare the GNI to the linear and nonlinear systems. The visual and numerical comparisons are shown in Figure 31 and Table 7.

Similar trends seen in the gap inerter cases were observed for the geometrically nonlinear inerter case. Figure 31 shows the GNI absolute displacement converging to the linear without RIM case and the reduction in transmitted forces as length, L is increased. It is important to note that the change in numerical values for the linear simulations is due to using the MATLAB generated white noise rather than the marine loading. Utilizing the GNI results in a reduced absolute displacement transfer function peak for all lengths compared to the linear systems, but the H_2 norm absolute displacement transfer function is increased for all GNI lengths compared to the conventional RIM system. The GNI H_2 norm absolute displacement transfer function remains below the linear system without the RIM for all cases. Therefore, the GNI may reduce the peak of the absolute displacement transfer function, but it is not as efficient at reducing displacements as the conventional RIM system. The reduced peak could be due to the inclusion of inertance in the damping coefficient for the system. The natural frequency of the GNI with $L=.001$ m is equal to the linear system with the RIM, but at increased lengths, the natural frequency is also increased. For all lengths considered, the natural frequency of the GNI is less than the natural frequency of the linear system without the RIM; however, the GNI's natural frequency would converge to the linear without RIM system at even longer lengths. The isolator force, or transmitted force was also analyzed for the GNI. It is shown in Figure 31 and Table 7 that as GNI length is increased, the isolator force transfer function H_2 norm is decreased, but the isolator force transfer function peak is increased.

Despite the reduced displacement transfer function peak for the considered GNI lengths, the absolute displacement H_2 norm for the estimated transfer function was not reduced compared to the with or without RIM cases. Additionally, transmitted forces are reduced, but like the numerically simulated gap concepts, the reduction of force is at the expense of increased displacements. As previously mentioned, the lengths were chosen to show the nonlinear effects of the GNI, but the lengths that make the device act in a nonlinear manner, are not physically realizable for marine applications. For example, $L=.001$ m would typically not be realistic or applicable to marine equipment isolation systems. Consequently, the GNI will not be considered further in this thesis.

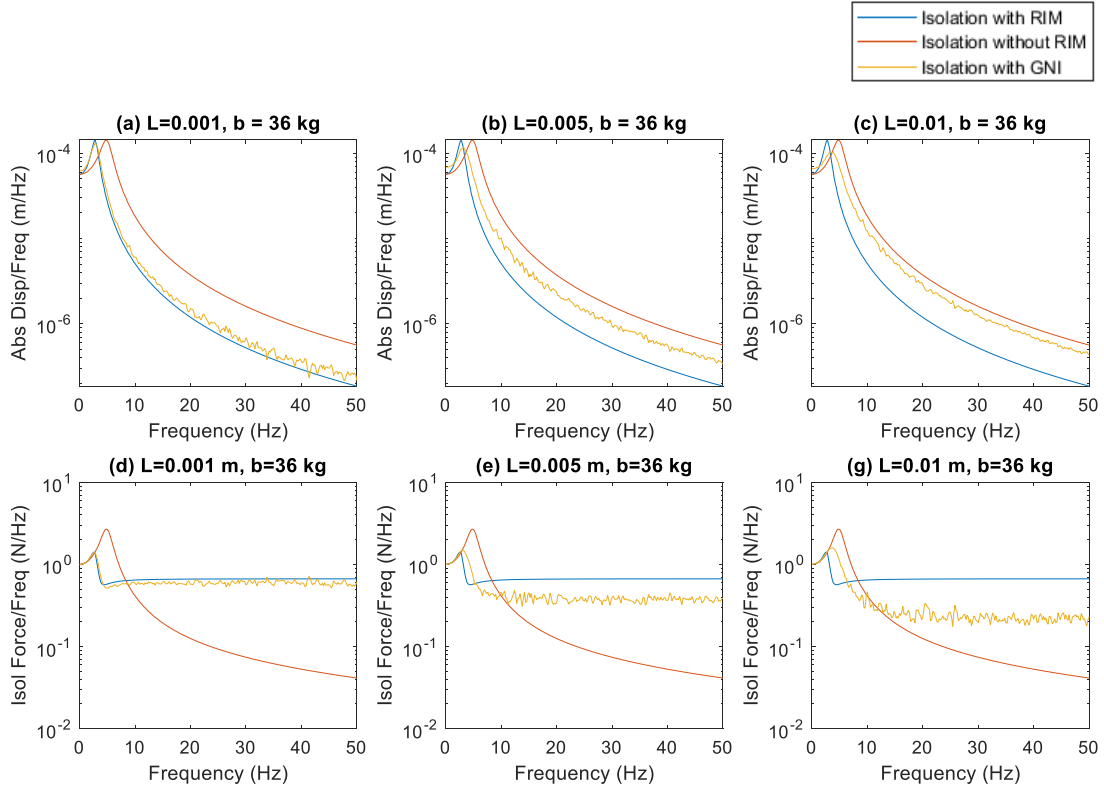


Figure 31 Geometrically Nonlinear Inerter, a-b: Absolute displacement transfer function, e-g: Isolator Force transfer function

Table 7 Geometrically nonlinear inerter compared to linear simulations

| | L = .001 m | L = .005 m | L = .01 m | With RIM | Without RIM |
|--|------------|------------|-----------|-----------|-------------|
| Peak Absolute Displacement TF | 0.000131 | 0.000116 | 0.000103 | 0.000143 | 0.000142 |
| Frequency of Peak Absolute Displacement TF | 2.80 Hz | 3.20 Hz | 3.40 Hz | 2.80 Hz | 4.80 Hz |
| Peak Isolator Force TF | 1.41 | 1.50 | 1.59 | 1.42 | 2.68 |
| H₂ Norm Absolute Displacement TF | 0.0000729 | 0.0000761 | 0.0000757 | 0.0000717 | 0.0000969 |
| H₂ Norm Isolator Force TF | 2.45 | 1.78 | 1.47 | 2.70 | 1.85 |

Chapter 5 Experimental Design

The experimental portion of this thesis was separated into three phases. The purpose of phase 1 was to investigate and understand the behavior of the test apparatus. The purpose of phase 2 was to understand how experimentally adding a conventional rotational inertial mechanism to the isolation layer can change the behavior of the test apparatus. Additionally, a gap inerter prototype was physically realized and fabricated. Phase 3 investigated the effectiveness and efficiency of the displacement gap inerter concept and device. The same z-direction white noise loading, rather than the marine loading discussed in chapter 3, was primarily used for all three experimental phases.

5.1 Phase 1 Experimental Testing

The test apparatus used for the experimental portion of this thesis is built up around a piece of equipment traditionally named a die set. The die set will be explained in further detail in the next chapter. The die set was mounted on a shake table at the University of Tennessee. The shake table is a 4 ft x 4 ft table with actuators that control movement in 6 degrees of freedom. The actuators can control 3 degrees of rotational movement, as well as displacement in the x, y, and z direction. The shake table has a wide range of loading capabilities. A z-motion acceleration white noise signal was loaded onto the shake table computer and used to excite the system. Additionally, accelerometers were used to measure acceleration data from the test apparatus and shake table in the x, y, and z direction. The test apparatus, instrumentation used to measure responses, data analysis, and phase 1 conclusions are outlined in detail below.

5.1.1 Die Set Apparatus & Modifications

The motivation behind the development of the die set test apparatus was to create a simplified SDOF environment to test any physically realized inerter-based devices. The conventional purpose of a die set is to cut and form sheet metal into a desired shape or profile. Figure 32 shows a picture of the unmodified die set purchased for the experimental portion of this thesis.

The die set is attractive for this testing because there are four guide pins that function with guide bushings and ball bearings to precisely align the upper and lower mass plates. Dynamic oscillating mass systems often have issues with alignment, but die sets are manufactured to be precisely aligned. Alignment issues are more likely to be avoided by using a die set for this type of experimental testing. Additionally, the die set configuration assists in limiting motion to be primarily vertical.

The die set was modified to have the same characteristics as the SDOF systems modeled in the numerical simulation chapter. The die set had a 16"x16" 7075 aluminum top plate. One modification that was necessary to simulate the numerically simulated SDOF system was the addition of springs. Four springs were selected based on the spring coefficient of stiffness and size. Spring retainer plates were designed and fabricated to mechanically connect the springs to the top and bottom plates and ensure the engagement of the spring for the entirety of the tests. Essentially, this is done to prevent the top mass plate from lifting off the springs during the upward motion, which would result in the springs disengaging with the system. With these retainer plates, the springs are fully engaged in both compression and tensile states. Figure 33 shows the die set spring modifications that were necessary to properly experimentally test the SDOF system that was numerically modeled. The top of the spring was welded to the top spring retainer plate and the bottom of the spring was welded to the bottom spring retainer plate. The welded spring and plate were placed over the die set guide rods. The spring retainer plate was then bolted to the bottom of the top mass plate and the top of the bottom mass plate.



Figure 32 Die set that the test apparatus is built up around

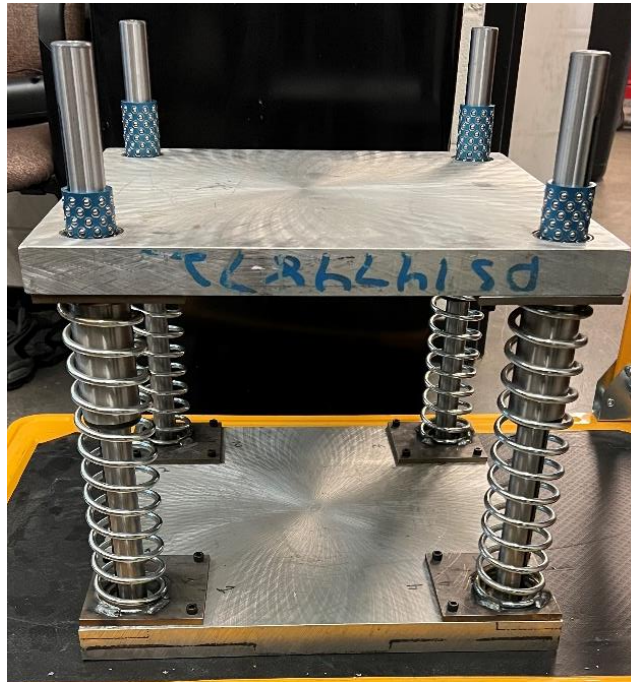


Figure 33 Die set test apparatus with springs

Additional modifications made to the die set consisted of tapped holes in the top and bottom mass plate to attach a designed adapter plate. The purpose of the adapter plate was to have one plate on the bottom and one plate on the top that the inerter device would attach to. This would prevent unnecessary holes in the die set and would allow the die set to be used for additional projects in the future. The total mass of the top plate consisted of the 16"x16" top plate, top adapter plate, and 4 spring retainer plates. The total moving mass of the experimental system was very close to the numerically modeled mass. The drawings for the spring retainer plates, adapter plates, and tapped die set holes can be found in Appendix B.

5.1.2 Instrumentation & Sensor Layout

Eight PCB piezoelectric accelerometers were secured to the die set and shake table. The accelerometers were strategically placed to ensure readings in the x, y, and z directions. Figure 34 shows the sensor placement on the die set and Table 8 corresponds the accelerometer identification number with the location on the test apparatus and the intended measured direction. A national instruments data acquisition system (DAQ) was used during the tests to process the samples taken from the accelerometers. The sampling rate used was 10,240 samples per second. The DAQ system was connected to a computer and synchronized with LabVIEW. LabVIEW is a graphical programming system that is typically used in experimental applications to visualize, record, and save data. The measured data was then saved in a file where it could be analyzed in MATLAB.

5.1.3 Data Analysis & Discussion

The data collected from the experimental tests was imported into MATLAB and analyzed. Figure 35 shows the cross power spectral density plots (CPSD) for the amplified band-limited white noise that was used to excite the system. The band-limited white noise has a frequency range of 2 - 80 Hz, therefore any data prior to 2 Hz is not valid, or relevant to this system. This data was collected from an accelerometer on the shake table and was used to confirm the white noise was amplified correctly. Additionally, it can be observed that the signal levels out at 2 Hz which is important for this system because the estimated natural frequency of the die set is about 5.2 Hz. The white noise was amplified by 0.2, 0.4, 0.8, 1.6 and 2.0.

Sensor 2 was secured to the bottom mass plate of the die set. Figure 36 shows the transfer function plot for the ground motion to sensor 2 data. From 2 Hz to 50 Hz, the value of the transfer function is equal to about one. This is expected and shows the die set is properly secured to the shake table. A transfer function is an input-output ratio, so because it is equal to one the die set motion is equal to the motion of the shake table, therefore the die set is sufficiently secured. There is deviation from one around 50 to 60 Hz. Sensors 5, 6 and 7 measured the die set top plate motion in the z direction. Sensors 5, 6, and 7 all had similar behavior and responses. Figure 37 shows the transfer function plots for the sensors secured to the top plate for all the amplitudes tested. As previously mentioned, the noise seen in Figure 37 before 2 Hz is not valid data due to the broadband noise that was used. Additionally, the natural frequency of the system was estimated to be 5.2 Hz using the stiffness of the springs and the total mass of the top plate. As seen in Figure 37, this is the true natural frequency of the system due to the peak around 5 Hz. The die set exhibited nonlinear behavior for 0.2 and 0.4 amplitudes. This is possibly due to friction. There are additional frequency peaks observed between 30 and 40 Hz, around 60 Hz, and around 90 Hz at higher amplitudes. The additional frequency peaks observed coincide with the deviation from 50 to 60 Hz seen in Figure 36. The damping ratio of the die set was also calculated using the sensor 5 data for each amplitude. The damping ratio was calculated using the half power method and the results are shown in Table 9. A higher damping value was evaluated for the 0.8 amplitude compared to amplitude = 1.6 and amplitude = 2.0. This higher damping ratio for 0.8 amplitude is expected because of the friction previously mentioned at lower amplitudes.

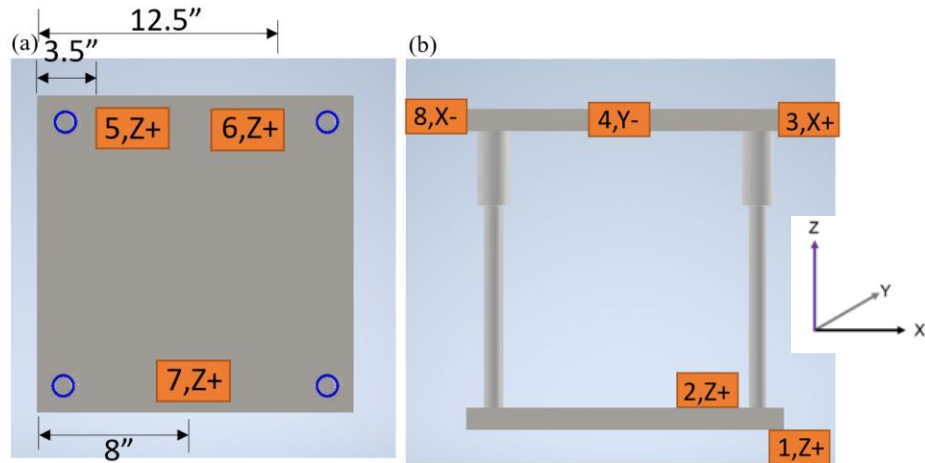


Figure 34 Accelerometer layout. (a) top of die set (b) front of die set

Table 8 Sensor identification number, model number, serial number, location, and direction for experimental testing

| Sensor Number | Sensor Model Number | Sensor Serial Number | Location | Direction |
|---------------|---------------------|----------------------|---------------------------------|-----------|
| 1 | 352C33 | LW223366 | Shake table | Z+ |
| 2 | 352C33 | LW223362 | Bottom mass plate, top of plate | Z+ |
| 3 | 352C33 | LW223364 | Top mass plate, side of plate | X+ |
| 4 | 352C33 | LW223361 | Top mass plate, front of plate | Y- |
| 5 | 352C33 | LW223388 | Top mass plate, top of plate | Z+ |
| 6 | 352C33 | LW223390 | Top mass plate, top of plate | Z+ |
| 7 | 352C33 | LW223386 | Top mass plate, top of plate | Z+ |
| 8 | 352C33 | LW223365 | Top mass plate, side of plate | X- |

Table 9 Damping ratio of die set at amplitude = 0.8, 1.6, 2.0

| Amplitude | Damping Ratio |
|-----------|---------------|
| 0.8 | 0.0576 |
| 1.6 | 0.0166 |
| 2.0 | 0.0166 |

Sensor 4 measured the front top plate of the die set in the y-direction. The frequency peaks in the auto power spectral density plot (APSD) shown in Figure 38 are consistent with the peaks observed in Figure 37, however, there is not as drastic of a peak at the natural frequency of the system, or around 5 Hz. This can be expected because the y direction of the die set is not as affected by the spring contribution creating this natural frequency observed in the z direction. Sensors 8 and 3 were used to measure the x direction from the side of the top plate of the die set. These sensors were used to determine if there was torsion of the top mass about the z axis. To analyze possible torsion, the CPSD plots for sensor 3 to sensor 8 were produced. Using MATLAB, the phase angle was then determined. Figure 39 shows the CPSD of the x sensors and the angle plot. When the angle is equal to π , or negative π , the sensors are out of phase. Due to the placement of the sensors and direction in which the sensors are measuring, an out-of-phase reading means the die set is moving laterally or left to right. When the angle is equal to 0 or 2π , the sensors are in phase with each other. An in-phase reading suggests that torsion is occurring. Table 10 shows the frequency at which peaks occur and the angle that corresponds to that frequency. Using the angle plot in Figure 39, the die set is exhibiting torsion behavior between 0 to 5 Hz frequency, but at all other frequencies up to 100 Hz, the die set is exhibiting lateral behavior, or more of a side-to-side motion. Ideally, the die set would not exhibit lateral behavior or torsion. Due to the nature of the testing, x-direction, or lateral motion of the die set, is inevitable.

5.1.4 Conclusions

Initial testing of the die set was successful in helping understand the behavior of the test apparatus. By completing phase 1, appropriate amplitudes of loading that will be used for subsequent testing were confirmed, the die set was adequately secured to the shake table, the calculated natural frequency for the system is the true natural frequency which was observed during testing, and there are additional peak frequencies observed during testing. The fundamental mode is primarily vertical. The additional peaks observed at higher frequencies may be plate modal frequencies of the die set. The die set has inherent dynamics that are not purely vertical. These plate modes are excited. Additionally, a better understanding of the die set motion in the x-direction was revealed. The die set top plate is mostly exhibiting lateral, or side-to-side motion, rather than torsion. Visually, the die set exhibited significant vertical motion, or z-motion displacements. Additionally, the springs remained engaged for the entirety of the tests despite amplitude changes, so the spring retainer plates were sufficient for spring engagement in tension and compression. Phase 1 testing demonstrated that the die set exhibits behavior sufficient and consistent for isolation system testing and that the die set would provide a basis for comparison once additional devices were incorporated into the isolation layer.

5.2 Phase 2 Experimental Testing

Phase 2 of experimental testing incorporated a conventional RIM device into the die set test apparatus. The tested RIM device, the modifications that were necessary to incorporate the RIM into the die set, and the instrumentation and sensor layout used during the tests are outlined in detail below. The white noise signal and amplitudes used in phase 1 were used for phase 2 as well. The data collected from phase 2 is presented below. The data was analyzed to understand how the conventional RIM behaves in isolation systems and how well that behavior was captured in the numerical simulations for the conventional RIM

5.2.1 Conventional RIM Device

The conventional RIM fabricated for phase 2 of experimental testing consisted of a lead screw, leadscrew nut, flywheel centerpiece, and bolts that acted as the flywheel. Figure 40 shows the labeled components of the conventional RIM. Figure 41 shows a more detailed figure of the pieces used to install the RIM in the die set. The RIM was secured to the die set on each end of the lead screw. The lead screw nut was bolted to the bottom of the top die set plate which can be seen in Figure 40.

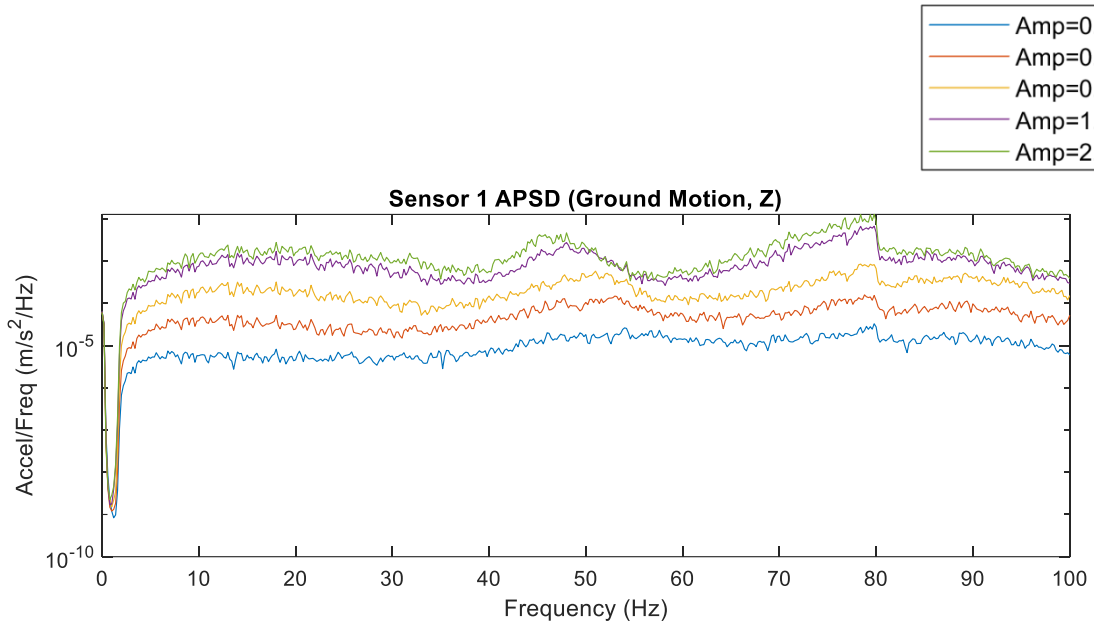


Figure 35 Figure 33 Ground Motion CPSD, Z direction

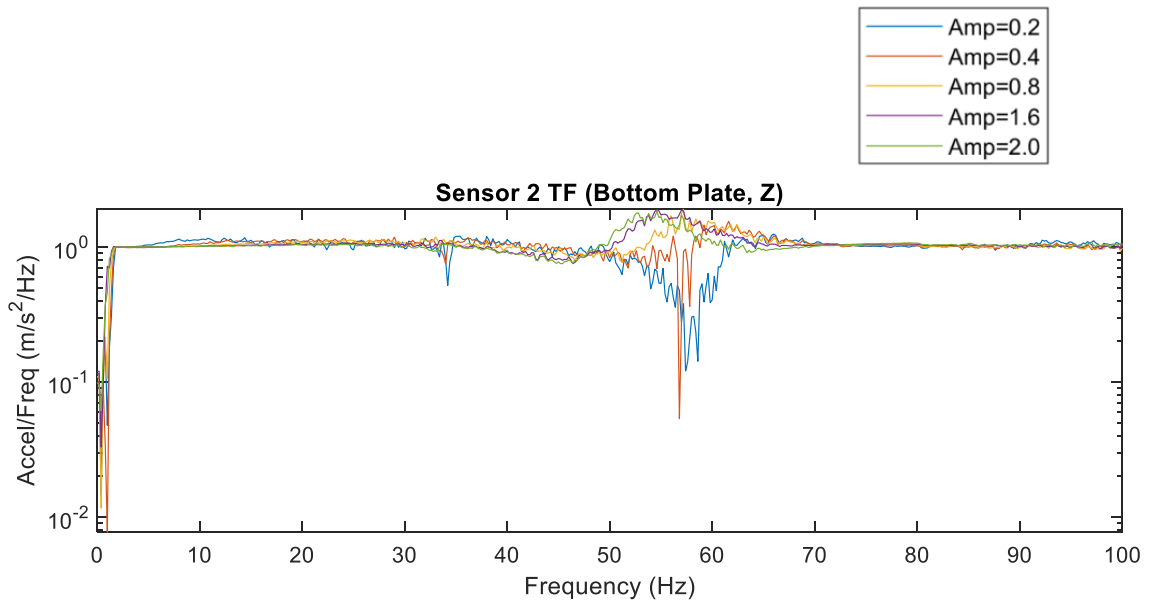


Figure 36 Sensor 2 CPSD, Z direction

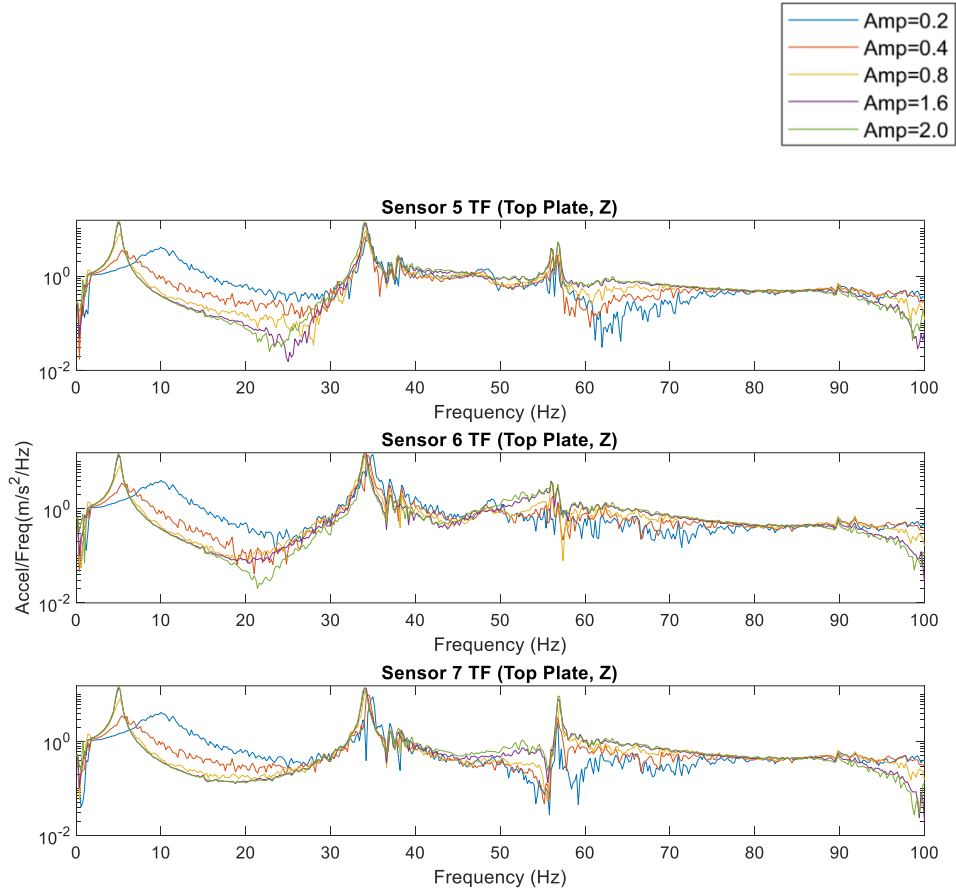


Figure 37 Sensor 5, 6 and 7 transfer function estimate, Z direction

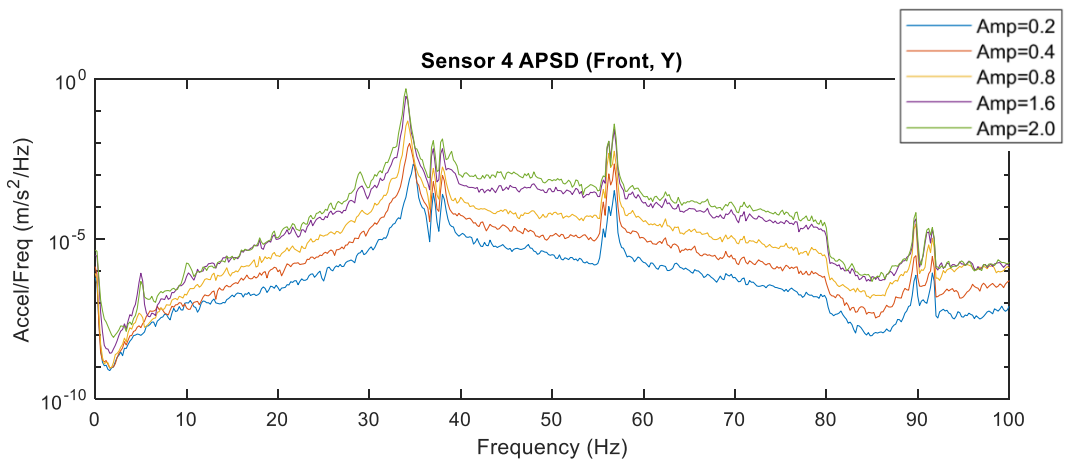


Figure 38 Sensor 4 auto power spectral density plot, Y Direction

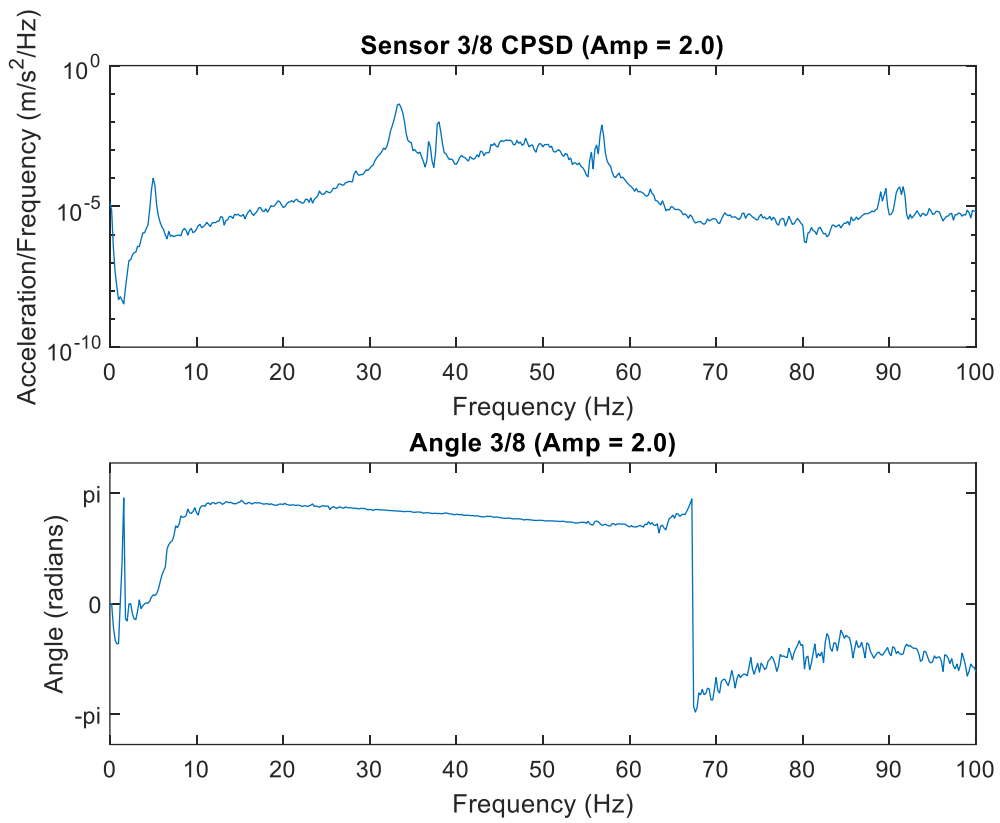


Figure 39 Sensor 3/8 CPSD and angle plot for amplitude = 2.0

Table 10 Sensor 3 to Sensor 8 CPSD, Frequency Peaks and Angle

| Frequency Peak (Hz) | Angle (radians) |
|---------------------|-----------------|
| 4.99 | 0.25 |
| 33.2 | 2.64 |
| 38.0 | 2.57 |
| 56.8 | 2.21 |
| 91.6 | -1.42 |

A shaft collar and thrust bearing were placed on the lead screw. The thrust bearing sits directly on the adapter plate and the lead screw is inserted through the center of the adapter plate. Another thrust bearing sits directly under the adapter plate and a second shaft collar secures the leadscrew and thrust bearing in position. The shaft collars hold the lead screw nut in place while rotating with the lead screw. The advantage of using shaft collars and thrust bearings is they do not contribute a significant amount of inertance to the system. Other bearings to secure the lead screw were investigated but a common problem was the inertance contribution was far too great for the mass used in this experimental testing. If other components of the system were contributing extreme amounts of inertance, the flywheel effects, or low levels of inertance, would not be able to be examined. Vibration-damping sandwich mounts were used to mount the adapter plate to allow clearance for the thrust bearing and shaft collar. The mounts also helped the lead screw self-align in the die set.

The inertance of the inerter can be modified by changing the geometry, or dimensions of the flywheel, or the mechanism that results in rotation. A 4 start lead screw with a 2 mm pitch and 8 mm lead was selected for the inerter due to its availability and success in previous inerter experimental designs. For this application, it is essential that the lead screw can backdrive. For this thesis, the inertance was solely altered by changing the flywheel geometry. The flywheel centerpiece, shown in Figure 42, was fabricated using a small steel cylinder with four threaded holes on the sides. Two, 1.25" set screws were used in each configuration to secure the flywheel to the lead screw. Two additional bolts were screwed into the other threaded holes to complete the flywheel, as shown in Figure 43. The inertance of the system consisted of the inertance from the lead screw, the flywheel, and two shaft collars. The shaft collars were included because any component rotating with the flywheel contributes inertance. The inertance of each component was calculated using the equation: $b = \left(\frac{2\pi}{l}\right)^2 * I$, l being the lead of the lead screw and I being the moment of inertia of the component. The total inertance in the system was determined by summing the inertance of each component. The calculations used to calculate the inertance values for the conventional RIM can be found in Appendix A. Various bolt sizes were used to change flywheel geometry and evaluate performance at different inertance levels. The total isolated mass included the mass of the aluminum 16"x16" die set plate, the top adapter plate, and the four top spring retainer plates. The desired inertance levels were around 25%, 50%, 100%, and 200% of the total isolated mass. Table 11 lists the flywheel inertance values (kg), the inertance percentage of mass (%), the set screws and bolts used in the configuration, and the natural frequency (Hz) of the system including inertance. As bolt length increased, the inertance value increased. Additionally, as inertance increased, the natural frequency decreased.

5.2.3 Instrumentation & Sensor Layout

The instrumentation and sensor layout used in phase 1 was also used for phase 2 of experimental testing.

5.2.4 Data Analysis & Discussion

The data collected from phase 2 of the experimental tests was imported into MATLAB and analyzed. The APSD for the ground motion taken from sensor 1 for phase 1 and phase 2 of experimental testing was plotted in Figure 44. Amplitude = 0.2 is the lowest signal in the figure, from there the amplitude increases to 0.4, 0.8, 1.6 and 2.0. The phase 1 and phase 2 ground motion data was plotted on one figure to ensure that the ground motion used was the same, or comparable to the ground motion used in phase 1. This is important because the data collected from phase 1, or the no flywheel case, will be compared to the flywheel configurations in this chapter. Additionally, this figure shows the scaling of the ground motion and ensures consistency throughout the tests.

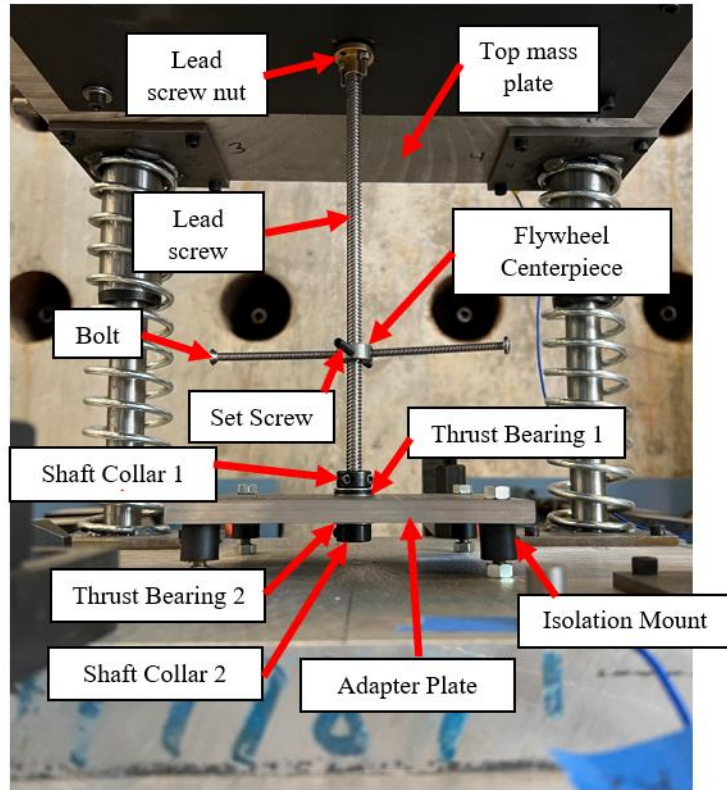


Figure 40 Conventional RIM installed in die set for phase 2 testing

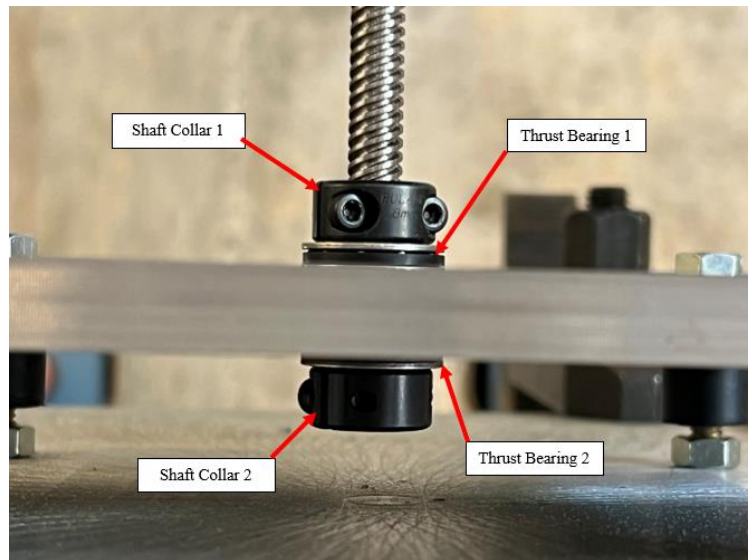


Figure 41 Thrust bearing and shaft collar used to secure the conventional RIM in the die set



Figure 42 Fabricated flywheel hub

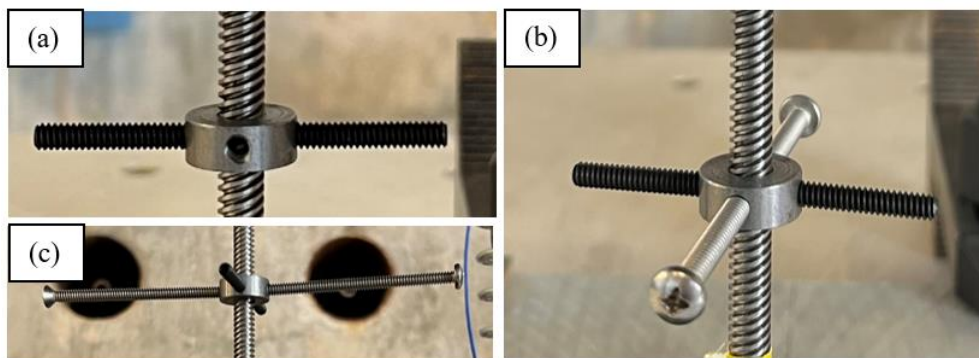


Figure 43 Examples of flywheel configurations (a) $b=24.6\%$ (b) $b=39.7\%$ (c) $b=194.5\%$

Table 11 Phase 2 flywheel inertance values, percent of mass, and natural frequency of the system considering inertance

| Total Inertance Value (kg) | Percent of Mass (%) | Set Screws / Bolts | Calculated Natural Frequency (Hz) |
|----------------------------|---------------------|---------------------------------------|-----------------------------------|
| 4.51 kg | 24.6% | 2- 1.25" set screws | 4.69 Hz |
| 7.28 kg | 39.7% | 2- 1.25" set screws 2- 1.25" bolts | 4.43 Hz |
| 18.3 kg | 100% | 2- 1.25" set screws 2- 2.25" bolts | 3.70 Hz |
| 35.7 kg | 194.5% | 2- 1.25" set screws 2- 3" bolts | 3.05 Hz |

Sensor 5 was attached to the top plate of the die set and measured motion in the Z direction. Figure 45 compares the estimated transfer functions for all flywheel configurations, as well as no flywheel, for each amplitude.

For the remainder of the experimental testing, the flywheel configurations will be referred to by their inertance percentage of mass value. Generally, as amplitude increases the frequency peaks become more drastic, or sharp. At an amplitude of 0.2, there is a significant reduction in response with 24.6% inertance, but there is no change in natural frequency of the system. The lack of shift in natural frequency is due to a lack of engagement of the inerter. If there is not a strong enough load to engage the flywheel, the inertance will not contribute to the system due to backlash in the lead screw. At an amplitude of 0.8 and greater, there is a significant natural frequency peak around 5 Hz. 24.6% and 39.7% inertance flywheels consistently reduce the peak and shift the natural frequency compared to the no flywheel case from phase 1. 100% and 194.5% inertance, both reduce the peak and shift the natural frequency, but also create a new 'peak-like' frequency around 20 Hz. This second peak is seen most drastically for amplitudes equal to 1.6 and 2.0 and shows the issue with post-isolation mode higher transmitted forces that are prevalent in inerter-based isolation systems. 24.6% and 39.7% also exhibit these transmitted forces, but they are not as drastic as the 100% and 194.5% inertance flywheels.

The inertance was back calculated using the mass of the top mass plate, the known stiffness of the springs in the system, and the natural frequency peak value obtained from Figure 47. Figure 47 was used to obtain the peaks because the nfft value, or the number of discrete Fourier transform points was increased compared to the other figures in the data analysis presented in this thesis. The nfft impacts the number of points plotted for the data, so this helps identify a more accurate true peak of the system. The inertance values calculated from the experimental identified natural frequency, shown in Table 12, are relatively close to the calculated inertance values. Slight error could be due to difficulty obtaining the true peak from the experimental data. For example, b=100% and b=194.5% are essentially straight lines, so there could be error in the calculated inertance values from the experimental data.

When looking at the later frequency peaks that are visible in Figure 45 and were observed in phase 1 testing, the peaks were not significantly reduced, or shifted at any inertance values. This is also seen in Figure 46 which shows the 0-500 Hz estimated transfer functions for all flywheel configurations, as well as no flywheel for an amplitude of 2.0.

Sensors 6 and 7 were also secured to the top mass plate and measured motion in the z-direction. Both sensors exhibited consistent behavior with sensor 5. Sensor 4 was secured to the front of the top mass plate and measured motion in the y direction. Figure 48 compares the y-direction APSD for all flywheel configurations, including no flywheel, at each amplitude. The natural frequency peak observed in the z-direction is not observed at low amplitudes and is very minimal at amplitudes 1.6 and 2.0. The peak observed in those higher amplitudes is only seen for the no flywheel case. It is not expected to see the mode around 5 Hz for this y-dominated sensor that was seen for the z-dominated sensor. The same peaks at later frequencies are consistent with phase 1 results and the z-direction results for phase 2.

Figure 49 shows a similar trend for x-direction measurements taken with sensor 8. Sensor 8 was applied to the side of the top plate of the die set. Figure 49 shows no natural frequency peak at lower amplitudes for the no flywheel case and all the flywheel configurations. At higher amplitudes, the die set with no flywheel exhibits a frequency peak around 5 Hz, but like sensor 4 the flywheel configurations do not exhibit this peak. The additional frequency peaks observed in the previous results are consistent locations and are not affected by the additional inertance. For all amplitudes, the flywheel configuration cases deviate from the no flywheel case between 65 and 90 Hz.

5.2.5 Conclusions

Phase 2 of experimental testing was intended to help investigate the changes in a system observed due to incorporating an inerter into the isolation layer. Flywheels of varying inertance levels were compared to phase 1 testing, or the no flywheel case to determine how the inerter fundamentally changes the behavior of a system.

It has been observed that incorporating an inerter in an isolation system can reduce the natural frequency peak corresponding to the main vertical mode of the system and shift or reduce this natural frequency of the system. As inertance increases, the peak is reduced and natural frequency is shifted, however, as inertance increases over 100% of the mass value, there are significant transmitted forces. This shows there is an optimum inertance level for a system with a linear inerter and it is largely dependent on the mass of the system. It is visually seen in the z-direction that another peak forms at a later frequency, despite reducing the natural frequency that has been observed at 5 Hz. Although a new peak forms at a later frequency, the new peak is significantly softer than the original. The experimental results are similar to the base loaded absolute acceleration figures that were numerically modeled previously. Additionally, it was observed in the x and y-direction that the addition of a flywheel, no matter the inertance level, reduced the natural frequency peak for the no flywheel case. The results were the same for low and high inertance flywheel configurations. There exist some frequency peaks, or possible plate modes at higher frequencies that are not affected or reduced by the flywheel configurations. The inerter may not have the capability of reducing plate mode frequencies, or other inherent frequencies in the system due to its inability to reduce peaks that occurred at later frequencies. The inerter solely impacted the main vertical mode of the system. For future testing on this structure, the inertance additions and changes to the system are only expected to influence the response from the 0-30 Hz range.

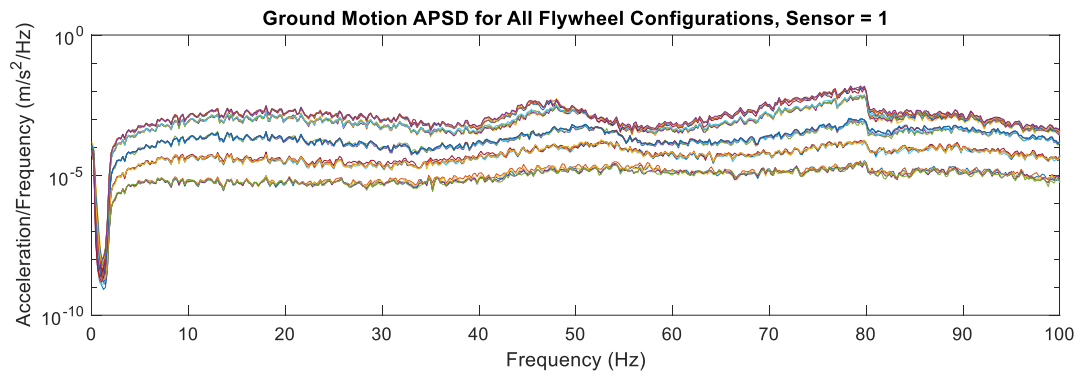


Figure 44 Ground motion APD for all flywheel configurations and phase 1 testing

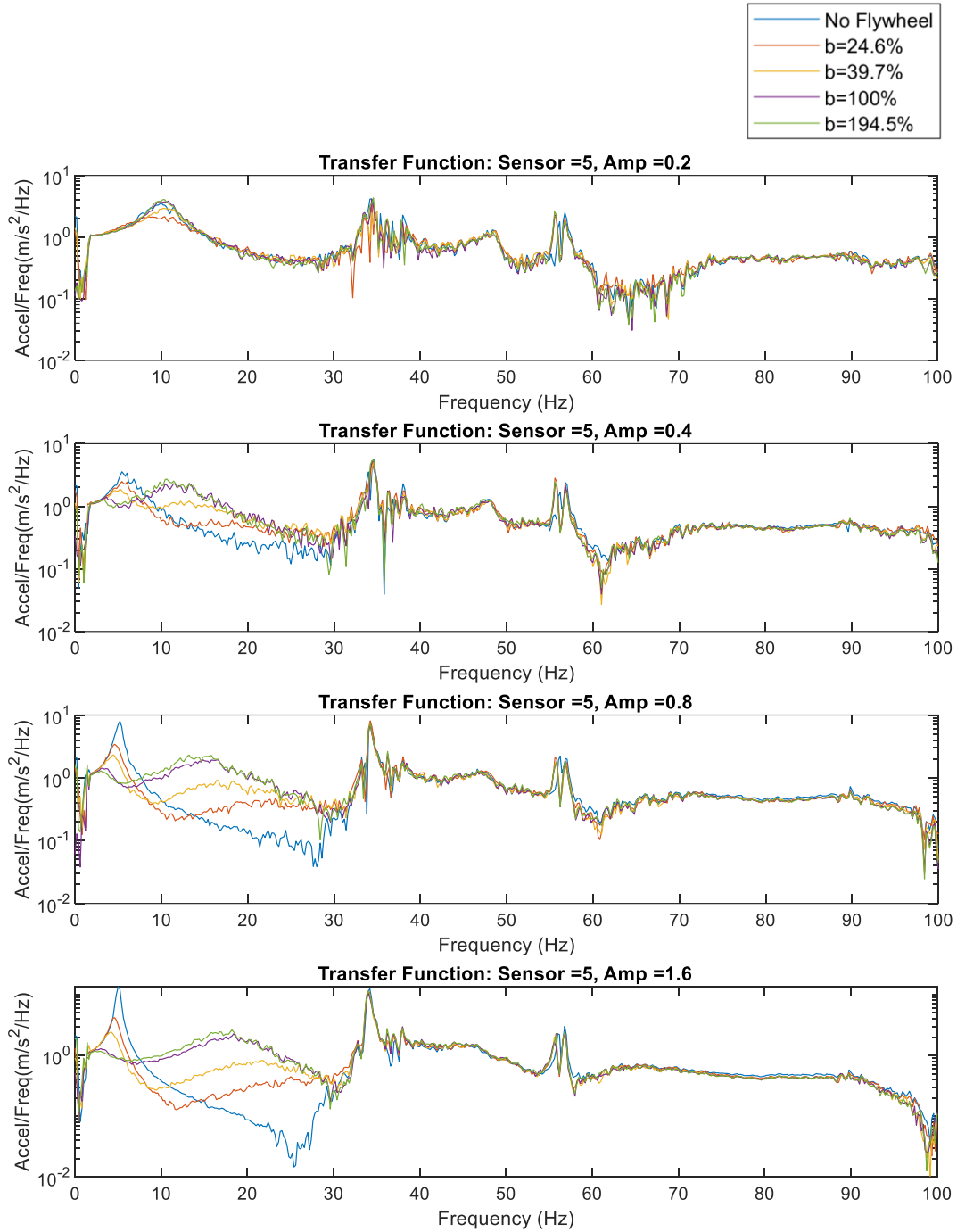


Figure 45 Sensor 5, 0-100 Hz Estimated Transfer Function for all Flywheel Configurations at Amp = 0.2, 0.4, 0.8, 1.6, 2.0

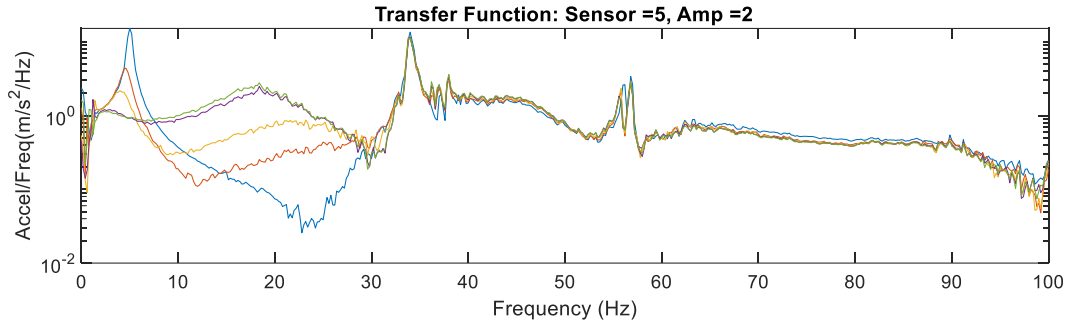


Figure 45 continued

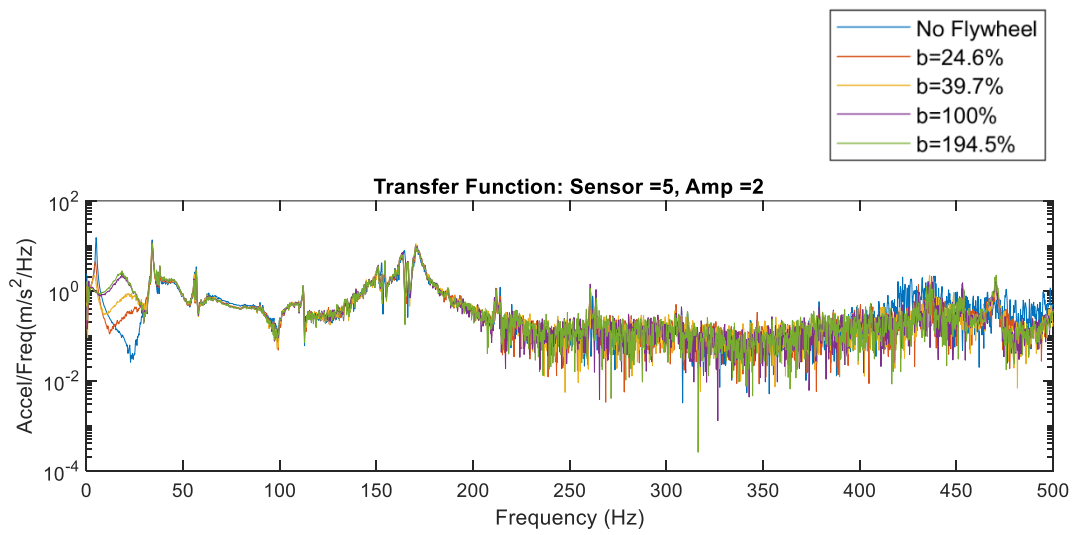


Figure 46 Sensor 5, 0-500 Hz Estimated Transfer Function for all Flywheel Configurations at Amp = 0.2, 0.4, 0.8, 1.6, 2.0

Table 12 Phase 2 Identified natural frequency from experimental results and calculated inertance values from identified natural frequency

| | Amp = 0.8 | | Amp = 2.0 | |
|---|---|---|---|---|
| Percent of Mass from Calculated Inertance (%) | Identified Natural Frequency from Experimental Results (Hz) | Calculated Inertance from Identified Natural Frequency (kg) | Identified Natural Frequency from Experimental Results (Hz) | Calculated Inertance from Identified Natural Frequency (kg) |
| 24.6% | 4.53 Hz | 6.18 kg | 4.47 Hz | 6.80 kg |
| 39.7% | 4.60 Hz | 5.44 kg | 3.93 Hz | 14.2 kg |
| 100% | 3.67 Hz | 19.0 kg | 3.07 Hz | 35.0 kg |
| 194.5% | 3.07 Hz | 35.0 kg | 2.33 Hz | 74.3 kg |

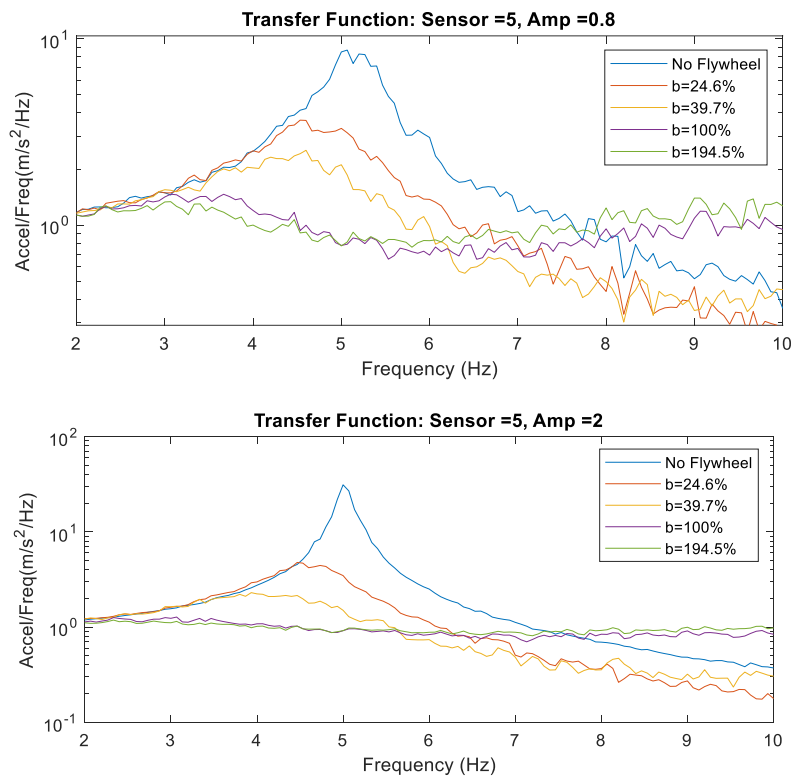


Figure 47 Phase 2 Estimated transfer function with increased nfft value used for calculated inertance values from identified natural frequency

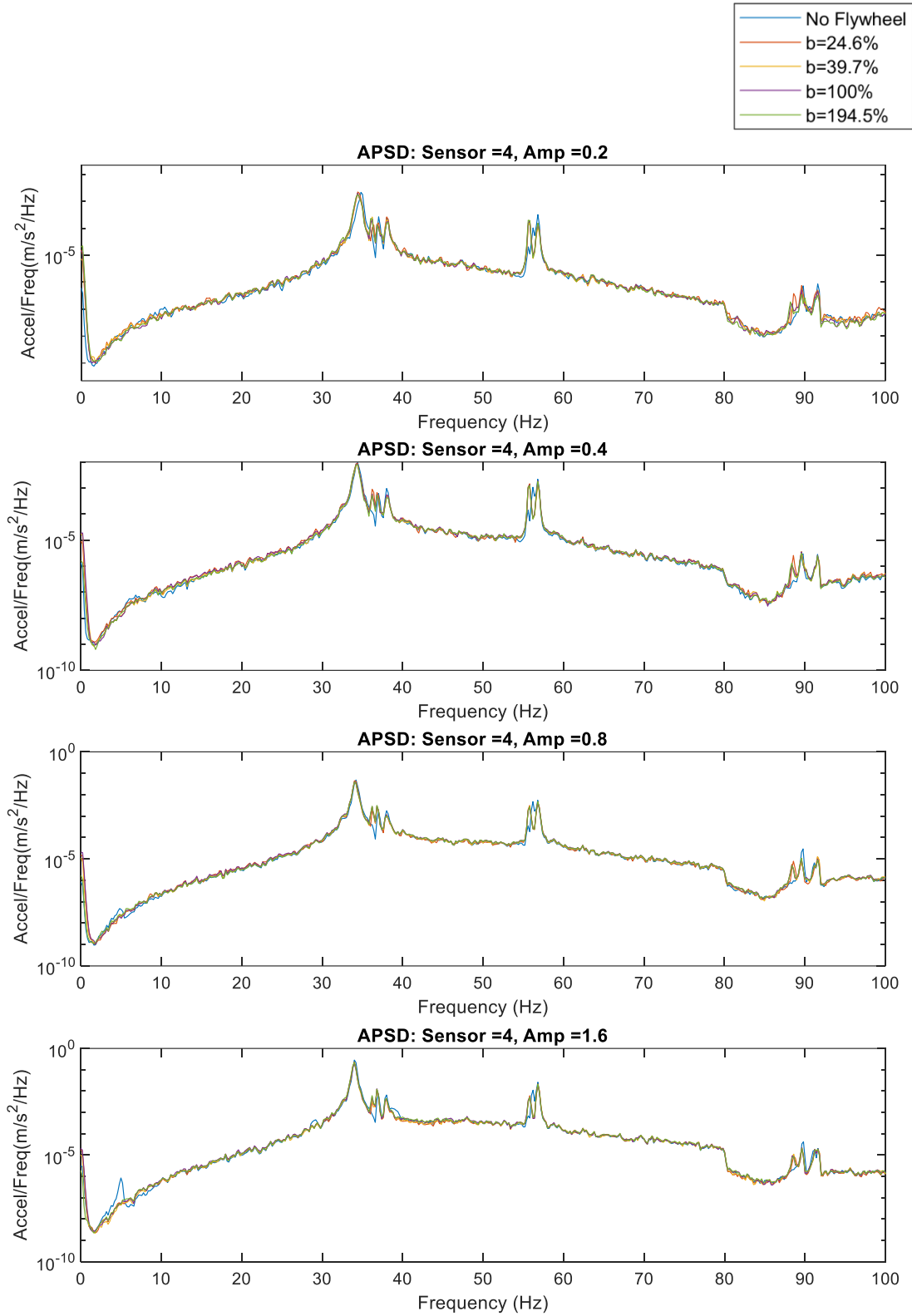


Figure 48 Sensor 4, 0-100 Hz APSD for all Flywheel Configurations at Amp = 0.2, 0.4, 0.8, 1.6, 2.0

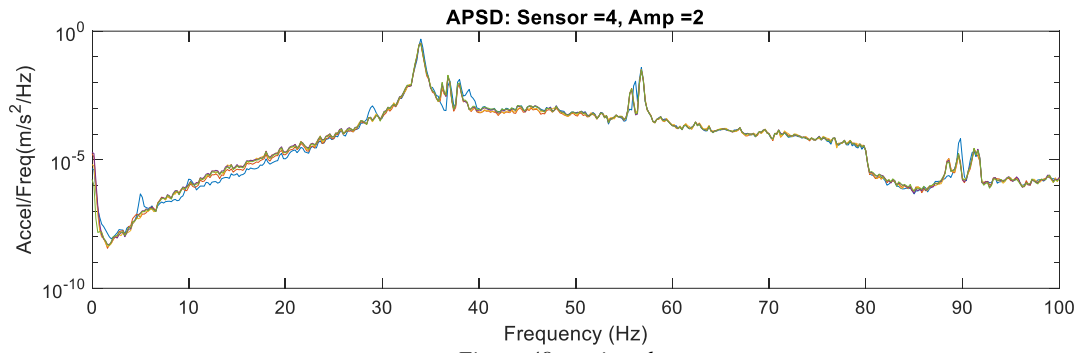


Figure 48 continued

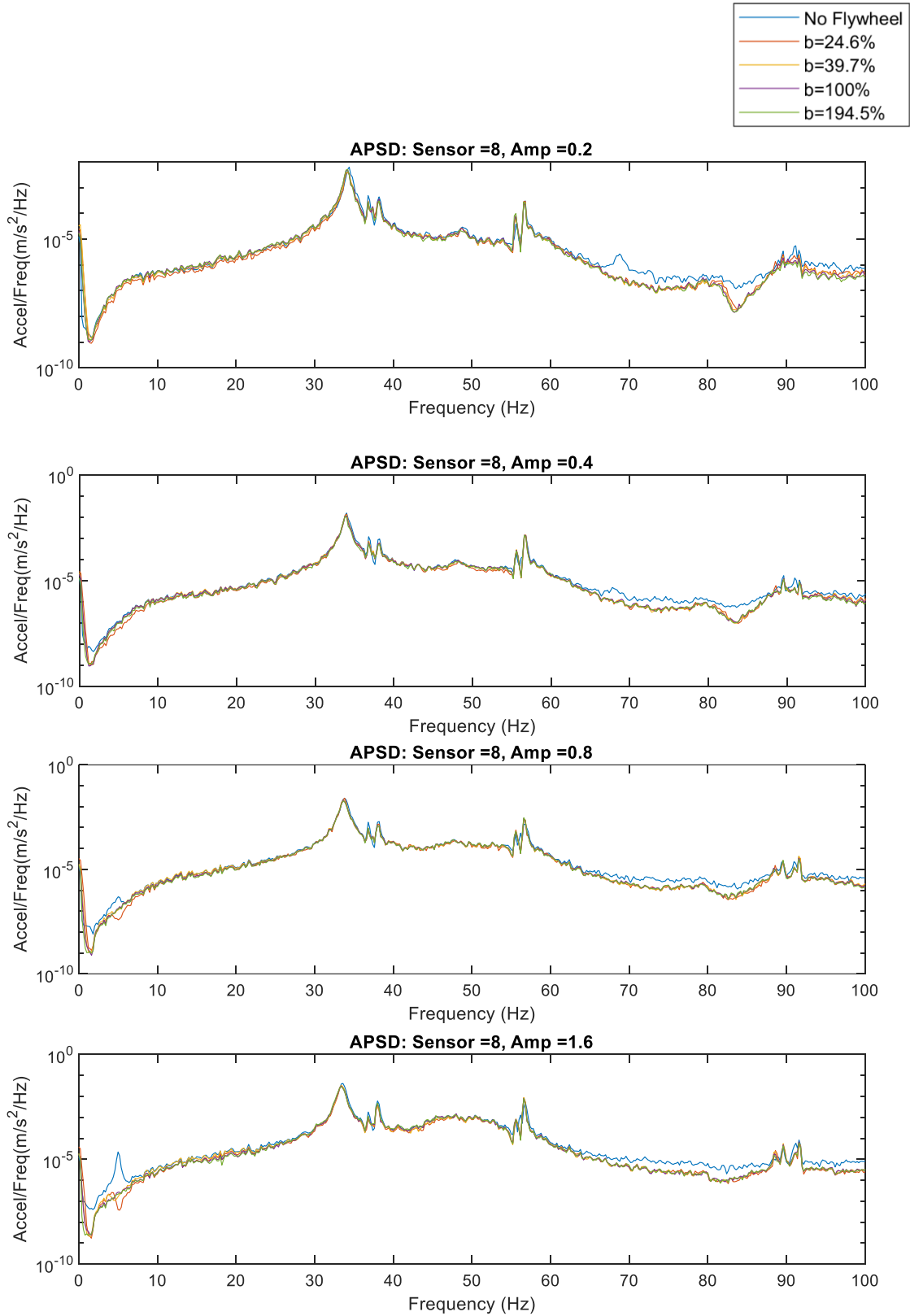


Figure 49 Sensor 8, 0-100 Hz APSD for all Flywheel Configurations at Amp = 0.2, 0.4, 0.8, 1.6, 2.0

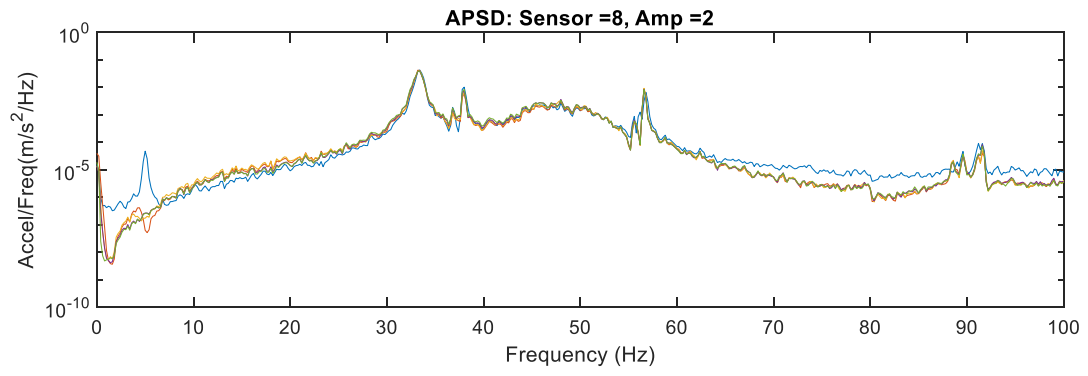


Figure 49 continued

5.3 Phase 3 Experimental Testing

Transmitted forces observed in phase 2 testing show the desire for NRIMs to reduce transmitted forces while also reducing the natural frequency peak and natural frequency of the system. As previously mentioned, the displacement gap inerter was more physically realizable compared to the acceleration gap inerter. A displacement gap inerter referred to as the bushing-crown gap inerter was fabricated to experimentally explore nonlinear inertial mechanisms. The white noise used for the previous phases was also used for phase 3 experimental testing. The following chapter outlines the device, the instrumentation and sensor layout, and presents collected data and conclusions on the viability of incorporating a gap-type inerter into an isolation system.

5.3.1 Bushing – Crown Gap Inerter Device

As previously mentioned, a version of the displacement gap inerter discussed in Chapter 4 was physically realizable. This is mainly due to the engagement and disengagement of the inerter being dependent on the displacement of the mass rather than the acceleration of the mass. The displacement gap inerter idea was physically realized using an 8 mm lead screw and flywheel that would engage and disengage based on the primary mass displacement. Two interlocking parts, the notched bushing and notched crown, were designed and fabricated to ensure dependency of the mass displacement. The parts were made from UHMW plastic due to its slippery nature which would limit friction and allow the parts to easily interlock and unlock. Figure 50 shows the notched bushing and crown in the engaged position when the parts are interlocked, and the disengaged position when the parts are not interlocked. The notched bushing is attached to the mass plate and the notched crown is attached to a lead screw nut. The bushing and crown will interlock when the mass and bushing displace a certain gap amount because the bushing is attached to the mass plate. The interlocking mechanism will subsequently engage the flywheel. The gap was measured based on the distance of travel required to completely interlock the bushing and crown. This gap distance was measured from point A to point B labeled in Figure 50.

While this is a gap inerter, the physical realization of this gap differs from the numerically simulated displacement gap inerter in Chapter 4. In the numerical simulations, a two-sided gap inerter was modeled where engagement occurred if the displacement of the mass was greater than the gap and less than the negative of the gap. The physically realized gap will engage when the displacement of the mass is greater than the negative of the gap, or when the mass displaces downward the full length of the gap and more, but the flywheel will not engage upward. The two-sided gap inerter that was numerically simulated would be physically realized if the inerter engaged when the mass displaced downward the full length of the gap and more and when the mass displaced upward a distance greater than the gap.

Figure 51 shows the labeled gap inerter installed in the die set. The gap inerter was installed with thrust bearings and shaft collars the same way the conventional RIM was installed, shown in Figure 41. The intended purpose of the shaft collar, thrust bearing, and spring labeled in Figure 51 was to assist the lead screw nut in returning to its initial position, thus resulting in the engagement and disengagement of the flywheel. A stiff spring was selected for the device due to gap size inconsistencies as engagement of the flywheel occurred. The gap increase inconsistencies were less drastic for a stiff spring compared to a less stiff spring. The lead screw nut with the notched crown then sat directly on the spring washer which acted as a contact surface between the bottom of the lead screw nut and top of the spring.

Table 13 shows the phase 3 flywheel inertance values, inertance percentage of mass, set screw, bolt, and nut configuration. Due to limited bolt lengths available, nuts were added to the bolts to increase the inertance in some cases. Compared to phase 2, additional configurations were tested. In the configurations

where the bolt sizes were the same, the inertance values changed to include the additional shaft collar labeled in Figure 51.

5.3.2 Instrumentation & Sensor Layout

The instrumentation and sensor layout used in phase 1 and phase 2 was used for phase 3 of the experimental testing for accurate comparison among tests.

5.3.3 Data Analysis & Discussion

The various flywheel configurations in Table 13 were tested in the bushing-crown gap inerter. Each configuration was tested with the same ground motion used in previous phases, but only with amplitudes equal to 0.8, 1.6 and 2.0. The gap between the bushing and crown, as explained in Figure 50, was equal to 0.2900” for all the tests. Using preliminary observations, gaps that were too large were not engaging enough. The gap of 0.2900” had an appropriate amount of engagement and disengagement of the flywheel. Figure 52 shows the z direction transfer function, from 2 to 30 Hz for all 8 gap-type NRIM configurations listed in Table 13 compared to the no flywheel case from phase 1 at amplitudes equal to 0.8, 1.6, and 2.0.

Frequency equals 2 to 30 Hz is presented because the behavior observed in previous phases has shown that after 30 Hz the inerter is unlikely to change the behavior of the die set. Regardless of amplitude, the transmitted forces from 10-30 Hz follows the general pattern of the no flywheel case. Figure 53 shows the same set of data as Figure 52, but from 2 to 10 Hz to show the impact the gap inerter has on the peak and natural frequency based on increases in inertance.

At an amplitude of 0.8, all the gap configurations behave similarly to the no flywheel case. It was observed that there was a relatively low amount of engagement of the flywheel at this amplitude. It makes sense that the behavior resembles the no flywheel case as there was low amounts of flywheel engagement. At amplitudes of 1.6 and 2.0, the gap inerter results deviate from the no flywheel case. For all gap inerter flywheel configurations, the peak is reduced. While each gap inerter peak is reduced, the natural frequencies are all slightly increased compared to the no flywheel case. The 300% gap-type NRIM flywheel configuration has the most drastically reduced peak, but it can also be seen in Figure 53 that the transmitted forces after 10 Hz for the 300% flywheel configuration still follow the no flywheel case relatively closely. Due to the 300% gap-type NRIM having the lowest peak and relatively low transmitted forces compared to the no flywheel case, Figure 54 compares the 300% gap-type NRIM seen in Figure 52 and Figure 53 with the no flywheel case and the 4 conventional flywheel configurations tested and analyzed in phase 2.

As previously discussed, at amplitude = 0.8, the no flywheel case and the gap-type NRIM have similar responses both in terms of the peak and the transmitted forces from 10 – 30 Hz due to a lack of engagement. At amplitude = 1.6, the gap-type NRIM peak is substantially reduced compared to the no flywheel case, but larger than the conventional cases. The transmitted forces from 10 – 30 Hz largely follows the no flywheel case and is significantly lower than all the linear flywheel configurations.

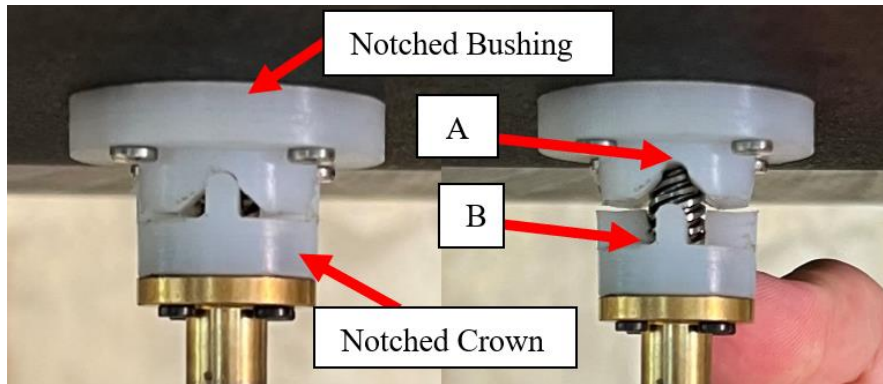


Figure 50 Gap inerter notched bushing and crown engaged (left) and disengaged (right)

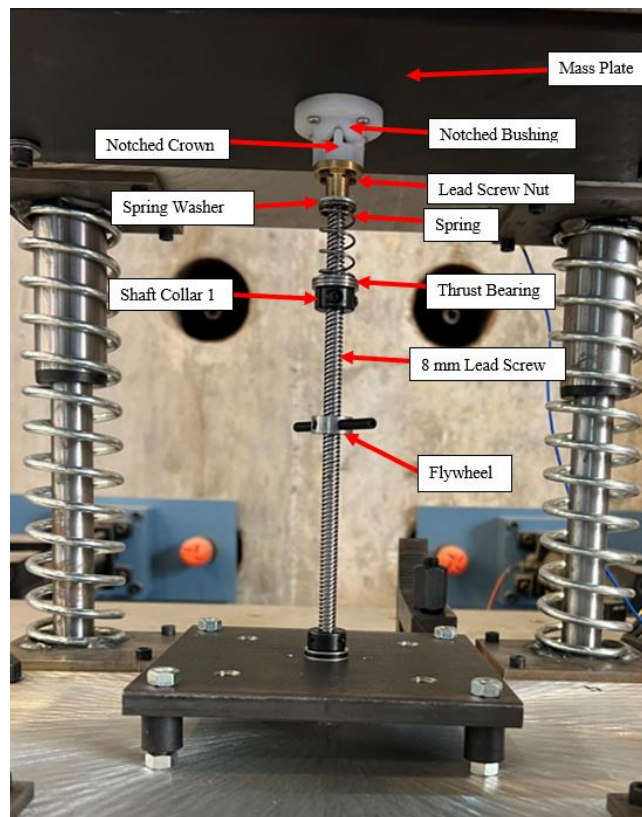


Figure 51 Displacement gap inerter with labeled components

Table 13 Phase 3 flywheel inertance values, percent of mass, and set screw, bolt, and nut configurations

| Inertance Value (kg) | Percent of Mass (%) | Set Screws / Bolts |
|----------------------|---------------------|---|
| 4.95 kg | 27.0% | 2- 1.25" steel set screws |
| 9.47 kg | 51.7% | 2- 1.25" steel set screws 2- 1.50" steel bolts |
| 18.8 kg | 102.5% | 2- 1.25" steel set screws 2- 2.25" steel bolts |
| 36.1 kg | 196.9% | 2- 1.25" steel set screws 2- 3" steel bolts |
| 54.8 | 298.7% | 2- 1.25" steel set screws 2- 3" steel bolts + 2 Nuts EA |
| 73.6 | 401.3% | 2- 1.25" steel set screws 2- 3.5" zinc bolts + 2 Nuts EA |
| 101.6 | 554.3% | 2- 1.25" set screws 2- 4" zinc bolts + 2 nuts EA |
| 116.8 | 636.9% | 2- 1.25" set screws 2- 4" zinc bolts + 3 nuts EA |

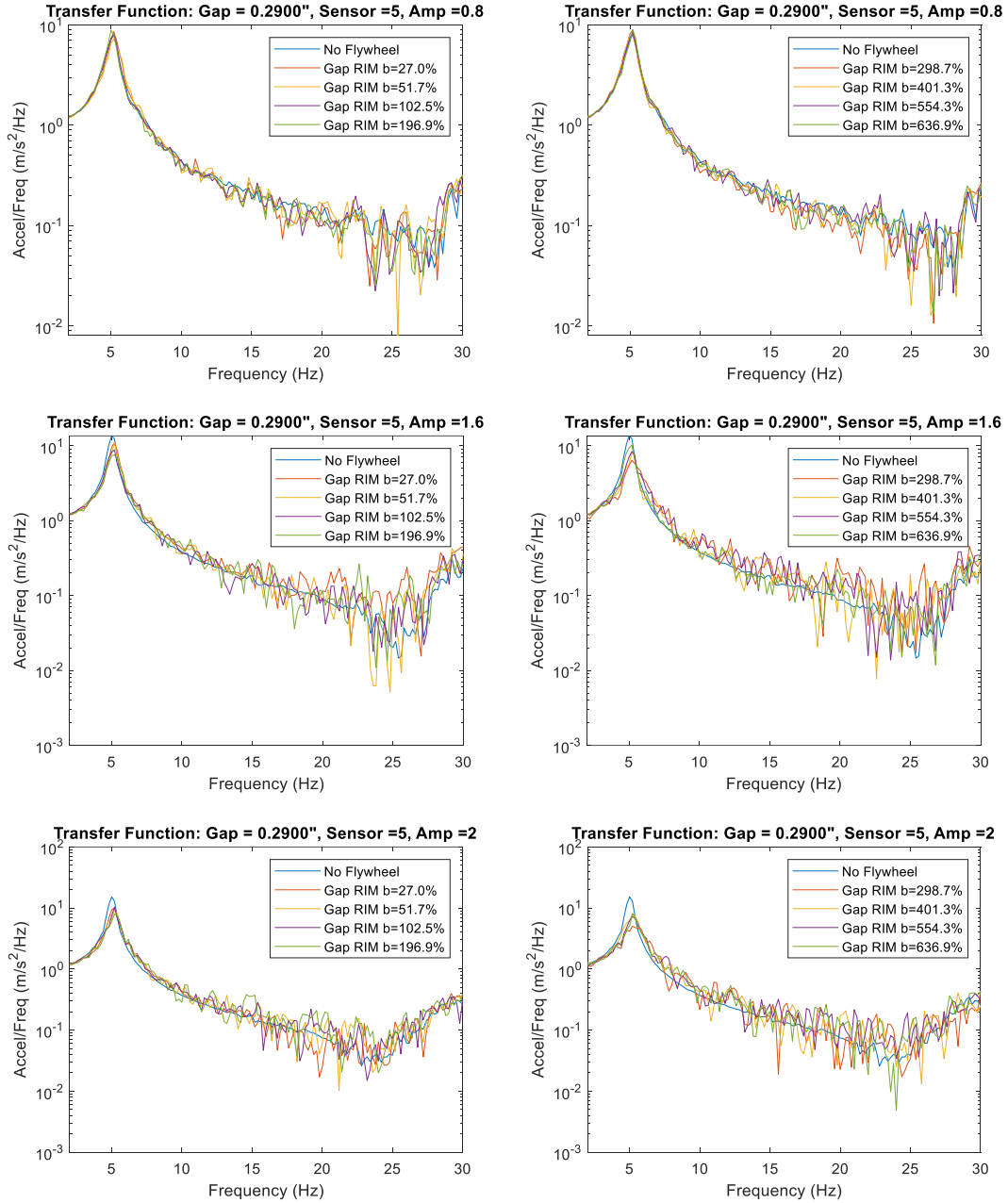


Figure 52 Sensor 5 estimated transfer function for all flywheel configurations, 2 – 30 Hz, compared to no flywheel case at Amp = 0.8, 1.6, and 2.0

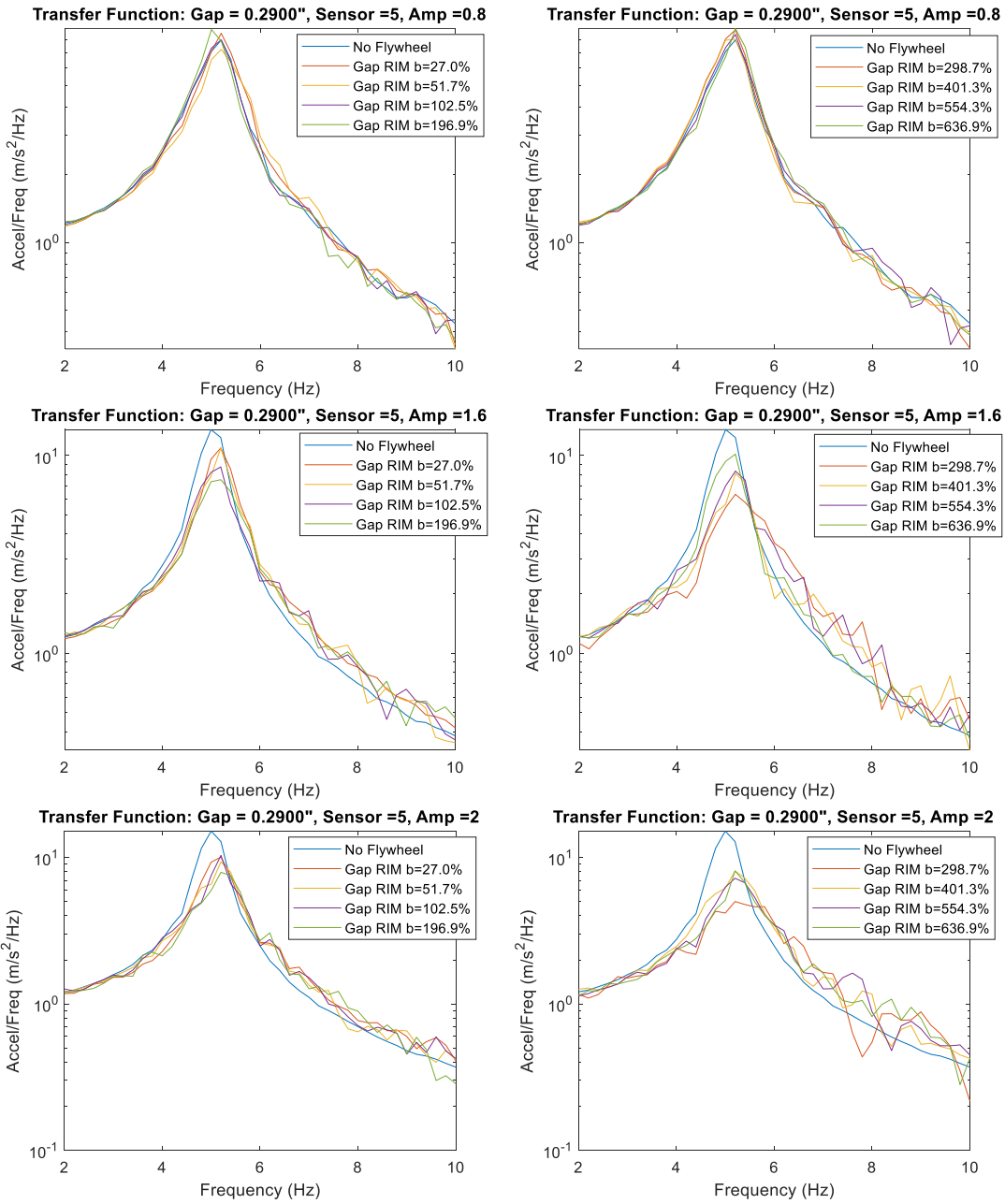


Figure 53 Sensor 5 estimated transfer function for all flywheel configurations, 2 – 10 Hz, compared to no flywheel case at Amp = 0.8, 1.6, and 2.0

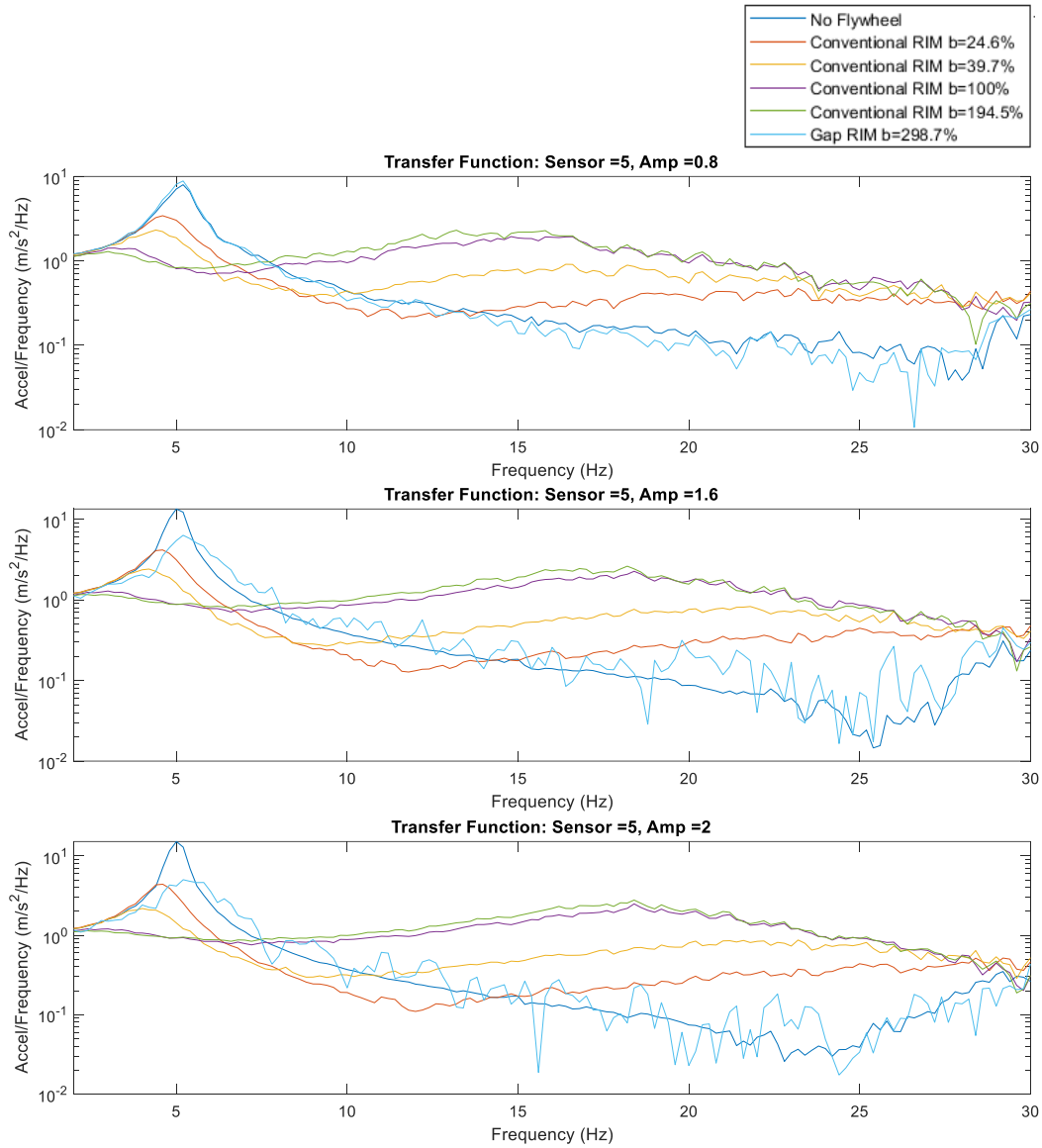


Figure 54 Sensor 5 estimated transfer function for 300% gap-type NRIM configuration compared to no flywheel case and linear flywheel cases from phase 2 at Amp = 0.8, 1.6, and 2.0

At amplitude = 2.0, the peak is reduced further than at amplitude = 1.6 and is visually equal to the 24.6% conventional inerter configuration. The transmitted forces for the gap-type NRIM are still significantly lower than all the conventional inerters, including the 24.6% configuration. It can also be visually seen that the location of the gap-type NRIM peak, or natural frequency, is increased significantly compared to the conventional cases and increased slightly compared to the no flywheel case.

Relevant numerical values from the without RIM, linear RIM, and gap-type NRIM are shown in Table 14 for amplitude=0.8, Table 15 for amplitude = 1.6, and Table 16 for amplitude = 2.0. The numerical values were computed using the base acceleration and sensor 5 data which collected data in the z- direction for the top mass plate. The time history response for each test was low pass filtered to 30 Hz in MATLAB. This was done because it was confirmed in the previous data figures that the inerter only impacted the response from 2-30 Hz. The peak acceleration of the top mass plate and the root mean square (RMS) of the top mass plate was then captured from the time history data. The peak was captured by taking the maximum value of the absolute valued filtered response. The RMS is the mean, or average, of the squares of the response. This value is important because it provides a measure of the overall amplitude of a response. The MATLAB command rms and the filtered time history signal were used to evaluate the RMS of the time history response. Low peak and low RMS values are desired for this application.

Additionally, MATLAB was used to evaluate the peak value, the H_2 analog of the estimated transfer function from the ground acceleration to the top mass acceleration considering the frequency range of 2-30 Hz, and the H_2 analog of the estimated transfer function from the ground acceleration to the top mass acceleration considering the frequency range of 10-30 Hz. Matlab was used to evaluate the transfer function for each test at each amplitude. This has been shown in previous figures and was previously explained. The transfer function result was then bounded for the frequency range of 2-30 Hz. The MATLAB command max was then used to capture the maximum, absolute value of the transfer function, or the peak that occurs at the natural frequency. The H_2 analog of the ground motion to top mass acceleration transfer function was evaluated for a frequency range of 2-30 Hz and 10-30 Hz. The frequency range of 10-30 Hz is of interest to show the effect the gap-type NRIM has on higher-frequency transmitted forces. The H_2 analog was previously explained and calculated in Chapter 4.1 and the same procedure was used to evaluate the H_2 analog of the bounded transfer function for each test at each amplitude. It is desired that both the peak and H_2 analog of the bounded transfer function from the ground motion to the top mass acceleration be as low as possible.

The observations previously stated from Figure 52, Figure 53, and Figure 54 are supported by the numerical values in Table 14. Table 14 describes the results for low amplitudes, or amplitude = 0.8. At 0.8 amplitude, the peak of the top mass from the time history response is generally higher for all gap NRIMs compared to the no RIM case and linear RIM cases. As inertance of the gap NRIM is increased the peak continues to increase. At high inertance values, the gap NRIM peak seems to stabilize around 0.4. Generally, the linear RIM peaks are slightly more or less than half the value of the gap NRIM peaks. A similar trend is also observed for the RMS of the top mass plate, where the gap NRIM RMS values are slightly higher than the no RIM case and consistently higher than the linear RIM cases. The RMS of the gap NRIM does not change as inertance is increased. The peak transfer function value from the ground motion to the top mass acceleration from 2-30 Hz is also the location of the natural frequency. It is desired that this peak be reduced as much as possible. The no RIM peak is much higher than the with RIM cases which was shown numerically in Chapter 4.1 and experimentally in Chapter 5. The gap NRIM has a reduced or equal peak to the no RIM case for inertance percentage values of 102.5%, or less. At this amplitude, higher values of inertance are showing to increase the peak. Additionally, it is shown that there is a threshold for linear RIMS where the peak is decreased to a point and then it is increased for higher inertance values.

Table 14 Numerical values from all experimental values tested at Amplitude = 0.8

| | Peak of Top Mass Plate from Time History Response (m/s²) | RMS of Top Mass Plate from Time History Response | Peak TF Value from the Ground Motion to the Top Mass Acceleration (m/s² / Hz) | H₂ of the TF from the Ground Motion to the Top Mass Acceleration | H₂ of the TF from the Ground Motion to the Top Mass Acceleration (10- 30 Hz) |
|---------------------------------|--|---|---|--|--|
| No RIM | 0.29 | 0.06 | 7.98 | 3.24 | 0.34 |
| Linear RIM b= 24.6% | 0.15 | 0.03 | 3.43 | 1.94 | 0.60 |
| Linear RIM b= 39.7% | 0.12 | 0.03 | 2.32 | 1.76 | 1.07 |
| Linear RIM b= 100% | 0.16 | 0.04 | 1.94 | 2.38 | 2.09 |
| Linear RIM b= 194.5% | 0.19 | 0.05 | 2.31 | 2.65 | 2.37 |
| Gap NRIM b= 27.0% | 0.33 | 0.07 | 8.55 | 3.34 | 0.34 |
| Gap NRIM b= 51.7% | 0.34 | 0.06 | 7.24 | 3.13 | 0.34 |
| Gap NRIM b= 102.5% | 0.38 | 0.07 | 7.99 | 3.24 | 0.33 |
| Gap NRIM b=196.9% | 0.40 | 0.07 | 8.89 | 3.35 | 0.33 |
| Gap NRIM b=298.7% | 0.37 | 0.07 | 8.85 | 3.48 | 0.31 |
| Gap NRIM b=401.3% | 0.39 | 0.07 | 8.05 | 3.34 | 0.33 |
| Gap NRIM b=554.3% | 0.39 | 0.07 | 8.45 | 3.33 | 0.34 |
| Gap NRIM b=636.9% | 0.40 | 0.07 | 8.98 | 3.36 | 0.33 |

Table 15 Numerical values from all experimental values tested at Amplitude = 1.6

| | Peak of Top Mass Plate from Time History Response (m/s²) | RMS of Top Mass Plate from Time History Response | Peak TF Value from the Ground Motion to the Top Mass Acceleration (m/s² / Hz) | H₂ of the TF from the Ground Motion to the Top Mass Acceleration | H₂ of the TF from the Ground Motion to the Top Mass Acceleration (10- 30 Hz) |
|---------------------------------|--|---|---|--|--|
| No RIM | 0.77 | 0.20 | 13.5 | 4.54 | 0.28 |
| Linear RIM b= 24.6% | 0.30 | 0.07 | 4.18 | 2.09 | 0.53 |
| Linear RIM b= 39.7% | 0.24 | 0.05 | 2.42 | 1.73 | 1.02 |
| Linear RIM b= 100% | 0.31 | 0.07 | 2.27 | 2.55 | 2.32 |
| Linear RIM b= 194.5% | 0.36 | 0.08 | 2.63 | 2.85 | 2.64 |
| Gap NRIM b= 27.0% | 0.80 | 0.17 | 10.9 | 3.89 | 0.39 |
| Gap NRIM b= 51.7% | 0.88 | 0.18 | 10.9 | 3.73 | 0.34 |
| Gap NRIM b= 102.5% | 0.81 | 0.17 | 8.73 | 3.43 | 0.32 |
| Gap NRIM b=196.9% | 0.88 | 0.17 | 7.52 | 3.26 | 0.34 |
| Gap NRIM b=298.7% | 0.80 | 0.15 | 6.35 | 2.97 | 0.42 |
| Gap NRIM b=401.3% | 0.85 | 0.17 | 8.08 | 3.10 | 0.35 |
| Gap NRIM b=554.3% | 0.91 | 0.18 | 8.32 | 3.36 | 0.41 |
| Gap NRIM b=636.9% | 1.06 | 0.19 | 10.1 | 3.70 | 0.33 |

Table 16 Numerical values from all experimental values tested at Amplitude = 2.0

| | Peak of Top Mass Plate from Time History Response (m/s²) | RMS of Top Mass Plate from Time History Response | Peak TF Value from the Ground Motion to the Top Mass Acceleration (m/s² / Hz) | H₂ of the TF from the Ground Motion to the Top Mass Acceleration (2- 30 Hz) | H₂ of the TF from the Ground Motion to the Top Mass Acceleration (10- 30 Hz) |
|---------------------------------|--|---|---|---|--|
| No RIM | 1.13 | 0.28 | 15.2 | 4.87 | 0.30 |
| Linear RIM b= 24.6% | 0.39 | 0.09 | 4.40 | 2.14 | 0.53 |
| Linear RIM b= 39.7% | 0.28 | 0.06 | 2.17 | 1.71 | 1.08 |
| Linear RIM b= 100% | 0.40 | 0.09 | 2.49 | 2.62 | 2.40 |
| Linear RIM b= 194.5% | 0.47 | 0.10 | 2.78 | 2.95 | 2.74 |
| Gap NRIM b= 27.0% | 0.85 | 0.20 | 10.1 | 3.73 | 0.32 |
| Gap NRIM b= 51.7% | 1.12 | 0.21 | 9.36 | 3.51 | 0.34 |
| Gap NRIM b= 102.5% | 1.27 | 0.23 | 10.4 | 3.53 | 0.34 |
| Gap NRIM b=196.9% | 1.02 | 0.23 | 7.94 | 3.25 | 0.38 |
| Gap NRIM b=298.7% | 1.08 | 0.18 | 5.01 | 2.70 | 0.37 |
| Gap NRIM b=401.3% | 1.37 | 0.23 | 8.10 | 3.40 | 0.36 |
| Gap NRIM b=554.3% | 1.18 | 0.22 | 7.23 | 3.15 | 0.37 |
| Gap NRIM b=636.9% | 1.23 | 0.22 | 8.12 | 3.10 | 0.41 |

The peak is decreased for $b = 24.6\%$, $b=39.7\%$, and $b=100\%$, but the peak is then increased for $b=194.5\%$. This is not referencing the original peak around 5 Hz, but this is the value of the new peak that forms, otherwise referred to as the high-frequency transmitted forces. Generally, the H_2 analog from 2-30 Hz for the gap NRIM exceeds the no RIM case, except for the gap NRIM case of $b=102.5\%$ where the H_2 analog is equal to the no RIM case and the gap NRIM case of $b=51.7\%$ where the H_2 norm is less than the no RIM case. The gap NRIM H_2 analog from 2-30 Hz exceeds the linear RIM for all cases. For 10-30 Hz, the gap NRIM H_2 analog is substantially lower than all the linear RIMs, but slightly higher than the no RIM case. For the linear RIM cases, the 10-30 Hz H_2 analog is increased as the inertance is increased, but there isn't a clear relationship between the H_2 analog and the inertance level of the gap NRIM. Although there is not a clear pattern of transmitted force reduction based on inertance level, at low amplitudes, it is apparent that the gap-type NRIM reduces high-frequency transmitted forces.

The results for amplitude =1.6 are shown in Table 15. Similar trends for the peak of the top mass from the time history are seen for 1.6 amplitude, as was seen for 0.8 amplitude where the gap NRIM peak is higher than the no RIM and linear RIM case. Also, like the 0.8 amplitude, the peak is increased for the gap NRIM as the inertance is increase. Previously, the peaks stabilized as inertance increased, but for this amplitude, the peak consistently increases in increments as the inertance increases. This is specifically seen where $b=298.7\%$ and greater. Additionally, there is a bigger difference between the linear RIM peaks and the gap NRIM peaks as was previously seen for the 0.8 amplitude case. The RMS of the top mass plate from the time history response differs than the previous amplitude. While the gap NRIM RMS values are still consistently larger than the linear RIM cases, all the gap NRIM RMS values are less than the no RIM case. Additionally, all gap NRIM peak transfer function values from the ground motion to the top mass acceleration from 2-30 Hz are consistently lower than the no flywheel case. The reductions are greater than what was seen for the 0.8 amplitude. Gap NRIM with $b=298.7\%$ had the furthest peak reduction which was previously shown in Figure 54. The gap NRIMs with inertance greater than 298.7% had a peak increase. As described for the 0.8 amplitude, the linear RIM with $b = 194.5\%$ had a peak increase compared to lower inertance values. Similar to the peak trends previously discussed, the H_2 norm has a similar trend where the gap NRIM H_2 norm is less than the no RIM case, but greater than the linear flywheels. Additionally, similar to how the gap NRIM had the lowest peak with $b=298.7\%$, the H_2 norm for $b=298.7\%$ is also the lowest compared to the other gap NRIMs. Similar trends that were shown for the 0.8 amplitude are shown for the 10-30 Hz H_2 analog at 1.6 amplitude. Again, the gap-type NRIM H_2 analog is substantially lower than all the linear RIMs, but slightly higher than the no RIM case. The linear H_2 analogs are substantially higher than both the no RIM case and all the gap-type NRIM cases. Additionally, like 0.8 amplitude, there is no clear relationship between inertance value and H_2 analog, but the gap-type NRIM has substantially lower transmitted forces in 10-30 Hz frequency range for amplitude=1.6.

Table 16 shows the results for amplitude = 2.0. The gap NRIM peak of the top mass from the time history response is less than the no RIM case for some inertance values. This differs from the previous amplitudes where the gap NRIM peaks were greater than the no RIM and linear RIM cases. The gap NRIMs with $b=27.0\%$, $b=51.7\%$, $b=196.9\%$, and $b= 298.7\%$ have peaks less than the no RIM case, but still greater than the linear RIM cases. Like amplitude = 1.6, the RMS values for the gap NRIMs are all consistently smaller than the no RIM case, however, the values are about two times greater than the linear RIM cases. The peak of the transfer function from the ground motion to the top mass acceleration has the same trend as amplitude = 1.6. The gap NRIM peak is decreased compared to the no RIM case, but is larger than the linear RIM. The gap RIM with $b=298.7\%$ also had the greatest reduction out of all the gap NRIMs. While the reduction was significant, the linear RIM had lower peaks for all inertance levels compared to $b=298.7\%$ gap NRIM. This was also seen in Figure 54. The H_2 norm of the transfer function

from the ground motion to the top mass acceleration from 2-30 Hz had a similar trend to 1.6 amplitude, but with one significant difference. While the gap NRIM H_2 norms are generally greater than the linear RIMs, the gap NRIM $b=298.7\%$ has a lower H_2 norm than the linear RIM of $b=194.5\%$. Previously, the gap NRIM H_2 norms were only less than the no RIM case. There isn't an explicit trend linking H_2 norm values with inertance values for the gap NRIM, but as inertance increases past 401.3%, the H_2 analog looks to be on a trending decline. Similar trends that were shown for the previous amplitudes are shown for the 10-30 Hz H_2 analog at 2.0 amplitude. The gap-type NRIM H_2 analog is substantially lower than all the linear RIMs, but slightly higher than the no RIM case for this amplitude as well. Additionally, the linear H_2 analogs are substantially higher than both the no RIM case and all the gap-type NRIM cases. For this amplitude, higher inertance values for the gap-type NRIM appear to have an increased H_2 analog. Despite these higher values, the gap-type NRIM has substantially lower transmitted forces in 10-30 Hz frequency range for all cases.

5.3.4 Conclusions

The gap inerter configurations investigated subjected to broadband loading shows the potential of the gap inerter concept at reducing transmitted forces in an isolation layer in comparison to the no RIM case and reducing transmitted forces at higher frequencies in comparison to the conventional RIM. It was observed that at an amplitude = 0.8, there was a relatively low amount of engagement of the flywheel. The gap inerter is dependent on the displacement of the mass which is largely dependent on the amplitude of the loading. The observation of lack of engagement indicates that it may be appropriate for a reduced gap size for certain loading conditions. As was visually shown and numerically expressed, at amplitudes of 1.6 and 2.0, the gap inerter peak was reduced, but the apparent natural frequencies were all slightly increased compared to the no flywheel case. The 300% gap-type NRIM configuration had the most drastically reduced peak out of all the flywheel configurations, but also kept the tail of the transmitted forces relatively low. The natural frequency of the system was increased significantly compared to the conventional RIM cases and increased slightly compared to the no flywheel case. The gap-type NRIM configuration has potential to reduce the amplitude of the natural frequency peak while avoiding high-frequency transmitted forces when subjected to broadband loading, however, the amount of peak reduction is dependent on the gap size and/or the amplitude of loading.

The numerical model created did not fully capture the behavior of the bushing-crown gap inerter due to differences in the mechanism of the physically realized design compared to what was numerically modeled. As previously mentioned, the device physically realized was a one-way gap device where engagement occurred when the displacement of the mass was greater than the negative of the gap, or when the mass displaced downward the full length of the gap and more. The physical device did not engage with the upward motion of the mass. The numerically modeled device was a two-way gap device where engagement also occurred if the displacement of the mass was greater than the gap distance, or if the mass displaced upward a distance greater than the gap. For example, in the physical realization, the gap size varied with response. As engagement increased, the gap became larger. This was not numerically modeled. Additionally, the spring component between the lead screw nut and thrust bearing took time to move. This movement was also not captured in the numerical model. It was also observed that the flywheel rotated in a one-way direction at times. Testing and results showed that the gap may need to be adjusted based on loading level, or amplitude. There may be an optimum gap size based on loading, but the lack of a numerical model that accurately captures the behavior has made it more difficult to discover the optimal gap size. Despite the differences in mechanics between the numerical model and the behavior of the physical realization, the numerical model did capture the reduction in transmitted forces trend, but the reduction differed from the physical gap NRIM results. The physical gap NRIM closely followed the no flywheel trend at later frequencies, while the numerical model, while reduced, was still consistently higher than the no flywheel system. It appears transmitted forces were reduced further in the physical realization, despite some inconsistencies in the design, than what was numerically modeled and expected.

Chapter 6 Conclusion & Recommendation for Future Work

The work presented in this thesis is part of a larger project that intends to design an effective isolation layer incorporating nonlinear rotational inertial mechanisms in marine isolation systems. Although linear rotational inertial mechanisms are commercially available and have been studied in a variety of different industries, there is a limited number of applications and experimental studies that have been done including inerter-based vibration control systems. Additionally, the disadvantages of linear inerters have been widely identified by researchers which has encouraged expansion into the design of nonlinear rotational inertial mechanisms. A potential NRIM can involve using inherent nonlinearities and exploiting them to benefit the inertial performance, or intentionally designing the inerter to behave in a nonlinear manner. The final marine isolation system will incorporate a nonlinear rotational inertial mechanism. Therefore, the goal of this thesis was to numerically simulate, design, fabricate, and test a NRIM with the intention of better understanding how the nonlinearities effect performance compared to linear inerters.

The process of developing the physical gap-type NRIM, or bushing-crown gap inerter, started with researching the inherent backlash, or play that occurs in gears. Play creates an inherent 'gap-like' effect between mating components of a system which results in the loss of motion. The play, or 'gap-like' effect was exploited to engage the flywheel at certain frequencies and disengage at others. A numerical model was created using the acceleration as the engagement, or disengagement criteria, but this idea proved to be difficult to physically realize in a passive way. Due to this, the displacement of the mass then became the qualifying criteria of engagement, or disengagement of the flywheel. The displacement is largely dependent on the amplitude of loading which is relatively simple to control in an experimental setting. After the numerical simulation was created, the bushing-crown gap inerter was designed and fabricated. A test apparatus, or die set, was purchased, and modified to simulate a SDOF system and test the bushing-crown gap inerter. The conventional inerter and bushing-crown gap inerter were installed and tested in the modified die set with various flywheel configurations, or inertance levels. While the bushing-crown gap inerter was a gap inerter, the physics of the numerical model varied from the physics of the experimental system.

The conventional inerter with various inertance levels showed the positive and negative effects of incorporating linear rotational inertial mechanisms in isolation layers. The conventional inerter experimentally showed reductions in the peak that occurs at the natural frequency and the reduction of the natural frequency. Numerically the conventional inerter has proven to be effective at reducing displacement. Displacement reduction was observed in experiments but was not confirmed by numerical measurements. Additionally, the conventional inerter proved to be consistent in experimental testing and behaves consistently with how it is numerically modeled. The negative effects of the conventional inerter mainly revolve around the impact of inertance levels that are too high. Although high inertance levels reduced the natural frequency and peak, another peak was essentially formed in the effect of transmitted forces. As the inertance increases, the higher-frequency transmitted forces increase. This is a huge drawback for incorporating linear inerters in machine isolation. Additionally, the inertance of a conventional inerter may need to be tuned or adjusted if there are mass changes in the isolated system being isolated. The experimental tests showed the relationship between inertance in the system and resulting transmitted forces. As inertance was increased, the transmitted forces subsequently increased. The increased transmitted forces were more significant for inertance levels over 100% of the mass. Needing to retune or adjust the system has always been an issue in passive structural control. It was previously mentioned that the need for retuning based on mass is a drawback for TMDs because if the device is not retuned, the device will not perform optimally. If the isolated system has any mass change

throughout its lifetime, the inertance in the inerter would need to be adjusted, or the transmitted forces could severely impact the system.

The bushing-crown gap inerter was also tested with various inertance levels and showed the positive and negative effects of incorporating nonlinear rotational inertial mechanisms in isolation layers. When compared to the system without a flywheel, the bushing-crown gap inerter proved to be effective in reducing the peak at the natural frequency and substantially decreasing the transmitted forces that followed the response of the system without the flywheel. These benefits came at the cost of slightly increasing the natural frequency. The main goal of an isolation system is to shift the natural frequency away from the loading frequency, thus avoiding resonance condition. Therefore, an increased natural frequency is not ideal. Additionally, the bushing-crown gap inerter did not reduce the peak compared to the linear inerter. While testing, there were inconsistencies relating to the gap size. As engagement of the flywheel occurred, the gap size became increasingly larger.

The gap inerter concept has potential for reducing in amplitude the isolation mode natural frequency peak compared to a system with no inertial mechanism and reducing the transmitted forces compared to a system isolated with a conventional inerter. A new gap inerter design that resembles the numerically simulated two-way displacement gap has been designed, fabricated, and installed in the test apparatus. The gap size inconsistencies observed in the bushing-crown gap inerter tests were not observed for the two-way gap, however, there have been other setbacks involving the flywheel engagement and disengagement mechanism. This device will need to be redesigned to better capture the engagement mechanism of the flywheel according to the displacements of the mass plate.

Additionally, other NRIM configurations and designs can be physically realized and tested. For example, the geometrically nonlinear inerter that was numerically simulated should be investigated further to physically realize the device for broadband loading. In addition to designing and fabricating a nonlinear device, the device needs to be tested with applicable marine loading. Due to the early design stage of this project and to gain better understanding of the nonlinear device, the marine white noise was not used experimentally. Once the nonlinear device is fabricated and efficient, the device should be installed in a marine isolation mount system and then can be incorporated into a marine environment.

References

- Balaji, P. S., and K. Karthik SelvaKumar. 2021. "Applications of Nonlinearity in Passive Vibration Control: A Review." *Journal of Vibration Engineering & Technologies* 9 (2): 183–213. <https://doi.org/10.1007/s42417-020-00216-3>.
- Brzeski, P., and P. Perlikowski. 2017. "Effects of Play and Inerter Nonlinearities on the Performance of Tuned Mass Damper." *Nonlinear Dynamics* 88 (2): 1027–41. <https://doi.org/10.1007/s11071-016-3292-1>.
- Carrella, A., M.J. Brennan, and T.P. Waters. 2007. "Static Analysis of a Passive Vibration Isolator with Quasi-Zero-Stiffness Characteristic." *Journal of Sound and Vibration* 301 (3–5): 678–89. <https://doi.org/10.1016/j.jsv.2006.10.011>.
- Deshpande, Sagar, Sudhir Mehta, and G. Nakhaie Jazar. 2006. "Optimization of Secondary Suspension of Piecewise Linear Vibration Isolation Systems." *International Journal of Mechanical Sciences* 48 (4): 341–77. <https://doi.org/10.1016/j.ijmecsci.2005.11.006>.
- Fu-Cheng Wang and Wei-Jiun Su. 2008. "Inerter Nonlinearities and the Impact on Suspension Control." In *2008 American Control Conference*, 3245–50. Seattle, WA: IEEE. <https://doi.org/10.1109/ACC.2008.4586992>.
- Gonzalez-Buelga, Alicia, Irina F. Lazar, Jason Z. Jiang, Simon A. Neild, and Daniel J. Inman. 2017. "Assessing the Effect of Nonlinearities on the Performance of a Tuned Inerter Damper: Effect of Nonlinearities on a Tuned Inerter Damper Performance." *Structural Control and Health Monitoring* 24 (3): e1879. <https://doi.org/10.1002/stc.1879>.
- Hu, Yinlong, Michael Z.Q. Chen, Zhan Shu, and Lixi Huang. 2015. "Analysis and Optimisation for Inerter-Based Isolators via Fixed-Point Theory and Algebraic Solution." *Journal of Sound and Vibration* 346 (June): 17–36. <https://doi.org/10.1016/j.jsv.2015.02.041>.
- Javidialesaadi, Abdollah, and Nicholas E. Wierschem. 2019a. "An Inerter-Enhanced Nonlinear Energy Sink." *Mechanical Systems and Signal Processing* 129 (August): 449–54. <https://doi.org/10.1016/j.ymssp.2019.04.047>.
- . 2019b. "Energy Transfer and Passive Control of Single-Degree-of-Freedom Structures Using a One-Directional Rotational Inertia Viscous Damper." *Engineering Structures* 196 (October): 109339. <https://doi.org/10.1016/j.engstruct.2019.109339>.
- Lazar, I. F., S.A. Neild, and D.J. Wagg. 2014. "Using an Inerter-Based Device for Structural Vibration Suppression: USING AN INERTER-BASED DEVICE FOR STRUCTURAL VIBRATION SUPPRESSION." *Earthquake Engineering & Structural Dynamics* 43 (8): 1129–47. <https://doi.org/10.1002/eqe.2390>.
- Lu, Zeqi, Michael J. Brennan, and Li-Qun Chen. 2016. "On the Transmissibilities of Nonlinear Vibration Isolation System." *Journal of Sound and Vibration* 375 (August): 28–37. <https://doi.org/10.1016/j.jsv.2016.04.032>.
- Ma, Ruisheng, Kaiming Bi, and Hong Hao. 2021. "Inerter-Based Structural Vibration Control: A State-of-the-Art Review." *Engineering Structures* 243 (September): 112655. <https://doi.org/10.1016/j.engstruct.2021.112655>.
- Makris, Nicos, M Asce, and Georgios Kampas. 2016. "Seismic Protection of Structures with Supplemental Rotational Inertia." *J. Eng. Mech.*, 11.

- Marian, Laurentiu, and Agathoklis Giaralis. 2014. "Optimal Design of a Novel Tuned Mass-Damper-Inerter (TMDI) Passive Vibration Control Configuration for Stochastically Support-Excited Structural Systems." *Probabilistic Engineering Mechanics* 38 (October): 156–64. <https://doi.org/10.1016/j.pro bengmech.2014.03.007>.
- Military Specification (MIL-STD 740-2(SH), Structureborne Vibratory Acceleration Measurements and Acceptance Criteria of Shipboard Equipment (DOD, 30 December 1986).
- Pradono, Mulyo Harris, Hirokazu Iemura, Akira Igarashi, and Afshin Kalantari. 2008. "Application of Angular-Mass Dampers to Base-Isolated Benchmark Building." *Structural Control and Health Monitoring* 15 (5): 737–45. <https://doi.org/10.1002/stc.270>.
- Scheibe, Frank, and Malcolm C. Smith. 2009. "A Behavioral Approach to Play in Mechanical Networks." *SIAM Journal on Control and Optimization* 47 (6): 2967–90. <https://doi.org/10.1137/070704605>.
- Shaw, S.W. 1986. "On the Dynamic Response of a System with Dry Friction." *Journal of Sound and Vibration* 108 (2): 305–25. [https://doi.org/10.1016/S0022-460X\(86\)80058-X](https://doi.org/10.1016/S0022-460X(86)80058-X).
- Smith, Malcolm C. 2020. "The Inerter: A Retrospective." *Annual Review of Control, Robotics, and Autonomous Systems* 3 (1): 361–91. <https://doi.org/10.1146/annurev-control-053018-023917>.
- Sun, X. Q., L. Chen, S. H. Wang, X. L. Zhang, and X. F. Yang. 2016. "Performance Investigation of Vehicle Suspension System with Nonlinear Ball-Screw Inerter." *International Journal of Automotive Technology* 17 (3): 399–408. <https://doi.org/10.1007/s12239-016-0041-x>.
- Wagg, David J. 2021. "A Review of the Mechanical Inerter: Historical Context, Physical Realisations and Nonlinear Applications." *Nonlinear Dynamics* 104 (1): 13–34. <https://doi.org/10.1007/s11071-021-06303-8>.
- Yang, Jian, Jason Zheng Jiang, and Simon A. Neild. 2020. "Dynamic Analysis and Performance Evaluation of Nonlinear Inerter-Based Vibration Isolators." *Nonlinear Dynamics* 99 (3): 1823–39. <https://doi.org/10.1007/s11071-019-05391-x>.
- Zhang, Ye-Wei, Yan-Nan Lu, Wei Zhang, Ying-Yuan Teng, Hui-Xin Yang, Tian-Zhi Yang, and Li-Qun Chen. 2019. "Nonlinear Energy Sink with Inerter." *Mechanical Systems and Signal Processing* 125 (June): 52–64. <https://doi.org/10.1016/j.ymssp.2018.08.026>.
- Zhang, Zhen, Ze-Qi Lu, Hu Ding, and Li-Qun Chen. 2019. "An Inertial Nonlinear Energy Sink." *Journal of Sound and Vibration* 450 (June): 199–213. <https://doi.org/10.1016/j.jsv.2019.03.014>.
- Zhang, Zhen, Ye-Wei Zhang, and Hu Ding. 2020. "Vibration Control Combining Nonlinear Isolation and Nonlinear Absorption." *Nonlinear Dynamics* 100 (3): 2121–39. <https://doi.org/10.1007/s11071-020-05606-6>.

Appendices

Appendix A: Codes and Calculations

Explanation of Documents:

A.1 Type 1 Equipment Marine Loading

A.2 Type 2 Equipment Marine Loading

A.3 Type 3 Equipment Marine Loading

A.4 Type 4 Equipment Marine Loading

A.5 Base Loaded Linear Systems Code

A.6 Mass Loaded Linear Systems Code

A.7 Base Loaded Acceleration Gap System Code

A.8 Base Loaded Acceleration Gap Figure & Numerical Values

A.9 Mass Loaded Acceleration Gap System Code

A.10 Mass Loaded Acceleration Gap Figure & Numerical Values

A.11 Base Loaded Displacement Gap System Code

A.12 Base Loaded Displacement Gap Figure & Numerical Values

A.13 Mass Loaded Displacement Gap System Code

A.14 Mass Loaded Displacement Gap Figure & Numerical Values

A.15 Geometrically Nonlinear Inerter Acceleration Derivation

A.16 Geometrically Nonlinear Inerter Code

A.17 Geometrically Nonlinear Inerter Figure & Numerical Values

A.18 RIM and NRIM Inertance Calculation – Flywheel 1

A.19 RIM Inertance Calculation – Flywheel 2A

A.20 NRIM Inertance Calculation – Flywheel 2B

A.21 RIM and NRIM Inertance Calculation Flywheel 3

A.22 RIM and NRIM Inertance Calculation Flywheel 4

A.23 RIM and NRIM Inertance Calculation Flywheel 5

A.24 RIM and NRIM Inertance Calculation Flywheel 6

A.25 RIM and NRIM Inertance Calculation Flywheel 7

A.26 RIM and NRIM Inertance Calculation Flywheel 8

A.1 TYPE 1 EQUIPMENT MARINE LOADING

```

%% 1/3 Octave Filtering Code
% Time Range and Sampling Frequency
Fs = 25000; %Sampling Rate
t = 0:1/Fs:100; %Scaled Time
L= 250000*2*10;
f = Fs*(0:(L/2))/L;

% White Noise
x = randn(length(t),1); % Original white noise signal generated from Matlab

%%Center Frequency(Hz) %Imported from MATLAB library
F0_all = [25.119 31.623 39.811 ...
          50.119 63.096 79.433 100 ...
          125.89 158.49 199.53 251.19 ...
          316.23 398.11 501.19 630.96 ...
          794.33 1000 1258.9 1584.9 ...
          1995.3 2511.9 3162.3 3981.1 ...
          5011.9 6309.6 7943.3 10000];

%%Type 1 Equipment (Reference MIL-STD 740;Figure 2)
dB = [78 81 83.5 ...
      86 89 91.5 94 ...
      96.5 99 102 103 ...
      104 105 106 107 ...
      108 109 110 111 ...
      112 113 114 115 ...
      116 117 118 119];

for a=1:length(F0_all) %using filter builder in MATLAB, this can be done
    %for 1 center frequency at a time, but we have 27 that we are interested in,
    %so we made a loop to do all center frequencies at once

    B = 3; % Bands per octave (we are wanting 1/3 Octave)
    N = 10; % Order
    F0 = F0_all(a) % Center Frequency
    h = fdesign.octave(B, 'Class 0', 'N,F0', N, F0, Fs);
    Hd(a) = design(h, 'butter', ...
        'SOSScaleNorm', 'Linf'); %Buttworth Filter is deisgn methods commonly used a
    frequency domain filter

% Filter White Noise
y(:,a) = filter(Hd(a),x); %Filter White Noise
yRMS(a) = rms(y(:,a)); %Take RMS of Each Column of Filtered White Noise

%Scale Filtered White Noise
%%Type 1 Equipment
for u=1:length(dB)
    SigRMS(u)=(10^-6)*(10^(dB(u)/20)); %This Equation is from the Military Standard (La
    (dB)= 20*Log(a/10) -> 10^-6 because micro gs
    b(a) = SigRMS(a)/yRMS(a); %Scale Factor = SignalRMS(using dB from Mil Std) / yRMS of
Signal

```

```
    yscaled(:,a)=y(:,a)*b(a); %Multiply Filtered Signal by Scale Factor
    yscaledRMS(a)=rms(yscaled(:,a)); %Take the RMS of each column of the scaled signal, ✓
this should be equal to SigRMS
end

end

% Add Filtered and Scaled Signal Together
ytotalsignal = sum(yscaled,2); %Adds each column of the scaled filtered signal together, ✓
so you have one number for each center frequency

%CPSD Parameters
nfft = floor(length(t)/20);
noverlap = nfft/2;
window = hann(nfft);

% Produce CPSD for noise before and after filtering
[YY,f] = cpsd(ytotalsignal,ytotalsignal,window,noverlap,nfft,Fs);
[XX,f] = cpsd(x,x,window,noverlap,nfft,Fs);

% Plot unfiltered and filtered white noise CPSD - Frequency Domain
%Unfiltered Noise
figure();
subplot(2,1,1)
semilogy(f,abs(XX))
xlabel('Frequency (Hz)')
ylabel('Accel/Freq (m/sec^2 /Hz)')
title('Unfiltered White Noise')
ylim([10^-20,10^0])

%Filtered Noise
subplot(2,1,2)
semilogy(f,abs(YY))
xlabel('Frequency (Hz)')
ylabel('Accel/Freq (m/sec^2 /Hz)')
title('Filtered White Noise - Type I Equipment ')

% Plot unfiltered and filtered white noise CPSD - Time Domain
%Unfiltered Noise
figure();
subplot(2,1,1)
plot(t,x)
xlabel('Time (sec)')
ylabel('Acceleration (m/sec^2)')
title('Unfiltered White Noise')
ylim([-10,10])

%Filtered Noise
subplot(2,1,2)
plot(t,ytotalsignal)
```

```
xlabel('Time (sec)')
ylabel('Acceleration (m/sec^2)')
title('Filtered White Noise - Type I Equipment ')

save('OctaveFilt_Type1_signal_100s', 'dB', 'Fs', 'F0_all','ytotalsignal') %Save Signal to
MATLAB File
```


A.2 TYPE 2 EQUIPMENT MARINE LOADING

```

%% 1/3 Octave Filtering Code
% Time Range and Sampling Frequency
Fs = 25000;
t = 0:1/Fs:100;
L= 250000*2*10;
f = Fs*(0:(L/2))/L;

% White Noise
x = randn(length(t),1);% Original white noise signal generated from MATLAB.

%%Center Frequency %Imported from MATLAB library
F0_all = [25.119 31.623 39.811 ...
          50.119 63.096 79.433 100 ...
          125.89 158.49 199.53 251.19 ...
          316.23 398.11 501.19 630.96 ...
          794.33 1000 1258.9 1584.9 ...
          1995.3 2511.9 3162.3 3981.1 ...
          5011.9 6309.6 7943.3 10000];

%%Type 2 Equipment (Reference MIL-STD 740;Figure 2)
dB = [79.5 80.5 81 ...
      82 83 83.5 84.5 ...
      85 86 87 88 ...
      88.5 89.5 90 ...
      91 92 92.5 93.5 ...
      94.5 95 96 97 98 ...
      98.5 99.5 100 101];

for a=1:length(F0_all)

B = 3;          % Bands per octave - 1/3 octave
N = 10;        % Order
F0 = F0_all(a) % Center Frequency
h = fdesign.octave(B, 'Class 0', 'N,F0', N, F0, Fs);
Hd(a) = design(h, 'butter', ...
              'SOSScaleNorm', 'Linf');

% Filter White Noise and Scale
%Type 2 Equipment
y(:,a) = filter(Hd(a),x);
yRMS(a) = rms(y(:,a));

%Type 2 Equip
for u=1:length(dB)
    SigRMS(u)=(10^-6)*(10^(dB(u)/20));
    b(a) = SigRMS(a)/yRMS(a);
    yscaled(:,a)=y(:,a)*b(a);
    yscaledRMS(a)=rms(yscaled(:,a));
end

```

```
end

% Add Filtered and Scaled Signals Together
ytotalsignal = sum(yscaled,2); %adds each row of every frequency together

%CPSD Parameters
nfft = floor(length(t)/20);
noverlap = nfft/2;
window = hann(nfft);

% Produce CPSD for noise before and after filtering
[YY,f] = cpsd(ytotalsignal,ytotalsignal,window,noverlap,nfft,Fs);
[XX,f] = cpsd(x,x,window,noverlap,nfft,Fs);

% Plot unfiltered and filtered white noise CPSD - Frequency Domain
figure();
subplot(2,1,1)
semilogy(f,abs(XX))
xlabel('Frequency (Hz)')
ylabel('Acceleration/Frequency (m/sec^2 /Hz)')
title('Unfiltered')

subplot(2,1,2)
semilogy(f,abs(YY))
xlabel('Frequency (Hz)')
ylabel('Acceleration/Frequency (m/sec^2 /Hz)')
title('Filtered')

save('OctaveFilt_Type2_signal_100s', 'dB', 'Fs', 'F0_all','ytotalsignal')
```

A.3 TYPE 3 EQUIPMENT MARINE LOADING

```

%% 1/3 Octave Filtering Example
% Time Range
Fs = 25000;
t = 0:1/Fs:100;
L= 250000*2*10;
f = Fs*(0:(L/2))/L;

% White Noise
x = randn(length(t),1); % Original white noise signal generated from MATLAB.

%%Center Frequency %Imported from MATLAB library
F0_all = [25.119 31.623 39.811 ...
          50.119 63.096 79.433 100 ...
          125.89 158.49 199.53 251.19 ...
          316.23 398.11 501.19 630.96 ...
          794.33 1000 1258.9 1584.9 ...
          1995.3 2511.9 3162.3 3981.1 ...
          5011.9 6309.6 7943.3 10000];

%%Type 3 Equipment (Reference MIL-STD 740;Figure 2)
dB = [85 85 85 ...
      85 85 85 85 ...
      85 85 85 85 ...
      85 85 85 85 ...
      85 85 85 85 ...
      85 85 85 85 ...
      85 85 85 85];

for a=1:length(F0_all)

B = 3; % Bands per octave (1/3)
N = 10; % Order
F0 = F0_all(a) % Center Frequency
h = fdesign.octave(B, 'Class 0', 'N,F0', N, F0, Fs);
Hd(a) = design(h, 'butter', ...
              'SOSScaleNorm', 'Linf');

% Filter White Noise and Scale
y(:,a) = filter(Hd(a),x);
yRMS(a) = rms(y(:,a));

%Type 3 Equip, SigRMS=85 dB for all frequencies (MIL STD FIG 2)
for u=1:length(dB)
    SigRMS(u)=(10^-6)*(10^(dB(u)/20));
    b(a) = SigRMS(a)/yRMS(a);
    yscaled(:,a)=y(:,a)*b(a);
    yscaledRMS(a)=rms(yscaled(:,a));
end

end

```

```
% Add Filtered and Scaled Signals Together
ytotalsignal = sum(yscaled,2); %adds each row of every frequency together

%CPSD Parameters
nfft = floor(length(t)/20);
noverlap = nfft/2;
window = hann(nfft);

% Produce CPSD for noise before and after filtering
[YY,f] = cpsd(ytotalsignal,ytotalsignal,window,noverlap,nfft,Fs);
[XX,f] = cpsd(x,x,window,noverlap,nfft,Fs);

% Plot unfiltered and filtered white noise CPSD - Frequency Domain
figure();
subplot(2,1,1)
semilogy(f,abs(XX))
xlabel('Frequency (Hz)')
ylabel('Acceleration/Frequency (m/sec^2 /Hz)')
title('Unfiltered')

subplot(2,1,2)
semilogy(f,abs(YY))
xlabel('Frequency (Hz)')
ylabel('Acceleration/Frequency (m/sec^2 /Hz)')
title('Filtered')

save('OctaveFilt_Type3_signal_100s', 'dB', 'Fs', 'F0_all','ytotalsignal')
```

A.4 TYPE 4 EQUIPMENT MARINE LOADING

```

%% 1/3 Octave Filtering Example
% Time Range
Fs = 25000;
t = 0:1/Fs:100;
L= 250000*2*10;
f = Fs*(0:(L/2))/L;

% White Noise
x = randn(length(t),1);% Original white noise signal generated from MATLAB.

%%Center Frequency %Imported from MATLAB library
F0_all = [25.119 31.623 39.811 ...
          50.119 63.096 79.433 100 ...
          125.89 158.49 199.53 251.19 ...
          316.23 398.11 501.19 630.96 ...
          794.33 1000 1258.9 1584.9 ...
          1995.3 2511.9 3162.3 3981.1 ...
          5011.9 6309.6 7943.3 10000];

%%Type 4 Equipment (Reference MIL-STD 740;Figure 2)
dB = [74.5 75 76 ...
      77 78 78.5 79.5 ...
      80 81 82 83 ...
      83.5 84.5 85 86 ...
      87 87.5 88.5 89.5 ...
      90 91 92 92.5 ...
      93.5 94 95 96];

for a=1:length(F0_all)

B = 3;          % Bands per octave - 1/3 octave
N = 10;        % Order
F0 = F0_all(a) % Center Frequency
h = fdesign.octave(B, 'Class 0', 'N,F0', N, F0, Fs);
Hd(a) = design(h, 'butter', ...
              'SOSScaleNorm', 'Linf');

% Filter White Noise and Scale
%Type 4 Equipment
y(:,a) = filter(Hd(a),x);
yRMS(a) = rms(y(:,a));

%Type 4 Equip, SigRMS=85 dB for all frequencies (MIL STD FIG 2)
for u=1:length(dB)
    SigRMS(u)=(10^-6)*(10^(dB(u)/20));
    b(a) = SigRMS(a)/yRMS(a);
    yscaled(:,a)=y(:,a)*b(a);
    yscaledRMS(a)=rms(yscaled(:,a));
end

```

```
end

% Add Filtered and Scaled Signals Together
ytotalsignal = sum(yscaled,2); %adds each row of every frequency together

%CPSD Parameters
nfft = floor(length(t)/20);
noverlap = nfft/2;
window = hann(nfft);

% Produce CPSD for noise before and after filtering
[YY,f] = cpsd(ytotalsignal,ytotalsignal,window,noverlap,nfft,Fs);
[XX,f] = cpsd(x,x,window,noverlap,nfft,Fs);

% Plot unfiltered and filtered white noise CPSD - Frequency Domain
figure();
subplot(2,1,1)
semilogy(f,abs(XX))
xlabel('Frequency (Hz)')
ylabel('Acceleration/Frequency (m/sec^2 /Hz)')
title('Unfiltered')
% ylim([10^-10,10^0])

subplot(2,1,2)
semilogy(f,abs(YY))
xlabel('Frequency (Hz)')
ylabel('Acceleration/Frequency (m/sec^2 /Hz)')
title('Filtered')
% ylim([10^-10,10^0])

save('OctaveFilt_Type4_signal_100s', 'dB', 'Fs', 'F0_all','ytotalsignal')
```

A .5 BASE LOADED LINEAR SYSTEMS CODE

```

clear all
close all
warning('off')
load('OctaveFilt_Type1_signal_100s.mat'); %Marine white noise for Type 1 equipment

%DOF
% y = Absolute Displacement of Top plate
% w = Relative Displacement of Top Plate

%System Parameters
m=17.92; %Mass (kg)
k=19858.68; %Spring coefficient (N/m)--4 springs @ 28.349 lb/in EA
zeta=.2; %Damping ratio = 20%
b=17.92; %Inertance (kg)
cb=2*zeta*sqrt(k*(m+b)); %Damping coefficient(with inerter)
c=2*zeta*sqrt(k*m); %Damping coefficient (without inerter)
k2= 9948.6; %Low Stiffness Spring Coefficient (N/m) (Nat Freq = 3.6 Hz)

%State Space Representations
%Linear System Without RIM:
A=[0 1;-k/(m) -c/(m)];
B=[0; -1];
C=[1 0 ; 0 1; -k/(m) -c/(m); -k/(m) -c/(m)];
D=[0 ; 0; -1; 0];
A=double(A);
B=double(B);
C=double(C);
D=double(D);
sys=ss(A,B,C,D);

%Linear System with RIM:
Ab=[0 1;-k/(m+b) -cb/(m+b)];
Bb=[0 ; -m/(m+b)];
Cb=[1 0 ; 0 1; -k/(m+b) -cb/(m+b); -k/(m+b) -cb/(m+b)];
Db=[0 ; 0 ; (-m/(m+b)); (-m/(m+b))+1];
Ab=double(Ab);
Bb=double(Bb);
Cb=double(Cb);
Db=double(Db);
sysb=ss(Ab,Bb,Cb,Db);

%Linear System With Low Stiffness:
Ak=[0 1;-k2/(m) -c/(m)];
Bk=[0; -1];
Ck=[1 0 ; 0 1; -k2/(m) -c/(m); -k2/(m) -c/(m)];
Dk=[0 ; 0; -1; 0];
Ak=double(Ak);
Bk=double(Bk);
Ck=double(Ck);
Dk=double(Dk);
sysk=ss(Ak,Bk,Ck,Dk);

```

```

%Simulate Linear Responses
%ytotalsignal = acceleration
fs= 25000;
SF = 100; %Scale Factor used to scale marine white noise frequency down
t=[0:1/fs:100]*SF; %Time
P=[ytotalsignal]; %Load = Acceleration
ugdot=cumtrapz(t,ytotalsignal); %Velocity ground signal
ug=cumtrapz(t,ugdot); %Displacement ground signal
xO=[0 0]; %Initial Conditions
xb=lsim(sysb,P,t,xO); %Simulation with RIM
x=lsim(sys,P,t,xO); %Simulation w/o RIM
xk=lsim(sysk,P,t,xO); %Simulation with Low Stiffness

%Results with RIM
wb=xb(:,1); %Relative displacement
wdotb=xb(:,2); %Relative velocity
wdotdotb= xb(:,3); %Relative acceleration
yb=wb + ug; %Absolute displacement
ydotb=wdotb + ugdot; %Absolute velocity
ydotdotb=xb(:,4); %Absolute acceleration

%Results without RIM
w=x(:,1); %Relative displacement
wdot=x(:,2); %Relative velocity
wdotdot= x(:,3); %Relative acceleration
y=w + ug; %Absolute displacement
ydot=wdot + ugdot; %Absolute velocity
ydotdot=x(:,4); %Absolute acceleration

%Results with low stiffness
wk= xk(:,1); %Relative displacement
wdotk= xk(:,2);%Relative velocity
wdotdotk= xk(:,3); %Relative acceleration
yk=wk + ug; %Absolute displacement
ydotk=wdotk + ugdot; %Absolute velocity
ydotdotk=xk(:,4); %Absolute acceleration

%CPSD Parameters
nfft = floor(length(t)/20);
window = hann(nfft);
noverlap = floor(nfft/2);
fs2=fs/SF; %Marine white noise frequency scaling

%Relative Displacement Transfer Function Estimate & Plots
[txwb,f]=tfestimate(P,wb>window,noverlap,nfft,fs2); %with RIM
[txw,f]=tfestimate(P,w>window,noverlap,nfft,fs2); %without RIM
[txwk,f]=tfestimate(P,wk>window,noverlap,nfft,fs2); %Low Stiffness
f1=figure
subplot(1,2,1)
semilogy(f,abs(txwb))

```



```

hold on
semilogy(f,abs(twx))
hold on
semilogy(f,abs(twxk),'m')
xlabel('Frequency (Hz)')
ylabel('Relative Displacement/Frequency (m/Hz)')
legend('Isolation with RIM','Isolation without RIM','Isolation with Low Stiffness')
title('Relative Displacement Transfer Function')
xlim([0,50])

%Absolute Acceleration Transfer Function Estimate & Plots
[txyba,f]=tfestimate(P,ydotdotb>window,noverlap,nfft,fs2); %with RIM
[txya,f]=tfestimate(P,ydotdot>window,noverlap,nfft,fs2); %Without RIM
[txyka,f]=tfestimate(P,ydotdotk>window,noverlap,nfft,fs2); %Low Stiffness
figure(f1)
subplot(1,2,2)
semilogy(f,abs(txyba))
hold on
semilogy(f,abs(txya))
hold on
semilogy(f,abs(txyka),'m')
xlabel('Frequency (Hz)')
ylabel('Absolute Acceleration/Frequency (m/s^2/Hz)')
legend('Isolation with RIM','Isolation without RIM','Isolation with Low Stiffness')
title('Absolute Acceleration Transfer Function')
xlim([0,50])

%Time History Response
%Displacement with RIM
f2=figure
subplot(1,3,1)
plot(t,wb) %Relative Displacement with RIM
xlabel('Time(sec)')
ylabel('Displacement (m)')
legend('Isolation with RIM')
%Displacement without RIM
figure(f2)
subplot(1,3,2)
plot(t,w,'r') %Relative Displacement without RIM
xlabel('Time(sec)')
ylabel('Displacement (m)')
legend('Isolation without RIM')
%Displacement Low stiffness
figure(f2)
subplot(1,3,3)
plot(t,wk,'m') %Relative Displacement without RIM
xlabel('Time(sec)')
ylabel('Displacement (m)')
legend('Isolation with Low Stiffness')

%Natural Frequency of Linear System

```

```

wn_winerter = sqrt(k/(m+b))/(2*pi)
wn_woinerter = sqrt(k/m)/(2*pi)
wn_lowstiffness = sqrt(k2/m)/(2*pi)

%Peak Max Displacement Transfer Function
w_inertermaxdisp= max(abs(txwb))
wo_inertermaxdisp=max(abs(txw))
lowstiffnesss_maxdisp=max(abs(txwk))

%Freq where peak occurs:
ttt=[f,abs(txwb)];
idx = find(ttt(:,2) == w_inertermaxdisp)
freq_winerter=f(idx)

%Peak Absolute Acceleration Transfer Function
w_inertermaxabsaccel= max(abs(txyba))
wo_inertermaxabsaccel=max(abs(txya))
lowstiffness_maxabsaccel=max(abs(txyka))

%H2 Norm Calculations
%Frequency Bounds: 1-100 Hz
fstart=find(f==1);
fend=find(f==100);
fstep=0.002;
fbounded=[f(fstart):fstep:f(fend)]';

%Relative Displacement Transfer Function H2 Norm
txwb=abs(txwb);
txwb_bounded=txwb(fstart:fend,:);
area4=cumtrapz(fbounded,txwb_bounded.^2);
H2n_disp_w_inerter = sqrt((1/(2*pi))*area4(end))

txw=abs(txw);
txw_bounded=txw(fstart:fend,:);
area5=cumtrapz(fbounded,txw_bounded.^2);
H2n_disp_wo_inerter =sqrt((1/(2*pi))*area5(end))

txwk=abs(txwk);
txwk_bounded=txwk(fstart:fend,:);
area5=cumtrapz(fbounded,txwk_bounded.^2);
H2n_disp_lowstiffness =sqrt((1/(2*pi))*area5(end))

%Absolute Acceleration Transfer Function H2 Norm
txyba=abs(txyba);
txyba_bounded=txyba(fstart:fend,:);
area7=cumtrapz(fbounded,txyba_bounded.^2);
H2n_isol_w_inerter = sqrt((1/(2*pi))*area7(end))

txya=abs(txya);
txya_bounded=txya(fstart:fend,:);
area8=cumtrapz(fbounded,txya_bounded.^2);

```

```
H2n_isol_wo_inerter = sqrt((1/(2*pi))*area8(end))

txyka=abs(txyka);
txyka_bounded=txyka(fstart:fend,:);
area8=cumtrapz(fbounded,txyka_bounded.^2);
H2n_isol_lowstiffness = sqrt((1/(2*pi))*area8(end))
```

A.6 MASS LOADED LINEAR SYSTEMS CODE

```

clear all
close all
warning('off')
load('OctaveFilt_Type1_signal_100s.mat'); %Marine white noise for Type 1 equipment

%DOF
% y = Absolute Displacement of Top plate

%System Parameters
m=17.92; %Mass (kg)
k=19858.68; %Spring coefficient (N/m) -- 4 springs @ 28.349 lb/in EA
zeta=0.2; %Damping Ratio = 20%
b=17.92; %Inertance (kg)
cb=2*zeta*sqrt(k*(m+b)); %Damping coefficient(with inerter)
c=2*zeta*sqrt(k*m); %Damping coefficient (without inerter)

%State Space Representations
%Linear System Without RIM:
A=[0 1;-k/(m) -c/(m)];
B=[0 ; 1/(m)];
C=[1 0 ; 0 1 ; -k/(m) -c/(m)];
D=[0 ; 0; 1/(m)];
A=double(A);
B=double(B);
C=double(C);
D=double(D);
sys=ss(A,B,C,D);

%Linear System with RIM:
Ab=[0 1;-k/(m+b) -cb/(m+b)];
Bb=[0 ; 1/(m+b)];
Cb=[1 0 ; 0 1;-k/(m+b) -cb/(m+b)];
Db=[0 ; 0 ; 1/(m+b)];
Ab=double(Ab);
Bb=double(Bb);
Cb=double(Cb);
Db=double(Db);
sysb=ss(Ab,Bb,Cb,Db);

%Simulate Response
%ytotalsignal=acceleration
fs=25000;
SF=100; %Scale Factor used to scale marine white noise frequency down
t=[0:1/fs:100]*SF; %Time
noise = ytotalsignal*m; %Load (F = m*a)
P=noise; %Load
xO=[0 0]; %Initial Conditions
xb=lsim(sysb,P,t,xO); %Simulation with RIM
x=lsim(sys,P,t,xO); %Simulation w/o RIM

%Results with Inerter

```

```

yb=xb(:,1);%Absolute displacement
ydotb=xb(:,2); %Absolute velocity
ydotdotb=xb(:,3); %Absolute acceleration
isolforceb = (k*yb)+(cb*ydotb)+(b*ydotdotb); %Isolator force

%Results without Inerter
y=x(:,1); %Absolute displacement
ydot=x(:,2); %Absolute velocity
ydotdot=x(:,3); %Absolute acceleration
isolforce=(k*y)+(c*ydot); %Isolator force

%CPSD Parameters
nfft = floor(length(noise)/20);
window = hann(nfft);
noverlap = floor(nfft/2);
fs2=fs/SF %Marine white noise natural frequency scaling

%Absolute Displacement Transfer Function Estimate & Plots
[txyb,f]=tfestimate(P,yb>window,noverlap,nfft,fs2); %With RIM
[txy,f]=tfestimate(P,y>window,noverlap,nfft,fs2); %Without RIM
f1=figure
subplot(1,2,1)
semilogy(f,abs(txyb))
hold on
semilogy(f,abs(txy))
xlabel('Frequency (Hz)')
ylabel('Absolute Displacement/Frequency (m/Hz)')
legend('Isolation with RIM','Isolation without RIM')
title('Absolute Displacement Transfer Function')
ylim([10^-7,10^-3])
xlim([0,50])

%Isolator Force Transfer Function Estimate & Plots
[txybisol,f]=tfestimate(P,isolforceb>window,noverlap,nfft,fs2); %With RIM
[txyisol,f]=tfestimate(P,isolforce>window,noverlap,nfft,fs2); %Without RIM
figure(f1)
subplot(1,2,2)
semilogy(f,abs(txybisol))
hold on
semilogy(f,abs(txyisol))
xlabel('Frequency (Hz)')
ylabel('Isolator Force/Frequency (N/Hz)')
legend('Isolation with RIM','Isolation without RIM')
title('Isolator Force Transfer Function')
xlim([0,50])

%Time History Response
f2=figure
subplot(1,2,1)
plot(t,yb) %Absolute Displacement with RIM
xlabel('Time(sec)')

```

```

ylabel('Displacement (m)')
legend('Isolation with RIM')
%Displacement without RIM
figure(f2)
subplot(1,2,2)
plot(t,y,'r')
xlabel('Time(sec)')
ylabel('Displacement (m)')
legend('Isolation without RIM')

%Natural Frequency of Linear System
wn_winerter = sqrt(k/(m+b))/(2*pi)
wn_woinerter = sqrt(k/m)/(2*pi)

%Peak Max Displacement Transfer Function
w_inertermaxdisp= max(abs(txyb))
wo_inertermaxdisp=max(abs(txy))
%Freq where peak occurs:
ttt=[f,abs(txyb)];
idx = find(ttt(:,2) == w_inertermaxdisp)
freq_winerter=f(idx)

%Peak Isolator Force Transfer Function
w_inertermaxisol= max(abs(txybisol))
wo_inertermaxisol=max(abs(txyisol))

%H2 Norm Calculations
%Frequency Bounds: 1- 100 Hz
fstart=find(f==1);
fend=find(f==100);
fstep=0.002;
fbounded=[f(fstart):fstep:f(fend)]';

%Absolute Displacement Transfer Function H2 Norm:
txyb=abs(txyb);
txyb_bounded=txyb(fstart:fend,:);
area4=cumtrapz(fbounded,txyb_bounded.^2);
H2n_disp_w_inerter = sqrt((1/(2*pi))*area4(end))
txy=abs(txy);
txy_bounded=txy(fstart:fend,:);
area5=cumtrapz(fbounded,txy_bounded.^2);
H2n_disp_wo_inerter =sqrt((1/(2*pi))*area5(end))

%Isolator Force Transfer Function H2 Norm:
txybisol=abs(txybisol);
txybisol_bounded=txybisol(fstart:fend,:);
area7=cumtrapz(fbounded,txybisol_bounded.^2);
H2n_isol_w_inerter = sqrt((1/(2*pi))*area7(end))
txyisol=abs(txyisol);
txyisol_bounded=txyisol(fstart:fend,:);
area8=cumtrapz(fbounded,txyisol_bounded.^2);

```

```
H2n_isol_wo_inerter = sqrt((1/(2*pi))*area8(end))
```

A.7 BASE LOADED ACCELERATION GAP SYSTEM CODE

```

clear all
close all
warning('off')
load('OctaveFilt_Type1_signal_100s.mat'); %Marine white noise for Type 1 equipment

%DOF
% y = Absolute Displacement of Top plate
% w = Relative Displacement of Top Plate

%System Parameters
m=17.92; %Mass (kg)
k=19858.68; %Spring coefficient (N/m)--4 springs @ 28.349 lb/in EA
zeta=.2; %Damping ratio = 20%
b=17.92; %Inertance (kg)
cb=2*zeta*sqrt(k*(m+b)); %Damping coefficient(with inerter)
c=2*zeta*sqrt(k*m); %Damping coefficient (without inerter)
g=1.3; %Acceleration Gap (m/s^2)

%State Space Representations
%Linear System Without RIM:
A=[0 1;-k/(m) -c/(m)];
B=[0; -1];
C=[1 0 ; 0 1; -k/(m) -c/(m); -k/(m) -c/(m)];
D=[0 ; 0; -1; 0];
A=double(A);
B=double(B);
C=double(C);
D=double(D);
sys=ss(A,B,C,D);

%Linear System with RIM:
Ab=[0 1;-k/(m+b) -cb/(m+b)];
Bb=[0 ; -m/(m+b)];
Cb=[1 0 ; 0 1; -k/(m+b) -cb/(m+b); -k/(m+b) -cb/(m+b)];
Db=[0 ; 0 ; (-m/(m+b)); (-m/(m+b))+1];
Ab=double(Ab);
Bb=double(Bb);
Cb=double(Cb);
Db=double(Db);
sysb=ss(Ab,Bb,Cb,Db);

%Gap Inerter
%System with RIM Engaged:
Ag=[0 1;-k/(m+b) -cb/(m+b)];
Bg=[0 ; -m/(m+b)];
Cg=[1 0 ; 0 1; -k/(m+b) -cb/(m+b); -k/(m+b) -cb/(m+b)];
Dg=[0 ; 0 ; (-m/(m+b)); (-m/(m+b))+1];
Ag=double(Ag);
Bg=double(Bg);
Cg=double(Cg);
Dg=double(Dg);

```



```

sysgb=ss(Ag,Bg,Cg,Dg);
%System without RIM:
An=[0 1;-k/(m) -c/(m)];
Bn=[0; -1];
Cn=[1 0 ; 0 1; -k/(m) -c/(m); -k/(m) -c/(m)];
Dn=[0 ; 0; -1; 0];
An=double(An);
Bn=double(Bn);
Cn=double(Cn);
Dn=double(Dn);
sysgb2=ss(An,Bn,Cn,Dn);

%Simulate Response
%ytotalsignal = acceleration
fs= 25000;
SF=100; %Scale Factor used to scale marine white noise frequency down
t=[0:1/fs:100]*SF; %Time
P=[ytotalsignal]; %Load = acceleration
ugdot=cumtrapz(t/1000,ytotalsignal); %Velocity ground signal
ug=cumtrapz(t/1000,ugdot); %Displacement ground signal
xO=[0 0]; %Initial Conditions
xb=lsim(sysb,P,t,xO); %Simulation with RIM
x=lsim(sys,P,t,xO); %Simulation w/o RIM

%Results with RIM
wb=xb(:,1); %Relative displacement
wdotb=xb(:,2); %Relative velocity
wdotdotb= xb(:,3); %Relative acceleration
yb=wb + ug; %Absolute displacement
ydotb=wdotb + ugdot; %Absolute velocity
ydotdotb=xb(:,4); %Absolute acceleration

%Results without RIM
w=x(:,1); %Relative displacement
wdot=x(:,2); %Relative velocity
wdotdot= x(:,3); %Relative acceleration
y=w + ug; %Absolute displacement
ydot=wdot + ugdot; %Absolute velocity
ydotdot=x(:,4); %Absolute acceleration

%Gap Inerter Results
wg=[0]; %Relative displacement
wgdot=[0]; %Relative velocity
wgdotdot=[0]; %Relative acceleration
yg=[0]; %Absolute displacement
ydotg=[0]; %Absolute velocity
ydotdotg=[0]; %Absolute acceleration

for a=2:length(t)-1;

    if abs(wgdotdot(end)) > g %Inerter Engaged

```

```

    Pbg=P;
    sys = sysgb;
    TrackStateLSIM(a) = 1; %Track Inerter Engagement
    x0=[yg(end) ydotg(end)];
    xg=lsim(sys,Pbg(a:a+1,:),t(a:a+1),x0);
else
    sys = sysgb2; %Inerter Disengaged
    TrackStateLSIM(a) = 2; %Track Inerter Disengagement
    x0=[yg(end) ydotg(end)];
    xg=lsim(sys,P(a:a+1),t(a:a+1),x0);
end

%Assign new variables for next iteration
wgnew=xg(:,1);
wgdotnew=xg(:,2);
wgdotdotnew=xg(:,3);
ydotdotnew=xg(:,4);
wg_new=wgnew(end);
wgdot_new=wgdotnew(end);
wgdotdot_new=wgdotdotnew(end);
ydotdot_new=ydotdotnew(end);
wg(a+1)=wg_new;
wgdot(a+1)=wgdot_new;
wgdotdot(a+1)=wgdotdot_new;
ydotdotg(a+1)=ydotdot_new;

yg(a+1) = wg(a+1) + ug(a+1); %Absolute Displacement
ydotg(a+1)=wgdot(a+1)+ugdot(a+1); %Absolute Velocity
end

%CPSD Parameters
nfft = floor(length(t)/20);
window = hann(nfft);
noverlap = floor(nfft/2);
fs2=fs/SF %marine white noise frequency scaling

%Absolute Acceleration Transfer Function Estimate & Plots
[txyba,f]=tfestimate(P,ydotdotb>window,noverlap,nfft,fs2); %with RIM
[txya,f]=tfestimate(P,ydotdot>window,noverlap,nfft,fs2); %without RIM
[txyga,f]=tfestimate(P,ydotdotg>window,noverlap,nfft,fs2); %Accel Gap RIM
f5=figure
semilogy(f,abs(txyba))
hold on
semilogy(f,abs(txya))
hold on
semilogy(f,abs(txyga))
xlabel('Frequency (Hz)')
ylabel('Absolute Acceleration/Frequency (m/s^2/Hz)')
legend('Isolation with RIM','Isolation without RIM','Isolation with Gap RIM')
title('Absolute Acceleration Transfer Function (Gap = 0.7 m/s^2)')
xlim([0,50])

```

```
ylim([10^-3,10^1])

%Relative Displacement Transfer Function Estimate & Plots
[txwb,f]=tfestimate(P,wb>window,noverlap,nfft,fs2); %with RIM
[txw,f]=tfestimate(P,w>window,noverlap,nfft,fs2); %without RIM
[txwg,f]=tfestimate(P,wg>window,noverlap,nfft,fs2); %Accel Gap RIM
f5=figure
semilogy(f,abs(txwb))
hold on
semilogy(f,abs(txw))
hold on
semilogy(f,abs(txwg))
xlabel('Frequency (Hz)')
ylabel('Relative Displacement/Frequency (m/Hz)')
legend('Isolation with RIM','Isolation without RIM','Isolation with Gap RIM')
title('Relative Displacement Transfer Function (Gap = 0.7 m/s^2)')
xlim([0,50])
ylim([10^-7,10^-2])

%Inerter Engagement Percentage
NumberofTimesInerterEngaged = numel(find(TrackStateLSIM==1))
NumberofTimesInerterDisengaged = numel(find(TrackStateLSIM==2))
PercentEngaged = (NumberofTimesInerterEngaged / 2500000)*100

%Save Results for Figure and Calculation Code
save('GroundLoaded_AccelGap_13',
'g','f','txwb','txw','txwg','txyba','txya','txyga','PercentEngaged') %Save Signal to
MATLAB File
```

A .8 BASE LOADED ACCELERATION GAP FIGURE & NUMERICAL VALUES

```
%Accel Gap Figure, Important Values & H2 Norm Calculations
```

```
%-----
```

```
%Gap = 0.1 (Variable 00)
```

```
load('GroundLoaded_AccelGap_01') %Load Saved Data
```

```
%Reassign Variables
```

```
txw00=txw;
```

```
txwb00=txwb;
```

```
txwg00=txwg;
```

```
txya00=txya;
```

```
txyba00=txyba;
```

```
txyga00=txyga;
```

```
%Frequency Bounds
```

```
fstart=find(f==1);
```

```
fend=find(f==100);
```

```
fstep=0.002;
```

```
fbounded=[f(fstart):fstep:f(fend) ]';
```

```
%Peak Relative Displacement TF & Natural Frequency
```

```
txwg00=abs(txwg00);
```

```
txwg00_bounded=txwg00(fstart:fend,:);
```

```
p00=[fbounded, txwg00_bounded];
```

```
gap_inertermaxdisp00=max(txwg00_bounded)
```

```
idxg = find(p00(:,2) == gap_inertermaxdisp00);
```

```
freq_gapinerter00=fbounded(idxg)
```

```
%Peak Absolute Acceleration TF (Transmitted force)
```

```
txyga00=abs(txyga00);
```

```
txyga00_bounded=txyga00(fstart:fend,:);
```

```
gap_inertermaxabsaccel00=max(txyga00_bounded)
```

```
%Relative Displacement TF Estimate, Gap = 0.1
```

```
f1=figure
```

```
subplot(2,4,1)
```

```
semilogy(f,abs(txwb00))
```

```
hold on
```

```
semilogy(f,abs(txw00))
```

```
hold on
```

```
semilogy(f,abs(txwg00))
```

```
xlabel('Frequency (Hz)')
```

```
ylabel('Rel Disp/Freq (m/Hz)')
```

```
title('(a) Gap = 0.1 m/s^2')
```

```
xlim([0,50])
```

```
ylim([10^-7,10^-2])
```

```
%Relative Displacement H2 norm:
```

```
area6=cumtrapz(fbounded,txwg00_bounded.^2);
```

```
H2n_disp_gap01_inerter = sqrt((1/(2*pi))*area6(end))
```

```
%Absolute Acceleration TF Estimate, Gap = 0.1
```

```
figure(f1)
```

```

subplot(2,4,5)
semilogy(f,abs(txyba00))
hold on
semilogy(f,abs(txya00))
hold on
semilogy(f,abs(txyga00))
xlabel('Frequency (Hz)')
ylabel('Abs Accel/Freq (m/s^2/Hz)')
title('(e) Gap = 0.1 m/s^2')
ylim([10^-3,10^1])
xlim([0,50])

%Absolute Acceleration H2 Norm:
txyga00=abs(txyga00);
txyga00_bounded=txyga00(fstart:fend,:);
area9=cumtrapz(fbounded,txyga00_bounded.^2);
H2n_AbsAcc_gap01_inerter = sqrt((1/(2*pi))*area9(end))

% -----
% %Gap = 0.3 (Variable 0)
% load('GroundLoaded_AccelGap_03.mat') %Load Saved Data
% % Reassign Variables
% txw0=txw;
% txwb0=txwb;
% txwg0=txwg;
% txya0=txya;
% txyba0=txyba;
% txyga0=txyga;
%
% %Frequency Bounds
% fstart=find(f==1);
% fend=find(f==100);
% fstep=0.002;
% fbounded=[f(fstart):fstep:f(fend)]';
%
% %Peak Relative Disp TF & Natural Frequency
% txwg0=abs(txwg0);
% txwg0_bounded=txwg0(fstart:fend,:);
% p0=[fbounded, txwg0_bounded];
% gap_inertermaxdisp0=max(txwg0_bounded)
% idxg = find(p0(:,2) == gap_inertermaxdisp0);
% freq_gapinerter0=fbounded(idxg)
%
% %Peak Absolute Acceleration TF (Transmitted force)
% txyga0=abs(txyga0);
% txyga0_bounded=txyga0(fstart:fend,:);
% gap_inertermaxabsaccel0=max(txyga0_bounded)
%
% %Relative Displacement TF Estimate, Gap = 0.3
% figure(f1)
% subplot(1,7,2)

```

```

% semilogy(f,abs(txwb0))
% hold on
% semilogy(f,abs(txw0))
% hold on
% semilogy(f,abs(txwg0))
% xlabel('Frequency (Hz)')
% ylabel('Rel Disp/Freq (m/Hz)')
% title('Gap = 0.3 m/s^2')
% xlim([0,50])
% ylim([10^-7,10^-2])
%
% %Relative Displacement H2 norm:
% area6=cumtrapz(fbounded,txwg0_bounded.^2);
% H2n_disp_gap03_inerter = sqrt((1/(2*pi))*area6(end))
%
% %Absolute Acceleration TF Estimate, Gap = 0.3
% figure(f1)
% subplot(1,7,2)
% semilogy(f,abs(txyba0))
% hold on
% semilogy(f,abs(txya0))
% hold on
% semilogy(f,abs(txyga0))
% xlabel('Frequency (Hz)')
% ylabel('Abs Accel/Freq (m/s^2/Hz)')
% title('Gap = 0.3 m/s^2')
% ylim([10^-3,10^1])
% xlim([0,50])
%
% %Absolute Acceleration H2 Norm:
% txyga0=abs(txyga0);
% txyga0_bounded=txyga0(fstart:fend,:);
% area9=cumtrapz(fbounded,txyga0_bounded.^2);
% H2n_AbsAcc_gap03_inerter = sqrt((1/(2*pi))*area9(end))
%
% -----
% %Gap = 0.5 (Variable 1)
% load('GroundLoaded_AccelGap_05.mat') %Load Saved Data
% %Resassign Variables
% txw1=txw;
% txwb1=txwb;
% txwg1=txwg;
% txya1=txya;
% txyba1=txyba;
% txyga1=txyga;
%
% %Frequency Bounds
% fstart=find(f==1);
% fend=find(f==100);
% fstep=0.002;
% fbounded=[f(fstart):fstep:f(fend)]';

```

```

%
% %Peak Relative Displacement TF Peak & Natural Frequency
% txwg1=abs(txwg1);
% txwg1_bounded=txwg1(fstart:fend,:);
% p1=[fbounded, txwg1_bounded];
% gap_inertermaxdispl=max(txwg1_bounded)
% idxg = find(p1(:,2) == gap_inertermaxdispl);
% freq_gapinerter1=fbounded(idxg)
%
% %Peak Absolute Acceleration TF (Transmitted force)
% txygal=abs(txygal);
% txygal_bounded=txygal(fstart:fend,:);
% gap_inertermaxabsaccel=max(txygal_bounded)
%
% %Relative Displacement TF Estimate, Gap = 0.5
% figure(f1)
% subplot(1,7,3)
% semilogy(f,abs(txwb1))
% hold on
% semilogy(f,abs(txw1))
% hold on
% semilogy(f,abs(txwg1))
% xlabel('Frequency (Hz)')
% ylabel('Rel Disp/Freq (m/Hz)')
% title('Gap = 0.5 m/s^2')
% xlim([0,50])
% ylim([10^-7,10^-2])
%
% %Relative Displacement H2 Norm:
% area6=cumtrapz(fbounded,txwg1_bounded.^2);
% H2n_disp_gap05_inerter = sqrt((1/(2*pi))*area6(end))
%
% %Absolute Acceleration TF Estimate, Gap = 0.5
% figure(f1)
% subplot(1,7,3)
% semilogy(f,abs(txyba1))
% hold on
% semilogy(f,abs(txya1))
% hold on
% semilogy(f,abs(txygal))
% xlabel('Frequency (Hz)')
% ylabel('Abs Accel/Freq (m/s^2/Hz)')
% title('Gap = 0.5 m/s^2')
% ylim([10^-3,10^1])
% xlim([0,50])
%
% %Abs Acceleration H2 Norm:
% txygal=abs(txygal);
% txygal_bounded=txygal(fstart:fend,:);
% area9=cumtrapz(fbounded,txygal_bounded.^2);
% H2n_AbsAcc_gap05_inerter = sqrt((1/(2*pi))*area9(end))

```

```

%-----
%Gap = 0.7 (Variable 2)
load('GroundLoaded_AccelGap_07.mat') %Load Saved Data
%Reassign Variables
txw2=txw;
txwb2=txwb;
txwg2=txwg;
txya2=txya;
txyba2=txyba;
txyga2=txyga;

%Frequency Bounds
fstart=find(f==1);
fend=find(f==100);
fstep=0.002;
fbounded=[f(fstart):fstep:f(fend)]';

%Peak Relative Displacement TF & Natural Frequency
txwg2=abs(txwg2);
txwg2_bounded=txwg2(fstart:fend,:);
p2=[fbounded, txwg2_bounded];
gap_inertermaxdisp2=max(txwg2_bounded)
idxg = find(p2(:,2) == gap_inertermaxdisp2);
freq_gapinexter2=fbounded(idxg)

%Peak Absolute Acceleration TF (Transmitted force)
txyga2=abs(txyga2);
txyga2_bounded=txyga2(fstart:fend,:);
gap_inertermaxabsaccel2=max(txyga2_bounded)

%Relative Displacement TF Estimate & Plots, Gap = 0.7
figure(f1)
subplot(2,4,2)
semilogy(f,abs(txwb2))
hold on
semilogy(f,abs(txw2))
hold on
semilogy(f,abs(txwg2))
xlabel('Frequency (Hz)')
ylabel('Rel Disp/Freq (m/Hz)')
title('(b) Gap = 0.7 m/s^2')
xlim([0,50])
ylim([10^-7,10^-2])

%Relative Displacement H2 norm:
area6=cumtrapz(fbounded,txwg2_bounded.^2);
H2n_disp_gap07_inerter = sqrt((1/(2*pi))*area6(end))

%Absolute Acceleration TF Estimate, Gap = 0.7
figure(f1)

```



```

subplot(2,4,6)
semilogy(f,abs(txyba2))
hold on
semilogy(f,abs(txya2))
hold on
semilogy(f,abs(txyga2))
xlabel('Frequency (Hz)')
ylabel('Abs Accel/Freq (m/s^2/Hz)')
title('(f) Gap = 0.7 m/s^2')
ylim([10^-3,10^1])
xlim([0,50])

%Absolute Acceleration H2 Norm:
txyga2=abs(txyga2);
txyga2_bounded=txyga2(fstart:fend,:);
area9=cumtrapz(fbounded,txyga2_bounded.^2);
H2n_AbsAcc_gap07_inerter = sqrt((1/(2*pi))*area9(end))

% -----
% %Gap = 0.9 (Variable 3)
% load('GroundLoaded_AccelGap_09.mat') %Load Saved Data
% Reassign Variables
% txw3=txw;
% txwb3=txwb;
% txwg3=txwg;
% txya3=txya;
% txyba3=txyba;
% txyga3=txyga;
%
% %Frequency Bounds
% fstart=find(f==1);
% fend=find(f==100);
% fstep=0.002;
% fbounded=[f(fstart):fstep:f(fend)]';
%
% %Peak Relative Displacement TF & Natural Frequency
% txwg3=abs(txwg3);
% txwg3_bounded=txwg3(fstart:fend,:);
% p3=[fbounded, txwg3_bounded];
% gap_inertermaxdisp3=max(txwg3_bounded)
% idxg = find(p3(:,2) == gap_inertermaxdisp3);
% freq_gapinerter3=fbounded(idxg)
%
% %Peak Absolute Acceleration TF (Transmitted force)
% txyga3=abs(txyga3);
% txyga3_bounded=txyga3(fstart:fend,:);
% gap_inertermaxabsaccel3=max(txyga3_bounded)
%
% %Relative Displacement TF Estimate, Gap = 0.9
% figure(f1)
% subplot(1,7,5)

```

```

% semilogy(f,abs(txwb3))
% hold on
% semilogy(f,abs(txw3))
% hold on
% semilogy(f,abs(txwg3))
% xlabel('Frequency (Hz)')
% ylabel('Rel Disp/Freq (m/Hz)')
% title('Gap = 0.9 m/s^2')
% xlim([0,50])
% ylim([10^-7,10^-2])
%
% %Relative Displacement H2 Norm:
% area6=cumtrapz(fbounded,txwg3_bounded.^2);
% H2n_disp_gap09_inerter = sqrt((1/(2*pi))*area6(end))
%
% %Absolute Acceleration TF Estimate, Gap = 0.9
% figure(f1)
% subplot(1,7,5)
% semilogy(f,abs(txyba3))
% hold on
% semilogy(f,abs(txya3))
% hold on
% semilogy(f,abs(txyga3))
% xlabel('Frequency (Hz)')
% ylabel('Abs Accel/Freq (m/s^2/Hz)')
% title('Gap = 0.9 m/s^2')
% ylim([10^-3,10^1])
% xlim([0,50])
%
% %Absolute Acceleration H2 Norm
% txyga3=abs(txyga3);
% txyga3_bounded=txyga3(fstart:fend,:);
% area9=cumtrapz(fbounded,txyga3_bounded.^2);
% H2n_AbsAcc_gap09_inerter = sqrt((1/(2*pi))*area9(end))

% % -----
% %Gap = 1.1 (Variable 4)
% load('GroundLoaded_AccelGap_11.mat') %Load Saved Data
% Reassign Variables
% txw4=txw;
% txwb4=txwb;
% txwg4=txwg;
% txya4=txya;
% txyba4=txyba;
% txyga4=txyga;
%
% %Frequency Bounds
% fstart=find(f==1);
% fend=find(f==100);
% fstep=0.002;
% fbounded=[f(fstart):fstep:f(fend)]';

```

```

%
% %Peak Relative Displacement TF & Natural Frequency
% txwg4=abs(txwg4);
% txwg4_bounded=txwg4(fstart:fend,:);
% p4=[fbounded, txwg4_bounded];
% gap_inertermaxdisp4=max(txwg4_bounded)
% idxg = find(p4(:,2) == gap_inertermaxdisp4);
% freq_gapinerter4=fbounded(idxg)
%
% %Peak Absolute Acceleration TF(Transmitted force)
% txyga4=abs(txyga4);
% txyga4_bounded=txyga4(fstart:fend,:);
% gap_inertermaxabsaccel4=max(txyga4_bounded)
%
% %Relative Displacement TF Estimate, Gap = 1.1
% figure(f1)
% subplot(1,7,6)
% semilogy(f,abs(txwb4))
% hold on
% semilogy(f,abs(txw4))
% hold on
% semilogy(f,abs(txwg4))
% xlabel('Frequency (Hz)')
% ylabel('Rel Disp/Freq (m/Hz)')
% title('Gap = 1.1 m/s^2')
% xlim([0,50])
% ylim([10^-7,10^-2])
%
% %Relative Displacement H2 norm:
% area6=cumtrapz(fbounded,txwg4_bounded.^2);
% H2n_disp_gap11_inerter = sqrt((1/(2*pi))*area6(end))
%
% %Absolute Acceleration TF Estimate, Gap = 1.1
% figure(f1)
% subplot(1,7,6)
% semilogy(f,abs(txyba4))
% hold on
% semilogy(f,abs(txya4))
% hold on
% semilogy(f,abs(txyga4))
% xlabel('Frequency (Hz)')
% ylabel('Abs Accel/Freq (m/s^2/Hz)')
% title('Gap = 1.1 m/s^2')
% ylim([10^-3,10^1])
% xlim([0,50])
%
% %Absolute Acceleratino H2 Norm:
% txyga4=abs(txyga4);
% txyga4_bounded=txyga4(fstart:fend,:);
% area9=cumtrapz(fbounded,txyga4_bounded.^2);
% H2n_AbsAcc_gap11_inerter = sqrt((1/(2*pi))*area9(end))

```

```
%-----  
%Gap = 1.3 (Variable 5)  
load('GroundLoaded_AccelGap_13.mat') %Load Saved Data  
%Reassign Variables  
txw5=txw;  
txwb5=txwb;  
txwg5=txwg;  
txya5=txya;  
txyba5=txyba;  
txyga5=txyga;  
  
%Frequency Bounds  
fstart=find(f==1);  
fend=find(f==100);  
fstep=0.002;  
fbounded=[f(fstart):fstep:f(fend)]';  
  
%Peak Relative Displacement TF & Natural Frequency  
txwg5=abs(txwg5);  
txwg5_bounded=txwg5(fstart:fend,:);  
p5=[fbounded, txwg5_bounded];  
gap_inertermaxdisp=max(txwg5_bounded)  
idxg = find(p5(:,2) == gap_inertermaxdisp);  
freq_gapinerter=fbounded(idxg)  
  
%Peak Absolute Acceleration TF (Transmitted force)  
txyga5=abs(txyga5);  
txyga5_bounded=txyga5(fstart:fend,:);  
gap_inertermaxabsaccel5=max(txyga5_bounded)  
  
%Relative Displacement TF Estimate, Gap = 1.3  
figure(f1)  
subplot(2,4,3)  
semilogy(f,abs(txwb5))  
hold on  
semilogy(f,abs(txw5))  
hold on  
semilogy(f,abs(txwg5))  
xlabel('Frequency (Hz)')  
ylabel('Rel Disp/Freq (m/Hz)')  
title('(c) Gap = 1.3 m/s^2')  
xlim([0,50])  
ylim([10^-7,10^-2])  
  
%Relative Displacement H2 Norm:  
area6=cumtrapz(fbounded,txwg5_bounded.^2);  
H2n_disp_gap13_inerter = sqrt((1/(2*pi))*area6(end))  
  
%Absolute Acceleration TF Estimate, = 1.3  
figure(f1)
```

```

subplot(2,4,7)
semilogy(f,abs(txyba5))
hold on
semilogy(f,abs(txya5))
hold on
semilogy(f,abs(txyga5))
xlabel('Frequency (Hz)')
ylabel('Abs Accel/Freq (m/s^2/Hz)')
title('(g) Gap = 1.3 m/s^2')
ylim([10^-3,10^1])
xlim([0,50])

%Absolute Acceleration H2 Norm:
txyga5=abs(txyga5);
txyga5_bounded=txyga5(fstart:fend,:);
area9=cumtrapz(fbounded,txyga5_bounded.^2);
H2n_AbsAcc_gap13_inerter = sqrt((1/(2*pi))*area9(end))

% -----
% %Gap = 1.1 (Variable 6)
% load('GroundLoaded_AccelGap_11.mat') %Load Saved Data
% Reassign Variables
% txw6=txw;
% txwb6=txwb;
% txwg6=txwg;
% txya6=txya;
% txyba6=txyba;
% txyga6=txyga;
%
% %Frequency Bounds
% fstart=find(f==1);
% fend=find(f==100);
% fstep=0.002;
% fbounded=[f(fstart):fstep:f(fend)]';
%
% %Peak Relative Displacement TF Peak & Natural Frequency
% txwg6=abs(txwg6);
% txwg6_bounded=txwg6(fstart:fend,:);
% p6=[fbounded, txwg6_bounded];
% gap_inertermaxdisp6=max(txwg6_bounded)
% idxg = find(p6(:,2) == gap_inertermaxdisp6);
% freq_gapinerter6=fbounded(idxg)
%
% %Peak Absolute Acceleration TF(Transmitted force)
% txyga6=abs(txyga6);
% txyga6_bounded=txyga6(fstart:fend,:);
% gap_inertermaxabsaccel6=max(txyga6_bounded)
%
% %Relative Displacement TF Estimate, Gap = 1.1
% figure(f1)
% subplot(1,7,6)

```

```

% semilogy(f,abs(txwb6))
% hold on
% semilogy(f,abs(txw6))
% hold on
% semilogy(f,abs(txwg6))
% xlabel('Frequency (Hz)')
% ylabel('Rel Disp/Freq (m/Hz)')
% title('Gap = 1.1 m/s^2')
% xlim([0,50])
% ylim([10^-7,10^-2])
%
% %Relative Displacement H2 Norm:
% area6=cumtrapz(fbounded,txwg4_bounded.^2);
% H2n_disp_gap11_inerter = sqrt((1/(2*pi))*area6(end))
%
% %Absolute Acceleration TF Estimate, Gap = 1.1
% figure(f1)
% subplot(1,7,6)
% semilogy(f,abs(txyba6))
% hold on
% semilogy(f,abs(txya6))
% hold on
% semilogy(f,abs(txyga6))
% xlabel('Frequency (Hz)')
% ylabel('Abs Accel/Freq (m/s^2/Hz)')
% title('Gap = 1.1 m/s^2')
% ylim([10^-3,10^1])
% xlim([0,50])
%
% %Absolute Acceleration H2 Norm:
% txyga6=abs(txyga6);
% txyga6_bounded=txyga6(fstart:fend,:);
% area9=cumtrapz(fbounded,txyga6_bounded.^2);
% H2n_AbsAcc_gap11_inerter = sqrt((1/(2*pi))*area9(end))

%-----
%Gap = 2.6 (Variable 7)
load('GroundLoaded_AccelGap_26.mat') %Load Saved Data
%Reassign Variables
txw7=txw;
txwb7=txwb;
txwg7=txwg;
txya7=txya;
txyba7=txyba;
txyga7=txyga;

%Frequency Bounds
fstart=find(f==1);
fend=find(f==100);
fstep=0.002;
fbounded=[f(fstart):fstep:f(fend)];

```

```

%%Peak Relative Displacement TF & Natural Frequency
txwg7=abs(txwg7);
txwg7_bounded=txwg7(fstart:fend,:);
p7=[fbounded, txwg7_bounded];
gap_inertermaxdisp7=max(txwg7_bounded)
idxg = find(p7(:,2) == gap_inertermaxdisp7);
freq_gapinerter7=fbounded(idxg)

%%Peak Absolute Acceleration TF (Transmitted force)
txyga7=abs(txyga7);
txyga7_bounded=txyga7(fstart:fend,:);
gap_inertermaxabsaccel7=max(txyga7_bounded)

%%Relative Displacement TF Estimate, Gap = 2.6
figure(f1)
subplot(2,4,4)
semilogy(f,abs(txwb7))
hold on
semilogy(f,abs(txw7))
hold on
semilogy(f,abs(txwg7))
xlabel('Frequency (Hz)')
ylabel('Rel Disp/Freq (m/Hz)')
title('(d) Gap = 2.6 m/s^2')
xlim([0,50])
ylim([10^-7,10^-2])

%%Relative Displacement H2 Norm:
area6=cumtrapz(fbounded,txwg7_bounded.^2);
H2n_disp_gap26_inerter = sqrt((1/(2*pi))*area6(end))

%%Absolute acceleration TF Estimate, Gap = 2.6
figure(f1)
subplot(2,4,8)
semilogy(f,abs(txyba7))
hold on
semilogy(f,abs(txya7))
hold on
semilogy(f,abs(txyga7))
xlabel('Frequency (Hz)')
ylabel('Abs Accel/Freq (m/s^2/Hz)')
title('(h) Gap = 2.6 m/s^2')
ylim([10^-3,10^1])
xlim([0,50])

%%Absolute Acceleration H2 Norm:
area9=cumtrapz(fbounded,txyga7_bounded.^2);
H2n_AbsAcc_gap26_inerter = sqrt((1/(2*pi))*area9(end))

```

A .9 MASS LOADED ACCELERATION GAP SYSTEM CODE

```

clear all
close all
warning('off')
load('OctaveFilt_Type1_signal_100s.mat'); %Marine White noise for Type 1 Equipment

%DOF
% y = Absolute Displacement of Top plate

% Die Set System Parameters
m=17.92; %Mass (kg)
k=19858.68; %Spring coefficient (N/m) -- 4 springs @ 28.349 lb/in EA
zeta=0.2; %Damping Ratio = 20%
b=17.92; %Inertance (kg)
cb=2*zeta*sqrt(k*(m+b)); %Damping coefficient(with inerter)
c=2*zeta*sqrt(k*m); %Damping coefficient (without inerter)
g=2.6; %Acceleration Gap (m/s^2)

%State Space Representations
%Linear System Without RIM:
A=[0 1;-k/(m) -c/(m)];
B=[0 ; 1/(m)];
C=[1 0 ; 0 1 ; -k/(m) -c/(m)];
D=[0 ; 0; 1/(m)];
A=double(A);
B=double(B);
C=double(C);
D=double(D);
sys=ss(A,B,C,D);

%Linear System with RIM:
Ab=[0 1;-k/(m+b) -cb/(m+b)];
Bb=[0 ; 1/(m+b)];
Cb=[1 0 ; 0 1;-k/(m+b) -cb/(m+b)];
Db=[0 ; 0 ; 1/(m+b)];
Ab=double(Ab);
Bb=double(Bb);
Cb=double(Cb);
Db=double(Db);
sysb=ss(Ab,Bb,Cb,Db);

%Gap Inerter:
%System with RIM Engaged
Ag=[0 1;-k/(m+b) -cb/(m+b)];
Bg=[0 0; 1/(m+b) 1/(m+b)];
Cg=[1 0 ; 0 1;-k/(m+b) -cb/(m+b)];
Dg=[0 0; 0 0; 1/(m+b) 1/(m+b)];
Ag=double(Ag);
Bg=double(Bg);
Cg=double(Cg);
Dg=double(Dg);
sysgb=ss(Ag,Bg,Cg,Dg);

```



```

%System without RIM:
An=[0 1;-k/(m) -c/(m)];
Bn=[0 ; 1/(m)];
Cn=[1 0 ; 0 1 ; -k/(m) -c/(m)];
Dn=[0 ; 0; 1/(m)];
An=double(An);
Bn=double(Bn);
Cn=double(Cn);
Dn=double(Dn);
sysgb2=ss(An,Bn,Cn,Dn);

%Simulate Response
%ytotalsignal = acceleration
fs= 25000;
SF=100; %Scale Factor used to scale marine white noise frequency down
t=[0:1/fs:100]*SF; %Time
noise = ytotalsignal*m; %Load (F=m*a)
P=noise; %Load
xO=[0 0]; %Initial Conditions
xb=lsim(sysb,P,t,xO); %Simulation with RIM
x=lsim(sys,P,t,xO); %Simulation w/o RIM

%Results with Inerter
yb=xb(:,1); %Absolute displacement
ydotb=xb(:,2); %Absolute velocity
ydotdotb=xb(:,3); %Absolute acceleration
isolforceb =(k*yb)+(cb*ydotb)+(b*ydotdotb); %Isolator Force

%Results without Inerter
y=x(:,1); %Absolute displacement
ydot=x(:,2); %Absolute velocity
ydotdot=x(:,3); %Absolute acceleration
isolforce=(k*y)+(c*ydot); %Isolator Force

%Results for Gap Inerter
yg=[0]; %Absolute displacement
ydotg=[0]; %Absolute velocity
ydotdotg=[0]; %Absolute acceleration
isolforceg=[0]; %Isolatr Force

for a=2:length(t)-1;

    if abs(ydotdotg(end)) > g %Inerter Engaged
        Pbg=[P (b.*g*(sign(ydotdotg(end)))) .*ones(length(t),1)];
        sys = sysgb;
        TrackStateLSIM(a) = 1; %Track Inerter Engagement
        xO=[yg(end) ydotg(end)];
        xg=lsim(sys,Pbg(a:a+1,:),t(a:a+1),xO);
    else
        sys = sysgb2; %Inerter Disengaged
        TrackStateLSIM(a) = 2; %Track Inerter Disengagement
    end
end

```

```

        x0=[yg(end) ydotg(end)];
        xg=lsim(sys,P(a:a+1),t(a:a+1),x0);
    end

    %Assign new variables for next iteration
    ygnew=xg(:,1);
    ydotgnew=xg(:,2);
    ydotdotgnew=xg(:,3);
    yg_new=ygnew(end);
    ydotg_new=ydotgnew(end);
    ydotdotg_new=ydotdotgnew(end);
    yg(a+1)=yg_new;
    ydotg(a+1)=ydotg_new;
    ydotdotg(a+1)=ydotdotg_new;

    %Isolator Force Calculation
    if ydotdotg(a+1) > g
        isolforceg(a+1)=(k*yg(a+1))+(cb*ydotg(a+1))+(b*(ydotdotg(a+1)-g));
        TrackStateISOLLSIM(a+1) = 1;
    elseif -1*ydotdotg(a+1) > g
        isolforceg(a+1)=(k*yg(a+1))+(cb*ydotg(a+1))+(b*(ydotdotg(a+1)+g));
        TrackStateISOLLSIM(a+1) = 2;
    else
        isolforceg(a+1)=(k*yg(a+1))+(cb*ydotg(a+1));
        TrackStateISOLLSIM(a+1) = 3;
    end

end

%CPSPD Parameters
nfft = floor(length(noise)/20);
window = hann(nfft);
noverlap = floor(nfft/2);
fs2=fs/SF

%Absolute Displacement TF Estimate & Plots
[txybdisp,f]=tfestimate(P,yb>window,noverlap,nfft,fs2); %With RIM
[txydisp,f]=tfestimate(P,y>window,noverlap,nfft,fs2); %Without RIM
[txygdisp,f]=tfestimate(P,yg>window,noverlap,nfft,fs2); %Gap RIM
f4=figure
semilogy(f,abs(txybdisp))
hold on
semilogy(f,abs(txydisp))
hold on
semilogy(f,abs(txygdisp))
xlabel('Frequency (Hz)')
ylabel('Absolute Displacement/Frequency (m/Hz)')
legend('Isolation with RIM','Isolation without RIM','Isolation with Gap RIM')
title('Absolute Displacement (Gap = 2.6 m/s^2)')
xlim([0,100])
ylim([10^-7,10^-2])

```

```
%Isolator Force Transfer Function Estimate & Plots
[txybisol,f]=tfestimate(P,isolforceb>window,noverlap,nfft,fs2); %With RIM
[txyisol,f]=tfestimate(P,isolforce>window,noverlap,nfft,fs2); %Without RIM
[txygisol,f]=tfestimate(P,isolforceg>window,noverlap,nfft,fs2); %Gap RIM
f4=figure
semilogy(f,abs(txybisol))
hold on
semilogy(f,abs(txyisol))
hold on
semilogy(f,abs(txygisol))
xlabel('Frequency (Hz)')
ylabel('Isolator Force/Frequency (N/Hz)')
legend('Isolation with RIM','Isolation without RIM','Isolation with Gap RIM')
title('Isolator Force (Gap=2.6 m/s^2)')
xlim([0,100])
ylim([10^-3,10^1])

%Inerter Engagement Percentage
NumberofTimesInerterEngaged = numel(find(TrackStateLSIM==1))
NumberofTimesInerterDisengaged = numel(find(TrackStateLSIM==2))
PercentEngaged = (NumberofTimesInerterEngaged / 2500000)*100

%Save results for Figure and Calculation Code
save('MassLoaded_AccelGap_26_c',
'g','f','txybisol','txyisol','txygisol','txybdisp','txydisp','txygdisp','PercentEngaged',
'yg','ydotg','ydotdotg','isolforceg') %Save Signal to MATLAB File
```

A .10 MASS LOADED ACCELERATION GAP FIGURE & NUMERICAL VALUES

%Accel Gap Thesis Figure

```

%-----
%Gap = 0.1 (Variable 00)
load('MassLoaded_AccelGap_01_c.mat') %Load Saved Data
%Reassign Variables
txybdisp00=txybdisp;
txydisp00=txydisp;
txygdisp00=txygdisp;
txyisol00=txyisol;
txybisol00=txybisol;
txygisol00=txygisol;

%Frequency Bounds
fstart=find(f==1);
fend=find(f==100);
fstep=0.002;
fbounded=[f(fstart):fstep:f(fend)];

%Peak absolute Disp TF & Natural Frequency
txygdisp00=abs(txygdisp00);
txygdisp00_bounded=txygdisp00(fstart:fend,:);
p00=[fbounded,txygdisp00_bounded];
gap_inertermaxdisp00=max(txygdisp00_bounded)
idxg = find(p00(:,2) == gap_inertermaxdisp00);
freq_gapinerter00=fbounded(idxg)

%Peak Isol Force TF (Transmitted force)
txygisol00=abs(txygisol00);
txygisol00_bounded=txygisol00(fstart:fend,:);
gap_inertermaxisol00=max(txygisol00_bounded)

%Absolute Displacement Transfer Function Estimate, Gap = 0.1
f1=figure
subplot(2,4,1)
semilogy(f,abs(txybdisp00))
hold on
semilogy(f,abs(txydisp00))
hold on
semilogy(f,abs(txygdisp00))
xlabel('Frequency (Hz)')
ylabel('Abs Disp/Freq (m/Hz)')
title('(a) Gap = 0.1 m/s^2')
xlim([0,50])
ylim([10^-7,10^-3])

%Absolute Displacement H2 Norm:
area6=cumtrapz(fbounded,txygdisp00_bounded.^2);
H2n_disp_gap01_inerter = sqrt((1/(2*pi))*area6(end))

%Isolator Force Transfer Function Estimate, Gap = 0.1

```

```

figure(f1)
subplot(2,4,5)
semilogy(f,abs(txybisol00))
hold on
semilogy(f,abs(txyisol00))
hold on
semilogy(f,abs(txygisol00))
xlabel('Frequency (Hz)')
ylabel('Isol Force/Freq (N/Hz)')
title('(e) Gap = 0.1 m/s^2')
ylim([10^-2,10^1])
xlim([0,50])

%Isolator Force H2 Norm:
txygisol00=abs(txygisol00);
txygisol00_bounded=txygisol00(fstart:fend,:);
area9=cumtrapz(fbounded,txygisol00_bounded.^2);
H2n_isol_gap01_inerter = sqrt((1/(2*pi))*area9(end))

% -----
% %Gap = 0.3 (Variable 0)
% load('MassLoaded_AccelGap_03_c.mat') %Load Saved Data
% Reassign Variables
% txybdisp0=txybdisp;
% txydisp0=txydisp;
% txygdisp0=txygdisp;
% txyisol0=txyisol;
% txybisol0=txybisol;
% txygisol0=txygisol;

% %Frequency Bounds
% fstart=find(f==.99);
% fend=find(f==100.0024);
% fstep=0.003;
% fbounded=[f(fstart):fstep:f(fend)]';

% %Peak Relative Displacement TF & Natural Frequency
% txygdisp0=abs(txygdisp0);
% txygdisp0_bounded=txygdisp0(fstart:fend,:);
% p0=[fbounded, txygdisp0_bounded];
% gap_inertermaxdisp0=max(txygdisp0_bounded)
% idxg = find(p0(:,2) == gap_inertermaxdisp0);
% freq_gapinerter0=fbounded(idxg)

% %Peak Isolator Force TF(Transmitted force)
% txygisol0=abs(txygisol0);
% txygisol0_bounded=txygisol0(fstart:fend,:);
% gap_inertermaxisol0=max(txygisol0_bounded)

% %Absolute Displacement Transfer Function, Gap = 0.3
% figure(f1)

```

```

% subplot(1,7,2)
% semilogy(f,abs(txybdisp0))
% hold on
% semilogy(f,abs(txydisp0))
% hold on
% semilogy(f,abs(txygdisp0))
% xlabel('Frequency (Hz)')
% ylabel('Transfer Function Magnitude')
% title('Gap = 0.3 m/s^2')
% xlim([0,50])
% ylim([10^-7,10^-3])
%
% %Absolute Displacement H2 Norm:
% area6=cumtrapz(fbounded,txygdisp0_bounded.^2);
% H2n_disp_gap01_inerter = sqrt((1/(2*pi))*area6(end))
%
% %Isolator Force TF Estimate, Gap = 0.3
% figure(f1)
% subplot(1,7,2)
% semilogy(f,abs(txybisol0))
% hold on
% semilogy(f,abs(txyisol0))
% hold on
% semilogy(f,abs(txygisol0))
% xlabel('Frequency (Hz)')
% ylabel('Transfer Function Magnitude')
% title('Gap = 0.3 m/s^2')
% ylim([10^-2,10^1])
% xlim([0,50])
% %
% %Isolator Force H2 Norm
% txygisol0=abs(txygisol0);
% txygisol0_bounded=txygisol0(fstart:fend,:);
% area9=cumtrapz(fbounded,txygisol0_bounded.^2);
% H2n_isol_gap03_inerter = sqrt((1/(2*pi))*area9(end))

% %-----
% %Gap = 0.5 (Variable 1)
% load('MassLoaded_AccelGap_05_c.mat') %Load Saved Data
% Reassign Variables
% txybdisp1=txybdisp;
% txydisp1=txydisp;
% txygdisp1=txygdisp;
% txyisol1=txyisol;
% txybisol1=txybisol;
% txygisol1=txygisol;

% %Frequency Bounds
% fstart=find(f==.99);
% fend=find(f==100.0024);

```

```

% fstep=0.003;
% fbounded=[f(fstart):fstep:f(fend)]';

% %Peak Absolute Displacement TF & Natural Frequency
% txygdispl=abs(txygdispl);
% txygdispl_bounded=txygdispl(fstart:fend,:);
% pl=[fbounded, txygdispl_bounded];
% gap_inertermaxdispl=max(txygdispl_bounded)
% idxg = find(pl(:,2) == gap_inertermaxdispl);
% freq_gapinerter1=fbounded(idxg)

% %Peak Isolator Force TF (Transmitted force)
% txygisol1=abs(txygisol1);
% txygisol1_bounded=txygisol1(fstart:fend,:);
% gap_inertermaxisol1=max(txygisol1_bounded)

%
% %Absolute Displacement TF Estimate, Gap = 0.5
% figure(f1)
% subplot(1,7,3)
% semilogy(f,abs(txybdispl))
% hold on
% semilogy(f,abs(txydispl))
% hold on
% semilogy(f,abs(txygdispl))
% xlabel('Frequency (Hz)')
% ylabel('Transfer Function Magnitude')
% title('Gap = 0.5 m/s^2')
% xlim([0,50])
% ylim([10^-7,10^-3])
%

% %Absolute Displacement H2 norm:
% area6=cumtrapz(fbounded,txygdispl_bounded.^2);
% H2n_disp_gap05_inerter = sqrt((1/(2*pi))*area6(end))

% %Isolator Force TF Estimate, Gap = 0.5
% figure(f1)
% subplot(1,7,3)
% semilogy(f,abs(txybisol1))
% hold on
% semilogy(f,abs(txyisol1))
% hold on
% semilogy(f,abs(txygisol1))
% xlabel('Frequency (Hz)')
% ylabel('Transfer Function Magnitude')
% title('Gap = 0.5 m/s^2')
% ylim([10^-2,10^1])
% xlim([0,50])

% %Isolator Force H2 Norm:

```

```

% txygisol1=abs(txygisol1);
% txygisol1_bounded=txygisol1(fstart:fend,:);
% area9=cumtrapz(fbounded,txygisol1_bounded.^2);
% H2n_isol_gap05_inerter = sqrt((1/(2*pi))*area9(end))

%-----
%Gap = 0.7 (Variable 2)
load('MassLoaded_AccelGap_07_c.mat') %Load Saved Data
%Reassign Variables
txybdisp2=txybdisp;
txydisp2=txydisp;
txygdisp2=txygdisp;
txyisol2=txyisol;
txybisol2=txybisol;
txygisol2=txygisol;

%Frequency Bounds
fstart=find(f==1);
fend=find(f==100);
fstep=0.002;
fbounded=[f(fstart):fstep:f(fend)]';

%Peak Absolute Displacement Transfer Function & Natural Frequency
txygdisp2=abs(txygdisp2);
txygdisp2_bounded=txygdisp2(fstart:fend,:);
p2=[fbounded, txygdisp2_bounded];
gap_inertermaxdisp2=max(txygdisp2_bounded)
idxg = find(p2(:,2) == gap_inertermaxdisp2);
freq_gapinerter2=fbounded(idxg)

%Peak Isolator Force TF (Transmitted force)
txygisol2=abs(txygisol2);
txygisol2_bounded=txygisol2(fstart:fend,:);
gap_inertermaxisol2=max(txygisol2_bounded)

%Absolute Displacement Transfer Function & Estimate, Gap = 0.7
figure(f1)
subplot(2,4,2)
semilogy(f,abs(txybdisp2))
hold on
semilogy(f,abs(txydisp2))
hold on
semilogy(f,abs(txygdisp2))
xlabel('Frequency (Hz)')
ylabel('Abs Disp/Freq (m/Hz)')
title('(b) Gap = 0.7 m/s^2')
xlim([0,50])
ylim([10^-7,10^-3])

%Absolute Displacement H2 Norm:

```



```

area6=cumtrapz(fbounded,txygdisp2_bounded.^2);
H2n_disp_gap07_inerter = sqrt((1/(2*pi))*area6(end))

%Isolator Force Transfer Function Estimate, Gap = 0.7
figure(f1)
subplot(2,4,6)
semilogy(f,abs(txybisol2))
hold on
semilogy(f,abs(txyisol2))
hold on
semilogy(f,abs(txygisol2))
xlabel('Frequency (Hz)')
ylabel('Isol Force/Freq (N/Hz)')
title('(f) Gap = 0.7 m/s^2')
ylim([10^-2,10^1])
xlim([0,50])

%Isolator Force H2 Norm:
txygisol2=abs(txygisol2);
txygisol2_bounded=txygisol2(fstart:fend,:);
area9=cumtrapz(fbounded,txygisol2_bounded.^2);
H2n_isol_gap07_inerter = sqrt((1/(2*pi))*area9(end))

```

```

% % -----
% %Gap = 0.9 (Variable 3)
% load('MassLoaded_AccelGap_09_c.mat') %Load saved data
% Reassign Variables
% txybdisp3=txybdisp;
% txydisp3=txydisp;
% txygdisp3=txydisp;
% txyisol3=txyisol;
% txybisol3=txybisol;
% txygisol3=txygisol;

% %Frequency Bounds
% fstart=find(f==.99);
% fend=find(f==100.0024);
% fstep=0.003;
% fbounded=[f(fstart):fstep:f(fend)]';

% %Peak Absolute Displacement TF & Natural Frequency
% txygdisp3=abs(txygdisp3);
% txygdisp3_bounded=txygdisp3(fstart:fend,:);
% p3=[fbounded, txygdisp3_bounded];
% gap_inertermaxdisp3=max(txygdisp3_bounded)
% idxg = find(p3(:,2) == gap_inertermaxdisp3);
% freq_gapinerter3=fbounded(idxg)
%
% %Peak Isolator Force TF(Transmitted force)
% txygisol3=abs(txygisol3);

```

```

% txygisol3_bounded=txygisol3(fstart:fend,:);
% gap_inertermaxisol3=max(txygisol3_bounded)

% %Absolute Displacement Transfer Function Estimate, Gap = 0.9
% figure(f1)
% subplot(1,7,5)
% semilogy(f,abs(txybdisp3))
% hold on
% semilogy(f,abs(txydisp3))
% hold on
% semilogy(f,abs(txygdisp3))
% xlabel('Frequency (Hz)')
% ylabel('Transfer Function Magnitude')
% title('Gap = 0.9 m/s^2')
% xlim([0,50])
% ylim([10^-7,10^-2])

% %Absolute Displacement H2 Norm:
% area6=cumtrapz(fbounded,txydisp3_bounded.^2);
% H2n_disp_gap09_inerter = sqrt((1/(2*pi))*area6(end))

% %Isolator Force Transfer Function Estimate, Gap = 0.9
% figure(f1)
% subplot(1,7,5)
% semilogy(f,abs(txybisol3))
% hold on
% semilogy(f,abs(txyisol3))
% hold on
% semilogy(f,abs(txygisol3))
% xlabel('Frequency (Hz)')
% ylabel('Transfer Function Magnitude')
% title('Gap = 0.9 m/s^2')
% ylim([10^-2,10^1])
% xlim([0,50])

% %Isolator Force H2 Norm:
% txygisol3=abs(txygisol3);
% txygisol3_bounded=txygisol3(fstart:fend,:);
% area9=cumtrapz(fbounded,txygisol3_bounded.^2);
% H2n_isol_gap09_inerter = sqrt((1/(2*pi))*area9(end))

%
% % -----
% %Gap = 1.1 (Variable 4)
% load('MassLoaded_AccelGap_11_c.mat') %Load Saved Data
% Reassign Variables
% txybdisp4=txybdisp;
% txydisp4=txydisp;
% txygdisp4=txygdisp;
% txyisol4=txyisol;
% txybisol4=txybisol;

```

```

% txygisol4=txygisol;

% %Frequency Bounds
% fstart=find(f==.99);
% fend=find(f==100.0024);
% fstep=0.003;
% fbounded=[f(fstart):fstep:f(fend)]';

% %Peak Absolute Displacement TF & Natural Frequency
% txygdisp4=abs(txygdisp4);
% txygdisp4_bounded=txygdisp4(fstart:fend,:);
% p4=[fbounded, txygdisp4_bounded];
% gap_inertermaxdisp4=max(txygdisp4_bounded)
% idxg = find(p4(:,2) == gap_inertermaxdisp4);
% freq_gapinerter4=fbounded(idxg)

% %Peak Isolator Force TF (Transmitted force)
% txygisol4=abs(txygisol4);
% txygisol4_bounded=txygisol4(fstart:fend,:);
% gap_inertermaxisol4=max(txygisol4_bounded)

% %Absolute Displacement H2 norm:
% area6=cumtrapz(fbounded,txygdisp4_bounded.^2);
% H2n_disp_gap11_inerter = sqrt((1/(2*pi))*area6(end))

% %Absolute Displacement Transfer Function Estimate, Gap = 1.1
% figure(f1)
% subplot(1,7,6)
% semilogy(f,abs(txybdisp4))
% hold on
% semilogy(f,abs(txydisp4))
% hold on
% semilogy(f,abs(txygdisp4))
% xlabel('Frequency (Hz)')
% ylabel('Transfer Function Magnitude')
% title('Gap = 1.1 m/s^2')
% xlim([0,50])
% ylim([10^-7,10^-3])
%
% %Isolator Force Transfer Function Estimate, Gap = 1.1
% figure(f1)
% subplot(1,7,6)
% semilogy(f,abs(txybisol4))
% hold on
% semilogy(f,abs(txyisol4))
% hold on
% semilogy(f,abs(txygisol4))
% xlabel('Frequency (Hz)')
% ylabel('Transfer Function Magnitude')
% title('Gap = 1.1 m/s^2')
% ylim([10^-2,10^1])

```

```

% xlim([0,50])

% %Isolator Force H2 Norm:
% txygisol4=abs(txygisol4);
% txygisol4_bounded=txygisol4(fstart:fend,:);
% area9=cumtrapz(fbounded,txygisol4_bounded.^2);
% H2n_isol_gap11_inerter = sqrt((1/(2*pi))*area9(end))
%
%-----
%Gap = 1.3 (Variable 5)
load('MassLoaded_AccelGap_13_c.mat') %Load saved data
%Reassign Variables
txybdisp5=txybdisp;
txydisp5=txydisp;
txygdisp5=txygdisp;
txyisol5=txyisol;
txybisol5=txybisol;
txygisol5=txygisol;

%Frequency Bounds
fstart=find(f==1);
fend=find(f==100);
fstep=0.002;
fbounded=[f(fstart):fstep:f(fend)'];

%Peak Absolute Displacement TF & Natural Frequency
txygdisp5=abs(txygdisp5);
txygdisp5_bounded=txygdisp5(fstart:fend,:);
p5=[fbounded,txygdisp5_bounded];
gap_inertermaxdisp5=max(txygdisp5_bounded)
idxg = find(p5(:,2) == gap_inertermaxdisp5);
freq_gapinerter5=fbounded(idxg)

%Peak Isolator Force TF (Transmitted force)
txygisol5=abs(txygisol5);
txygisol5_bounded=txygisol5(fstart:fend,:);
gap_inertermaxisol5=max(txygisol5_bounded)

%Absolute Displacement Transfer Function Estimate, Gap = 1.3
figure(f1)
subplot(2,4,3)
semilogy(f,abs(txybdisp5))
hold on
semilogy(f,abs(txydisp5))
hold on
semilogy(f,abs(txygdisp5))
xlabel('Frequency (Hz)')
ylabel('Abs Disp/Freq (m/Hz)')
title('(c) Gap = 1.3 m/s^2')
xlim([0,50])
ylim([10^-7,10^-3])

```

```

%Absolute Displacement H2 Norm
area6=cumtrapz(fbounded,txydisp5_bounded.^2);
H2n_disp_gap13_inerter = sqrt((1/(2*pi))*area6(end))

%Isolator Force Transfer Function Estimate, Gap = 1.3
figure(f1)
subplot(2,4,7)
semilogy(f,abs(txybisol5))
hold on
semilogy(f,abs(txyisol5))
hold on
semilogy(f,abs(txygisol5))
xlabel('Frequency (Hz)')
ylabel('Isol Force/Freq (N/Hz)')
title('(g) Gap = 1.3 m/s^2')
ylim([10^-2,10^1])
xlim([0,50])

%Isolator Force H2 Norm:
txygisol5=abs(txygisol5);
txygisol5_bounded=txygisol5(fstart:fend,:);
area9=cumtrapz(fbounded,txygisol5_bounded.^2);
H2n_isol_gap13_inerter = sqrt((1/(2*pi))*area9(end))

%-----
%Gap = 2.6 (Variable 6)
load('MassLoaded_AccelGap_26_c.mat') %Load Saved Data
%Reassign Variables
txybdisp6=txybdisp;
txydisp6=txydisp;
txygdisp6=txygdisp;
txyisol6=txyisol;
txybisol6=txybisol;
txygisol6=txygisol;

%Frequency Bounds
fstart=find(f==1);
fend=find(f==100);
fstep=0.002;
fbounded=[f(fstart):fstep:f(fend)'];

%Peak Absolute Displacement TF & Natural Frequency
txygdisp6=abs(txygdisp6);
txygdisp6_bounded=txygdisp6(fstart:fend,:);
p6=[fbounded,txygdisp6_bounded];
gap_inertermaxdisp6=max(txygdisp6_bounded)
idxg = find(p6(:,2) == gap_inertermaxdisp6);
freq_gapinerter6=fbounded(idxg)

%Peak Isolator Force TF (Transmitted force)

```

```
txygisol6=abs(txygisol6);
txygisol6_bounded=txygisol6(fstart:fend,:);
gap_inertermaxisol6=max(txygisol6_bounded)

%Absolute Displacement Transfer Function Estimate, Gap = 2.6
figure(f1)
subplot(2,4,4)
semilogy(f,abs(txybdisp6))
hold on
semilogy(f,abs(txydisp6))
hold on
semilogy(f,abs(txygdisp6))
xlabel('Frequency (Hz)')
ylabel('Abs Disp/Freq (m/Hz)')
title('(d) Gap = 2.6 m/s^2')
xlim([0,50])
ylim([10^-7,10^-3])

%Absolute Displacement H2 Norm:
area6=cumtrapz(fbounded,txydisp6_bounded.^2);
H2n_disp_gap26_inerter = sqrt((1/(2*pi))*area6(end))

%Isolator Force Transfer Function, Gap = 2.6
figure(f1)
subplot(2,4,8)
semilogy(f,abs(txybisol6))
hold on
semilogy(f,abs(txyisol6))
hold on
semilogy(f,abs(txygisol6))
xlabel('Frequency (Hz)')
ylabel('Isol Force/Freq (m/Hz)')
title('(h) Gap = 2.6 m/s^2')
ylim([10^-2,10^1])
xlim([0,50])

%Isolator Force H2 Norm:
txygisol6=abs(txygisol6);
txygisol6_bounded=txygisol6(fstart:fend,:);
area9=cumtrapz(fbounded,txygisol6_bounded.^2);
H2n_isol_gap26_inerter = sqrt((1/(2*pi))*area9(end))
```

A.11 BASE LOADED DISPLACEMENT GAP SYSTEM CODE

```

clear all
close all
warning('off')
load('OctaveFilt_Type1_signal_100s.mat'); %Marine white noise for Type 1 equipment

%DOF
% y = Absolute Displacement of Top plate
% w = Relative Displacement of Top Plate

%System Parameters
m=17.92; %Mass (kg)
k=19858.68; %Spring coefficient (N/m)--4 springs @ 28.349 lb/in EA
zeta=.2; %Damping ratio = 20%
b=17.92; %Inertance (kg)
cb=2*zeta*sqrt(k*(m+b)); %Damping coefficient(with inerter)
c=2*zeta*sqrt(k*m); %Damping coefficient(without inerter)
e=0.001; %Displacement Gap (m)

%State Space Representations
%Linear System Without RIM:
A=[0 1;-k/(m) -c/(m)];
B=[0; -1];
C=[1 0 ; 0 1; -k/(m) -c/(m); -k/(m) -c/(m)];
D=[0 ; 0; -1; 0];
A=double(A);
B=double(B);
C=double(C);
D=double(D);
sys=ss(A,B,C,D);

%Linear System With RIM:
Ab=[0 1;-k/(m+b) -cb/(m+b)];
Bb=[0 ; -m/(m+b)];
Cb=[1 0 ; 0 1; -k/(m+b) -cb/(m+b); -k/(m+b) -cb/(m+b)];
Db=[0 ; 0 ; (-m/(m+b)); (-m/(m+b))+1];
Ab=double(Ab);
Bb=double(Bb);
Cb=double(Cb);
Db=double(Db);
sysb=ss(Ab,Bb,Cb,Db);

%Gap Inerter
%Sys1 : (y=u+e) Inerter Engaged & Extended
Ag=[0 1;-k/(m+b) -cb/(m+b)];
Bg=[0 ; -m/(m+b)];
Cg=[1 0 ; 0 1; -k/(m+b) -cb/(m+b); -k/(m+b) -cb/(m+b)];
Dg=[0 ; 0; (-m/(m+b)); (-m/(m+b))+1];
Ag=double(Ag);
Bg=double(Bg);
Cg=double(Cg);
Dg=double(Dg);

```

```

sys1=ss(Ag,Bg,Cg,Dg);
%Sys 2 : (y=u-e) Inerter Engaged & Compressed
Ag=[0 1;-k/(m+b) -cb/(m+b)];
Bg=[0 ; -m/(m+b)];
Cg=[1 0 ;0 1; -k/(m+b) -cb/(m+b); -k/(m+b) -cb/(m+b)];
Dg=[0 ; 0; (-m/(m+b)); (-m/(m+b))+1];
Ag=double(Ag);
Bg=double(Bg);
Cg=double(Cg);
Dg=double(Dg);
sys2=ss(Ag,Bg,Cg,Dg);
%Sys 3 : Inerter Disengaged
Ag=[0 1;-k/(m) -c/(m)];
Bg=[0; -1];
Cg=[1 0 ;0 1; -k/(m) -c/(m); -k/(m) -c/(m)];
Dg=[0; 0; -1; 0];
Ag=double(Ag);
Bg=double(Bg);
Cg=double(Cg);
Dg=double(Dg);
sys3=ss(Ag,Bg,Cg,Dg);

%Simulate Response
%ytotalsignal = acceleration
fs=25000;
SF=100; %Scale Factor used to scale marine white noise frequency down
t=[0:1/fs:100]*SF; %Time
P=[ytotalsignal]; %Load = Acceleration
ugdot=cumtrapz(t/1000,ytotalsignal); %Velocity ground signal
ug=cumtrapz(t/1000,ugdot); %Displacement ground signal
x0=[0 0]; %Initial Conditions
xb=lsim(sysb,P,t,x0); %Simulation with RIM
x=lsim(sys,P,t,x0); %Simulation w/o RIM

%Results with RIM
wb=xb(:,1); %Relative displacement
wdotb=xb(:,2); %Relative velocity
wdotdotb= xb(:,3); %Relative acceleration
yb=wb + ug; %Absolute displacement
ydotb=wdotb + ugdot; %Absolute velocity
ydotdotb=xb(:,4); %Abslute acceleration

%Results without RIM
w=x(:,1); %Relative displacement
wdot=x(:,2);%Relative velocity
wdotdot= x(:,3); %Relative acceleration
y=w + ug; %Absolute displacement
ydot=wdot + ugdot; %Absolute velocity
ydotdot=x(:,4); %Absolute acceleration

%Gap Inerter Results

```



```

wg=[0]; %Relative displacement
wgdot=[0]; %Relative velocity
wgdotdot=[0]; %Relative acceleration
yg=[0]; %Absolute displacement
ydotg=[0]; %Absolute velocity
ydotdotg=[0]; %Absolute acceleration

%Displacement Gap Loop
for a=2:length(t);

    if yg(a-1) > e    %Inerter Engaged & Extended (SYS1: y-u=e)
        Pbg=[P]; %Load
        sys = sys1;
        TrackStateLSIM(a) = 1; %Track Inerter Engagement
        x0=[yg(end) ydotg(end)];
        xg=lsim(sys,Pbg(a-1:a,:),t(a-1:a),x0);

        %Assign New Variables for Next Iteration
        wgnew=xg(:,1);
        wgdnew=xg(:,2);
        wgdnewdot=xg(:,3);
        ydotdotnew=xg(:,4);
        wg_new=wgnew(end);
        wgd_new=wgdnew(end);
        wgdnewdot_new=wgdnewdotnew(end);
        ydotdot_new=ydotdotnew(end);
        wg(a)=wg_new;
        wgd(a)=wgd_new;
        wgdnewdot(a)=wgdnewdot_new;
        ydotdotg(a)=ydotdot_new;

        yg(a) = wg(a) + ug(a); %yg = wg + ug(Absolute disp signal)
        ydotg(a)=wgd(a)+ugd(a); %ydotg= wdotg + ugd(Absolute velocity signal)

    elseif yg(a-1) < -e    %inerter Engaged & Compressed (SYS2: y-u=-e)
        Pbg=[P]; %Load
        sys = sys2;
        TrackStateLSIM(a) = 2; %Track Inerter Engagement
        x0=[yg(end) ydotg(end)];
        xg=lsim(sys,Pbg(a-1:a,:),t(a-1:a),x0);

        %Assign new variables for next iteration
        wgnew=xg(:,1);
        wgdnew=xg(:,2);
        wgdnewdot=xg(:,3);
        ydotdotnew=xg(:,4);
        wg_new=wgnew(end);
        wgd_new=wgdnew(end);
        wgdnewdot_new=wgdnewdotnew(end);
        ydotdot_new=ydotdotnew(end);
        wg(a)=wg_new;

```

```

    wgdot(a)=wgdot_new;
    wgdotdot(a)=wgdotdot_new;
    ydotdotg(a)=ydotdot_new;

    yg(a) = wg(a) + ug(a); %yg = wg + ug(Absolute disp signal)
    ydotg(a)=wgdot(a)+ugdot(a); %ydotg= wdotg + ugdot(Absolute velocity signal)

else      %Inerter Disengaged (SYS 3:Fb=0)
Pbg=[P]; %Load
sys = sys3;
TrackStateLSIM(a) = 3; %Track Inerter Disengagement
x0=[yg(end) ydotg(end)];
xg=lsim(sys,Pbg(a-1:a,:),t(a-1:a),x0);

%Assign new variables for next iteration
wgnew=xg(:,1);
wgdotnew=xg(:,2);
wgdotdotnew=xg(:,3);
ydotdotnew=xg(:,4);
wg_new=wgnew(end);
wgdot_new=wgdotnew(end);
wgdotdot_new=wgdotdotnew(end);
ydotdot_new=ydotdotnew(end);
wg(a)=wg_new;
wgdot(a)=wgdot_new;
wgdotdot(a)=wgdotdot_new;
ydotdotg(a)=ydotdot_new;

    yg(a) = wg(a) + ug(a); %yg = wg + ug(Abs disp signal)
    ydotg(a)=wgdot(a)+ugdot(a); %ydotg= wdotg + ugdot(Abs velocity signal)
end

end

%CPD Parameters
nfft = floor(length(t)/20);
window = hann(nfft);
noverlap = floor(nfft/2);
fs2=fs/SF

%Absolute Acceleration Transfer Function Estimate & Plots
[txyba,f]=tfestimate(P,ydotdotb>window,noverlap,nfft,fs2); %with RIM
[txya,f]=tfestimate(P,ydotdot>window,noverlap,nfft,fs2); %without RIM
[txyga,f]=tfestimate(P,ydotdotg>window,noverlap,nfft,fs2); %Disp Gap RIM
f5=figure
semilogy(f,abs(txyba))
hold on
semilogy(f,abs(txya))
hold on
semilogy(f,abs(txyga))
xlabel('Frequency (Hz)')
ylabel('Abs Accel/Frequency (m/s^2/Hz)')

```

```
legend('Isolation with RIM','Isolation without RIM','Isolation with Gap RIM')
title('Absolute Acceleration Transfer Function (Gap = 0.0009 m)')
xlim([0,100])
ylim([10^-3,10^1])

%Relative Displacement Transfer Function Estimate & Plots
[txwb,f]=tfestimate(P,wb>window,noverlap,nfft,fs2); %with RIM
[txw,f]=tfestimate(P,w>window,noverlap,nfft,fs2); %without RIM
[txwg,f]=tfestimate(P,wg>window,noverlap,nfft,fs2); %Disp Gap Rim
f5=figure
semilogy(f,abs(txwb))
hold on
semilogy(f,abs(txw))
hold on
semilogy(f,abs(txwg))
xlabel('Frequency (Hz)')
ylabel('Relative Displacement/Frequency (m/Hz)')
legend('Isolation with RIM','Isolation without RIM','Isolation with Gap RIM')
title('Relative Displacement (Gap = 0.0009 m)')
xlim([0,100])
ylim([10^-7,10^-2])

%Inerter Engagement Percentage
NumberofTimesInerterEngaged = numel(find(TrackStateLSIM==1))+numel(find(TrackStateLSIM==2))
NumberofTimesInerterDisengaged = numel(find(TrackStateLSIM==3))
PercentEngaged = (NumberofTimesInerterEngaged / 2500001)*100

%Save Results for Figure and Calculation Code
save('GroundLoaded_DispGap_001',
'e','f','txwb','txw','txwg','txyba','txya','txyga','PercentEngaged') %Save Signal to
MATLAB File
```

A .12 BASE LOADED DISPLACEMENT GAP FIGURE & NUMERICAL VALUES

```

%Disp Gap Thesis Figure
%-----
%Gap = 0.0001 (Variable 00)
load('GroundLoaded_DisGap_0001_c.mat') %Load Saved Data
%Reassign Variables
txw00=txw;
txwb00=txwb;
txwg00=txwg;
txya00=txya;
txyba00=txyba;
txyga00=txyga;

%Frequency Bounds
fstart=find(f==1);
fend=find(f==100);
fstep=0.002;
fbounded=[f(fstart):fstep:f(fend)]';

%Peak Displacement TF & Natural Frequency, Gap = 0.0001
txwg00=abs(txwg00);
txwg00_bounded=txwg00(fstart:fend,:);
p00=[fbounded, txwg00_bounded];
gap_inertermaxdisp00=max(txwg00_bounded)
idxg = find(p00(:,2) == gap_inertermaxdisp00);
freq_gapinerter00=fbounded(idxg)

%Peak Absolute Acceleration TF (Transmitted force)
txyga00=abs(txyga00);
txyga00_bounded=txyga00(fstart:fend,:);
gap_inertermaxabsaccel00=max(txyga00_bounded)

%Relative Displacement TF Estimate, Gap = 0.0001
f1=figure
subplot(2,4,1)
semilogy(f,abs(txwb00))
hold on
semilogy(f,abs(txw00))
hold on
semilogy(f,abs(txwg00))
xlabel('Frequency (Hz)')
ylabel('Rel Disp/Freq (m/Hz)')
title('(a) Gap = 0.0001 m')
xlim([0,50])
ylim([10^-7,10^-2])

%Absolute Acceleration TF Estimate, Gap = 0.0001
figure(f1)
subplot(2,4,5)
semilogy(f,abs(txyba00))
hold on
semilogy(f,abs(txya00))

```

```

hold on
semilogy(f,abs(txyga00))
xlabel('Frequency (Hz)')
ylabel('Abs Accel/Freq (m/s^2/Hz)')
title('(e) Gap = 0.0001 m')
ylim([10^-3,10^1])
xlim([0,50])

%Relative Displacement H2 Norm:
area6=cumtrapz(fbounded,txwg00_bounded.^2);
H2n_disp_gap01_inerter = sqrt((1/(2*pi))*area6(end))

%Absolute Acceleration H2 Norm:
txyga00=abs(txyga00);
txyga00_bounded=txyga00(fstart:fend,:);
area9=cumtrapz(fbounded,txyga00_bounded.^2);
H2n_AbsAcc_gap01_inerter = sqrt((1/(2*pi))*area9(end))

%-----
%Gap = 0.0003 (Variable 0)
load('GroundLoaded_DispGap_0003_c.mat') %Load Saved Data
%Reassign Variables
txw0=txw;
txwb0=txwb;
txwg0=txwg;
txya0=txya;
txyba0=txyba;
txyga0=txyga;

%Frequency Bounds
fstart=find(f==1);
fend=find(f==100);
fstep=0.002;
fbounded=[f(fstart):fstep:f(fend)'];

%Peak TF Displacement & Natural Frequency, Gap = 0.0001
txwg0=abs(txwg0);
txwg0_bounded=txwg0(fstart:fend,:);
p0=[fbounded,txwg0_bounded];
gap_inertermaxdisp0=max(txwg0_bounded)
idxg = find(p0(:,2) == gap_inertermaxdisp0);
freq_gapinerter0=fbounded(idxg)

%Peak Absolute Acceleration TF (Transmitted force)
txyga0=abs(txyga0);
txyga0_bounded=txyga0(fstart:fend,:);
gap_inertermaxabsaccel0=max(txyga0_bounded)

%Relative Displacement TF Estimate Plots, Gap = 0.0003
figure(f1)
subplot(2,4,2)

```

```

semilogy(f,abs(txwb0))
hold on
semilogy(f,abs(txw0))
hold on
semilogy(f,abs(txwg0))
xlabel('Frequency (Hz)')
ylabel('Rel Disp/Hz (m/Hz)')
title('(b) Gap = 0.0003 m')
xlim([0,50])
ylim([10^-7,10^-2])

%Absolute Acceleration TF Estimate,Gap = 0.0003
figure(f1)
subplot(2,4,6)
semilogy(f,abs(txyba0))
hold on
semilogy(f,abs(txya0))
hold on
semilogy(f,abs(txyga0))
xlabel('Frequency (Hz)')
ylabel('Abs Accel/Freq (m/s^2/Hz)')
title('(f) Gap = 0.0003 m')
ylim([10^-3,10^1])
xlim([0,50])

%Relative Displacement H2 Norm:
area6=cumtrapz(fbounded,txwg0_bounded.^2);
H2n_disp_gap0003_inerter = sqrt((1/(2*pi))*area6(end))

%Absolute Acceleration H2 Norm:
txyga0=abs(txyga0);
txyga0_bounded=txyga0(fstart:fend,:);
area9=cumtrapz(fbounded,txyga0_bounded.^2);
H2n_AbsAcc_gap0003_inerter = sqrt((1/(2*pi))*area9(end))

%-----
%Gap = 0.0005 (Variable 1)
load('GroundLoaded_DispGap_0005_c.mat') %Load Saved Data
%Reassign Variables
txw1=txw;
txwb1=txwb;
txwg1=txwg;
txya1=txya;
txyba1=txyba;
txyga1=txyga;

%Frequency Bounds
fstart=find(f==1);
fend=find(f==100);
fstep=0.002;
fbounded=[f(fstart):fstep:f(fend)];

```

```
%Peak Displacement TF & Natural Frequency, Gap = 0.0001
txwg1=abs(txwg1);
txwg1_bounded=txwg1(fstart:fend,:);
p1=[fbounded, txwg1_bounded];
gap_inertermaxdisp1=max(txwg1_bounded)
idxg = find(p1(:,2) == gap_inertermaxdisp1);
freq_gapinerter1=fbounded(idxg)

%Peak Absolute Acceleration TF (Transmitted force)
txygal=abs(txygal);
txygal_bounded=txygal(fstart:fend,:);
gap_inertermaxabsaccl1=max(txygal_bounded)

%Relative Displacement TF Estimate Plots, Gap = 0.0005
figure(f1)
subplot(2,4,3)
semilogy(f,abs(txwb1))
hold on
semilogy(f,abs(txw1))
hold on
semilogy(f,abs(txwg1))
xlabel('Frequency (Hz)')
ylabel('Rel Disp/Freq (m/Hz)')
title('(c) Gap = 0.0005 m')
xlim([0,50])
ylim([10^-7,10^-2])

%Absolute acceleration TF Estimate & Plots, Gap = 0.0005
figure(f1)
subplot(2,4,7)
semilogy(f,abs(txybal))
hold on
semilogy(f,abs(txya1))
hold on
semilogy(f,abs(txygal))
xlabel('Frequency (Hz)')
ylabel('Abs Accel/Freq (m/s^2/Hz)')
title('(g) Gap = 0.0005 m')
ylim([10^-3,10^1])
xlim([0,50])

%Relative Displacement TF H2 Norm:
area6=cumtrapz(fbounded,txwg1_bounded.^2);
H2n_disp_gap0005_inerter = sqrt((1/(2*pi))*area6(end))

%Absolute Acceleration H2 Norm:
txygal=abs(txygal);
txygal_bounded=txygal(fstart:fend,:);
area9=cumtrapz(fbounded,txygal_bounded.^2);
H2n_AbsAcc_gap0005_inerter = sqrt((1/(2*pi))*area9(end))
```

```

% -----
%Gap = 0.001 (Variable 2)
load('GroundLoaded_DisGap_001_c.mat') %Load Saved Data
%Reassign Variables
txw2=txw;
txwb2=txwb;
txwg2=txwg;
txya2=txya;
txyba2=txyba;
txyga2=txyga;

%Frequency Bounds
fstart=find(f==1);
fend=find(f==100);
fstep=0.002;
fbounded=[f(fstart):fstep:f(fend)]';

%Peak Relative Displacement TF & Natural Frequency
txwg2=abs(txwg2);
txwg2_bounded=txwg2(fstart:fend,:);
p2=[fbounded, txwg2_bounded];
gap_inertermaxdisp2=max(txwg2_bounded)
idxg = find(p2(:,2) == gap_inertermaxdisp2);
freq_gapinerter2=fbounded(idxg)

%Peak Absolute Acceleration TF (Transmitted force)
txyga2=abs(txyga2);
txyga2_bounded=txyga2(fstart:fend,:);
gap_inertermaxabsaccel2=max(txyga2_bounded)

%Relative Displacement TF Estimate & Plots, Gap = 0.0009
figure(f1)
subplot(2,4,4)
semilogy(f,abs(txwb2))
hold on
semilogy(f,abs(txw2))
hold on
semilogy(f,abs(txwg2))
xlabel('Frequency (Hz)')
ylabel('Rel Disp/Hz (m/Hz)')
title('(d) Gap = 0.001 m')
xlim([0,50])
ylim([10^-7,10^-2])

%Relative Displacement H2 Norm
area6=cumtrapz(fbounded,txwg2_bounded.^2);
H2n_disp_gap001_inerter = sqrt((1/(2*pi))*area6(end))

%Absolute Acceleration TF Estimate & Plots - Gap = 0.0007
figure(f1)

```



```
subplot(2,4,8)
semilogy(f,abs(txyba2))
hold on
semilogy(f,abs(txya2))
hold on
semilogy(f,abs(txyga2))
xlabel('Frequency (Hz)')
ylabel('Abs Accel/Freq (m/s^2/Hz)')
title('(h) Gap = 0.001 m')
ylim([10^-3,10^1])
xlim([0,50])

%Absolute Acceleration H2 Norm
txyga2=abs(txyga2);
txyga2_bounded=txyga2(fstart:fend,:);
area9=cumtrapz(fbounded,txyga2_bounded.^2);
H2n_AbsAcc_gap001_inerter = sqrt((1/(2*pi))*area9(end))
```

A.13 MASS LOADED DISPLACEMENT GAP SYSTEM CODE

```

clear all
close all
warning('off')
load('OctaveFilt_Type1_signal_100s.mat'); %Marine White noise for Type 1 Equipment

%DOF
% y = Absolute Displacement of Top plate

% Die Set System Parameters
m=17.92; %Mass (kg)
k=19858.68; %Spring coefficient (N/m) -- 4 springs @ 28.349 lb/in EA
zeta=0.2; %Damping Ratio = 20%
b=17.92; %Inertance (kg)
cb=2*zeta*sqrt(k*(m+b)); %Damping coefficient(with inerter)
c=2*zeta*sqrt(k*m); %Damping coefficient (without inerter)
e=.001; %Displacement Gap (m)

%State Space Representations
%Linear System Without RIM:
A=[0 1;-k/(m) -c/(m)];
B=[0 ; 1/(m)];
C=[1 0 ; 0 1 ; -k/(m) -c/(m)];
D=[0 ; 0; 1/(m)];
A=double(A);
B=double(B);
C=double(C);
D=double(D);
sys=ss(A,B,C,D);

%Linear System with RIM:
Ab=[0 1;-k/(m+b) -cb/(m+b)];
Bb=[0 ; 1/(m+b)];
Cb=[1 0 ; 0 1;-k/(m+b) -cb/(m+b)];
Db=[0 ; 0 ; 1/(m+b)];
Ab=double(Ab);
Bb=double(Bb);
Cb=double(Cb);
Db=double(Db);
sysb=ss(Ab,Bb,Cb,Db);

%Gap Inerter
%Sys1 : (y=u+e) Inerter Engaged & Extended
Ag=[0 1;(-k)/(m+b) (-cb)/(m+b)];
Bg=[0; 1/(m+b)];
Cg=[1 0;0 1; (-k)/(m+b) (-cb)/(m+b)];
Dg=[0 ; 0; 1/(m+b)];
Ag=double(Ag);
Bg=double(Bg);
Cg=double(Cg);
Dg=double(Dg);

```

```

sys1=ss(Ag,Bg,Cg,Dg);
%Sys 2 : (y=u-e) Inerter Engaged & Compressed
Ag=[0 1;(-k)/(m+b) (-cb)/(m+b)];
Bg=[0; 1/(m+b)];
Cg=[1 0;0 1; (-k)/(m+b) (-cb)/(m+b)];
Dg=[0 ; 0; 1/(m+b)];
Ag=double(Ag);
Bg=double(Bg);
Cg=double(Cg);
Dg=double(Dg);
sys2=ss(Ag,Bg,Cg,Dg);
%Sys 3 : Inerter Disengaged
Ag=[0 1;(-k)/(m) (-c)/(m)];
Bg=[0; 1/(m)];
Cg=[1 0;0 1; (-k)/(m) (-c)/(m)];
Dg=[0 ; 0; 1/(m)];
Ag=double(Ag);
Bg=double(Bg);
Cg=double(Cg);
Dg=double(Dg);
sys3=ss(Ag,Bg,Cg,Dg);

%Simulate Response
%ytotalsignal = acceleration
fs= 25000;
SF=100; %Scale Factor used to scale marine white noise frequency down
t=[0:1/fs:100]*SF; %Time
noise = ytotalsignal*m; %Load (F=m*a)
P=noise; %Load
x0=[0 0]; %Initial Conditions
xb=lsim(sysb,P,t,x0); %Simulation with RIM
x=lsim(sys,P,t,x0); %Simulation w/o RIM

%Results with Inerter
yb=xb(:,1); %Absolute displacement
ydotb=xb(:,2); %Absolute velocity
ydotdotb=xb(:,3); %Absolute acceleration
isolforceb =(k*yb)+(cb*ydotb)+(b*ydotdotb);

%Results without Inerter
y=x(:,1); %Absolute displacement
ydot=x(:,2); %Absolute velocity
ydotdot=x(:,3); %Absolute acceleration
isolforce=(k*y)+(c*ydot);

%Gap Inerter
yg=[0]; %%Absolute displacement
ydotg=[0]; %Absolute velocity
ydotdotg=[0]; %Absolute acceleration
ug=[0]; %Displacement of Inerter
isolforceg=[0]; %Isolator Force

```

```

for a=2:length(t);

    if yg(a-1) > e    %Inerter Engaged & Extended (SYS1: y-u=e)
        Pbg=[P];    %Load
        sys = sys1;
        TrackStateLSIM(a) = 1; %Track Inerter Engagement
        x0=[yg(end) ydotg(end)];
        xg=lsim(sys,Pbg(a-1:a,:),t(a-1:a),x0);

        %Assign New Variables for Next Iteration
        ynew=xg(:,1);
        ydotnew=xg(:,2);
        ydotdotnew=xg(:,3);
        yg_new=ynew(end);
        ydotg_new=ydotnew(end);
        ydotdotg_new=ydotdotnew(end);
        yg(a)=yg_new;
        ydotg(a)=ydotg_new;
        ydotdotg(a)=ydotdotg_new;
        ug(a) = (-(k*e)+P(a)-((m+b)*ydotdotg(a))-(cb*ydotg(a))) / k ;
        isolforceg(a)=(k*yg(a))+(cb*ydotg(a))+(b*(ydotdotg(a)));

    elseif yg(a-1) < -e    %inerter Engaged & Compressed (SYS2: y-u=-e)
        Pbg=[P];    %Load
        sys = sys2;
        TrackStateLSIM(a) = 2; %Track Inerter Engagement
        x0=[yg(end) ydotg(end)];
        xg=lsim(sys,Pbg(a-1:a,:),t(a-1:a),x0);

        %Assign new variables for next iteration
        ynew=xg(:,1);
        ydotnew=xg(:,2);
        ydotdotnew=xg(:,3);
        yg_new=ynew(end);
        ydotg_new=ydotnew(end);
        ydotdotg_new=ydotdotnew(end);
        yg(a)=yg_new;
        ydotg(a)=ydotg_new;
        ydotdotg(a)=ydotdotg_new;
        ug(a) = ((k*e)+P(a)-((m+b)*ydotdotg(a))-(cb*ydotg(a))) / k ;
        isolforceg(a)=(k*yg(a))+(cb*ydotg(a))+(b*(ydotdotg(a)));

    else    %Inerter Disengaged (SYS 3:Fb=0)
        Pbg=[P]; %Load
        sys = sys3;
        TrackStateLSIM(a) = 3; %Track Inerter Disengagement
        x0=[yg(end) ydotg(end)];
        xg=lsim(sys,Pbg(a-1:a,:),t(a-1:a),x0);

        %Assign new variables for next iteration

```

```

        ynew=xg(:,1);
        ydotnew=xg(:,2);
        ydotdotnew=xg(:,3);
        yg_new=ynew(end);
        ydotg_new=ydotnew(end);
        ydotdotg_new=ydotdotnew(end);
        yg(a)=yg_new;
        ydotg(a)=ydotg_new;
        ydotdotg(a)=ydotdotg_new;
        ug(a)=((-k*e)+P(a)-((m)*ydotdotg(a))-(cb*ydotg(a))+P(a))/k;
        isolforceg(a)=(k*yg(a)+(cb*ydotg(a)));
    end

end

%CPD Parameters
nfft = floor(length(noise)/20);
window = hann(nfft);
noverlap = floor(nfft/2);
fs2=fs/SF

%Absolute Displacement TF Estimate & Plots
[txybdisp,f]=tfestimate(P,yb>window,noverlap,nfft,fs2);
[txydisp,f]=tfestimate(P,y>window,noverlap,nfft,fs2);
[txygdisp,f]=tfestimate(P,yg>window,noverlap,nfft,fs2);
f4=figure
semilogy(f,abs(txybdisp))
hold on
semilogy(f,abs(txydisp))
hold on
semilogy(f,abs(txygdisp))
xlabel('Frequency (Hz)')
ylabel('Absolute Displacement/Frequency (m/Hz)')
legend('Isolation with RIM','Isolation without RIM','Isolation with Gap RIM')
title('Absolute Displacement TF Estimate')
xlim([0,100])

%Isolator Force Transfer Function Estimate & Plots
[txybisol,f]=tfestimate(P,isolforceb>window,noverlap,nfft,fs2);
[txyisol,f]=tfestimate(P,isolforce>window,noverlap,nfft,fs2);
[txygisol,f]=tfestimate(P,isolforceg>window,noverlap,nfft,fs2);
f2=figure
semilogy(f,abs(txybisol))
hold on
semilogy(f,abs(txyisol))
hold on
semilogy(f,abs(txygisol))
xlabel('Frequency (Hz)')
ylabel('Isolator Force/Frequency (N/Hz)')
legend('Isolation with RIM','Isolation without RIM','Isolation with Gap RIM')
title('Isolator Force TF')
xlim([0,100])

```

```
%Inerter Engagement Percentage
NumberofTimesInerterDisengaged = numel(find(TrackStateLSIM==3))
NumberofTimesInerterEngaged = numel(find(TrackStateLSIM==1))+numel(find
(TrackStateLSIM==2))
PercentEngaged = (NumberofTimesInerterEngaged / 2500001)*100

%Save results for Figure and Calculation Code
save('MassLoaded_DispGap_001_c',
'e','f','txybisol','txyisol','txygisol','txybdisp','txydisp','txygdisp','PercentEngaged',
'yg','ydotg','ydotdotg','isolforceg') %Save Signal to MATLAB File
```

A.14 MASS LOADED DISPLACEMENT GAP FIGURE & NUMERICAL VALUES

```

%Mass Loaded Displacement Gap Thesis Figure
%-----
%Gap = 0.0001 (Variable 00)
load('MassLoaded_DispGap_0001_c.mat') %Load Saved Data
%Reassign Variables
txybdisp00=txybdisp;
txydisp00=txydisp;
txygdisp00=txygdisp;
txyisol00=txyisol;
txybisol00=txybisol;
txygisol00=txygisol;

%Frequency Bounds
fstart=find(f==1);
fend=find(f==100);
fstep=0.002;
fbounded=[f(fstart):fstep:f(fend)]';

%Peak Absolute Displacement TF & Natural Frequency
txygdisp00=abs(txygdisp00);
txygdisp00_bounded=txygdisp00(fstart:fend,:);
p00=[fbounded,txygdisp00_bounded];
gap_inertermaxdisp00=max(txygdisp00_bounded)
idxg = find(p00(:,2) == gap_inertermaxdisp00);
freq_gapinerter00=fbounded(idxg)

%Peak Isolator Force TF (Transmitted force)
txygisol00=abs(txygisol00);
txygisol00_bounded=txygisol00(fstart:fend,:);
gap_inertermaxisol00=max(txygisol00_bounded)

%Absolute Displacement Transfer Function Estimate & Plots, Gap = 0.0001
f1=figure
subplot(2,4,1)
semilogy(f,abs(txybdisp00))
hold on
semilogy(f,abs(txydisp00))
hold on
semilogy(f,abs(txygdisp00))
xlabel('Frequency (Hz)')
ylabel('Abs Disp/Freq (m/Hz)')
title('(a) Gap = 0.0001 m')
xlim([0,50])
ylim([10^-8,10^-3])

%Absolute Displacement H2 Norm:
area6=cumtrapz(fbounded,txygdisp00_bounded.^2);
H2n_disp_gap0001_inerter = sqrt((1/(2*pi))*area6(end))

%Isolator Force Transfer Function Estimate & Plots, Gap = 0.001
figure(f1)

```

```

subplot(2,4,5)
semilogy(f,abs(txybisol00))
hold on
semilogy(f,abs(txyisol00))
hold on
semilogy(f,abs(txygisol00))
xlabel('Frequency (Hz)')
ylabel('Isol Force/Freq (N/Hz)')
title('(e) Gap = 0.0001 m')
ylim([10^-3,10^1])
xlim([0,50])

%Absolute Acceleration H2 Norm:
txygisol00=abs(txygisol00);
txygisol00_bounded=txygisol00(fstart:fend,:);
area9=cumtrapz(fbounded,txygisol00_bounded.^2);
H2n_isol_gap0001_inerter = sqrt((1/(2*pi))*area9(end))

%-----
%Gap = 0.0003 (Variable 0)
load('MassLoaded_DispGap_0003_c.mat') %Load Saved Data
%Reassign Variables
txybdisp0=txybdisp;
txydisp0=txydisp;
txygdisp0=txygdisp;
txyisol0=txyisol;
txybisol0=txybisol;
txygisol0=txygisol;

%Frequency Bounds
fstart=find(f==1);
fend=find(f==100);
fstep=0.002;
fbounded=[f(fstart):fstep:f(fend)'];

%Peak Absolute Displacement TF & Natural Frequency
txygdisp0=abs(txygdisp0);
txygdisp0_bounded=txygdisp0(fstart:fend,:);
p0=[fbounded,txygdisp0_bounded];
gap_inertermaxdisp0=max(txygdisp0_bounded)
idxg = find(p0(:,2) == gap_inertermaxdisp0);
freq_gapinerter0=fbounded(idxg)

%Peak Isolator Force TF (Transmitted force)
txygisol0=abs(txygisol0);
txygisol0_bounded=txygisol0(fstart:fend,:);
gap_inertermaxisol0=max(txygisol0_bounded)

%Absolute Displacement TF Estimate & Plots, Gap = 0.003
figure(f1)
subplot(2,4,2)

```



```

semilogy(f,abs(txybdisp0))
hold on
semilogy(f,abs(txydisp0))
hold on
semilogy(f,abs(txygdisp0))
xlabel('Frequency (Hz)')
ylabel('Abs Disp/Freq (m/Hz)')
title('(b) Gap = 0.0003 m')
xlim([0,50])
ylim([10^-8,10^-3])

%Absolute Displacement H2 Norm, Gap= 0.0003
area6=cumtrapz(fbounded,txygdisp0_bounded.^2);
H2n_disp_gap0003_inerter = sqrt((1/(2*pi))*area6(end))

%Isolator Force TF Estimate & Plot, Gap = 0.0003
figure(f1)
subplot(2,4,6)
semilogy(f,abs(txybisol0))
hold on
semilogy(f,abs(txyisol0))
hold on
semilogy(f,abs(txygisol0))
xlabel('Frequency (Hz)')
ylabel('Isol Force/Freq (N/Hz)')
title('(f) Gap = 0.0003 m')
ylim([10^-3,10^1])
xlim([0,50])

%Isolator Force H2 Norm:
txygisol0=abs(txygisol0);
txygisol0_bounded=txygisol0(fstart:fend,:);
area9=cumtrapz(fbounded,txygisol0_bounded.^2);
H2n_isol_gap0003_inerter = sqrt((1/(2*pi))*area9(end))

%-----
%Gap = 0.0005 (Variable 1)
load('MassLoaded_DispGap_0005_c.mat') %Load Saved Data
%Reassign Variables
txybdisp1=txybdisp;
txydisp1=txydisp;
txygdisp1=txygdisp;
txyisol1=txyisol;
txybisol1=txybisol;
txygisol1=txygisol;

%Frequency Bounds
fstart=find(f==1);
fend=find(f==100);
fstep=0.002;
fbounded=[f(fstart):fstep:f(fend)];

```

```

%Peak Displacement TF & Natural Frequency
txygdysl=abs(txygdysl);
txygdysl_bounded=txygdysl(fstart:fend,:);
p1=[fbounded, txygdysl_bounded];
gap_inertermaxdysl=max(txygdysl_bounded)
idxg = find(p1(:,2) == gap_inertermaxdysl);
freq_gapinerter1=fbounded(idxg)

%Peak Isolator Force TF (Transmitted force)
txygisol1=abs(txygisol1);
txygisol1_bounded=txygisol1(fstart:fend,:);
gap_inertermaxisol1=max(txygisol1_bounded)

%Absolute Displacement TF Estimate & Plots, Gap = 0.0005
figure(f1)
subplot(2,4,3)
semilogy(f,abs(txybdysl))
hold on
semilogy(f,abs(txydysl))
hold on
semilogy(f,abs(txygdysl))
xlabel('Frequency (Hz)')
ylabel('Abs Disp/Freq (m/Hz)')
title('(c) Gap = 0.0005 m')
xlim([0,50])
ylim([10^-8,10^-3])

%Absolute Displacement TF H2 Norm, Gap= 0.0005
area6=cumtrapz(fbounded,txygdysl_bounded.^2);
H2n_disp_gap0005_inerter = sqrt((1/(2*pi))*area6(end))

%Isolator Force TF Estimate & Plot, Gap = 0.0005
figure(f1)
subplot(2,4,7)
semilogy(f,abs(txybisol1))
hold on
semilogy(f,abs(txyisol1))
hold on
semilogy(f,abs(txygisol1))
xlabel('Frequency (Hz)')
ylabel('Isol Force/Freq (N/Hz)')
title('(g) Gap = 0.0005 m')
ylim([10^-3,10^1])
xlim([0,50])

%Isolator Force H2 Norm:
txygisol1=abs(txygisol1);
txygisol1_bounded=txygisol1(fstart:fend,:);
area9=cumtrapz(fbounded,txygisol1_bounded.^2);
H2n_isol_gap0005_inerter = sqrt((1/(2*pi))*area9(end))

```

```

%-----
%Gap = 0.001 (Variable 2)
load('MassLoaded_DispGap_001_c.mat') %Load Saved Data
%Reassign Variables
txybdisp2=txybdisp;
txydisp2=txydisp;
txygdisp2=txygdisp;
txyisol2=txyisol;
txybisol2=txybisol;
txygisol2=txygisol;

%Frequency Bounds
fstart=find(f==1);
fend=find(f==100);
fstep=0.002;
fbounded=[f(fstart):fstep:f(fend)]';

%Peak Displacement TF & Natural Frequency
txygdisp2=abs(txygdisp2);
txygdisp2_bounded=txygdisp2(fstart:fend,:);
p2=[fbounded,txygdisp2_bounded];
gap_inertermaxdisp2=max(txygdisp2_bounded)
idxg = find(p2(:,2) == gap_inertermaxdisp2);
freq_gapinerter2=fbounded(idxg)

%Peak Isol Force TF (Transmitted force)
txygisol2=abs(txygisol2);
txygisol2_bounded=txygisol2(fstart:fend,:);
gap_inertermaxisol2=max(txygisol2_bounded)

%Absolute Displacement TF Estimate & Plots
figure(f1)
subplot(2,4,4)
semilogy(f,abs(txybdisp2))
hold on
semilogy(f,abs(txydisp2))
hold on
semilogy(f,abs(txygdisp2))
xlabel('Frequency (Hz)')
ylabel('Abs Disp/Freq (m/Hz)')
title('(d) Gap = 0.001 m')
xlim([0,50])
ylim([10^-8,10^-3])

%Absolute Displacement H2 Norm
area6=cumtrapz(fbounded,txygdisp2_bounded.^2);
H2n_disp_gap0009_inerter = sqrt((1/(2*pi))*area6(end))

%Isolator Force TF Estimate & Plots, Gap = 0.001

```

```
figure(f1)
subplot(2,4,8)
semilogy(f,abs(txybisol2))
hold on
semilogy(f,abs(txyisol2))
hold on
semilogy(f,abs(txygisol2))
xlabel('Frequency (Hz)')
ylabel('Isol Force/Freq (N/Hz)')
title('(h) Gap = 0.001 m/s^2')
ylim([10^-3,10^1])
xlim([0,50])

%Isolator Force H2 Norm:
txygisol2=abs(txygisol2);
txygisol2_bounded=txygisol2(fstart:fend,:);
area9=cumtrapz(fbounded,txygisol2_bounded.^2);
H2n_isol_gap0009_inerter = sqrt((1/(2*pi))*area9(end))
```

A. 15 GEOMETRICALLY NONLINEAR INERTER ACCELERATION DERIVATION

Geometrically Nonlinear Inerter Acceleration Equation Derivation

$$f_b = f_{b1} + f_{b2} = 2b\left(\frac{x^2\ddot{x}}{l^2+x^2} + \frac{l^2x\dot{x}^2}{(l^2+x^2)^2}\right) \quad (\text{Yang, Jiang, and Neild 2020})$$

Equation of Motion for the mass loaded (P) SDOF System with damping, stiffness, and GNI:

$$m\ddot{x} + c\dot{x} + kx + f_b = P$$

$$m\ddot{x} + c\dot{x} + kx + \left(\frac{2bx^2\ddot{x}}{l^2+x^2} + \frac{2bl^2x\dot{x}^2}{(l^2+x^2)^2}\right) = P$$

$$m\ddot{x} + c\dot{x} + kx + \left(\frac{2bx^2}{l^2+x^2}\right)\ddot{x} + \left(\frac{2bl^2x\dot{x}^2}{(l^2+x^2)^2}\right) = P$$

$$\left(m + \left(\frac{2bx^2}{l^2+x^2}\right)\right)\ddot{x} + c\dot{x} + kx = P - \left(\frac{2bl^2x\dot{x}^2}{(l^2+x^2)^2}\right)$$

$$\ddot{x} = \frac{P - \left(\frac{2bl^2x\dot{x}^2}{(l^2+x^2)^2}\right) - c\dot{x} - kx}{\left(m + \left(\frac{2bx^2}{l^2+x^2}\right)\right)}$$

A. 16 GEOMETRICALLY NONLINEAR INERTER CODE

```

%Geometrically Nonlinear Inerter Code

clear all
close all
warning('off')

%System Parameters for Linear Systems
m=17.92; %Mass (kg)
k=17686.33; %Spring Coefficient(N/m) -- 4 springs @ 28.349 lb/in EA
zeta=.2; %Damping Ratio = 20%
b=36; %Inertance (kg)
bb=b/2; %Inertance per side (kg)
cb=2*zeta*sqrt(k*(m+b)); %Damping coefficient(with inerter)
c=2*zeta*sqrt(k*m); %Damping coefficient (without inerter)
L=0.005; %m
Parameters = [m k zeta b bb cb c L]; %Parameters used for ode45

%Simulate Response
fs= 1000;
tend=100;
toriginal=[0:1/fs:tend]; %Time
rng(1);
noise=wgn(length(toriginal),1,55);
x0=[0 0]; %Initial Conditions
scale = 1;
P=noise*scale; %Load

%State Space Representations
%Linear System Without RIM (DOF = u)
A=[0 1;-k/(m) -c/(m)];
B=[0 ; 1/(m)];
C=[1 0 ; 0 1 ; -k/(m) -c/(m)];
D=[0 ; 0; 1/(m)];
A=double(A);
B=double(B);
C=double(C);
D=double(D);
sys=ss(A,B,C,D);
%Results without Inerter
xx=lsim(sys,P,toriginal,x0);
u=xx(:,1); %Absolute displacement
udot=xx(:,2); %Absolute velocity
udotdot=xx(:,3); %Absolute acceleration
isolforce=(k.*u)+(c.*udot); %Isolator Force
MaxDisp_NoInerter_cm = max(u)*100 %Maximum Displacement (cm)

%Linear System with Inerter: (DOF = ub)
Ab=[0 1;-k/(m+b) -cb/(m+b)];
Bb=[0 ; 1/(m+b)];
Cb=[1 0 ; 0 1;-k/(m+b) -cb/(m+b)];
Db=[0 ; 0 ; 1/(m+b)];

```

```

Ab=double (Ab);
Bb=double (Bb);
Cb=double (Cb);
Db=double (Db);
sysb=ss (Ab, Bb, Cb, Db);
%Results with Inerter
xb=lsim (sysb, P, toriginal, x0);
ub=xb (:, 1); %Absolute displacement
udotb=xb (:, 2); %Absolute velocity
udotdotb=xb (:, 3); %Absolute acceleration
isolforceb = (k.*ub)+(cb.*udotb)+(b.*udotdotb); %Isolator Force
MaxDisp_wInerter_cm = max(ub)*100 %Maximum Displacement (cm)

%Geometrically Nonlinear Inerter: (DOF = x)
HighSamplingRate=100*fs; %Higher Sampling Rate to add more points to the system
NoiseVectorTime=[0:1/HighSamplingRate:100]; %New Time Vector
NoiseHighFs=interp1 (toriginal, P, NoiseVectorTime)'; %New Noise Vector to interpolate
between the old and new time vector
IC=[0 0]; %Initial Conditions
SolverOptions=odeset ('RelTol', 1e-10, 'AbsTol', 1e-10); %SolverOptions
[t, Y]= ode45 (@(t, x) inerter (t, x, NoiseHighFs, HighSamplingRate, Parameters), [0:1/fs:100], IC,
SolverOptions); %ODE45 Command
x=Y (:, 1); %Absolute displacement
xdot=Y (:, 2); %Absolute velocity

% Calculate acceleration using equations:
a1=(m+(2.*bb).*(x.^2./(L.^2+x.^2)));
a2=(2.*bb.*(L.^2).*x.*(xdot.^2))./(((L.^2)+(x.^2)).^2);
xdotdot=(1./a1).*(P-(xdot*cb)-(x*k)-a2); %Absolute acceleration
fb=(2.*bb).*((x.^2).*(xdotdot))./(L.^2+x.^2)+(((L.^2).*x.*(xdot.^2))./(((L.^2)+(x.^2)).^2)); %Force of GNI, Yang (2020)
isolforcex = (k.*x)+(cb.*xdot)+(fb); %Isolator Force
MaxDisp_GNI_m=max(x) %Max Displacemement (m)
MaxDisp_GNI_cm=MaxDisp_GNI_m*100 %Max Displacemement (cm)

%CPSD Parameters
nfft = floor (length (noise)/20);
window = hann (nfft);
noverlap = floor (nfft/2);

%Displacement Transfer Function Plot
[txyd_x, f]=tffestimate (P, x, window, noverlap, nfft, fs);
[txyd_u, f]=tffestimate (P, u, window, noverlap, nfft, fs);
[txyd_ub, f]=tffestimate (P, ub, window, noverlap, nfft, fs);
f4=figure
semilogy (f, abs (txyd_x))
hold on
semilogy (f, abs (txyd_u))
hold on
semilogy (f, abs (txyd_ub))
xlabel ('Frequency (Hz)')

```

```

ylabel('Absolute Displacement/Frequency (m/Hz)')
legend('Geometrically Nonlinear Inerter','Isolation without RIM','Isolation with RIM')
title('Absolute Displacement TF Estimate')

%Isolator Force Transfer Function Plot
[txyi_x,f]=tfestimate(P,isolforcex>window,noverlap,nfft,fs);
[txyi_u,f]=tfestimate(P,isolforce>window,noverlap,nfft,fs);
[txyi_ub,f]=tfestimate(P,isolforceb>window,noverlap,nfft,fs);
f5=figure
semilogy(f,abs(txyi_x))
hold on
semilogy(f,abs(txyi_u))
hold on
semilogy(f,abs(txyi_ub))
xlabel('Frequency (Hz)')
ylabel('Isolator Force/Frequency (N/Hz)')
legend('Geometrically Nonlinear Inerter','Isolation without RIM','Isolation with RIM')
title('Isolator Force TF')
xlim([0,100])

%H2 Norm Calcs -- Disp
area4=cumtrapz(f,abs(txyd_x.^2));
H2n_disp_geo_inerter = sqrt((1/(2*pi))*area4(end));
area5=cumtrapz(f,abs(txyd_u.^2));
H2n_disp_wo_inerter =sqrt((1/(2*pi))*area5(end));
area6=cumtrapz(f,abs(txyd_ub.^2));
H2n_disp_w_inerter= sqrt((1/(2*pi))*area6(end));

%H2 Norm Calcs -- Isolator Force
area7=cumtrapz(f,abs(txyi_x.^2));
H2n_isol_geo_inerter = sqrt((1/(2*pi))*area7(end));
area8=cumtrapz(f,abs(txyi_u.^2));
H2n_isol_wo_inerter = sqrt((1/(2*pi))*area8(end));
area9=cumtrapz(f,abs(txyi_ub.^2));
H2n_isol_w_inerter= sqrt((1/(2*pi))*area9(end));

%Effective natural Frequency
Wn_nonlinear = abs(sqrt(k./(m+fb)));
Wn_linear = sqrt(k./m);
Wn_ratio = Wn_nonlinear / Wn_linear ;
Wn_percent = Wn_ratio.*100;
Wn_percent_reduction = 100 - Wn_percent;
Greater90 = Wn_percent_reduction > 90; % if Wn percent reduction is greater than 90 ->
nonlinear effects observed
Count=sum(Greater90); % Percent Nonlinear effects observed

%Save Results for Figure and Calculation Code
save
('GNI_Lp005_b36','Count','L','b','f','x','xdot','xdotdot','txyd_x','txyd_u','txyd_ub',...
'txyi_x','txyi_u','txyi_ub','MaxDisp_NoInerter_cm','MaxDisp_wInerter_cm','MaxDisp_GNI_cm')

```



```
) %Save Signal to MATLAB File

% %Parameters = [m k zeta b bb cb c L];
function dx = inerter(t,x,NoiseHighFs,HighSamplingRate,Parameters)

    tIndex=round(t*HighSamplingRate)+1; %Finds nearest time step to current time
    p=NoiseHighFs(tIndex); %Selects noise value at tIndex which gives an approx✓
interpolation
    m=Parameters(1);
    k=Parameters(2);
    zeta=Parameters(3);
    bb=Parameters(5);
    cb=Parameters(6);
    L=Parameters(8);
    a1=(m+((2.*bb).*(x(1).^2./(L.^2+x(1).^2)));
    a2=(2.*bb.*(L.^2).*x(1).*(x(2).^2)./(((L.^2)+(x(1).^2)).^2);
    dx=[x(2); ...
        (1/a1)*(p-(x(2)*cb)-(x(1)*k)-(a2))];
end
```

A. 17 GEOMETRICALLY NONLINEAR INERTER FIGURE & NUMERICAL VALUES

```

%Geometrically Nonlinear Inerter Figure
clear all
close all

%L=0.001 m, b= 36 kg (Variable 00)
load('GNI_Lp001_b36.mat') %Load Saved Data
%Reassign Variables
txybdisp00=txyd_ub;
txydisp00=txyd_u;
txygdisp00=txyd_x;
txyisol00=txyi_u;
txybisol00=txyi_ub;
txygisol00=txyi_x;

%Frequency Bounds
fstart=find(f==1);
fend=find(f==100);
fstep=0.2;
fbounded=[f(fstart):fstep:f(fend)];

%Peak absolute Disp TF & Natural Frequency
txygdisp00=abs(txygdisp00);
txygdisp00_bounded=txygdisp00(fstart:fend,:);
p00=[fbounded, txygdisp00_bounded];
GNI_maxdisp00=max(txygdisp00_bounded)
idxg = find(p00(:,2) == GNI_maxdisp00);
GNI_Freq00=fbounded(idxg)

%Peak Isol Force TF (Transmitted force)
txygisol00=abs(txygisol00);
txygisol00_bounded=txygisol00(fstart:fend,:);
GNI_maxisol00=max(txygisol00_bounded)

%Absolute Displacement Transfer Function Estimate
f1=figure
subplot(2,3,1)
semilogy(f,abs(txybdisp00))
hold on
semilogy(f,abs(txydisp00))
hold on
semilogy(f,abs(txygdisp00))
xlabel('Frequency (Hz)')
ylabel('Abs Disp/Freq (m/Hz)')
title('(a) L=0.001, b = 36 kg')
xlim([0,50])
% ylim([10^-7,10^-3])

%Absolute Displacement H2 Norm:
area6=cumtrapz(fbounded,txygdisp00_bounded.^2);
H2n_GNI_disp_00 = sqrt((1/(2*pi))*area6(end))

```

```

%Isolator Force Transfer Function Estimate
figure(f1)
subplot(2,3,4)
semilogy(f,abs(txybisol00))
hold on
semilogy(f,abs(txyisol00))
hold on
semilogy(f,abs(txygisol00))
xlabel('Frequency (Hz)')
ylabel('Isol Force/Freq (N/Hz)')
title('(d) L=0.001 m, b=36 kg')
ylim([10^-2,10^1])
xlim([0,50])

%Isolator Force H2 Norm:
txygisol00=abs(txygisol00);
txygisol00_bounded=txygisol00(fstart:fend,:);
area9=cumtrapz(fbounded,txygisol00_bounded.^2);
H2n_GNI_isol_00 = sqrt((1/(2*pi))*area9(end))

%Linear Systems Table Values
%Without RIM: Peak Absolute Disp TF & Natural Frequency
txydisp00=abs(txydisp00);
txydisp00_bounded=txydisp00(fstart:fend,:);
p00=[fbounded, txydisp00_bounded];
WO_maxdisp=max(txydisp00_bounded)
idxg = find(p00(:,2) == WO_maxdisp);
WO_Freq=fbounded(idxg)
%Absolute Displacement H2 Norm:
area10=cumtrapz(fbounded,txydisp00_bounded.^2);
H2n_WO_disp = sqrt((1/(2*pi))*area10(end))
%Peak Isol Force TF (Transmitted force)
txyisol00=abs(txyisol00);
txyisol00_bounded=txyisol00(fstart:fend,:);
WO_maxisol=max(txyisol00_bounded)
%Isolator Force H2 Norm:
txyisol00=abs(txyisol00);
txyisol00_bounded=txyisol00(fstart:fend,:);
area11=cumtrapz(fbounded,txyisol00_bounded.^2);
H2n_WO_isol = sqrt((1/(2*pi))*area11(end))

%With RIM: Peak absolute Disp TF & Natural Frequency
txybdisp00=abs(txybdisp00);
txybdisp00_bounded=txybdisp00(fstart:fend,:);
p00=[fbounded, txybdisp00_bounded];
W_maxdisp=max(txybdisp00_bounded)
idxg = find(p00(:,2) == W_maxdisp);
W_Freq=fbounded(idxg)
%Absolute Displacement H2 Norm:
area12=cumtrapz(fbounded,txybdisp00_bounded.^2);
H2n_W_disp = sqrt((1/(2*pi))*area12(end))

```

```

%Peak Isol Force TF (Transmitted force)
txybisol00=abs(txybisol00);
txybisol00_bounded=txybisol00(fstart:fend,:);
W_maxisol=max(txybisol00_bounded)
%Isolator Force H2 Norm:
txybisol00=abs(txybisol00);
txybisol00_bounded=txybisol00(fstart:fend,:);
areal3=cumtrapz(fbounded,txybisol00_bounded.^2);
H2n_W_isol = sqrt((1/(2*pi))*areal3(end))

```

```

% % -----

```

```

%L=0.005 m, b= 36 kg (Variable 0)
load('GNI_Lp005_b36.mat') %Load Saved Data
%Reassign Variables
txybdisp0=txyd_ub;
txydisp0=txyd_u;
txygdisp0=txyd_x;
txyisol0=txyi_u;
txybisol0=txyi_ub;
txygisol0=txyi_x;

```

```

%Frequency Bounds
fstart=find(f==1);
fend=find(f==100);
fstep=0.2;
fbounded=[f(fstart):fstep:f(fend)'];

```

```

%Peak absolute Disp TF & Natural Frequency
txygdisp0=abs(txygdisp0);
txygdisp0_bounded=txygdisp0(fstart:fend,:);
p0=[fbounded, txygdisp0_bounded];
GNI_maxdisp0=max(txygdisp0_bounded)
idxg = find(p0(:,2) == GNI_maxdisp0);
GNI_Freq0=fbounded(idxg)

```

```

%Peak Isol Force TF (Transmitted force)
txygisol0=abs(txygisol0);
txygisol0_bounded=txygisol0(fstart:fend,:);
GNI_maxisol0=max(txygisol0_bounded)

```

```

%Absolute Displacement Transfer Function Estimate
figure(f1)
subplot(2,3,2)
semilogy(f,abs(txybdisp0))
hold on
semilogy(f,abs(txydisp0))
hold on
semilogy(f,abs(txygdisp0))
xlabel('Frequency (Hz)')
ylabel('Abs Disp/Freq (m/Hz)')
title('(b) L=0.005, b = 36 kg')

```

```

xlim([0,50])

%Absolute Displacement H2 Norm:
area6=cumtrapz(fbounded,txygdisp0_bounded.^2);
H2n_GNI_disp_0 = sqrt((1/(2*pi))*area6(end))

%Isolator Force Transfer Function Estimate
figure(f1)
subplot(2,3,5)
semilogy(f,abs(txybisol0))
hold on
semilogy(f,abs(txyisol0))
hold on
semilogy(f,abs(txygisol0))
xlabel('Frequency (Hz)')
ylabel('Isol Force/Freq (N/Hz)')
title('(e) L=0.005 m, b=36 kg')
ylim([10^-2,10^1])
xlim([0,50])

%Isolator Force H2 Norm:
txygisol0=abs(txygisol0);
txygisol0_bounded=txygisol0(fstart:fend,:);
area9=cumtrapz(fbounded,txygisol0_bounded.^2);
H2n_GNI_isol_0 = sqrt((1/(2*pi))*area9(end))

% % -----
%L=0.01 m, b= 36 kg (Variable 0)
load('GNI_Lp01_b36.mat') %Load Saved Data
%Reassign Variables
txybdisp1=txyd_ub;
txydisp1=txyd_u;
txygdisp1=txyd_x;
txyisol1=txyi_u;
txybisol1=txyi_ub;
txygisol1=txyi_x;

%Frequency Bounds
fstart=find(f==1);
fend=find(f==100);
fstep=0.2;
fbounded=[f(fstart):fstep:f(fend)]';

%Peak absolute Disp TF & Natural Frequency
txygdisp1=abs(txygdisp1);
txygdisp1_bounded=txygdisp1(fstart:fend,:);
p1=[fbounded,txygdisp1_bounded];
GNI_maxdisp1=max(txygdisp1_bounded)
idxg = find(p1(:,2) == GNI_maxdisp1);
GNI_Freq1=fbounded(idxg)

```

```
%Peak Isol Force TF (Transmitted force)
txygisol1=abs(txygisol1);
txygisol1_bounded=txygisol1(fstart:fend,:);
GNI_maxisol1=max(txygisol1_bounded)

%Absolute Displacement Transfer Function Estimate
figure(f1)
subplot(2,3,3)
semilogy(f,abs(txybdisp1))
hold on
semilogy(f,abs(txydisp1))
hold on
semilogy(f,abs(txygdisp1))
xlabel('Frequency (Hz)')
ylabel('Abs Disp/Freq (m/Hz)')
title('(c) L=0.01, b = 36 kg')
xlim([0,50])
% ylim([10^-7,10^-3])

%Absolute Displacement H2 Norm:
area6=cumtrapz(fbounded,txygdisp1_bounded.^2);
H2n_GNI_disp_1 = sqrt((1/(2*pi))*area6(end))

%Isolator Force Transfer Function Estimate, L=0.03 m
figure(f1)
subplot(2,3,6)
semilogy(f,abs(txybisol1))
hold on
semilogy(f,abs(txyisol1))
hold on
semilogy(f,abs(txygisol1))
xlabel('Frequency (Hz)')
ylabel('Isol Force/Freq (N/Hz)')
title('(g) L=0.01 m, b=36 kg')
ylim([10^-2,10^1])
xlim([0,50])

%Isolator Force H2 Norm:
txygisol1=abs(txygisol1);
txygisol1_bounded=txygisol1(fstart:fend,:);
area9=cumtrapz(fbounded,txygisol1_bounded.^2);
H2n_GNI_isol_1 = sqrt((1/(2*pi))*area9(end))
```

A.18 RIM AND NRIM INERTANCE CALCULATION - FLYWHEEL 1

FLYWHEEL INERTANCE CALCULATIONS (FLYWHEEL 1)

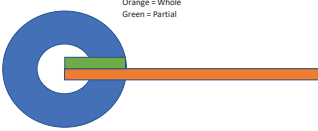
| Die Set Information | | Flywheel Bolts (STEEL ONLY) | | Flywheel Moment of Inertia Calculations | | | | Percent | | | | | |
|-------------------------|--------------------------------|-----------------------------------|---|--|-------------|----------------------|--------------------|---|---------------------------|-------------------------------|-----------------------------|-------------------|-------------|
| Mass (Total), kg | 18.3345434 | 0 | 0 | Component | Volume | I _{Partial} | I | Unit | Desired Inertance | Actual Gap Inertance | Actual Inertance Percentage | Natural Frequency | |
| Density of Steel | 0.000008 kg/mm ³ | 0 | 0 | Centerpiece | | | 0.585 | kg*mm ² | 25 | 4.583635849 | 4.99 | 27.0 | 4.647952448 |
| Density of Zinc | 0.000008 kg/mm ³ | 0 | 0 | Rod 1 | 2.248 | 0.042 | 2.206 | kg*mm ² | 50 | 9.167271698 | 9.47 | 51.7 | 4.253413992 |
| Die Set Nat Freq (Hz) | 5.24 | 0 | 0 | Rod 2 | 0.000 | 0.042 | -0.042 | kg*mm ² | 100 | 18.3345434 | 18.8 | 102.5 | 3.680497229 |
| | | | | Rod 3 | 2.248 | 0.042 | 2.206 | kg*mm ² | 200 | 36.66908679 | 36.1 | 196.9 | 3.039892645 |
| | | | | Rod 4 | 0.000 | 0.042 | -0.042 | kg*mm ² | | | | | |
| Lead Screw Dimensions | | Total Number of Nuts on Each Bolt | | Washer Moment of Inertia Calculations | | | | Mass Calculation | | | | | |
| Lead | 8 mm | 0 | 0 | Washer Number | Radius (mm) | I = MR ² | Unit | Member | Volume (mm ³) | Density (kg/mm ³) | Mass (kg) | | |
| Length | 300 mm | 0 | 0 | 1 | 0.863 | 0.002 | kg*mm ² | Die Set Top Plate | 5343860.502 | 0.00000281 | 14.73524803 | | |
| Radius | 4 mm | 0 | 0 | 2 | -2.274 | 0.014 | kg*mm ² | Spring retainer plates | 105783.5777 | 0.000008 | 0.846268622 | | |
| Volume | 15079.6320 mm ³ | | | 4 | -5.411 | 0.078 | kg*mm ² | Adaptive Plate | 344128.3455 | 0.000008 | 2.753026764 | | |
| Mass | 0.1206 kg | | | 5 | -11.685 | 0.362 | kg*mm ² | TOTAL | | | 18.3345434 | | |
| Moment of inertia | 0.965096448 kg*mm ² | | | 6 | -14.821 | 0.583 | kg*mm ² | | | | | | |
| Centerpiece Dimensions | | | | 7 | -17.658 | 0.855 | kg*mm ² | Linear Inerters | | | | | |
| O.D (inch) | 0.75 inch | 19.05 mm | | 8 | -21.095 | 1.180 | kg*mm ² | Inertance (kg) | Mass Percent (%) | Natural Frequency (Hz) | | | |
| Radius (O.D) | | 9.525 mm | | 9 | -24.232 | 1.557 | kg*mm ² | 4.51 | 24.57 | 4.691500182 | | | |
| I.D | 0.323 inch | 8.2042 mm | | 10 | -27.569 | 2.936 | kg*mm ² | 7.08 | 39.7 | 4.4115165064 | | | |
| Radius (I.D) | | 4.1021 mm | | TOTAL | | | 4.913 | kg*mm ² | 18.3 | 100 | 3.705528413 | | |
| Thickness | 0.3 inch | 7.62 mm | | | | | | | 35.7 | 194.5 | 3.051123566 | | |
| Mass | 0.01089 kg | | | | | | | | | | | | |
| Rod Dimensions | | | | Total Moment of Inertia, Flywheel = 4.913 kg*mm ² | | | | Inertance Calculations | | | | | |
| Rod 1: Set Screw | | | | Lead Screw | 0.595320009 | kg | | Inertance B (Two-way Gap Inerters) | | | | | |
| Radius | 2.413 mm | | | Flywheel | 3.630 | kg | | 4.50538131 | kg | | | | |
| Length | 1.25 inch | 31.75 mm | | Nuts | 0 | kg | | % of Mass | 24.57 | % | | | |
| Effective Length | | 35.8521 | | Shaft Collar A | 0.439862793 | kg | | Inertance B (Bushings-Crown Gap Inerters) | | | | | |
| Volume | 655.8110784 | mm ³ | | Shaft Collar B | 0.439862793 | kg | | 4.945244102 | kg | | | | |
| Total Mass | 0.005246489 | kg | | Shaft Collar C | 0.439862793 | kg | | % of Mass | 26.97 | % | | | |
| I-Partial | 9.525 | mm | | | | | | Inertance (Linear Inerters): | | | | | |
| Mass-Partial | 0.00139386 | kg | | | | | | 4.50538131 | kg | | | | |
| Rod 2: Bolt (Steel) | | | | | | | | % of Mass | 24.57 | % | | | |
| Radius | 2.413 mm | | | | | | | | | | | | |
| Length | 0 inch | 0 mm | | | | | | | | | | | |
| Effective Length | 0 | mm | | | | | | | | | | | |
| Volume | 0 | mm ³ | | | | | | | | | | | |
| Total Mass | 0 | kg | | | | | | | | | | | |
| I-Partial | 9.525 | mm | | | | | | | | | | | |
| Mass-Partial | 0.00139386 | kg | | | | | | | | | | | |
| Rod 3: Set Screw | | | | | | | | | | | | | |
| Radius | 2.413 mm | | | | | | | | | | | | |
| Length | 1.25 inch | 31.75 mm | | | | | | | | | | | |
| Effective Length | | 35.8521 | | | | | | | | | | | |
| Volume | 655.8110784 | mm ³ | | | | | | | | | | | |
| Total Mass | 0.005246489 | kg | | | | | | | | | | | |
| I-Partial | 9.525 | mm | | | | | | | | | | | |
| Mass-Partial | 0.00139386 | kg | | | | | | | | | | | |
| Rod 4: Bolt (Steel) | | | | | | | | | | | | | |
| Radius | 2.413 mm | | | | | | | | | | | | |
| Length | 0 inch | 0 mm | | | | | | | | | | | |
| Effective Length | 0 | mm | | | | | | | | | | | |
| Volume | 0 | mm ³ | | | | | | | | | | | |
| Total Mass | 0 | kg | | | | | | | | | | | |
| I-Partial | 9.525 | mm | | | | | | | | | | | |
| Mass-Partial | 0.00139386 | kg | | | | | | | | | | | |
| Shaft Collar Dimensions | | | | Total Moment of Inertia, Flywheel = 4.913 kg*mm ² | | | | Inertance Calculations | | | | | |
| O.D | 18 mm | | | Lead Screw | 0.595320009 | kg | | Inertance B (Two-way Gap Inerters) | | | | | |
| I.D | 8 mm | | | Flywheel | 3.630 | kg | | 4.50538131 | kg | | | | |
| Thickness | 9 mm | | | Nuts | 0 | kg | | % of Mass | 24.57 | % | | | |
| Volume | 1837.831702 | mm ³ | | Shaft Collar A | 0.439862793 | kg | | Inertance B (Bushings-Crown Gap Inerters) | | | | | |
| Mass | 0.014702654 | kg | | Shaft Collar B | 0.439862793 | kg | | 4.945244102 | kg | | | | |
| Moment of inertia | 0.715078701 | kg*mm ² | | Shaft Collar C | 0.439862793 | kg | | % of Mass | 26.97 | % | | | |
| Added Weight Dimensions | | | | | | | | Inertance (Linear Inerters): | | | | | |
| O.D | 9.2456 mm | | | | | | | 4.50538131 | kg | | | | |
| I.D | 4.2672 mm | | | | | | | % of Mass | 24.57 | % | | | |
| Thickness | 3.1369 mm | | | | | | | | | | | | |
| Volume | 165.7393734 | mm ³ | | | | | | | | | | | |
| Mass | 0.001320515 | kg | | | | | | | | | | | |
| Moment of inertia | 0.017185535 | kg*mm ² | | | | | | | | | | | |

A.19 RIM INERTANCE CALCULATION - FLYWHEEL 2A

FLYWHEEL INERTANCE CALCULATIONS (FLYWHEEL 2)

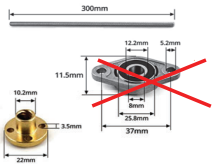
| Die Set Information | | Flywheel Bolts (STEEL ONLY) | | Flywheel Moment of Inertia Calculations | | | | Percent | | | | | |
|-----------------------|-----------------------------|-----------------------------------|-----|--|---------------------------|-------------------------------|--------------------|--------------------|--------------------|-------------------|----------------------|-----------------------------|-------------------|
| Mass (Total), kg | 18.3345434 | 1.5 | 1.5 | Component | I _{Whole} | I _{Partial} | I | Unit | Percent | Desired Inertance | Actual Gap Inertance | Actual Inertance Percentage | Natural Frequency |
| Density of Steel | 0.000008 kg/mm ³ | Total Number of Nuts on Each Bolt | | Centerpiece | 2.248 | 0.042 | 0.585 | kg*mm ² | 25 | 4.58303849 | 4.95 | 27.0 | 4.47952448 |
| Density of Zinc | 0.000008 kg/mm ³ | 0 | | Rod 1 | 2.248 | 0.042 | 2.206 | kg*mm ² | 50 | 9.16707698 | 9.47 | 51.7 | 4.25343992 |
| Die Set Nat Freq (Hz) | 5.24 Hz | | | Rod 2 | 3.666 | 0.042 | 3.624 | kg*mm ² | 100 | 18.3345434 | 36.1 | 102.5 | 3.680497229 |
| | | | | Rod 3 | 2.248 | 0.042 | 2.206 | kg*mm ² | 200 | 36.6690879 | 36.1 | 196.9 | 3.039892648 |
| | | | | Rod 4 | 3.666 | 0.042 | 3.624 | kg*mm ² | | | | | |
| | | | | Washer Moment of Inertia Calculations | | | | | | | | | |
| | | | | Washer Number | Radius (mm) | I = MR ² | Unit | | | | | | |
| | | | | 1 | 38.963 | 4.026 | kg*mm ² | | | | | | |
| | | | | 2 | 35.826 | 3.404 | kg*mm ² | | | | | | |
| | | | | 3 | 32.689 | 2.834 | kg*mm ² | | | | | | |
| | | | | 4 | 29.552 | 2.316 | kg*mm ² | | | | | | |
| | | | | 5 | 26.416 | 1.850 | kg*mm ² | | | | | | |
| | | | | 6 | 23.279 | 1.437 | kg*mm ² | | | | | | |
| | | | | 7 | 20.142 | 1.076 | kg*mm ² | | | | | | |
| | | | | 8 | 17.005 | 0.767 | kg*mm ² | | | | | | |
| | | | | 9 | 13.868 | 0.510 | kg*mm ² | | | | | | |
| | | | | 10 | 10.731 | 0.305 | kg*mm ² | | | | | | |
| | | | | TOTAL | | | | 0.000 | kg*mm ² | | | | |
| | | | | Mass Calculation | | | | | | | | | |
| | | | | Member | Volume (mm ³) | Density (kg/mm ³) | Mass (kg) | | | | | | |
| | | | | Die Set Top Plate | 5243860.502 | 0.00000281 | 14.73524801 | | | | | | |
| | | | | Spring retainer plates | 105783.5777 | 0.000008 | 0.846268622 | | | | | | |
| | | | | Adaptive Plate | 344128.3455 | 0.000008 | 2.753022764 | | | | | | |
| | | | | TOTAL | | | 18.3345434 | | | | | | |
| | | | | Linear Inertor | | | | | | | | | |
| | | | | Inertance (kg) | Mass Percent (%) | Natural Frequency (Hz) | | | | | | | |
| | | | | 4.51 | 24.57 | 4.692500182 | | | | | | | |
| | | | | 7.28 | 39.7 | 4.431515064 | | | | | | | |
| | | | | 18.3 | 100 | 3.705528413 | | | | | | | |
| | | | | 35.7 | 194.5 | 3.051123566 | | | | | | | |
| | | | | Centerpiece Dimensions | | | | | | | | | |
| | | | | O.D (inch) | 0.75 | 19.05 | mm | | | | | | |
| | | | | Radius (O.D) | | 9.525 | mm | | | | | | |
| | | | | I.D | 0.323 | 8.2042 | mm | | | | | | |
| | | | | Radius (I.D) | | 4.1021 | mm | | | | | | |
| | | | | Thickness | 0.3 | 7.62 | mm | | | | | | |
| | | | | Mass | | 0.01089 | kg | | | | | | |
| | | | | Rod Dimensions | | | | | | | | | |
| | | | | Rod 1: Set Screw | | | | | | | | | |
| | | | | Radius | 2.413 | mm | | | | | | | |
| | | | | Length | 1.25 | 31.75 | mm | | | | | | |
| | | | | Effective Length | | 35.8521 | | | | | | | |
| | | | | Volume | 655.8110784 | mm ³ | | | | | | | |
| | | | | Total Mass | 0.005246489 | kg | | | | | | | |
| | | | | I-Partial | | 9.525 | mm | | | | | | |
| | | | | Mass-Partial | 0.00139386 | kg | | | | | | | |
| | | | | Rod 2: Bolt (Steel) | | | | | | | | | |
| | | | | Radius | 2.413 | mm | | | | | | | |
| | | | | Length | 1.5 | 38.1 | mm | | | | | | |
| | | | | Effective Length | | 42.2021 | | | | | | | |
| | | | | Volume | 771.9660692 | mm ³ | | | | | | | |
| | | | | Total Mass | 0.006175729 | kg | | | | | | | |
| | | | | I-Partial | | 9.525 | mm | | | | | | |
| | | | | Mass-Partial | 0.00139386 | kg | | | | | | | |
| | | | | Rod 3: Set Screw | | | | | | | | | |
| | | | | Radius | 2.413 | mm | | | | | | | |
| | | | | Length | 1.25 | 31.75 | mm | | | | | | |
| | | | | Effective Length | | 35.8521 | | | | | | | |
| | | | | Volume | 655.8110784 | mm ³ | | | | | | | |
| | | | | Total Mass | 0.005246489 | kg | | | | | | | |
| | | | | I-Partial | | 9.525 | mm | | | | | | |
| | | | | Mass-Partial | 0.00139386 | kg | | | | | | | |
| | | | | Rod 4: Bolt (Steel) | | | | | | | | | |
| | | | | Radius | 2.413 | mm | | | | | | | |
| | | | | Length | 1.5 | 38.1 | mm | | | | | | |
| | | | | Effective Length | | 42.2021 | | | | | | | |
| | | | | Volume | 771.9660692 | mm ³ | | | | | | | |
| | | | | Total Mass | 0.006175729 | kg | | | | | | | |
| | | | | I-Partial | | 9.525 | mm | | | | | | |
| | | | | Mass-Partial | 0.00139386 | kg | | | | | | | |
| | | | | Shaft Collar Dimensions | | | | | | | | | |
| | | | | O.D | 18 | mm | | | | | | | |
| | | | | I.D | 8 | mm | | | | | | | |
| | | | | Thickness | 9 | mm | | | | | | | |
| | | | | Volume | 1837.831702 | mm ³ | | | | | | | |
| | | | | Mass | 0.014702654 | kg | | | | | | | |
| | | | | Moment of Inertia | 0.713078701 | kg*mm ² | | | | | | | |
| | | | | Added Weight Dimensions | | | | | | | | | |
| | | | | O.D | 9.2456 | mm | | | | | | | |
| | | | | I.D | 4.2672 | mm | | | | | | | |
| | | | | Thickness | 1.1369 | mm | | | | | | | |
| | | | | Volume | 165.7389734 | mm ³ | | | | | | | |
| | | | | Mass | 0.001325915 | kg | | | | | | | |
| | | | | Moment of Inertia | 0.017185535 | kg*mm ² | | | | | | | |

| Total Moment of Inertia, Flywheel | | = | 12.245 kg*mm ² |
|--|-------------|----|---------------------------|
| Inertance Calculations | | | |
| Lead Screw | 0.595320009 | kg | |
| Flywheel | 7.554 | kg | |
| Nuts | 0 | kg | |
| Shaft Collar A | 0.439862793 | kg | |
| Shaft Collar B | 0.439862793 | kg | |
| Shaft Collar C | 0.439862793 | kg | |
| Inertance B (Two-way Gap Inertor) | | | |
| Inertance B | 9.028571268 | kg | |
| % of Mass | 49.24 | % | |
| Inertance D (Bushing-Crown Gap Inertor) | | | |
| Inertance D | 9.468434061 | kg | |
| % of Mass | 51.64 | % | |
| Inertance (Linear Inertor): | | | |
| Inertance | 9.028571268 | kg | |
| % of Mass | 49.24 | % | |



Orange = Whole

Green = Partial



A.20 NRIM INERTANCE CALCULATION - FLYWHEEL 2B

| FLYWHEEL INERTANCE CALCULATIONS (FLYWHEEL 2B) | | | | | | | | | |
|---|-------------|------------------------------------|-------------------|--|--------------------------|---|-------------|------------------------------------|--------------------------------|
| Die Set Information | | Flywheel Bolts (STEEL ONLY) | | Flywheel Moment of Inertia Calculations | | | | Percent | |
| Mass (Total), kg | 18.3345434 | kg | 1.25 | Component | I_{Whole} | I_{Partial} | I | Unit | Desired Inertance |
| Density of Steel | 0.000008 | kg/mm ³ | 1.25 | Centerpiece | 2.248 | 0.042 | 0.585 | kg*mm ² | 4.583635849 |
| Density of Zinc | 0.000008 | kg/mm ³ | 0 | Rod 1 | 2.248 | 0.042 | 2.206 | kg*mm ² | 9.167271698 |
| Die Set Nat Freq (Hz) | 5.24 | Hz | | Rod 2 | 2.248 | 0.042 | 2.206 | kg*mm ² | 18.3345434 |
| | | | | Rod 3 | 2.248 | 0.042 | 2.206 | kg*mm ² | 36.66908679 |
| | | | | Rod 4 | 2.248 | 0.042 | 2.206 | kg*mm ² | 36.66908679 |
| Lead Screw Dimensions | | Centerpiece Dimensions | | Washer Moment of Inertia Calculations | | | | Mass Calculation | |
| Lead | 8 | mm | O.D (inch) | 0.75 | inch | 19.05 | mm | Member | Volume (mm³) |
| Length | 300 | mm | Radius (O.D) | 0.323 | inch | 8.2042 | mm | Die Set Top Plate | 5243860.502 |
| Radius | 4 | mm | Radius (I.D) | 0.3 | inch | 7.62 | mm | Spring retainer plates | 105783.5777 |
| Volume | 15079.6320 | mm ³ | Thickness | 0.3 | inch | 0.01089 | kg | Adaptive Plate | 344128.3455 |
| Mass | 0.1206 | kg | Mass | 0.01089 | kg | | | TOTAL | 18.3345434 |
| Moment of Inertia | 0.965096448 | kg*mm ² | | | | | | | |
| Rod Dimensions | | Rod 1: Set Screw | | Total Moment of Inertia, Flywheel | | | | Linear Inertor | |
| Radius | 2.413 | mm | Radius | 2.413 | mm | = | | 9.408 | kg*mm ² |
| Length | 1.25 | inch | Length | 1.25 | inch | | | | |
| Effective Length | 35.8521 | mm | Effective Length | 35.8521 | mm | | | | |
| Volume | 655.8110784 | mm ³ | Volume | 655.8110784 | mm ³ | | | | |
| Total Mass | 0.005246489 | kg | Total Mass | 0.005246489 | kg | | | | |
| L- Partial | 9.525 | mm | L- Partial | 9.525 | mm | | | | |
| Mass-Partial | 0.00139386 | kg | Mass-Partial | 0.00139386 | kg | | | | |
| Rod 2: Bolt (Steel) | | Rod 3: Set Screw | | Inertance Calculations | | | | Inertance & Mass Legend | |
| Radius | 2.413 | mm | Radius | 2.413 | mm | Lead Screw | 0.595320009 | kg | Orange = Whole |
| Length | 1.25 | inch | Length | 1.25 | inch | Flywheel | 5.804 | kg | Green = Partial |
| Effective Length | 35.8521 | mm | Effective Length | 35.8521 | mm | Nuts | 0 | kg | |
| Volume | 655.8110784 | mm ³ | Volume | 655.8110784 | mm ³ | Shaft Collar A | 0.439862793 | kg | |
| Total Mass | 0.005246489 | kg | Total Mass | 0.005246489 | kg | Shaft Collar B | 0.439862793 | kg | |
| L- Partial | 9.525 | mm | L- Partial | 9.525 | mm | Shaft Collar C | 0.439862793 | kg | |
| Mass-Partial | 0.00139386 | kg | Mass-Partial | 0.00139386 | kg | Inertance B (Two-way Gap Inertor) | 7.278614809 | kg | |
| Rod 4: Bolt (Steel) | | Rod 4: Bolt (Steel) | | Inertance & Mass Legend | | | | Inertance & Mass Legend | |
| Radius | 2.413 | mm | Radius | 2.413 | mm | % of Mass | 39.70 | % | |
| Length | 1.25 | inch | Length | 1.25 | inch | Inertance B (Bushing-Crown Gap Inertor) | 7.718477601 | kg | |
| Effective Length | 35.8521 | mm | Effective Length | 35.8521 | mm | % of Mass | 42.10 | % | |
| Volume | 655.8110784 | mm ³ | Volume | 655.8110784 | mm ³ | Inertance (Linear Inertor): | 7.278614809 | kg | |
| Total Mass | 0.005246489 | kg | Total Mass | 0.005246489 | kg | % of Mass | 39.70 | % | |
| L- Partial | 9.525 | mm | L- Partial | 9.525 | mm | | | | |
| Mass-Partial | 0.00139386 | kg | Mass-Partial | 0.00139386 | kg | | | | |
| Shaft Collar Dimensions | | Added Weight Dimensions | | Diagram | | | | Diagram | |
| O.D | 18 | mm | O.D | 9.2456 | mm | | | | |
| I.D | 8 | mm | I.D | 4.2672 | mm | | | | |
| Thickness | 9 | mm | Thickness | 3.1369 | mm | | | | |
| Volume | 1837.831702 | mm ³ | Volume | 15.7393734 | mm ³ | | | | |
| Mass | 0.014702654 | kg | Mass | 0.01329615 | kg | | | | |
| Moment of Inertia | 0.713078701 | kg*mm ² | Moment of Inertia | 0.017185535 | kg*mm ² | | | | |

A.21 RIM AND NRIM INERTANCE CALCULATION - FLYWHEEL 3

FLYWHEEL INERTANCE CALCULATIONS (FLYWHEEL 3)

| Die Set Information | | Flywheel Bolts (STEEL ONLY) | | Flywheel Moment of Inertia Calculations | | | | Percent | | | | | |
|------------------------|--------------------------------|---|--------------------------------|---|--------------------------|------------------------|---------------------------|-------------------------------|-------------------|----------------------|-----------------------------|-------------------|-------------------|
| Mass (Total), kg | 18.3345434 | 2.25 | 2.25 | Component | I _{Whole} | I _{Partial} | I | Unit | Desired Inertance | Actual Gap Inertance | Actual Inertance Percentage | Natural Frequency | Natural Frequency |
| Density of Steel | 0.000008 kg/mm ³ | 2.25 | 2.25 | Centerpiece | | | 0.585 | kg*mm ² | 25 | 4.583635849 | 4.95 | 27.0 | 4.647952448 |
| Density of Zinc | 0.000008 kg/mm ³ | 0 | 0 | Rod 1 | 2.248 | 0.042 | 2.206 | kg*mm ² | 50 | 9.167216098 | 9.47 | 51.7 | 4.253413993 |
| Die Set Nat Freq (Hz) | 5.24 | | | Rod 2 | 11.210 | 0.042 | 11.168 | kg*mm ² | 100 | 18.3345434 | 18.8 | 102.5 | 3.680497229 |
| | | | | Rod 3 | 2.248 | 0.042 | 2.206 | kg*mm ² | 200 | 36.66908679 | 36.1 | 196.9 | 3.038992648 |
| | | | | Rod 4 | 11.210 | 0.042 | 11.168 | kg*mm ² | | | | | |
| | | | | | | | | | | | | | |
| Lead Screw Dimensions | | Washer Moment of Inertia Calculations | | | | Mass Calculation | | | | | | | |
| Lead | 8 mm | Washer Number | Radius (mm) | I = MR ² | Unit | Member | Volume (mm ³) | Density (kg/mm ³) | Mass (kg) | | | | |
| Length | 300 mm | 1 | 58.013 | 8.925 | kg*mm ² | Die Set Top Plate | 5243860.502 | 0.00000281 | 14.73524801 | | | | |
| Radius | 4 mm | 2 | 54.876 | 7.986 | kg*mm ² | Spring retainer plates | 105783.5777 | 0.000008 | 0.846268622 | | | | |
| Volume | 15079.6320 mm ³ | 3 | 51.739 | 7.099 | kg*mm ² | Adaptive Plate | 344128.3455 | 0.000008 | 2.753026764 | | | | |
| Mass | 0.1206 kg | 4 | 48.602 | 6.264 | kg*mm ² | TOTAL | | | 18.3345434 | | | | |
| Moment of Inertia | 0.965096448 kg*mm ² | 5 | 45.466 | 5.482 | kg*mm ² | | | | | | | | |
| | | 6 | 42.329 | 4.751 | kg*mm ² | | | | | | | | |
| | | 7 | 39.192 | 4.073 | kg*mm ² | | | | | | | | |
| | | 8 | 36.055 | 3.447 | kg*mm ² | | | | | | | | |
| | | 9 | 32.918 | 2.873 | kg*mm ² | | | | | | | | |
| | | 10 | 29.781 | 2.352 | kg*mm ² | | | | | | | | |
| | | | TOTAL | 0.000 | kg*mm² | | | | | | | | |
| Centerpiece Dimensions | | Total Moment of Inertia, Flywheel = | | | | Linear Inertor | | | | | | | |
| O.D (inch) | 0.75 inch | 19.05 mm | 27.332 kg*mm ² | | | Inertance (kg) | Mass Percent (%) | Natural Frequency (Hz) | | | | | |
| Radius (O.D) | 9.525 mm | | | | | 4.51 | 24.57 | 4.692500182 | | | | | |
| I.D | 0.323 inch | 8.2042 mm | | | | 7.28 | 39.7 | 4.431515064 | | | | | |
| Radius (I.D) | 4.1021 mm | | | | | 18.8 | 100 | 3.705294413 | | | | | |
| Thickness | 0.3 inch | 7.62 mm | | | | 35.7 | 194.5 | 3.051123566 | | | | | |
| Mass | 0.01089 kg | | | | | | | | | | | | |
| Rod Dimensions | | Inertance Calculations | | | | | | | | | | | |
| Radius | 2.413 mm | Lead Screw | 0.595320009 | kg | | | | | | | | | |
| Length | 31.75 mm | Flywheel | 16.860 | kg | | | | | | | | | |
| Effective Length | 35.8521 | Nuts | 0 | kg | | | | | | | | | |
| Volume | 655.8110784 mm ³ | Shaft Collar A | 0.439862793 | kg | | | | | | | | | |
| Total Mass | 0.005246489 kg | Shaft Collar B | 0.439862793 | kg | | | | | | | | | |
| L- Partial | 9.525 mm | Shaft Collar C | 0.439862793 | kg | | | | | | | | | |
| Mass-Partial | 0.00139386 kg | Inertance B (Two-way Gap Inertor) | 18.33485298 | kg | | | | | | | | | |
| | | % of Mass | 100.00 | % | | | | | | | | | |
| | | Inertance B (Bushing-Crown Gap Inertor) | 18.77471577 | kg | | | | | | | | | |
| | | % of Mass | 102.40 | % | | | | | | | | | |
| | | Inertance (Linear Inertor): | 18.33485298 | kg | | | | | | | | | |
| | | % of Mass | 100.00 | % | | | | | | | | | |
| Rod 1: Set Screw | | Shaft Collar Dimensions | | | | | | | | | | | |
| Radius | 2.413 mm | O.D | 18 mm | | | | | | | | | | |
| Length | 31.75 mm | I.D | 8 mm | | | | | | | | | | |
| Effective Length | 35.8521 | Thickness | 9 mm | | | | | | | | | | |
| Volume | 655.8110784 mm ³ | Volume | 1837.831702 mm ³ | | | | | | | | | | |
| Total Mass | 0.005246489 kg | Mass | 0.014702654 kg | | | | | | | | | | |
| L- Partial | 9.525 mm | Moment of Inertia | 0.713078701 kg*mm ² | | | | | | | | | | |
| Mass-Partial | 0.00139386 kg | | | | | | | | | | | | |
| Rod 2: Bolt (Steel) | | Added Weight Dimensions | | | | | | | | | | | |
| Radius | 2.413 mm | O.D | 9.2456 mm | | | | | | | | | | |
| Length | 57.15 mm | I.D | 4.2672 mm | | | | | | | | | | |
| Effective Length | 61.2521 | Thickness | 3.1369 mm | | | | | | | | | | |
| Volume | 1120.431042 mm ³ | Volume | 165.7393734 mm ³ | | | | | | | | | | |
| Total Mass | 0.008963448 kg | Mass | 0.013329615 kg | | | | | | | | | | |
| L- Partial | 9.525 mm | Moment of Inertia | 0.017185535 kg*mm ² | | | | | | | | | | |
| Mass-Partial | 0.00139386 kg | | | | | | | | | | | | |
| Rod 3: Set Screw | | | | | | | | | | | | | |
| Radius | 2.413 mm | | | | | | | | | | | | |
| Length | 31.75 mm | | | | | | | | | | | | |
| Effective Length | 35.8521 | | | | | | | | | | | | |
| Volume | 655.8110784 mm ³ | | | | | | | | | | | | |
| Total Mass | 0.005246489 kg | | | | | | | | | | | | |
| L- Partial | 9.525 mm | | | | | | | | | | | | |
| Mass-Partial | 0.00139386 kg | | | | | | | | | | | | |
| Rod 4: Bolt (Steel) | | | | | | | | | | | | | |
| Radius | 2.413 mm | | | | | | | | | | | | |
| Length | 57.15 mm | | | | | | | | | | | | |
| Effective Length | 61.2521 | | | | | | | | | | | | |
| Volume | 1120.431042 mm ³ | | | | | | | | | | | | |
| Total Mass | 0.008963448 kg | | | | | | | | | | | | |
| L- Partial | 9.525 mm | | | | | | | | | | | | |
| Mass-Partial | 0.00139386 kg | | | | | | | | | | | | |

A.22 RIM AND NRIM INERTANCE CALCULATION - FLYWHEEL 4

FLYWHEEL INERTANCE CALCULATIONS (FLYWHEEL 4)

| Die Set Information | | Flywheel Bolts (STEEL ONLY) | | Flywheel Moment of Inertia Calculations | | | | Percent | | | | | |
|-----------------------|-----------------------------|-----------------------------------|---|---|--------------------|----------------------|--------------------|--------------------|-------------------|----------------------|-----------------------------|-------------------|-------------------|
| Mass (Total) kg | 18.3345434 | 3 | | Component | I _{Whole} | I _{Partial} | I | Unit | Desired Inertance | Actual Gap Inertance | Actual Inertance Percentage | Natural Frequency | Natural Frequency |
| Density of Steel | 0.000008 kg/mm ³ | Total Number of Nuts on Each Bolt | 0 | Centerpiece | | 0.585 | kg*mm ² | | 25 | 4.583039849 | 4.95 | 27.0 | 4.47952448 |
| Density of Zinc | 0.000008 kg/mm ³ | | | Rod 1 | 2.248 | 0.042 | 2.206 | kg*mm ² | 50 | 9.16721668 | 9.47 | 51.7 | 4.25343992 |
| Die Set Nat Freq (Hz) | 5.24 Hz | | | Rod 2 | 25.259 | 0.042 | 25.217 | kg*mm ² | 100 | 18.3345434 | 18.8 | 102.5 | 3.680497229 |
| | | | | Rod 3 | 2.248 | 0.042 | 2.206 | kg*mm ² | 200 | 36.66908679 | 36.1 | 196.9 | 3.039892648 |
| | | | | Rod 4 | 25.259 | 0.042 | 25.217 | kg*mm ² | | | | | |

| Lead Screw Dimensions | | Centerpiece Dimensions | | Rod Dimensions | | Rod 1: Set Screw | | Rod 2: Bolt (Steel) | | Rod 3: Set Screw | | Rod 4: Bolt (Steel) | | Shaft Collar Dimensions | | Added Weight Dimensions | |
|-----------------------|--------------------------------|------------------------|------------|------------------|-----------------------------|------------------|-----------------------------|---------------------|-----------------------------|------------------|-----------------------------|---------------------|--------------------------------|-------------------------|--------------------------------|-------------------------|--|
| Lead | 8 mm | O.D (inch) | 0.75 inch | Radius | 2.413 mm | Radius | 2.413 mm | Radius | 2.413 mm | Radius | 2.413 mm | O.D | 18 mm | O.D | 9.2456 mm | | |
| Length | 300 mm | Radius (O.D) | 9.525 mm | Length | 1.25 inch | Length | 1.25 inch | Length | 3 inch | Length | 1.25 inch | LD | 8 mm | LD | 4.2672 mm | | |
| Radius | 4 mm | ID | 8.2042 mm | Effective Length | 35.8521 | Effective Length | 35.8521 | Effective Length | 80.3021 | Effective Length | 80.3021 | Thickness | 9 mm | Thickness | 1.1369 mm | | |
| Volume | 15079.6320 mm ³ | Radius (I.D) | 4.1021 mm | Volume | 655.8110784 mm ³ | Volume | 655.8110784 mm ³ | Volume | 1468.896014 mm ³ | Volume | 655.8110784 mm ³ | Volume | 1837.831702 mm ³ | Volume | 165.7393734 mm ³ | | |
| Mass | 0.1206 kg | Thickness | 0.3 inch | Total Mass | 0.005246489 kg | Total Mass | 0.005246489 kg | Total Mass | 0.011751168 kg | Total Mass | 0.005246489 kg | Mass | 0.014702654 kg | Mass | 0.001325915 kg | | |
| Moment of Inertia | 0.965096448 kg*mm ² | Mass | 0.01089 kg | I-Partial | 9.525 mm | I-Partial | 9.525 mm | I-Partial | 9.525 mm | I-Partial | 9.525 mm | Moment of Inertia | 0.713078701 kg*mm ² | Moment of Inertia | 0.011785535 kg*mm ² | | |

| Washer Moment of Inertia Calculations | | Total Moment of Inertia, Flywheel | |
|---------------------------------------|-------------|-----------------------------------|--------------------------|
| Washer Number | Radius (mm) | I = MR ² | Unit |
| 1 | 77.063 | 15.748 | kg*mm ² |
| 2 | 73.926 | 14.492 | kg*mm ² |
| 3 | 70.789 | 13.289 | kg*mm ² |
| 4 | 67.652 | 12.137 | kg*mm ² |
| 5 | 64.516 | 11.038 | kg*mm ² |
| 6 | 61.379 | 9.990 | kg*mm ² |
| 7 | 58.242 | 8.995 | kg*mm ² |
| 8 | 55.105 | 8.052 | kg*mm ² |
| 9 | 51.968 | 7.162 | kg*mm ² |
| 10 | 48.831 | 6.323 | kg*mm ² |
| TOTAL | | 0.000 | kg*mm² |

| Mass Calculation | | Mass Calculation | | Linear Inertor | | | |
|------------------------|---------------------------|-------------------------------|-------------|-------------------|---------------------------|-------------------------------|-------------|
| Member | Volume (mm ³) | Density (kg/mm ³) | Mass (kg) | Member | Volume (mm ³) | Density (kg/mm ³) | Mass (kg) |
| Die Set Top Plate | 5243860.502 | 0.00000281 | 14.73524801 | Die Set Top Plate | 105783.5777 | 0.000008 | 0.846268622 |
| Spring retainer plates | | | | Adaptive Plate | 344128.3455 | 0.000008 | 2.753026764 |
| TOTAL | | | | 18.3345434 | | | |

| Inertance Calculations | | Inertance (Linear Inertor): | |
|------------------------|----------------|-----------------------------|----------------|
| Lead Screw | 0.595320009 kg | Inertance (Linear Inertor): | 35.66723963 kg |
| Flywheel | 34.192 kg | % of Mass | 194.54 % |
| Nuts | 0 kg | | |
| Shaft Collar A | 0.439862793 kg | | |
| Shaft Collar B | 0.439862793 kg | | |
| Shaft Collar C | 0.439862793 kg | | |

| Inertance (Two-way Gap Inertor) | | Inertance (Bushing-Crown Gap Inertor) | |
|---------------------------------|----------------|---------------------------------------|----------------|
| Inertance (Two-way Gap Inertor) | 35.66723963 kg | Inertance (Bushing-Crown Gap Inertor) | 36.10710242 kg |
| % of Mass | 194.54 % | % of Mass | 196.93 % |

Orange = Whole

Green = Partial

| Shaft Collar Dimensions | |
|-------------------------|--------------------------------|
| O.D | 18 mm |
| LD | 8 mm |
| Thickness | 9 mm |
| Volume | 1837.831702 mm ³ |
| Mass | 0.014702654 kg |
| Moment of Inertia | 0.713078701 kg*mm ² |

A.23 RIM AND NRIM INERTANCE CALCULATION - FLYWHEEL 5

FLYWHEEL INERTANCE CALCULATIONS (FLYWHEEL 5)

| Die Set Information | | Flywheel Bolts (STEEL ONLY) | |
|-----------------------|-----------------------------|-----------------------------------|---|
| Mass (Total), kg | 18.3345434 | 3 | |
| Density of Steel | 0.000008 kg/mm ³ | | |
| Density of Zinc | 0.000008 kg/mm ³ | | |
| Die Set Nat Freq (Hz) | 5.24 | Total Number of Nuts on Each Bolt | 2 |

| Flywheel Moment of Inertia Calculations | | | |
|---|--------|----------|--------------------|
| Component | LWhole | LPartial | Unit |
| Centerpiece | | 0.585 | kg*mm ² |
| Rod 1 | 2.248 | 0.042 | 2.206 |
| Rod 2 | 25.259 | 0.042 | 25.217 |
| Rod 3 | 2.248 | 0.042 | 2.206 |
| Rod 4 | 25.259 | 0.042 | 25.217 |

| Washer Moment of Inertia Calculations | | | |
|---------------------------------------|-------------|---------------------|--------------------------|
| Washer Number | Radius (mm) | I = MR ² | Unit |
| 1 | 77.063 | 15.748 | kg*mm ² |
| 2 | 73.926 | 14.492 | kg*mm ² |
| 3 | 70.789 | 13.236 | kg*mm ² |
| 4 | 67.652 | 12.137 | kg*mm ² |
| 5 | 64.516 | 11.038 | kg*mm ² |
| 6 | 61.379 | 9.990 | kg*mm ² |
| 7 | 58.242 | 8.996 | kg*mm ² |
| 8 | 55.105 | 8.052 | kg*mm ² |
| 9 | 51.968 | 7.162 | kg*mm ² |
| 10 | 48.831 | 6.323 | kg*mm ² |
| TOTAL | | 30.241 | kg*mm² |

| Lead Screw Dimensions | |
|-----------------------|--------------------------------|
| Lead | 8 mm |
| Length | 300 mm |
| Radius | 4 mm |
| Volume | 15079.6320 mm ³ |
| Mass | 0.1206 kg |
| Moment of inertia | 0.965096448 kg*mm ² |

| Centerpiece Dimensions | |
|------------------------|------------|
| O.D (inch) | 0.75 |
| Radius (O.D) | 9.525 mm |
| I.D | 8.2042 mm |
| Radius (I.D) | 4.1021 mm |
| Thickness | 7.62 mm |
| Mass | 0.01089 kg |

| Rod 1: Set Screw | |
|------------------|-----------------------------|
| Radius | 2.413 mm |
| Length | 1.25 inch |
| Effective Length | 35.8521 |
| Volume | 655.8110784 mm ³ |
| Total Mass | 0.005246489 kg |
| L- Partial | 9.525 mm |
| Mass- Partial | 0.00139386 kg |

| Rod 2: Bolt (Steel) | |
|---------------------|-----------------------------|
| Radius | 2.413 mm |
| Length | 3 inch |
| Effective Length | 80.3021 |
| Volume | 1468.896014 mm ³ |
| Total Mass | 0.011751168 kg |
| L- Partial | 9.525 mm |
| Mass- Partial | 0.00139386 kg |

| Rod 3: Set Screw | |
|------------------|-----------------------------|
| Radius | 2.413 mm |
| Length | 1.25 inch |
| Effective Length | 35.8521 |
| Volume | 655.8110784 mm ³ |
| Total Mass | 0.005246489 kg |
| L- Partial | 9.525 mm |
| Mass- Partial | 0.00139386 kg |

| Rod 4: Bolt (Steel) | |
|---------------------|-----------------------------|
| Radius | 2.413 mm |
| Length | 3 inch |
| Effective Length | 80.3021 |
| Volume | 1468.896014 mm ³ |
| Total Mass | 0.011751168 kg |
| L- Partial | 9.525 mm |
| Mass- Partial | 0.00139386 kg |

| Shaft Collar Dimensions | |
|-------------------------|--------------------------------|
| O.D | 18 mm |
| I.D | 8 mm |
| Thickness | 9 mm |
| Volume | 1837.831702 mm ³ |
| Mass | 0.014702654 kg |
| Moment of inertia | 0.715078701 kg*mm ² |

| Added Weight Dimensions | |
|-------------------------|--------------------------------|
| O.D | 9.2456 mm |
| I.D | 4.2672 mm |
| Thickness | 3.1369 mm |
| Volume | 105.7393734 mm ³ |
| Mass | 0.001320515 kg |
| Moment of inertia | 0.017185535 kg*mm ² |

| Flywheel Bolts (STEEL ONLY) | |
|-----------------------------------|---|
| 3 | |
| Total Number of Nuts on Each Bolt | 2 |

| Total Moment of Inertia, Flywheel | |
|-----------------------------------|---------------------------|
| = | 55.430 kg*mm ² |

| Inertance Calculations | | | |
|------------------------|-------------|----|--|
| Lead Screw | 0.595320009 | kg | |
| Flywheel | 34.152 | kg | |
| Nuts | 18.65413857 | kg | |
| Shaft Collar A | 0.439862793 | kg | |
| Shaft Collar B | 0.439862793 | kg | |
| Shaft Collar C | 0.439862793 | kg | |

| Inertance B (Two-way Gap Inserter) | |
|------------------------------------|----------------|
| Inertance | 54.32137819 kg |
| % of Mass | 296.28 % |

| Inertance B (Bushing-Crown Gap Inserter) | |
|--|----------------|
| Inertance | 54.76124099 kg |
| % of Mass | 296.08 % |

| Inertance (Linear Inserter) | |
|-----------------------------|----------------|
| Inertance | 54.32137819 kg |
| % of Mass | 296.28 % |

| Mass Calculation | | | | |
|------------------------|---------------------------|-------------------------------|-------------------|-------------------|
| Member | Volume (mm ³) | Density (kg/mm ³) | Mass (kg) | Natural Frequency |
| Die Set Top Plate | 5343860.502 | 0.00000281 | 1.473534803 | 27.0 |
| Spring retainer plates | 105783.5777 | 0.000008 | 0.846268622 | 102.5 |
| Adaptive Plate | 344128.3455 | 0.000008 | 2.753026764 | 196.9 |
| TOTAL | | | 18.3345434 | |

| Linear Inserter | | | |
|-----------------|------------------|------------------------|--|
| Inertance (kg) | Mass Percent (%) | Natural Frequency (Hz) | |
| 4.51 | 24.57 | 4.691500182 | |
| 7.08 | 38.7 | 4.4115165064 | |
| 18.3 | 100 | 3.705528413 | |
| 35.7 | 194.5 | 3.051123566 | |

Orange = Whole

Green = Partial

A.24 RIM AND NRIM INERTANCE CALCULATION - FLYWHEEL 6

FLYWHEEL INERTANCE CALCULATIONS (FLYWHEEL 6)

| Die Set Information | |
|-----------------------|-------------------------------|
| Mass (Total), kg | 18.3345434 kg |
| Density of Steel | 0.000028 kg/mm ³ |
| Density of Zinc | 0.00007133 kg/mm ³ |
| Die Set Nat Freq (Hz) | 5.24 Hz |

| Flywheel Bolts (ZINC ONLY) | |
|--|-----|
| | 3.5 |
| Total Number of Nuts on Each Bolt | 2 |

| Flywheel Moment of Inertia Calculations | | | |
|---|--------------------|----------------------|---------------------------|
| Component | L _{Whole} | L _{Partial} | I Unit |
| Centerpiece | 2.248 | 0.042 | 0.585 kg*mm ² |
| Rod 1 | 2.248 | 0.042 | 2.206 kg*mm ² |
| Rod 2 | 34.986 | 0.038 | 34.948 kg*mm ² |
| Rod 3 | 2.248 | 0.042 | 2.206 kg*mm ² |
| Rod 4 | 34.986 | 0.038 | 34.948 kg*mm ² |

| Washer Moment of Inertia Calculations | | | |
|---------------------------------------|-------------|---------------------|--------------------------|
| Washer Number | Radius (mm) | I = MR ² | Unit |
| 1 | 89.763 | 21.367 | kg*mm ² |
| 2 | 86.626 | 19.900 | kg*mm ² |
| 3 | 83.489 | 18.484 | kg*mm ² |
| 4 | 80.352 | 17.122 | kg*mm ² |
| 5 | 77.216 | 15.811 | kg*mm ² |
| 6 | 74.079 | 14.552 | kg*mm ² |
| 7 | 70.942 | 13.346 | kg*mm ² |
| 8 | 67.805 | 12.192 | kg*mm ² |
| 9 | 64.668 | 11.090 | kg*mm ² |
| 10 | 61.531 | 10.040 | kg*mm ² |
| TOTAL | | 41.266 | kg*mm² |

| Percent | Desired Inertance | Actual Gap Inertance | Actual Inertance Percentage | Natural Frequency |
|---------|-------------------|----------------------|-----------------------------|-------------------|
| 25 | 4.583635849 | 4.95 | 27.0 | 4.647952448 |
| 50 | 9.167271698 | 9.47 | 51.7 | 4.253413992 |
| 100 | 18.3345434 | 18.8 | 102.5 | 3.680497229 |
| 200 | 36.66908679 | 36.1 | 196.9 | 3.039892648 |

| Mass Calculation | | | |
|------------------------|---------------------------|-------------------------------|-------------------|
| Member | Volume (mm ³) | Density (kg/mm ³) | Mass (kg) |
| Die Set Top Plate | 5243860.502 | 0.0000281 | 14.73524801 |
| Spring retainer plates | 105783.5777 | 0.000008 | 0.846268622 |
| Adaptive Plate | 344128.3455 | 0.000008 | 2.753026764 |
| TOTAL | | | 18.3345434 |

| Linear Inertor | | |
|----------------|------------------|------------------------|
| Inertance (kg) | Mass Percent (%) | Natural Frequency (Hz) |
| 4.51 | 24.57 | 4.692500182 |
| 7.28 | 39.7 | 4.431515064 |
| 18.3 | 100 | 3.705528413 |
| 35.7 | 194.5 | 3.051123566 |

| Rod Dimensions | |
|---------------------------|-----------------------------|
| Rod 1: Set Screw | |
| Radius | 2.413 mm |
| Length | 1.25 inch 31.75 mm |
| Effective Length | 35.8521 |
| Volume | 655.8110784 mm ³ |
| Total Mass | 0.005246489 kg |
| L-Partial | 9.525 mm |
| Mass-Partial | 0.00139386 kg |
| Rod 2: Bolt (ZINC) | |
| Radius | 2.413 mm |
| Length | 3.5 inch 88.9 mm |
| Effective Length | 93.0021 |
| Volume | 1701.205996 mm ³ |
| Total Mass | 0.012134702 kg |
| L-Partial | 9.525 mm |
| Mass-Partial | 0.0012428 kg |
| Rod 3: Set Screw | |
| Radius | 2.413 mm |
| Length | 1.25 inch 31.75 mm |
| Effective Length | 35.8521 |
| Volume | 655.8110784 mm ³ |
| Total Mass | 0.005246489 kg |
| L-Partial | 9.525 mm |
| Mass-Partial | 0.00139386 kg |
| Rod 4: Bolt (ZINC) | |
| Radius | 2.413 mm |
| Length | 3.5 inch 88.9 mm |
| Effective Length | 93.0021 |
| Volume | 1701.205996 mm ³ |
| Total Mass | 0.012134702 kg |
| L-Partial | 9.525 mm |
| Mass-Partial | 0.0012428 kg |

| Shaft Collar Dimensions | |
|-------------------------|--------------------------------|
| O.D | 18 mm |
| I.D | 8 mm |
| Thickness | 9 mm |
| Volume | 1837.831702 mm ³ |
| Mass | 0.014702654 kg |
| Moment of Inertia | 0.713078701 kg*mm ² |

| Added Weight Dimensions | |
|-------------------------|--------------------------------|
| O.D | 9.2456 mm |
| I.D | 4.2672 mm |
| Thickness | 3.1369 mm |
| Volume | 165.7393734 mm ³ |
| Mass | 0.001325915 kg |
| Moment of Inertia | 0.017185535 kg*mm ² |

| Total Moment of Inertia, Flywheel | |
|-----------------------------------|---------------------------|
| = | 74.894 kg*mm ² |

| Inertance Calculations | |
|------------------------|----------------|
| Lead Screw | 0.595320009 kg |
| Flywheel | 46.198 kg |
| Washers | 25.45524304 kg |
| Shaft Collar A | 0.439862793 kg |
| Shaft Collar B | 0.439862793 kg |
| Shaft Collar C | 0.439862793 kg |

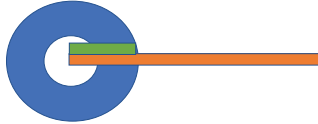
| Inertance.b (Two-way Gap Inertor) | |
|-----------------------------------|----------------|
| Inertance.b | 73.12841754 kg |
| % of Mass | 398.86 % |

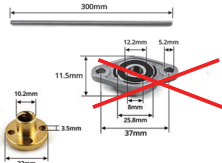
| Inertance.b (Bushing-Crown Gap Inertor) | |
|---|----------------|
| Inertance.b | 73.56828033 kg |
| % of Mass | 401.26 % |

| Inertance (Linear Inertor): | |
|-----------------------------|----------------|
| Inertance | 73.12841754 kg |
| % of Mass | 398.86 % |

Orange - Whole

Green - Partial





A.25 RIM AND NRIM INERTANCE CALCULATION - FLYWHEEL 7

FLYWHEEL INERTANCE CALCULATIONS (FLYWHEEL 7)

| Die Set Information | |
|-----------------------|--------------------------------|
| Mass (Total), kg | 18.334544 |
| Density of Steel | 0.000007133 kg/mm ³ |
| Density of Zinc | 0.000007133 kg/mm ³ |
| Die Set Nat Freq (Hz) | 5.24 |

| Flywheel Bolts (ZINC ONLY) | |
|-----------------------------------|---|
| Quantity | 4 |
| Total Number of Nuts on Each Bolt | 2 |

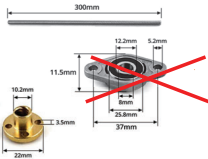
| Lead Screw Dimensions | |
|-----------------------|--------------------------------|
| Lead | 8 mm |
| Radius | 300 mm |
| Radius | 4 mm |
| Volume | 15079.6320 mm ³ |
| Mass | 0.1206 kg |
| Moment of Inertia | 0.965096448 kg*mm ² |

| Centerpiece Dimensions | | |
|------------------------|-------|------------|
| O.D (inch) | 0.75 | 19.05 mm |
| Radius (O.D) | | 9.525 mm |
| ID | 0.323 | 8.202 mm |
| Radius (ID) | | 4.1021 mm |
| Thickness | 0.3 | 7.62 mm |
| Mass | | 0.01089 kg |

| Rod Dimensions | | |
|---------------------------|-----------|-----------------------------|
| Rod 1: Set Screw | | |
| Radius | 2.413 mm | |
| Length | 1.25 inch | 31.75 mm |
| Effective Length | | 35.8521 |
| Volume | | 655.8110784 mm ³ |
| Total Mass | | 0.005246489 kg |
| L- Partial | | 9.525 mm |
| Mass-Partial | | 0.00139386 kg |
| Rod 2: Bolt (ZINC) | | |
| Radius | 2.413 mm | |
| Length | 4 inch | 101.6 mm |
| Effective Length | | 105.7021 |
| Volume | | 1933.515978 mm ³ |
| Total Mass | | 0.013791769 kg |
| L- Partial | | 9.525 mm |
| Mass-Partial | | 0.0012428 kg |
| Rod 3: Set Screw | | |
| Radius | 2.413 mm | |
| Length | 1.25 inch | 31.75 mm |
| Effective Length | | 35.8521 |
| Volume | | 655.8110784 mm ³ |
| Total Mass | | 0.005246489 kg |
| L- Partial | | 9.525 mm |
| Mass-Partial | | 0.00139386 kg |
| Rod 4: Bolt (ZINC) | | |
| Radius | 2.413 mm | |
| Length | 4 inch | 101.6 mm |
| Effective Length | | 105.7021 |
| Volume | | 1933.515978 mm ³ |
| Total Mass | | 0.013791769 kg |
| L- Partial | | 9.525 mm |
| Mass-Partial | | 0.0012428 kg |

| Shaft Collar Dimensions | |
|-------------------------|--------------------------------|
| O.D | 18 mm |
| ID | 8 mm |
| Thickness | 9 mm |
| Volume | 1837.831702 mm ³ |
| Mass | 0.014702654 kg |
| Moment of Inertia | 0.713078701 kg*mm ² |

| Added Weight Dimensions | |
|-------------------------|--------------------------------|
| O.D | 9.2456 mm |
| ID | 4.2672 mm |
| Thickness | 3.1369 mm |
| Volume | 165.7393734 mm ³ |
| Mass | 0.001325915 kg |
| Moment of Inertia | 0.017485533 kg*mm ² |



| Flywheel Moment of Inertia Calculations | | | | |
|---|--------------------|----------------------|--------|--------------------|
| Component | L _{whole} | L _{Partial} | I | Unit |
| Centerpiece | | | 0.585 | kg*mm ² |
| Rod 1 | 2.248 | 0.042 | 2.206 | kg*mm ² |
| Rod 2 | 51.365 | 0.038 | 51.327 | kg*mm ² |
| Rod 3 | 2.248 | 0.042 | 2.206 | kg*mm ² |
| Rod 4 | 51.365 | 0.038 | 51.327 | kg*mm ² |

| Washer Moment of Inertia Calculations | | | |
|---------------------------------------|-------------|-------------------|--------------------------|
| Washer Number | Radius (mm) | I=MR ² | Unit |
| 1 | 102.463 | 27.841 | kg*mm ² |
| 2 | 99.326 | 26.162 | kg*mm ² |
| 3 | 96.189 | 24.536 | kg*mm ² |
| 4 | 93.052 | 22.962 | kg*mm ² |
| 5 | 89.916 | 21.440 | kg*mm ² |
| 6 | 86.779 | 19.970 | kg*mm ² |
| 7 | 83.642 | 18.552 | kg*mm ² |
| 8 | 80.505 | 17.187 | kg*mm ² |
| 9 | 77.368 | 15.873 | kg*mm ² |
| 10 | 74.231 | 14.612 | kg*mm ² |
| TOTAL | | 54.003 | kg*mm² |

Total Moment of Inertia, Flywheel = 107.651 kg*mm²

| Inertance Calculations | |
|------------------------|----------------|
| Lead Screw | 0.595320009 kg |
| Flywheel | 65.405 kg |
| Washers | 33.31168865 kg |
| Shaft Collar A | 0.439862793 kg |
| Shaft Collar B | 0.439862793 kg |
| Shaft Collar C | 0.439862793 kg |

| | |
|-----------------------------------|----------------|
| Inertance,b (Two-way Gap Inertor) | 101.1915411 kg |
| % of Mass | 551.92 % |

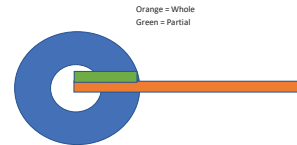
| | |
|---|----------------|
| Inertance,b (Bushing - Crown Gap Inertor) | 101.6314039 kg |
| % of Mass | 554.32 % |

| | |
|----------------------------|----------------|
| Inertance (Linear Inertor) | 101.1915411 kg |
| % of Mass | 551.92 % |

| Percent | Desired Inertance | Actual Gap Inertance | Actual Inertance Percentage | Natural Frequency |
|---------|-------------------|----------------------|-----------------------------|-------------------|
| 25 | 4.383635840 | 4.95 | 27.0 | 4.647952448 |
| 50 | 9.167271680 | 9.47 | 51.7 | 4.253413992 |
| 100 | 18.3345434 | 18.8 | 102.5 | 3.680497229 |
| 200 | 36.66908679 | 36.1 | 196.9 | 3.039892648 |

| Mass Calculation | | | |
|------------------------|---------------------------|-------------------------------|-------------------|
| Member | Volume (mm ³) | Density (kg/mm ³) | Mass (kg) |
| Die Set Top Plate | 5243860.502 | 0.00000281 | 14.73524801 |
| Spring retainer plates | 105783.5777 | 0.0000008 | 0.846268622 |
| Adaptive Plate | 344128.3455 | 0.0000008 | 2.753026764 |
| TOTAL | | | 18.3345434 |

| Linear Inertor | | |
|----------------|------------------|------------------------|
| Inertance (kg) | Mass Percent (%) | Natural Frequency (Hz) |
| 4.51 | 24.57 | 4.692500182 |
| 7.28 | 39.7 | 4.431515064 |
| 18.3 | 100 | 3.705529413 |
| 35.7 | 194.5 | 3.051123566 |



A.26 RIM AND NRIM INERTANCE CALCULATION - FLYWHEEL 8

FLYWHEEL INERTANCE CALCULATIONS (FLYWHEEL 8)

| Die Set Information | | Flywheel Bolts (ZINC ONLY) | | Flywheel Moment of Inertia Calculations | | | | Percent | | | | | | |
|--------------------------------|--------------------------------|-----------------------------------|---|---|--------------------|----------------------|--------------------|-------------------------|---------------------------|-------------------------------|-----------------------------|-------------------|-------------|--|
| Mass (Total), kg | 18.3345434 | 4 | | Component | L _{Whole} | L _{Partial} | l | Unit | Desired Inertance | Actual Gap Inertance | Actual Inertance Percentage | Natural Frequency | | |
| Density of Steel | 0.000008 kg/mm ³ | | | Centerpiece | | | | | 25 | 4.583635849 | 4.95 | 27.0 | 4.647952440 | |
| Density of Zinc | 0.00007133 kg/mm ³ | Total Number of Nuts on Each Bolt | 3 | Rod 1 | 2.248 | 0.042 | 2.206 | kg*mm ² | 50 | 9.167271698 | 9.47 | 51.7 | 4.213413992 | |
| Die Set Nat Freq (Hz) | 5.24 | | | Rod 2 | 51.365 | 0.038 | 51.327 | kg*mm ² | 100 | 18.3345434 | 18.8 | 102.5 | 3.680497229 | |
| | | | | Rod 3 | 2.248 | 0.042 | 2.206 | kg*mm ² | 200 | 36.66908679 | 36.1 | 156.9 | 3.039892648 | |
| | | | | Rod 4 | 51.365 | 0.038 | 51.327 | kg*mm ² | | | | | | |
| Lead Screw Dimensions | | | | Washer Moment of Inertia Calculations | | | | Mass Calculation | | | | | | |
| Lead | 8 mm | | | Washer Number | Radius (mm) | l = MR ² | Unit | Member | Volume (mm ³) | Density (kg/mm ³) | Mass (kg) | | | |
| Length | 300 mm | | | 1 | 102.463 | 27.841 | kg*mm ² | Die Set Top Plate | 5243860.502 | 0.00000281 | 14.73524801 | | | |
| Radius | 4 mm | | | 2 | 99.326 | 26.162 | kg*mm ² | Spring retainer plates | 105783.5777 | 0.000008 | 0.846268622 | | | |
| Volume | 15079.6300 mm ³ | | | 3 | 96.189 | 24.536 | kg*mm ² | Adaptive Plate | 344128.3455 | 0.000008 | 2.753026784 | | | |
| Mass | 0.1206 kg | | | 4 | 93.052 | 22.962 | kg*mm ² | TOTAL | | | 18.3345434 | | | |
| Moment of Inertia | 0.965096448 kg*mm ² | | | 5 | 89.916 | 21.440 | kg*mm ² | Linear Inertor | | | | | | |
| Centerpiece Dimensions | | | | 6 | 86.779 | 19.970 | kg*mm ² | Inertance (kg) | Mass Percent (%) | Natural Frequency (Hz) | | | | |
| O.D (Inch) | 0.75 inch | 19.05 mm | | 7 | 83.642 | 18.552 | kg*mm ² | 4.51 | 24.57 | 4.692500182 | | | | |
| Radius (O.D) | | 9.525 mm | | 8 | 80.505 | 17.187 | kg*mm ² | 7.28 | 39.7 | 4.431515064 | | | | |
| I.D | 0.323 inch | 8.2042 mm | | 9 | 77.368 | 15.873 | kg*mm ² | 18.3 | 100 | 3.70528413 | | | | |
| Radius (I.D) | | 4.1021 mm | | 10 | 74.231 | 14.612 | kg*mm ² | 35.7 | 194.5 | 3.051123566 | | | | |
| Thickness | 0.3 inch | 7.62 mm | | | | | | | | | | | | |
| Mass | | 0.01089 kg | | | | | | | | | | | | |
| Rod Dimensions | | | | Total Moment of Inertia, Flywheel = | | | | | | | | | | |
| Rod 1: Set Screw | | | | 107.651 kg*mm² | | | | | | | | | | |
| Radius | 2.413 mm | | | Inertance Calculations | | | | | | | | | | |
| Length | 1.25 inch | 31.75 mm | | Lead Screw | 0.595320009 kg | | | | | | | | | |
| Effective Length | | 35.8521 | | Flywheel | 66.405 kg | | | | | | | | | |
| Volume | | 655.8110784 mm ³ | | Washers | 48.44656811 kg | | | | | | | | | |
| Total Mass | | 0.005246489 kg | | Shaft Collar A | 0.439862793 kg | | | | | | | | | |
| l-Partial | | 9.525 mm | | Shaft Collar B | 0.439862793 kg | | | | | | | | | |
| Mass-Partial | | 0.00139386 kg | | Shaft Collar C | 0.439862793 kg | | | | | | | | | |
| Rod 2: Bolt (ZINC) | | | | Inertance, b (Two-way Gap Inertor) | | | | | | | | | | |
| Radius | 2.413 mm | | | 116.3264205 kg | | | | | | | | | | |
| Length | 4 inch | 101.6 mm | | % of Mass 634.47 % | | | | | | | | | | |
| Effective Length | | 105.7021 | | Inertance, b (Bushing - Crown Gap Inertor) | | | | | | | | | | |
| Volume | | 1933.515978 mm ³ | | 116.7662833 kg | | | | | | | | | | |
| Total Mass | | 0.013791769 kg | | % of Mass 636.86 % | | | | | | | | | | |
| l-Partial | | 9.525 mm | | Inertance (Linear Inertor): | | | | | | | | | | |
| Mass-Partial | | 0.0012428 kg | | 116.3264205 kg | | | | | | | | | | |
| Rod 3: Set Screw | | | | % of Mass 634.47 % | | | | | | | | | | |
| Radius | 2.413 mm | | | | | | | | | | | | | |
| Length | 1.25 inch | 31.75 mm | | | | | | | | | | | | |
| Effective Length | | 35.8521 | | | | | | | | | | | | |
| Volume | | 655.8110784 mm ³ | | | | | | | | | | | | |
| Total Mass | | 0.005246489 kg | | | | | | | | | | | | |
| l-Partial | | 9.525 mm | | | | | | | | | | | | |
| Mass-Partial | | 0.00139386 kg | | | | | | | | | | | | |
| Rod 4: Bolt (ZINC) | | | | | | | | | | | | | | |
| Radius | 2.413 mm | | | | | | | | | | | | | |
| Length | 4 inch | 101.6 mm | | | | | | | | | | | | |
| Effective Length | | 105.7021 | | | | | | | | | | | | |
| Volume | | 1933.515978 mm ³ | | | | | | | | | | | | |
| Total Mass | | 0.013791769 kg | | | | | | | | | | | | |
| l-Partial | | 9.525 mm | | | | | | | | | | | | |
| Mass-Partial | | 0.0012428 kg | | | | | | | | | | | | |
| Shaft Collar Dimensions | | | | | | | | | | | | | | |
| O.D | 18 mm | | | | | | | | | | | | | |
| I.D | 8 mm | | | | | | | | | | | | | |
| Thickness | 9 mm | | | | | | | | | | | | | |
| Volume | 1837.831702 mm ³ | | | | | | | | | | | | | |
| Mass | 0.014702654 kg | | | | | | | | | | | | | |
| Moment of Inertia | 0.713078701 kg*mm ² | | | | | | | | | | | | | |
| Added Weight Dimensions | | | | | | | | | | | | | | |
| O.D | 9.2456 mm | | | | | | | | | | | | | |
| I.D | 4.3612 mm | | | | | | | | | | | | | |
| Thickness | 3.1369 mm | | | | | | | | | | | | | |
| Volume | 165.7393734 mm ³ | | | | | | | | | | | | | |
| Mass | 0.001325915 kg | | | | | | | | | | | | | |
| Moment of Inertia | 0.017185535 kg*mm ² | | | | | | | | | | | | | |

Appendix B: Experimental Hardware

| | | | | | |
|----------|--|------------|--|------------------------|--|
| DRAWN | | 12/15/2021 | | | |
| CHECKED | | | | TITLE | |
| SK | | | | | |
| MFG | | | | | |
| APPROVED | | | | | |
| | | SIZE | | DWG NO | |
| | | D | | Gap Inserter Drawing 2 | |
| | | SCALE | | SHEET 1 of 4 | |

Alex Shafer
 ashafer4@vols.utk.edu
 University of Tennessee - Knoxville

Explanation of Documents:
 B.1 Gap Inserter
 B.2 Die Set and Modifications
 B.3 Adapter Plates
 B.4 Spring Retainer Plates

B.1 Gap Inerter

Contents:

This section includes the fabricated gap inerter pieces and various gap inerter configurations that will be investigated. The gap inerter pieces include the notched bushing, notched crown, bearing cap, and flywheel centerpiece.

| | | | |
|----------|------------|-------|-----------------------|
| DRAWN | 12/15/2021 | | |
| CHECKED | | TITLE | |
| SK | | | |
| WFG | | | |
| APPROVED | | SIZE | DWG NO |
| | | D | Gap Inerter Drawing 2 |
| | | SCALE | SHEET 2 of 4 |

Fabricated Gap Inerter Pieces

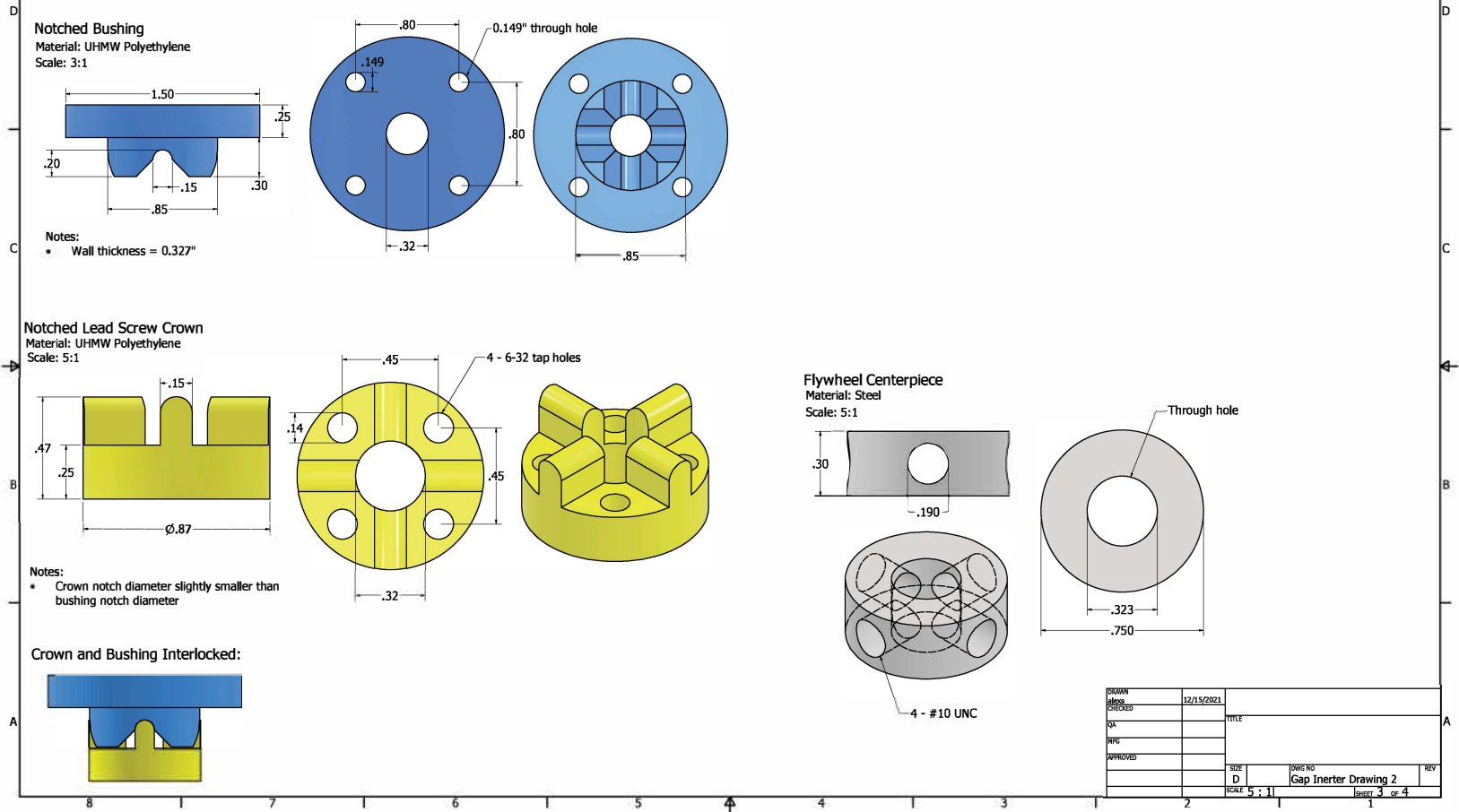


Figure B-1 Fabricated gap inerter pieces

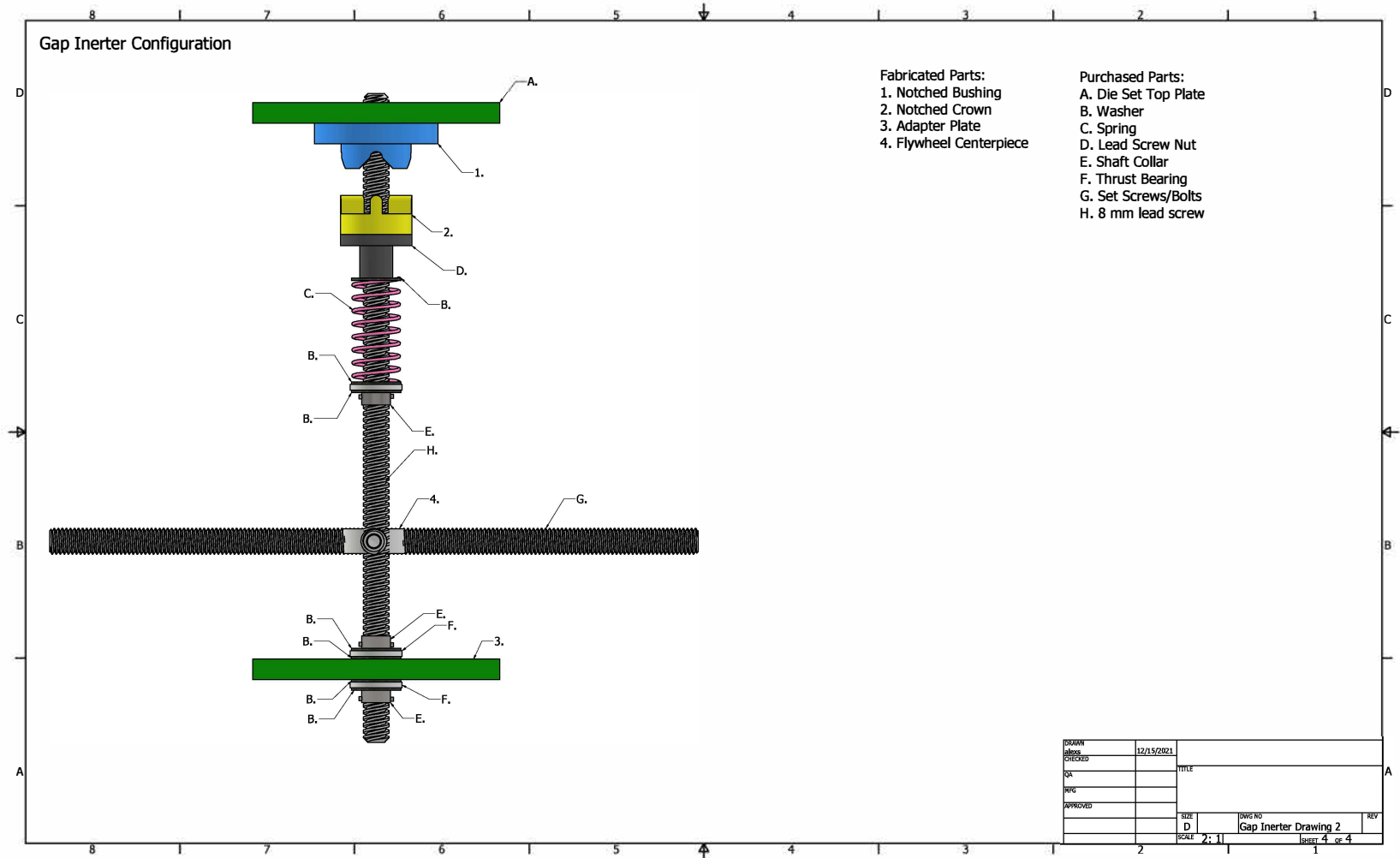


Figure B-2 Gap inerter configuration

B.2 Die Set and Modifications

Contents:

This section includes the purchased die set test apparatus and die set modifications. The die set drawings included in this Appendix were provided by the die set manufacturer, Superior Die Set. Die set modifications include tapped holes in the top and bottom mass plates to secure the fabricated adapter plates(B.3).

| | | | |
|----------|-----------|-------|-----------------------|
| DRAWN | 12/7/2021 | | |
| CHECKED | | TITLE | |
| SK | | | |
| REG | | | |
| APPROVED | | SIZE | ENG NO |
| | | D | AdapterPlate Drawings |
| | | SCALE | SHEET 1 OF 7 |

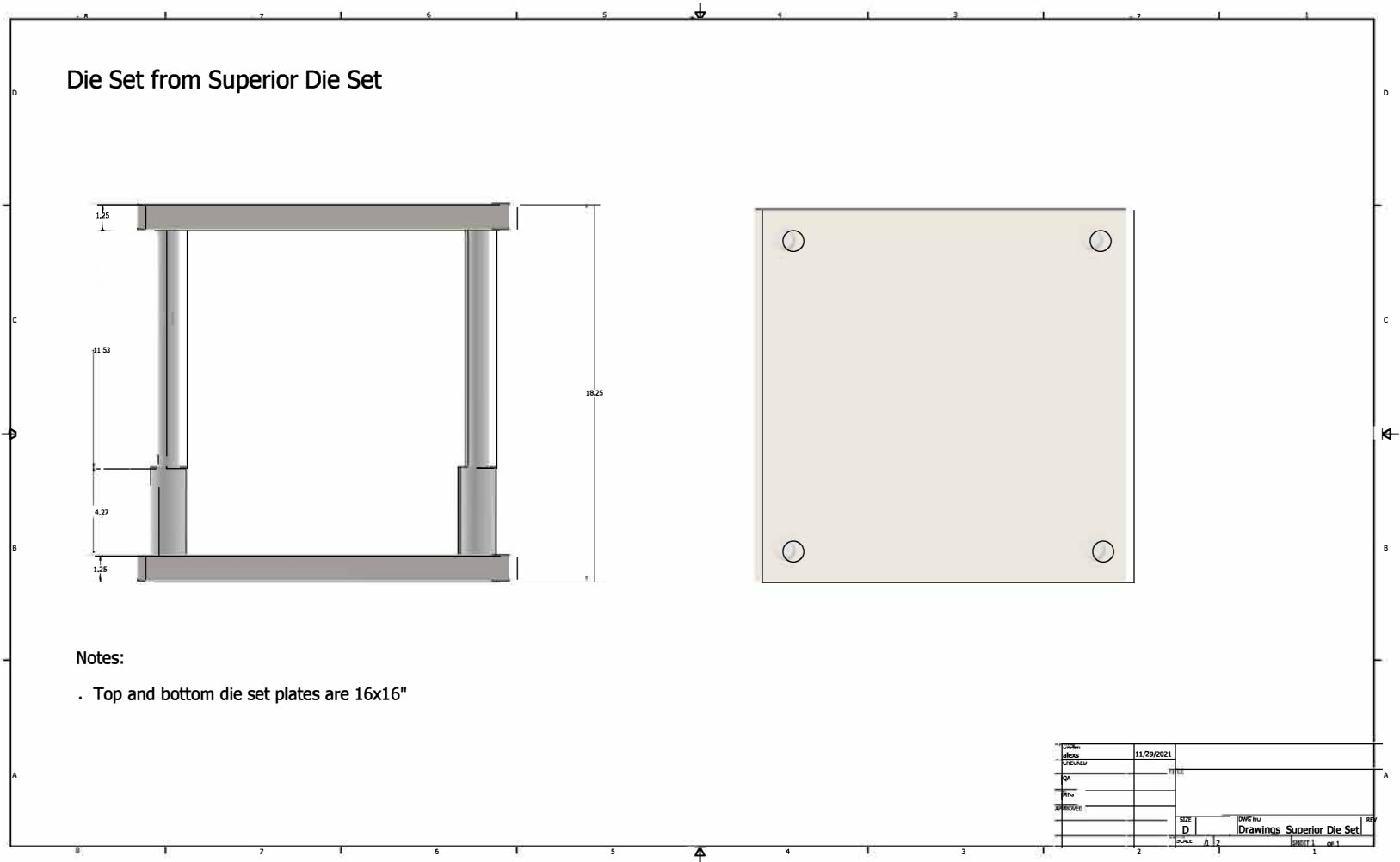


Figure B-3 Die set from Superior Die Set

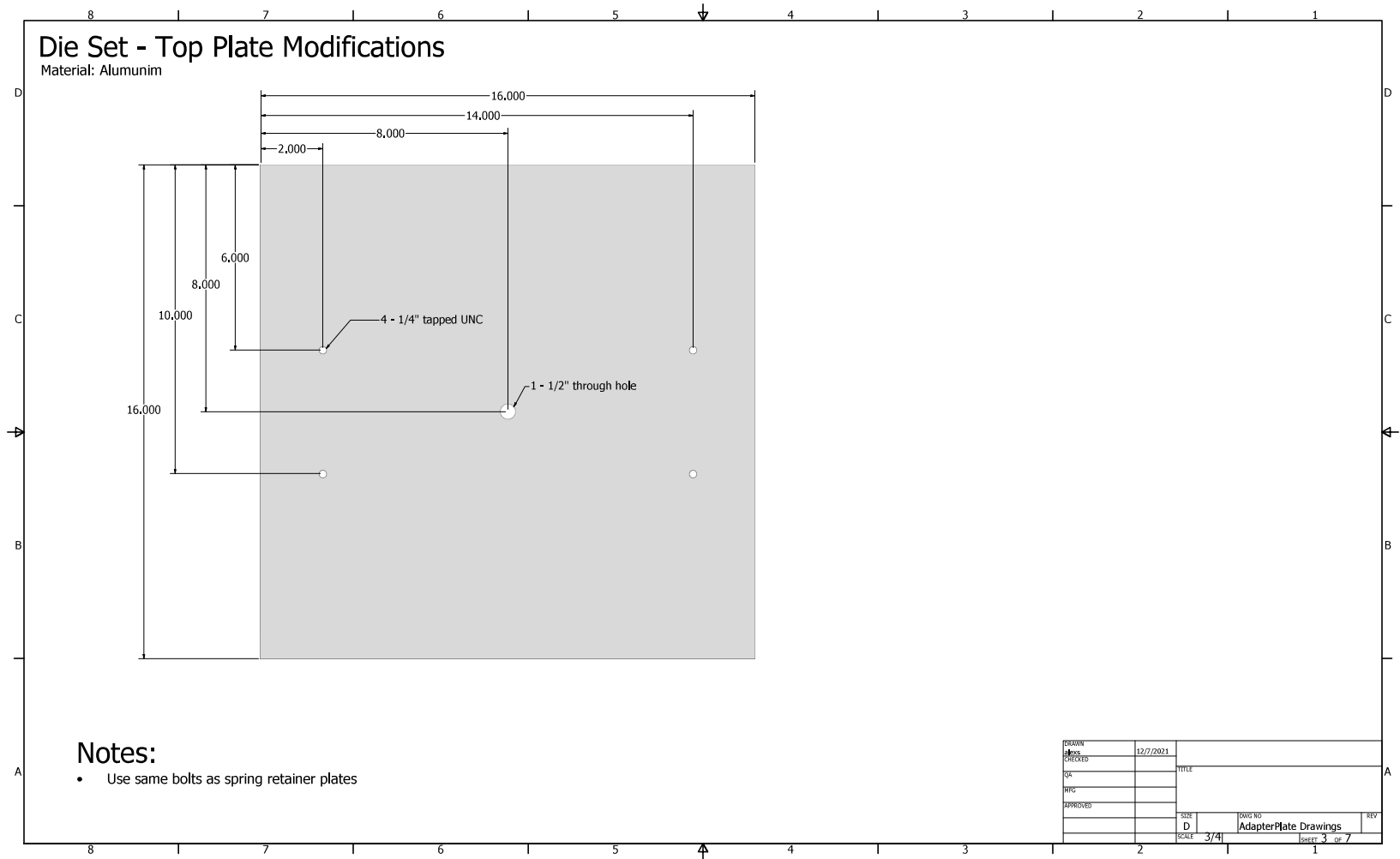


Figure B-4 Die set top plate modifications

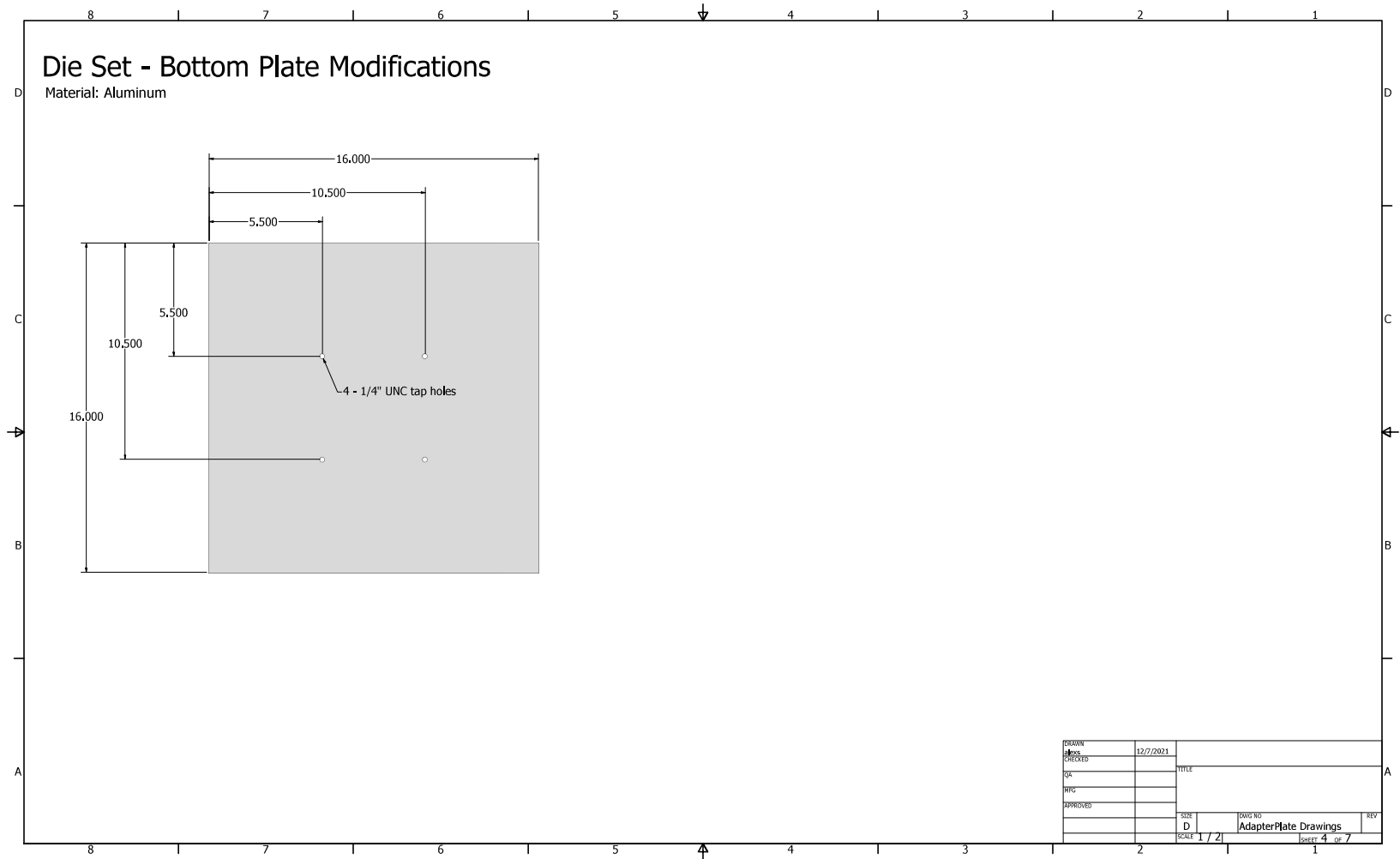


Figure B-5 Die Set Bottom Plate Modifications

B.3 Adapter Plates

Contents:

This section includes the fabricated adapter plates. The top adapter plate will be secured to the top die set plate and the bottom adapter plate will be secured to the bottom die set plate. The rotational inertial mechanism will attach to the adapter plates. The purpose of the adapter plate is to prevent unnecessary holes in the die set test apparatus. This would allow the die set to be used for other projects in the future.

| | | | |
|----------|-----------|-------|-----------------------|
| DRAWN | 12/7/2021 | | |
| CHECKED | | TITLE | |
| SK | | | |
| REF | | | |
| APPROVED | | SIZE | DWG NO |
| | | D | AdapterPlate Drawings |
| | | SCALE | SHEET 5 OF 7 |

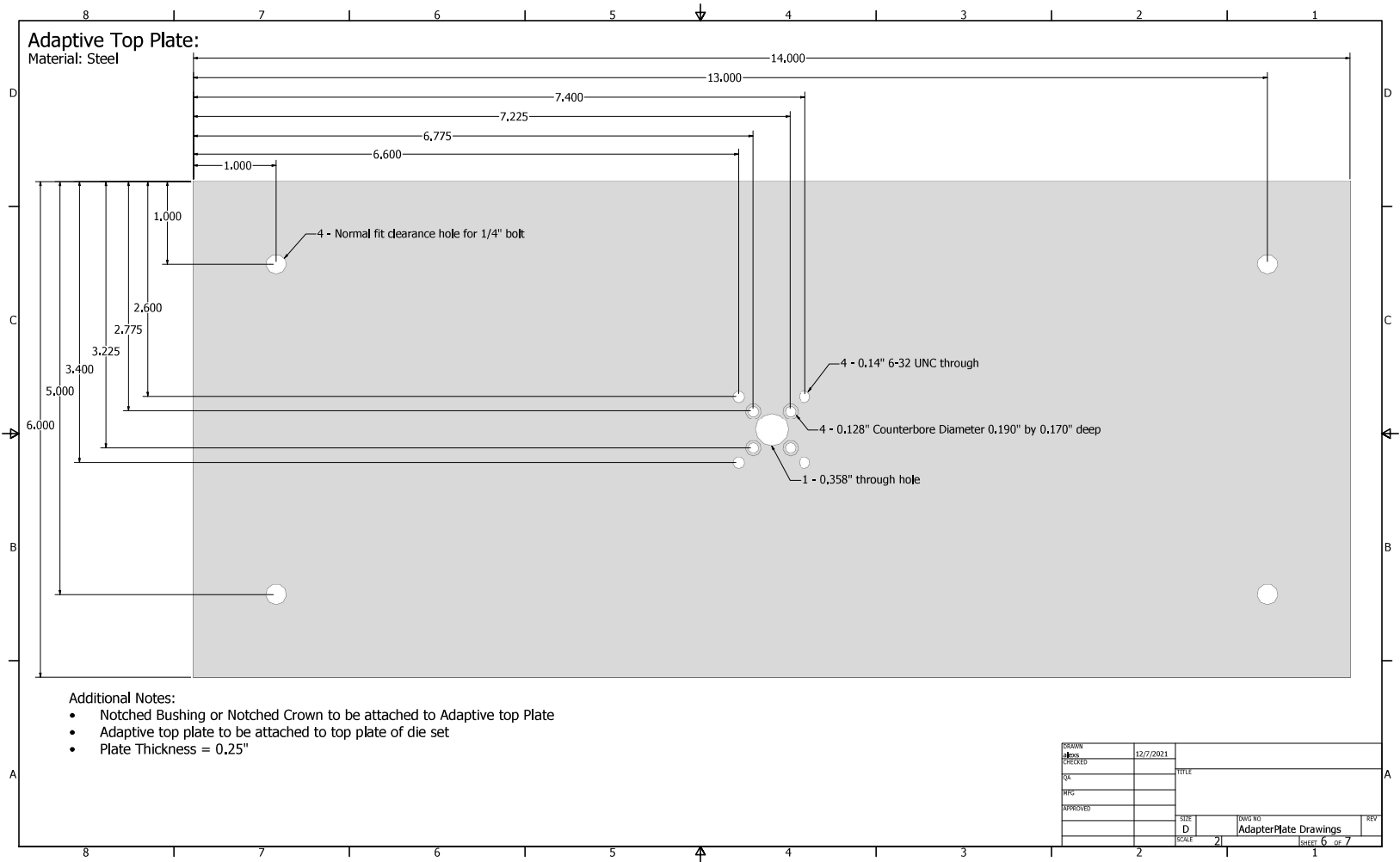


Figure B-6 Adaptive top plate

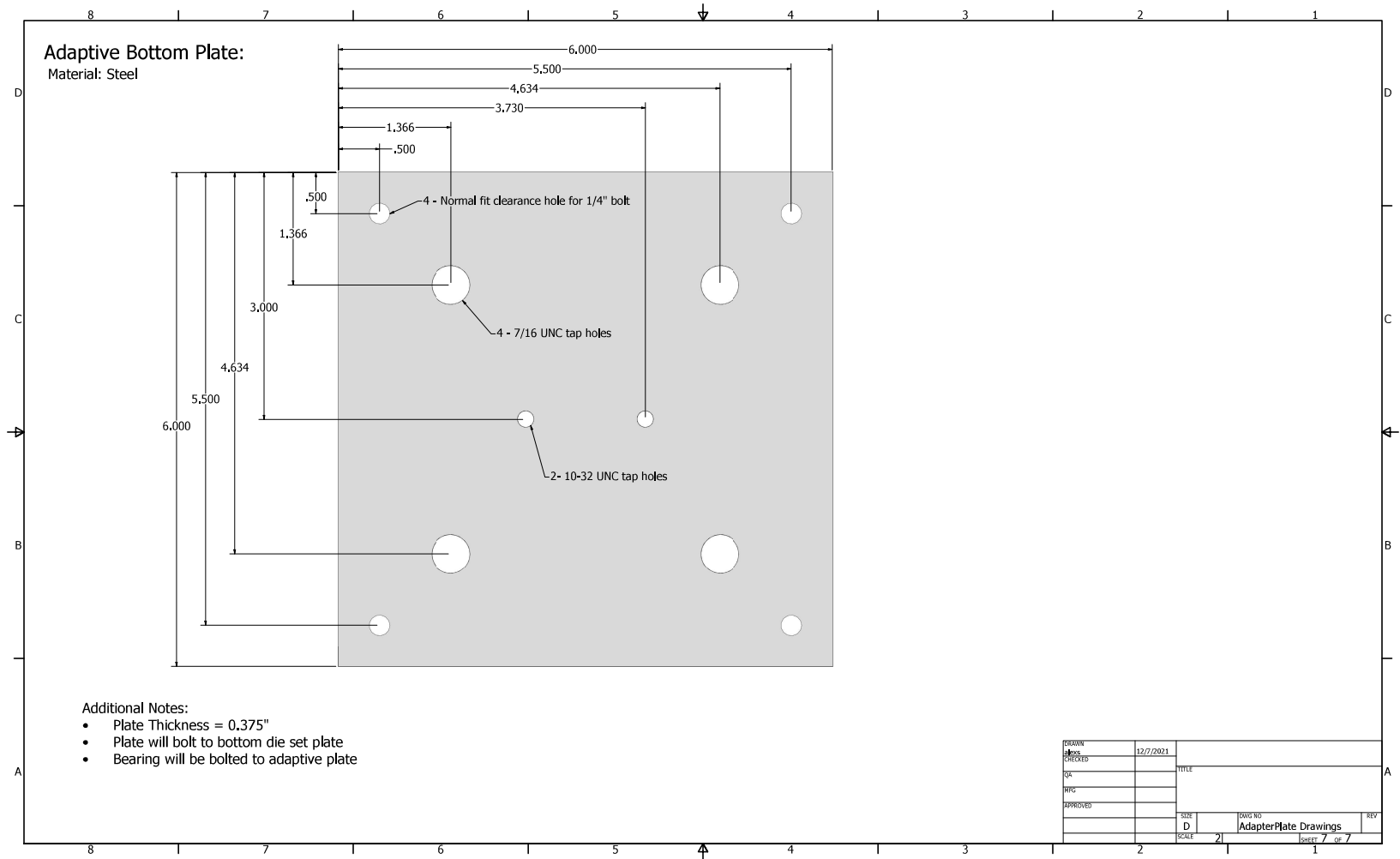


Figure B-7 Adaptive bottom plate

B.4 Spring Retainer Plates

Contents:

This section includes the fabricated spring retainer plates. The purchased springs were welded to a top spring retainer plate and bottom spring retainer plate. The welded spring and plate were placed over the guide rods. The spring retainer plates were bolted to the top and bottom of the die set mass plates to ensure the spring would be engaged in both tension and compression during experimental testing.

| | | | |
|----------|-----------|-------|-------------------------------|
| DRAWN | 1/31/2022 | | |
| CHECKED | | TITLE | |
| SK | | | |
| RFG | | | |
| APPROVED | | SIZE | DWG NO |
| | | D | Spring Retainer Plate Drawing |
| | | SCALE | SHEET 1 OF 3 |

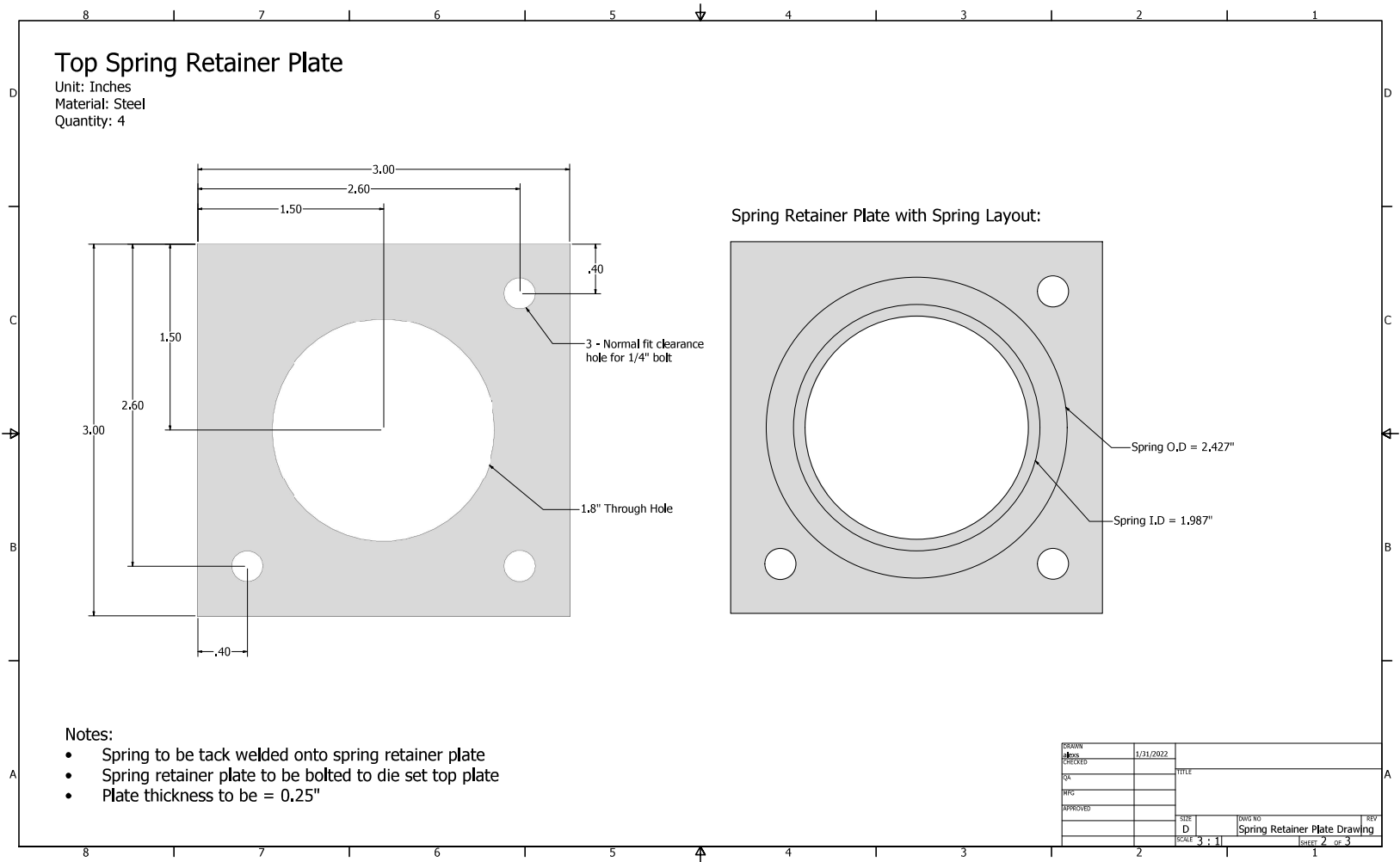


Figure B-8 Top spring retainer plate

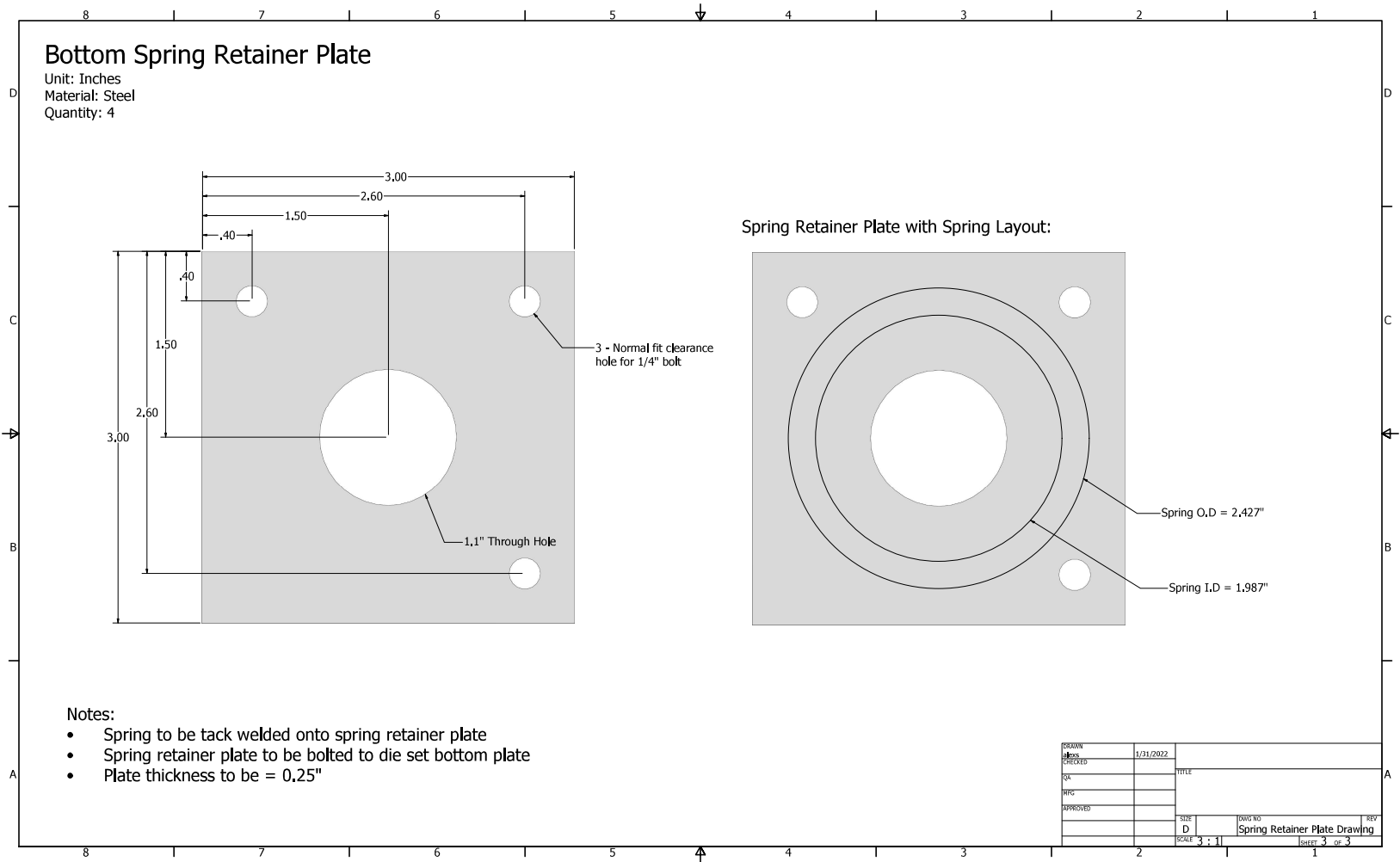


Figure B-9 Bottom spring retainer plate

Vita

Alex Shafer is originally from the Suburbs outside of Chicago, Illinois where she attended Huntley High School. She moved to Knoxville to continue her education at the University of Tennessee. In December 2020, Alex obtained her Bachelor of Science degree in Civil Engineering. She loved Tennessee so much she decided to stay at UT to complete her Master of Science in Structural Engineering. In January of 2021, she accepted a graduate research assistantship position where she studied passive isolation systems with linear and nonlinear rotational inertial mechanisms. Alex graduated with her Master of Science in August 2022 and is now pursuing a career as a structural engineer.